UNIVERSITY OF Southampton

University of Southampton Research Repository
ePrints Soton

Copyright © and Moral Rights for this thesis are retained by the author and/or other copyright owners. A copy can be downloaded for personal non-commercial research or study, without prior permission or charge. This thesis cannot be reproduced or quoted extensively from without first obtaining permission in writing from the copyright holder/s. The content must not be changed in any way or sold commercially in any format or medium without the formal permission of the copyright holders.

When referring to this work, full bibliographic details including the author, title, awarding institution and date of the thesis must be given e.g.

AUTHOR (year of submission) "Full thesis title", University of Southampton, name of the University School or Department, PhD Thesis, pagination

http://eprints.soton.ac.uk

UNIVERSITY OF Southampton

FACULTY OF ENGINEERING AND THE ENVIRONMENT
ENGINEERING SCIENCES

NATIONAL CENTRE FOR ADVANCED TRIBOLOGY AT SOUTHAMPTON (nCATS) RESEARCH GROUP

DEFENCE SCIENCE AND TECHNOLOGY LABORATORY (*DSTL*) FUNDED PROJECT THROUGH THE EUROPEAN DEFENCE AGENCY (*EDA*) PROJECT ENTITLED 'ANTIFOULING COATINGS FOR WARSHIPS' (*A*CWS)

METHOD DEVELOPMENT FOR ENHANCED ANTIFOULING TESTING USING NOVEL NATURAL PRODUCTS AGAINST MARINE BIOFILMS

By
Maria Salta

SUPERVISORS: DR JULIAN WHARTON, PROF ROBERT WOOD, DR DEBORA IGLESIAS RODRIGUEZ

THESIS SUBMITTED FOR THE DEGREE OF
DOCTOR OF PHILOSOPHY

April 2012

Abstract

Marine biofouling is the accumulation of organisms on underwater surfaces, causing increased ship hydrodynamic drag, which results in higher fuel consumption and decreased speed and range. Biofilms constitute a major component of the overall biofouling and may lead to a 14 % increase in ship fuel costs. Past solutions to antifouling (AF) have used toxic coatings which have subsequently been shown to severely affect marine life. The prohibited use of these antifoulants has led to the search for bio-inspired AF strategies. Current approaches towards the production of alternative coatings include the incorporation of natural AF compounds into paints.

Screening assays for novel AF compounds are often separated into two categories; toxicity and AF assays. Increasingly there is evidence that active compounds affect organisms at non-toxic concentrations, hence, the necessity for more insightful AF testing, such as bacterial and diatom attachment. This study assessed natural product (NP) antifouling performance of two marine seaweeds (*Chondrus crispus* and *Bifurcaria bifurcata*) and two isolated pure compounds from terrestrial sources (usnic acid and juglone) against two marine biofilm bacteria, *Cobetia marina* and *Marinobacter hydrocarbonoclasticus*. Overall it was found that all NPs affected bacterial attachment, however, juglone demonstrated the best AF performance against both bacterial species at a concentration range between 5 - 20 ppm.

Biofilm colonisation is a surface related phenomenon, thus novel bioassays have been developed to directly test biofilm attachment and growth on NP-containing coatings for both static and hydrodynamic conditions. This study has incorporated NPs into a model coating system, using two formulations in order to assess their effect on biofilm growth. Laboratory screening of NP-containing coatings is often largely unexplored mainly due to difficulties in assessing their activity over short experimental time scales (typically only a maximum of a few days). To date there are only a limited number of reports on laboratory assessment for antifouling paints and their effect on biofilm growth and/or attachment. In this study, NP-containing model paints were applied on to coupons, placed in 24-well plates and then inoculated with the marine biofilm forming bacteria. This has been achieved by the development of a novel bioassay protocol that has allowed the *in situ* observation of biofilm formation and growth, by corroborating different techniques such as a multidetection microplate reader and confocal laser scanning microscopy (through nucleic acid staining).

There was good correlation between the two techniques which showed that the NP containing coatings significantly inhibited biofilm growth and also revealed marked differences in biofilm structure (e.g. bio-volume, morphology and thickness). The goal of this study was to develop a new protocol to allow assessment of biofilm formation on coatings in a high throughput non-invasive manner.

New protocols and methods using microfluidic devices were developed for the assessment of bacterial attachments and initial biofilm formation in the presence and absence of a NP under hydrodynamic conditions. This led to the development and fabrication of a novel lab-on-a-chip device for the investigation of the biofilm response to different hydrodynamic conditions. The microfluidic flow channels were designed using computational fluid dynamic simulations so as to have a pre-defined, homogeneous wall shear stress in the channels, ranging from 0.03 to 4.30 Pa, which are relevant to in-service conditions on a ship hull.

Table of contents

Acknowledgements

Writing the acknowledgments was very difficult for me, since sometimes words are not enough to describe the overwhelming feelings one experiences throughout the PhD years and upon completing it. Nevertheless I'll try to do so.

First of all, I would like to thank my principal supervisor and dear friend *Dr Julian Wharton* who, most importantly, believed in me. My work would have never been so exciting, constructive and fun if it wasn't for his constant support and encouragement. His constructive criticism was there only to push me into a new way of thinking and realisation of my abilities. My crazy ideas over the last years were always welcomed which made me feel free to do the thing I love the most: *research*. And for this reason, I will always be thankful and consider myself incredibly lucky. The best supervisor one could ask for! A simple "thank you" won't suffice…nevertheless…Thank you so much for the amazing journey, Julian!

I would also like to heartily thank my secondary supervisor *Prof Robert Wood* and my advisor *Prof Keith Stokes* for their financial support but also constructive criticism which taught me how to communicate my work in many disciplines and fields and gave me the opportunity to carry on with my ideas. Thank you to Lily for introducing me into the world of Biofouling and for being such a positive personality! I would also like to thank all the members of the EDA project who have been very joyful to work with – and left me with great memories during our meetings across Europe (Toulon, Paris, Den Helder, Amsterdam). Special thanks to *Jean-Francois Briand* for the most interesting discussions on marine biofilms, also *Job Klijnstra* and *Anouk Bruin* for their fantastic hospitality during my visit at TNO (Den Helder).

Special thanks to my colleague and friend *Dr Simon Dennington* for his many advices and collaboration over the last 3 years. His constant excitement and positive outlook for research and life in general has always been a breath of fresh air. Our plans for artistically communicating environmental issues will one day be fulfilled ☺. I would also like to thank *Dr Paul Stoodley* for all his advices and for always being excited and enthusiastic during our discussions. Thank you Paul for helping me understand a little better the "magic" world of Biofilms ☺! Also, I would like to thank *Prof Paul Tyler* who, with his remarkable enthusiasm and love for his work, made me realise (year 1 BSc) I had to become a researcher. A big thank you to *Dr Debora Iglesias-Rodriguez* for giving me some amazing opportunities and for trusting me during my Masters course. Many thanks to all the people who I co-sailed with, in the research cruises D321 and JC031, they've been once-in –a-life-time journeys!

I would also like to thank all my friends who over the years stood by me! We have sheared moments of scientific stimulation but also moments of great foolishness – both of which I found essential and helped me to carry on through this difficult process. *Amir, Orestis, Lorenzo, Federico, Dario, Sophia, Orestis Jr, Peter, Liam, Jonathan, Tom, Rob, Mostafa, Anna, Hatice, Maria-Nefeli, Yiannis, Cynthia, Bronwyn, Eithne, Sinhue, Dave, Mark, Libby, Richard,*

Aggelikoula, Aphrodite, Marinakion, Giotanna, Vicky, Bakkerino: Thank you all for being part of my life!

Last but not least, I would like to thank my parents and brother for their love and incredible support throughout the years. If it wasn't for them, none of my dreams would have ever been fulfilled. I love you all so very much!

Finally, I would like to dedicate this work to my mother – *Ευτυχία* – who taught me how to be strong, never give up and how to turn life's difficutlies into positive experiences. Being incredibly patient, full of strength and love she is a perfect mother who always holds my hand while I'm following my dreams… Σε ευχαριστώ μανούλα.

"Σα βγεις στον πηγαιμό για την Ιθάκη,
να εύχεσαι να'ναι μακρύς ο δρόμος,
γεμάτος περιπέτειες, γεμάτος γνώσεις."
Κ.Π. Καβάφης

"As you set out for Ithaka,
hope the voyage is a long one,
full of adventure, full of discovery."
C.P. Cavafy

List of Figures

Figure 9.6. Stress *vs*. strain curves of a *C. marina* bacterial biofilm (Red line) and ASW controls (Blue lines). Biofilm maximum load = 4.95 mPa; Biofilm slope = 543.6 mPa mm^{-1}; ASW mean maximum load = 1.10 mPa

List of Tables

Table 5.1. Natural products (NP) used to assess bacterial attachment where, JUG = juglone, UA = usnic acid, CCT = *C. crispus* toluene soluble. Units: ppm = µg mL^{-1}.

Nomenclature

ACWS	Antifouling Coatings for Was Ships
AF	Antifouling
AFM	Atomic Force Microscopy
AMBIO	Advanced Nanostructured Surfaces for the Control of Biofouling
ANOVA	Analysis of Variances
ASW	Artificial Sea Water
ASWPH	Artificial Sea Water Peptone High
ASWPL	Artificial Sea Water Peptone Low
ATCC	American Type Culture Collection
ATP	Adenosine Triphosphate
BB	*Bifurcaria bifurcata*
CC	*Chondrus crispus*
CCT	*Chondrus crispus* Toluene
CDP	Controlled depletion rate
CLSM	Confocal Laser Scanning Microscopy
CON	Control
CV	Crystal Violet
DGGE	Denaturing gradient gel electrophoresis
DAPI	4',6-diamidino-2-phenylindole
DLVO	Derjagiun, Landau, Verwey and Overbeek
DMSO	Dimethyl sulfoxide
DSTL	Defence Science and Technology Laboratory
DSTO	Defence Science and Technology Organisation
EC_{50}	Effective Concentration 50 %
EDA	European Defence Agency
EPS	Extrapolymeric Substances
EtOH	Ethanol
FC81	Flow Cell 81
FISH	Fluorescence *in situ* hybridization
FRC	Foul-Release Coatings
GC-EIMS	Gas Chromatography –Electron Impact Mass Spectrometry
GFP	Green Fluorescent Pigment
IMO	International Maritime Organisation
JUG	Juglone
KW	Kruskal-Wallis
LC_{50}	Lethal Concentration 50 %
LED	Light Emitting Diode
MAPIEM	Le laboratoire des Matériaux - Polymères - Interfaces - Environnement Marin
MBC	Minimum Bactericidal Concentration
MIC	Minimum Inhibitory Concentration
MTM	Metamare B175™
nCATS	National Centre for Advanced Tribology at Southampton

NOCS	National Oceanography Centre, Southampton
NP	Natural product
NSPL	Natural Sea Water Peptone Low
NSW	Natural Sea Water
NSWPH	Natural Sea Water Peptone High
OD	Optical density
PBS	Phosphate Buffered Saline
PCR	Polymerase chain reaction
PI	Propidium Iodide
PMMA	Polymethylmethacrylate
PMT	Photomultiplier Tube
PPM	Part Per Million (μg mL^{-1})
QS	Quorum sensing
Re	Reynolds number
RFP	Red Fluorescent Pigment
RFU	Relative Fluorescence Units
ROS	Rosin
SEM	Scanning Electron Microscopy
SoC	Ship-on-a-Chip
SPC	Self Polishing Copolymers
SSP	Sea Salts Peptone
S9	Syto9
TBT	Tributyltin
TNO	Nederlandse Organisatie voor Toegepast
UA	(+)- Usnic Acid
w	Viscosity of working fluid
μ	Fluid viscosity (kg m^{-1} s^{-1})
τ_w	Wall shear stress (Pa)
$\frac{dv}{dy}$	Velocity gradient
h	Distance between flow cell plates (m)
b	Width of flow cell channel (m)
Q	Measured flow (m^3 s^{-1})
λ_{EM}	Emission wavelength (nm)
λ_{EX}	Excitation wavelength (nm)
Log K_{ow}	Log octanol-water partition coefficient
LogD	Logarithm of the distribution coefficient of an ionisable compound between octanol and water phases at defined pH values.

Declaration of authorship

I, Maria Salta, declare that the thesis entitled **"Method development for enhanced antifouling testing using novel natural products against marine biofilms"** is an account of the work carried out by me as part of the national Centre for Advanced Tribology, Southampton (nCATS), Engineering Sciences, Faculty of Engineering and the Environment, University of Southampton, UK.

The work presented in this thesis is my own, and has been generated by me as the result of my own original research. I confirm that:

- this work was done wholly or mainly while in candidature for a research degree at this University;
- where any part of this thesis has previously been submitted for a degree or any other qualification at this University or any other institution, this has been clearly stated;
- where I have consulted the published work of others, this is always clearly attributed;
- where I have quoted from work of others, the source is always given. With the exception of such quotations, this thesis is entirely my own work;
- I have acknowledged all main sources of help;
- where the thesis is based on work done by myself jointly with others, I have made clear exactly what was done by others and what I have contributed myself;
- parts of this work have been published as: see pages 208 - 210

Signed: …….

Date: 25/05/2012

Chapter 1

1. General introduction

The underwater hull of a ship is exposed not only to the corrosive seawater environment, but also to the constant accumulation of biofouling. Biofouling, or marine growth, includes any attaching organisms such as bacteria, diatoms, tubeworms, mussels, barnacles and algae. Marine growth is a major problem continually encountered when dealing with the underwater hull and platforms, which can affect a vessel's performance including: speed, hydrodynamic efficiency, fuel consumption and weight. With an estimated 300 million tonnes of bunker fuel oil consumed annually by the world's fleet, there is an ever increasing focus on shipping's environmental footprint. The International Maritime Organization (IMO, 2000) estimates that, without corrective action and the introduction of new technologies, air emissions due to increased bunker fuel consumption by the world's shipping fleet could increase by between 38 and 72 per cent by 2020. It is estimated that AF coatings provide the shipping industry with annual fuel savings of $60 billion and reduced emissions of 384 million and 3.6 million tonnes, respectively, for carbon dioxide and sulphur dioxide per annum.

The use of tributyltin (TBT) in coatings was widely used for its antifouling capacity. However, in September 2008 further applications of TBT coatings were prohibited in a treaty ratified by the IMO, due to its toxic effects in the wider marine environment, thus all structures must have the coating removed or overlay a protective barrier to prevent the further leakage of the TBT. Specifically, TBT has been shown to cause shell deformations in oysters; sex changes (imposex) in whelks; and immune response, neurotoxic and genetic effect in other marine species (IMO, 2002). TBT has also been described as the most toxic substance ever deliberately introduced into the marine environment (IMO 2002, Evans et al. 1995). Therefore, the need for new, effective and environmentally friendly coatings has been the focus and challenge for the scientific community.

In order to comply with the new legislations against toxic AF systems, the French, the Dutch and the Royal navies have collaborated to form the Antifouling Coatings for War Ships (ACWS) project under the aegis of the European Defence Agency (EDA). The ultimate objective of this EDA project is to identify environmentally acceptable systems that are capable of

providing effective and durable antifouling properties leading to increased dry-docking intervals (*i.e.* 6-10 years), high ship availability and a reduction in the degree of maintenance. This will be addressed through research into novel coating technologies. Specifically, the current PhD project is focused on the investigation of natural products (NPs) and their potential AF activity against marine biofilms, which will ultimately be incorporated into a coating system, resulting in an environmentally friendly AF system for (naval) ship hulls. The different research themes associated with antifouling products that will be investigated in this study include:

- Screening of NPs against bacterial attachment,
- Incorporation of selected NPs into a model coating system and subsequent testing against bacterial attachment and biofilm formation,
- Investigation of bacterial attachment and initial biofilm formation under different hydrodynamic condition in the presence and/or absence of NPs.

Colonisation of immersed substrates by biofouling organisms is a process often characterised by four main sequential steps that occur in the following order: 1) surface conditioning (seconds to minutes), 2) micro-fouling (biofilm) attachment and subsequent growth (minutes to hours), 3) larval and spore settlement of macro-organisms (macro-foulers) (days to weeks) and 4) macro-fouler growth and colonisation (weeks to years). Generally, marine biofilms are organised micro-communities of homogenous and mixed bacterial and diatom species typically surrounded by extrapolymeric substances (EPS). Water channels formed within and between these communities can transport nutrients or metabolites through convective flow (Stoodley et al. 1994, de Beer et al. 1994). Along with diatoms, bacteria constitute the major components of biofilms occurring in the marine environment, with both depending on location and seasonal variations. For example, a 14 % increase in ship fuel cost resulting from biofilms.

Several AF technologies have attempted to resolve the problem of biofouling. Currently, the maritime industry has primarily returned to using copper based coatings, the forerunner to TBT systems or has adopted foul-release coatings (FRC). The former has negative environmental connotations, which could possibly mean that they will be the subject of future legislation. They also have a shorter useful life than TBT, while the later coatings based on silicone elastomers with low surface free energies being the most successful in preventing macro-fouling attachment. However, FRCs are not immune from bacteria and diatom biofilms,

especially for extended times in dockyard / port, and the higher biofilm attachment strength on these hydrophobic surfaces (Holland *et al.* 2004) has been shown to resist speeds as high as 50 knots, *i.e.* 25.7 m s^{-1} (Townsin and Anderson 2009). Fuel penalties from increased surface roughness due to biofilms (5 µm – 1 mm) are commonly reported (*e.g.* Schultz 2007). To date, new tin free self-polishing / ablative antifouling coatings which have been reported as offering good performance on commercial ships has not been translated to naval platforms, particularly as naval platforms tend to remain moored alongside for at least 50% of their lives. Consequently, there remains a very real necessity to identify suitable new AF systems for effectively preventing the fouling and in particular biofilms. For these reasons biofilm inhibition was decided to be the main focus of the current investigation.

Chapter 2

2. Aims, objectives and thesis structure

2.1. Aims and objectives

The main aim of the current research project was to identify and exploit NPs that possess AF properties which could be incorporated into a paint system in order to protect marine platforms against fouling organisms. Specifically, inhibition of biofilm formation was the primary aim, since (*i*) current AF technologies have yet to identify methods for its prevention and (*ii*) biofilm formation is often considered to be the first step of the biofouling community succession thus positively affecting (or supporting) macrofouling settlement. This investigation's aims were addressed by:

- establishing a selection criteria and identifying NPs with potential AF (anti-biofilm) properties,
- assessing AF efficacy against (relevant) marine biofilm forming species,
- incorporation of NPs into a simplified model coating system,
- developing novel bioassays using NPs incorporated into coating formulations,
- understanding the overall effect of NPs on bacterial attachment at the surface-biofilm interface by corroborating different techniques, *e.g.* CLSM and microplate reader,
- measuring release rates of the NP from the coated surface in order to understand the molecule's (or extract's) kinetics with time and to evaluate its effect on bacterial attachment,
- testing bacterial attachment on NP-containing surfaces under a range of hydrodynamic scenarios that simulate the real environment, *i.e.* flow dynamics present when the ship is either moving or docked (*e.g.* tidal flows).

2.2 Thesis structure

The thesis consists of nine chapters. The literature survey can be found in **Chapter 3** and will review the current state of knowledge and scientific aspects related to this investigation. This chapter is divided into sections that are relevant to the current project, such as *i*) biofilm species diversity, *ii*) attachment mechanisms, *iii*) their effect on macro-fouling settlement, as well as *iv*) recently published literature on biofilms and AF are presented.

Chapter 4 assesses the techniques currently available for investigating the effect of NPs on biofilms; this requires a suite of laboratory based experiments, commonly known as bioassays. The initial growth conditions play a key role in cell biology, since the environment may affect the physiology and therefore the growth and kinetic response of an organism to a treatment. For this reason a series of tests were conducted in order to i) compare different experimental media, *i.e.* NSW *vs.* ASW and the levels of carbon typically used in bacterial bioassay testing, ii) optimise and establish both planktonic and biofilm assessment methods.

In **Chapter 5** three NPs were chosen for evaluation of their potential AF activity, two of which were pure compounds of terrestrial origin, namely juglone and usnic acid, and a crude extract from the marine environment, the alga *Chondrus crispus*. The NP selection criteria was informed by previous evidence supporting potential AF activity within the ACWS project (for marine NPs) as well as promising data from the published literature (for terrestrial NPs).

Chapters 5-7 describe novel high throughput bioassays which have been developed for NP screening against two marine biofilm forming species (*Cobetia marina* and *Marinobacter hydrocarbonoclasticus*). For initial screening purposes, three NPs were suspended in serial dilutions and bacterial attachment bioassays were conducted to identify AF activity (**Chapter 5**). Once the NP activity was confirmed through screening bioassays, novel protocols/methods were developed where NPs were incorporated into model coating formulations in order to assess AF efficacy at the NP coating-biofilm interface under both static (**Chapter 6**) and dynamic/flow (**Chapter 7**) conditions. The overall conclusions obtained from this work are summarised in **Chapter 8** and suggestions for further work are presented in **Chapter 9**.

2.3 Novelty

Several elements of novelty can be identified in the current work:

I. The development of a new bioassay that has allowed a rapid *in situ* assessment of newly attached bacteria using microtiter plates combined with nucleic acid staining and plate reader technology.

II. The investigation of one marine and two terrestrial NPs in terms of bacterial attachment response which revealed a range of anti-biofilm effects, including a hormetic response identified for the first time in a marine context.

III. Of the NPs screened, juglone which has never been used previously against marine biofilms (or any other fouling organisms) was identified as the best AF candidate, revealing anti-biofilm activity at low concentrations comparable to commercially available biocides.

IV. For the first time, the NPs were incorporated into model coating systems and a novel bioassay protocol was developed in order to allow the *in situ* observation, at the coating surface, of biofilm formation and growth. This was achieved by corroborating measurements from a multidetection microplate reader and confocal laser scanning microscopy.

V. Novel protocol and methods using microfluidic devices were developed for the assessment of bacterial attachments and initial biofilm formation in the absence and presence of a NP under hydrodynamic conditions.

VI. The hydrodynamic studies have led to the development and fabrication of a novel *lab-on-a-chip* device for the investigation of the biofilm response to different hydrodynamic conditions.

Chapter 3

3. Literature review

3.1 Marine biofilms: a brief introduction

Marine biofilms, often termed microfouling, are organised micro-communities of mixed species containing mainly bacteria and diatoms which are typically surrounded by a matrix of extrapolymeric substances (EPS). Water channels form between biofilm communities allowing nutrient and/or metabolite transportation through convective flow (Stoodley et al. 1994, de Beer et al. 1994). Along with diatoms, bacteria constitute the major components of biofilms occurring in the marine environment, where both are dependent on geographical and seasonal variations. The moment a clean surface is submerged into the sea, biofilm forming microorganisms will rapidly colonise it and subsequently form highly complex, dynamic 3D surface structures (Davey and O'toole 2000, Molino et al. 2009a, Huggett et al. 2009). Recent reviews into fouling control using textured and biomimetic surfaces have identified the numerous challenges of developing antifouling (AF) technologies (Salta et al. 2010, Scardino and de Nys, 2011). Importantly, it was highlighted that these technologies are usually targeting a limited number of taxonomic groupings, for instance coatings that inhibit macrofoulers (*e.g*. algae, barnacles and mussels) may not be active against biofilms. Scardino and de Nys (2011) primarily focused on the effect of surface modifications on macrofoulers, however, they noted that microbial biofilms can modify and/or mask the surface topographies/properties and they went on to state the need to control these complex biofilm communities. In the present review we will focus on biofilm / surface interactions bringing together the recent literature in this field.

In contrast to planktonic bacteria, biofilm bacteria are reported to have enhanced resistance against antibacterial agents (Costerton et al. 1999, Hall -Stoodley et al. 2004). A change in the bacterial phenotype (*i.e.* from planktonic to biofilm and *vice versa*) has been suggested to occur in a cell-density dependent manner, commonly known as quorum sensing

(QS) (*e.g*. Dobretsov et al. 2007). QS regulates a range of different processes, serving as a simple communication network by the secretion, accumulation and recognition of low molar mass compounds, leading to an improved access to nutrients, more rigid colonisation and greater resistance of the community to hostile environments (Reading and Sperandio 2005, Waters and Bassler 2005).

Man-made structures, as well as natural (inanimate or living) surfaces, are all affected by biofilm attachment and growth. Marine substrates including aquaculture nets, oil and gas installations, as well as ship hulls, often demonstrate a great diversity of micro and macrofoulers. In particular, on a ship there is a wide range of materials and structures providing a variety of fouling niches, see **Figure 3.1**. The economic impact of hull biofouling has been examined by Schultz et al. (2011) who showed that the primary associated costs with fouling was due to increased fuel consumption linked to frictional drag (estimated to be $56 million per year for a mid-sized ship). Several papers have described the effect of biofilms on the hydrodynamic performance of ship hull surfaces (reviewed in Howell 2009). For instance, even the formation of a 1 mm thick biofilm on a 23 m fleet tender, resulted in an 80% increase in skin friction coefficient and a 15% loss in ship speed, compared with the clean hull (Lewthwaite et al. 1985). In full-scale power trials for a frigate, Bohlander (1991) found that fouling mainly in the form of biofilms caused an increase of 8–18% in drag, while Schultz and Swain (1999, 2000) observed penalties in local skin friction coefficients of between 33–187 % on flat plates fouled with biofilms. This describes how, despite the fact that macrofouling organisms are primarily responsible for degrading ship hydrodynamic performance, microfouling organisms also play an important role, particularly in the colonisation processes.

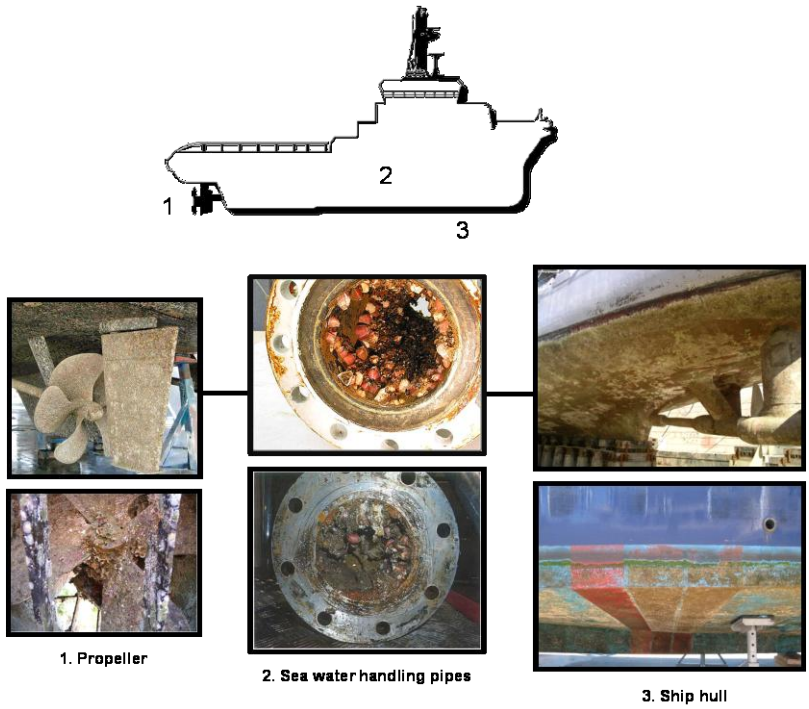

Figure 3.1 Schematic demonstrating the fouling niches typically found on a ship (Courtesy of Andrew Scardino and Chris Norwood, DSTO).

Overall, marine biofilms are now recognised to be a significant issue for a wide range of engineered structures, however, there is very limited published information about marine biofilm composition and how it varies with substrates and AF coatings. Marine biofilms often occur as the initial surface accumulation which culminates with the macrofouling colonisation. Thus, understanding the development of microfouling communities is an important aspect in the selection and management of antifouling coatings for marine operations. This **Section** aims to review marine biofilm composition on man-made materials with an additional focus on the positive or negative effects that biofilms may exert on macrofoulers.

3.2 Biofilm attachment mechanisms

The formation of an organic conditioning film precedes the formation of a biofilm on seawater submerged surfaces since organic molecules are transported faster to the surface (within a few seconds) than bacteria. The conditioning film of adsorbed organic molecules strongly affects surface properties, such as *i)* surface charge, *ii)* wettability and *iii)* surface free energy which has been shown to subsequently affect bacterial colonisation (Baier 1980; Baty et al. 1996; Schneider 1997; Bakker et al. 2003; Salerno et al. 2004).

Bacterial adhesion to a hard substratum is broadly described as a multi-level process that includes cell transport, initial bacterial attachment (irreversible and reversible) followed by adhesion and surface colonisation of cells. A brief description of these steps is reported here.

3.2.1 Transport

Initially, transport of cells to a substrate can be achieved through three different modes, *i.e.* i) through Brownian motion, ii) active movement and iii) convective motion, as shown schematically in **Figure 3.2**:

i) **Brownian motion (diffusion**): in the absence of flow/quiescence conditions, bacterial cells are passively transported by Brownian motion (average displacement, 40 μm h^{-1}; Marshall 1985), which allows their passage through the diffusion layer beyond which no convection can take place. Diffusive transport is several orders of magnitude slower than in convective flow.

ii) **Active motion**: many species of marine fouling bacteria are active swimmers (reviewed by Lauga and Powers 2009), to allow movement on small spatial scale, responding chemotactically towards a gradient of chemical cues in (of minute concentrations, 10^{-6} M) the interfacial region (Berg and Brown 1972).

iii) **Convective motion**: cell transport is achieved due to liquid flow. This may be faster than the Brownian motion by several orders of magnitude however, in some cases the final step prior surface encounter (passage though the diffusion sublayer) is diffusion controlled (van Loosdrecht et al. 1990).

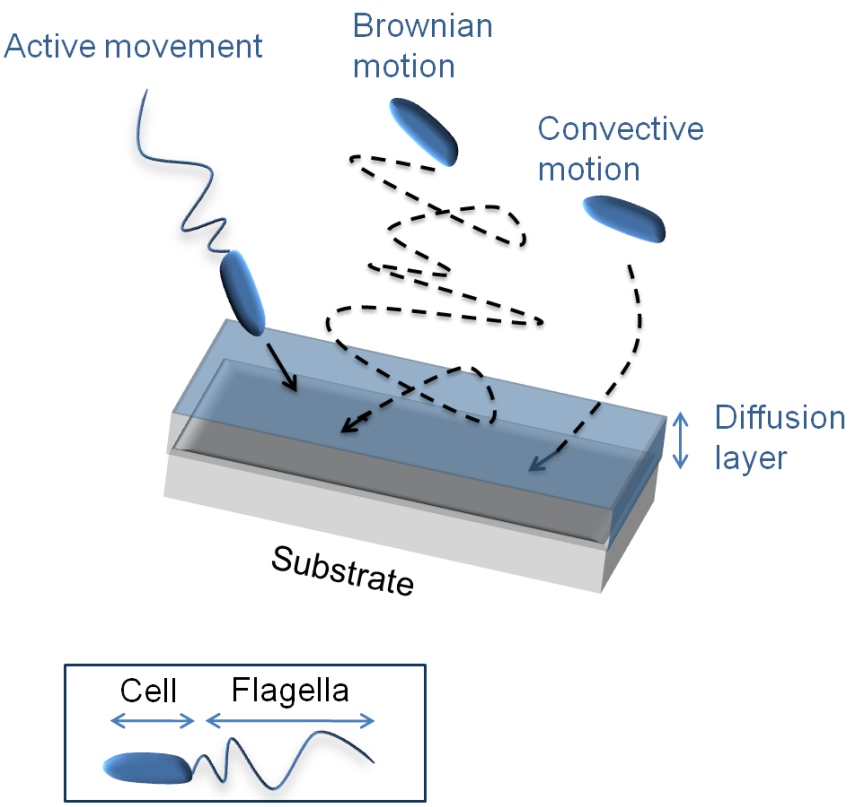

Figure 3.2 Bacterial cell transport mechanism on a substrate (adapted from Van Loosdrecht et al. 1990).

3.2.2 Bacterial initial adhesion/attachment

It is well-established that the main forces determining physical attachment are electrostatic and dispersive (van der Waals force) interactions (Derjaguin 1992). Adhesion on the basis of electrostatic and dispersive forces is described by the Derjagiun, Landau, Verwey and Overbeek (DLVO) theory (van Loosdrecht et al. 1989). The DLVO theory was initially created in order to explain colloid behaviour. DLVO states that the total energy of a system consisting of two closely positioned surfaces is the sum energies of their electrostatic and dispersive interactions. For adhesion/attachment to occur, the bacterium must be positioned at distances corresponding to the secondary (10-15 nm) or primary (0.5-1 nm) energy minimum.

The Gibbs interaction energy between a bacterium cell and a hard surface largely depends on the ionic strength of the surrounding medium. **Figure 3.3** shows the electrostatic (G_E), van der Waals (G_W), and total interaction Gibbs energy (G_{tot}) as a function of separation (H) for a bacterium and a solid surface, with the assumption that both bacterium and substrate

have the same charge. At low ionic strength, the electric double layer is large hence electrostatic repulsion dominates and G_{tot} has a positive maximum acting as a barrier for bacteria to overcome and adhere in the primary minimum (**Figure 3.3a**). At intermediate ionic strength, the electric double layer decreases and the G_{tot} maximum is low enough for some cells that contain sufficient thermal energy to overcome the barrier -slow *irreversible* adhesion/attachment- (**Figure 3.3b**), with the aid of EPS and/or other cellular components such as flagella, fimbrie and pilli (Ward and Berkeley 1980; Marshall 1985). At even higher ionic strength, all cells can reach the primary minimum (**Figure 3.3c**).

At a distance between 10-15 nm, the shallower secondary minimum exists in intermediate ionic strength, and is more profound for systems having a larger van der Waals attraction and larger particles, such as bacteria. The presence of bacteria within the range corresponding to the secondary energy minimum usually does not ensure its adhesion/attachment to the surface, since in this case, van der Waals attraction only slightly exceeds the electrostatic repulsion. The bacterium may be detached owing to external perturbations or its own locomotion. Conversely, in the primary minimum area, when the bacterium approaches the surface, at a distance less than 1 nm, adhesion/attachment is faster. These energy minima correspond to the *reversible* and *irreversible* forms of adhesion (Railkin 2004), see **Figure 3.4**. During reversible adhesion/attachement, where the cells are loosely "hovering" on the surface, EPS and/or other cellular components such as flagella, fimbrie and pilli (Ward and Berkeley 1980, Marshall 1985) may facilitate adhesion/attachment to the underlying substrate.

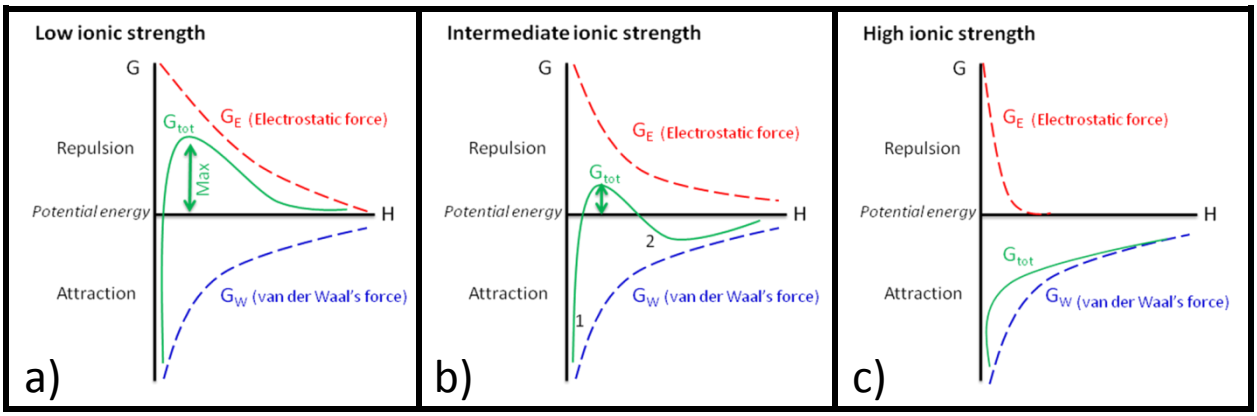

Figure 3.3 Gibbs energy of interaction between a sphere and a flat surface having the same charge sign, according to the DLVO theory. a) low, b) intermediate and c) high ionic strength. In b), 1= primary minimum and 2 = secondary minimum (adapted from Van Loosdrecht et al. 1990).

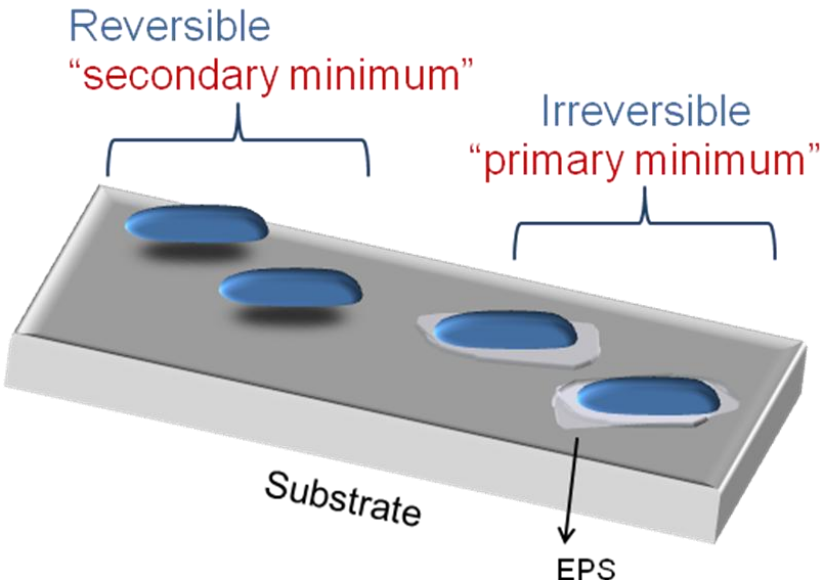

Figure 3.4 Initial bacterial adhesion/attachment on a substrate (adapted from Van Loosdrecht et al. 1990).

3.2.3 Bacterial attachment

Following irreversible adhesion/attachment, cell surface structures such as fimbriae, other proteins, lipo-polysaccharides, EPS and flagella all clearly play an important role in bacterial attachment. Cell surface polymers with nonpolar sites such as fimbriae appear to dominate attachment to hydrophobic substrata, while EPS and LPS are more important in attachment to hydrophilic materials. Fimbriae play a role in attachment, by overcoming the initial electrostatic repulsion barrier that exists between the cell and the substratum. Flagella are also important in attachment, although their role may be to overcome repulsive forces rather than to act as adsorbents or adhesives (Donlan 2002) (**Figure 3.5**).

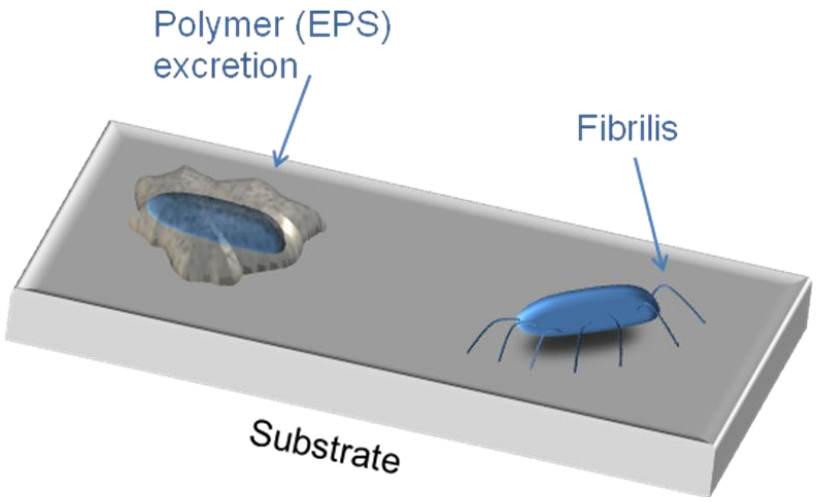

Figure 3.5 Bacterial attachment on surface (adapted from Van Loosdrecht et al. 1990).

3.2.4 Biofilm growth

Depending on the mode of attachment on a surface, bacteria may exhibit several patterns of growth: i) cells are irreversibly attached on the surface (*e.g.* EPS) but not to each other, forming a monolayer of cells on surface and ii) irreversibly attached cells to the surface and to each other, resulting in a three-dimensional biofilm (Van Loosdrecht et al. 1990, **Figure 3.6**).

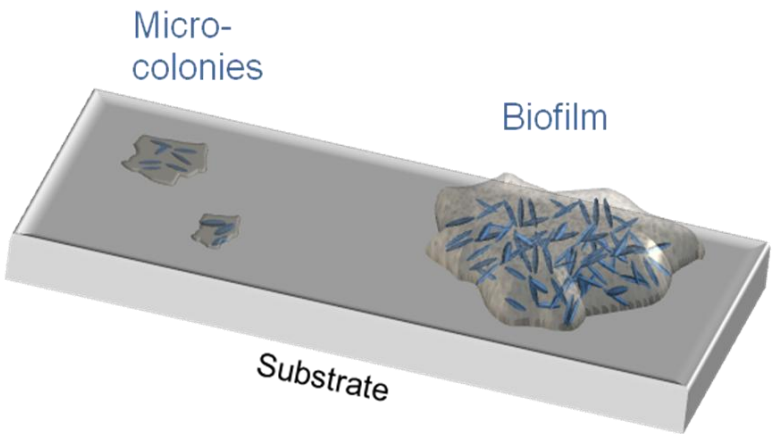

Figure 3.6 Initial stages of bacterial colonisation and biofilm formation (adapted from Van Loosdrecht et al. 1990).

3.2.5 EPS

The adhesion of bacterial biofilms on surfaces results from the excretion of extracellular "sticky" polymers once the cells come into contact with the surface. Bacterial cells are known to be attracted by some sugars and L-amino acids which are simultaneously absorbed by the surface once submerged into the water. The polymers excreted by bacteria are comprised mainly of glucose and fructose-based polysaccharide fibrilis (Abarzua and Jakubowski 1995). The shift in planktonic behaviour to an adapted biofilm metabolic state and the increase in EPS have been observed in marine bacteria (Marshall et al. 2006). It has been suggested that bacterial cells constitute about 2-5% of the biofilm mass, while the rest of the biofilm is composed of the EPS matrix typically containing exopolysaccharides, protein, released nucleic acids, glycoproteins, phospholipids and other surfactants (Kristensen et al. 2008). The main chemical composition components of EPS are illustrated in **Figure 3.7**.

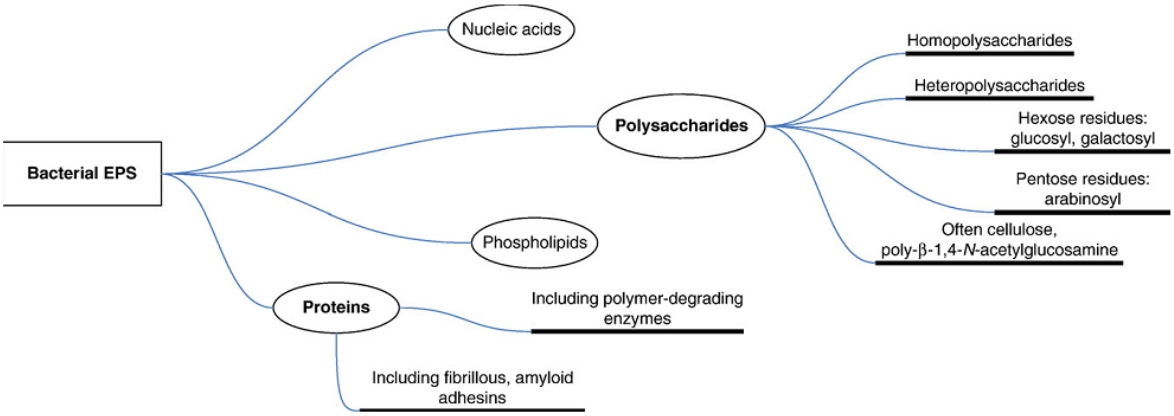

Figure 3.7 Overview of the structural component chemistry of extracellular polymeric substances (EPS) involved in bacterial biofilms (from Kristensen et al. 2008).

3.3 Marine biofilm diversity

Biofilm organisms are mainly represented by sessile bacteria, microalgae including diatoms, microscopic fungi, heterotrophic flagellates and sessile ciliates (heterotrophic protists). The abundance ratio between these organisms varies, however, with bacteria and diatoms often being the dominant taxa. In the White Sea (Russia), for example, microfouling communities that developed on polymer plates illustrated a bacteria / diatoms / heterotrophic flagellates ratio of 640:4:1, respectively (Railkin 2004). The proportion of other unicellular organisms (yeast, autotrophic flagellates and ciliates) was only about 0.15% of the total number of cells. Similar proportions of the main microfouler groups were also reported for the US Pacific Coast communities (Railkin 2004).

3.3.1 Impact of local environment on fouling community

Currently, only a limited number of studies have assessed biofilm composition over a range of man-made surfaces, nevertheless these have provided key insights into the importance of understanding the interactions occurring at the biofilm - substrate interface to the biofouling processes. Biofilms may interfere with the surface properties of the underlying substrate as reported by Hung et al. 2008 and Chung et al. 2010.

Comparative studies on early stage biofilm composition dynamics is challenging, since differences in immersion sites are associated with differences in environmental conditions (such as nutrient status, temperature, hydrodynamics and water chemistry) all of which influence both planktonic and biofilm ecophysiology (*e.g*. Hall-Stoodley et al. 2004). Although few studies have reported the environmental details of the immersion sites, it should be underlined that biofilm community composition is directly driven by its ecosystem, *i.e*. biogeochemical and physical interactions as well as seasonality. Biofilm dynamics should then preferably be evaluated in this context. For instance, temperature (Lau et al. 2005), as well as nutrients (Chiu et al. 2008), have been shown to affect the structure of biofilm microbial communities whereas salinity appeared to be less influential (Lau et al. 2005).

In an attempt to link changes in biofilm community composition with anthropogenic contamination in Antarctica, glass slides were immersed in three contaminated sites (scaling from low to highly impacted) (Webster and Negri 2006). Denaturing gradient gel electrophoresis (DGGE) analysis revealed that the bacterial sequences retrieved from the glass surfaces were affiliated to *γ-Proteobacteria,* Cytophaga / Flavobacteria of Bacteroidetes (CFB),

Verrucomicrobia and Planctomycetales. Biofilm community composition was found to be greater between different sites in Antarctica than within them, with *α-Proteobacteria*, *γ-Proteobacteria* and CFB dominating the least impacted site, while interestingly, sulphate reducing bacteria exhibited higher proportions at the more contaminated Antarctic sites.

3.3.1.1 Biofilms under motion / hydrodynamics

All marine structures are subject to hydrodynamic forces including drag, lift and acceleration. Effectively, being a part of the surface, biofilms will also be affected by these forces (Dusenbery 2009). For example, all ship births on the river Tyne are tidally influenced, and tidal streams in the river vary, reaching a maximum of 3 knots (Port of Tyne 2007). One of the largest docks in Europe, in Southampton Water, is tidally dominated, with a maximum tidal flow of 1.2 knots (Shi 2000).

In fluid mechanics, the Reynolds number (Re) is a measure of the ratio of inertial forces to viscous forces and quantifies the relative importance of these forces for given flow conditions. The world of microorganisms is the world of low Reynolds numbers ($\sim 10^{-5}$), a world where inertia plays little role and viscous damping is paramount.

Motile marine microorganisms are not large in comparison with the smallest hydrodynamic scales at which viscosity dissipates kinetic energy allowing them to utilise flagellar motion. However, these viscous hydrodynamic processes significantly influence the settlement processes allowing the bacteria and diatoms to identify an appropriate substratum surface. This contrasts with engineered marine structures where Reynolds numbers are usually between 10^3 to 10^9. When the bacterial cells enter the boundary layer near the wall, the velocity will be considerably less than the average bulk velocity due to the no-slip boundary condition. The flow velocity of the fluid, which is a key component of the Reynolds number, has been demonstrated to affect the attachment density (Magin et al. 2010).

The skin friction on some ship hull types can account for as much as 90% of the total drag even when the hull is free of fouling (Schultz 2007). Weinell et al. (2003) suggested that an increase of 5 μm in micro-roughness results in a ~4 % increase in drag resistance. For mid-sized merchant and naval vessels, such as frigates and destroyers which are typically 150 m in length, at cruising speed (7.7 m s^{-1} or 15 knots) or near maximum (15.4 m s^{-1} or 30 knots), an 8-29 % penalty in propulsive power has been attributed to a mature slime (bacteria and diatom film) (Holm et al. 2004; Schultz 2007). The effect of biofouling on drag is well-documented (e.g. Callow et al. 2002; Holm et al. 2004) specifically, Stoodley et al. (1998) found

a double increase in the friction factor in a smooth pipe due to thin biofilms (tens of microns). However, little information is available on biofilm adaptation to hydrodynamic conditions. Indeed, it has been observed that biofilms grown under hydrodynamic conditions can streamline their form to achieve lower drag, which indicates an adaptive response (Stoodley et al. 1998; Taherzadeh et al. 2009). Interestingly, Stoodley et al. (2002) have found that biofilms grown under high flow conditions have higher storage (elastic) and loss (viscous) moduli, necessitating greater shear stress to achieve biofilm detachment from a substrate when compared to biofilms grown under low flows. Overall, it can be concluded that biofilms grown under high hydrodynamic conditions illustrate a more tenacious attachment than biofilms grown at low flows.

Biofilms grown at low velocities (0.15 knots) exhibit low density and high effective diffusivity, whereas biofilms grown at high flow velocities (0.54 knots) have high density and low effective diffusion (Horn et al. 2003). External shear force will not only change the shape of biofilm, but it can also influence biofilm detachment (Horn et al. 2003), which in turn influences biofilm formation and the microbial ecology within it. Tsai (2005) investigated the impact of flow velocity on the dynamic behaviour of biofilm bacteria. It was found that the maximum biofilm biomass did not change when flow velocity was increased from 0.38 to 0.77 knots, but was significantly affected when flow velocity was further increased to 1.16 knots. The concentration of bacteria within the biofilm was substantially reduced by the higher shear stress.

Observations by van Loosdrecht (1995, 1997), suggest that at high shear forces the biofilm gets more compact with less growth taking place in the outer filamentous biofilm and more in the base of the colony therefore leading to less detachment (biofilm grown in a more compact form); while, detachment is dominant for protruding and filamentous structures since they are removed before growing out. Van Loosdrecht et al. (2002) reported that the faster a biofilm grows the better the balance between the detachment and the more heterogeneous and the thicker it becomes. However, a fast growing biofilm rapidly consumes the nutrients leading to stronger medium gradients, resulting in relatively faster growth at the protrusion tips than at the base of the biofilm, thus enhancing the formation of heterogeneous and porous biofilms. This can be counteracted by high shear stresses limiting the rapid outgrowth biofilm protrusions by detaching them, therefore resulting in a higher portion of the nutrients being converted by the base biofilm. The biofilm can in this context be seen as an adaptive system responding to the environmental factors (van Loosdrecht et al. 2002)(see **Figure 3.8**).

Diffusion gradients can occur when the potential nutrient consumption rate exceeds the maximum mass transport rates by diffusion or convection. Thus, the slower the diffusion processes relative to the growth processes the stronger the nutrient gradient will be. Picioreanu et al. (1998) through 2D modelling, demonstrated that when transport rates of the substrate are relatively slow, strongly porous or even filamentous biofilms can be formed.

Solute transport that is carried by the bulk flow of a fluid (convection) is generally much faster than the transport resulting from random molecular motion (diffusion) (Stewart 2003). Since there is no net convective flow of fluid into or out of the microbial cell, diffusion may become critical for moving the solute toward or away from the cell surface. The reason that diffusion does not limit this step is that the distances are small and diffusion is rapid. Diffusion limitation is commonly observed in biofilm systems due to fluid flow reduction and the increase in the diffusion distance. The biofilm and the surface to which it is attached will impede flow in the vicinity of the biofilm, restricting the convective transport. Locally high cell densities within cell clusters, as well as the presence of EPS hinder the flow of water, thus diffusion is the predominant transport process within cell aggregates (Stoodley et al. 1994, de Beer et al. 1997). This can easily represent an increase in the diffusion distance, compared to a single cell, of two orders of magnitude.

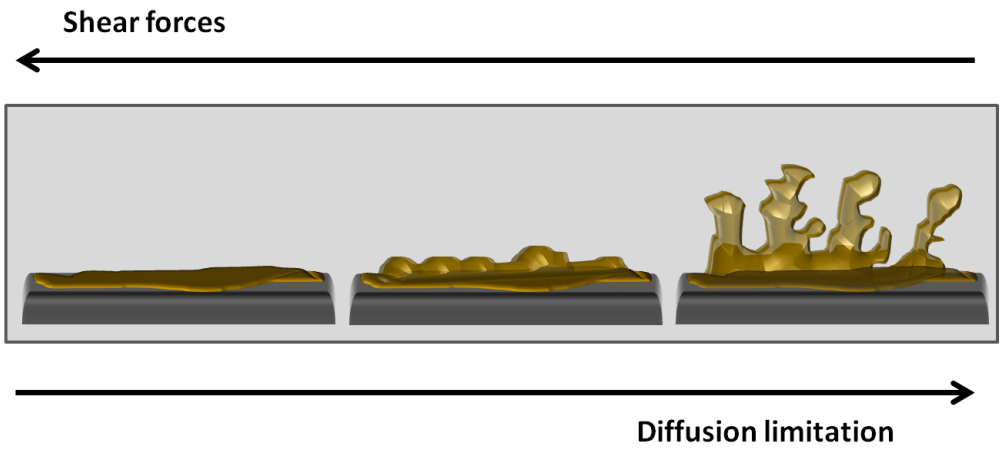

Figure 3.8. Schematic representation of the interaction between growth and detachment on the biofilm structure (adapted from Van Loosdrecht et al. 2002).

Evidence is emerging that multispecies communities that develop under high shear stress are less diverse than those that have developed at lower shear stress (reviewed by Howell 2009). Rochex et al. (2008) assessed the effect of shear stress (0.055 to 0.27 Pa) on biofilm diversity using the PCR- single strand conformation polymorphism fingerprinting

method and concluded that shear stress effected biofilm composition. They showed that biofilm species composition decreased with increasing shear stresses suggesting reduction of biofilm maturation and maintenance of young biofilms. Thus, increasingly demanding in the AF technologies is the incorporation of the hydrodynamic factor when assessing AF coating performance against biofilms.

3.3.2 Studies on artificial surfaces (without AF properties)

It has been reported that bacterial communities on dissimilar surfaces, stainless steel and polycarbonate (immersed in Delaware Bay, US), would evolve to a similar pattern over time (Jones et al. 2007). Likewise, biofilm community composition, as determined by a combined approach of DGGE and fluorescence *in situ* hybridization (FISH), was reported as similar across all surfaces, regardless of initial substrate wettability (ten chemical treatments of glass slides, immersed at Hawaii, US), and all these surfaces had distinct temporal shifts in community structure over a ten day period (Huggett et al. 2009). These results have been also confirmed using polystyrene and glass (Hung et al. 2008) or granite rocks (Chung et al. 2010) both immersed at the same site in Hong Kong waters (China).

3.3.2.1 Bacteria

The early stage biofilms were dominated by the same major classes of bacteria that were most abundant in planktonic communities with the latter demonstrating a higher diversity when compared to that of biofilm bacteria (Jones et al. 2007, Lee et al. 2008). Bacteria in the *Alteromonas* (γ-*Proteobacteria*) and *Roseobacter* (α-*Proteobacteria*) groups were identified as the main primary colonizers (9-72 h). Acidobacteria, Actinobacteria, Bacteroidetes, Chloroflexi, Cyanobacteria, Firmicutes, Planctomycetes, β-,δ- and ε-*Proteobacteria* and Verrucomicrobia were also identified as minor groups belonging to these biofilms dependent on the surfaces (glass, polycarbonate, polystyrene and steel) and immersion sites (Great Barrier Reef, Australia, Delaware bay, South Carolina and Hawaii, US, Sacheon harbour, Korea and Hong Kong, China) (Dang and Lovell 2000, 2002, Webster et al. 2004, Jones et al. 2007, Lee et al. 2007, Hugett et al. 2009, Chung et al. 2010). During the early stage development, between 24 h to 6 days, Archaea have not been detected on glass and polystyrene surfaces (Dang and Lowell 2002, Chung et al. 2010) or only at low densities on glass (Webster et al. 2004, Hugett et al. 2009). Pooled replicates from six day and twelve day

old biofilms developed on polystyrene Petri dishes were analysed using PhyloChip (DNA Microarray for Rapid Profiling of Microbial Populations) (Chung et al. 2010). This analysis showed a much higher species richness than previously described: 100 / 123 taxa in the 6 and 12-days old biofilm affiliated to 10 / 9 known phyla, respectively (see **Figure 3.9**). The global predominance of Proteobacteria (especially *α-Proteobacteria*) was confirmed but the structure of biofilm communities display dissimilarities depending on the study. In addition, when looking at the genus or species level within the same phylum, the dominance would be expected to change with time.

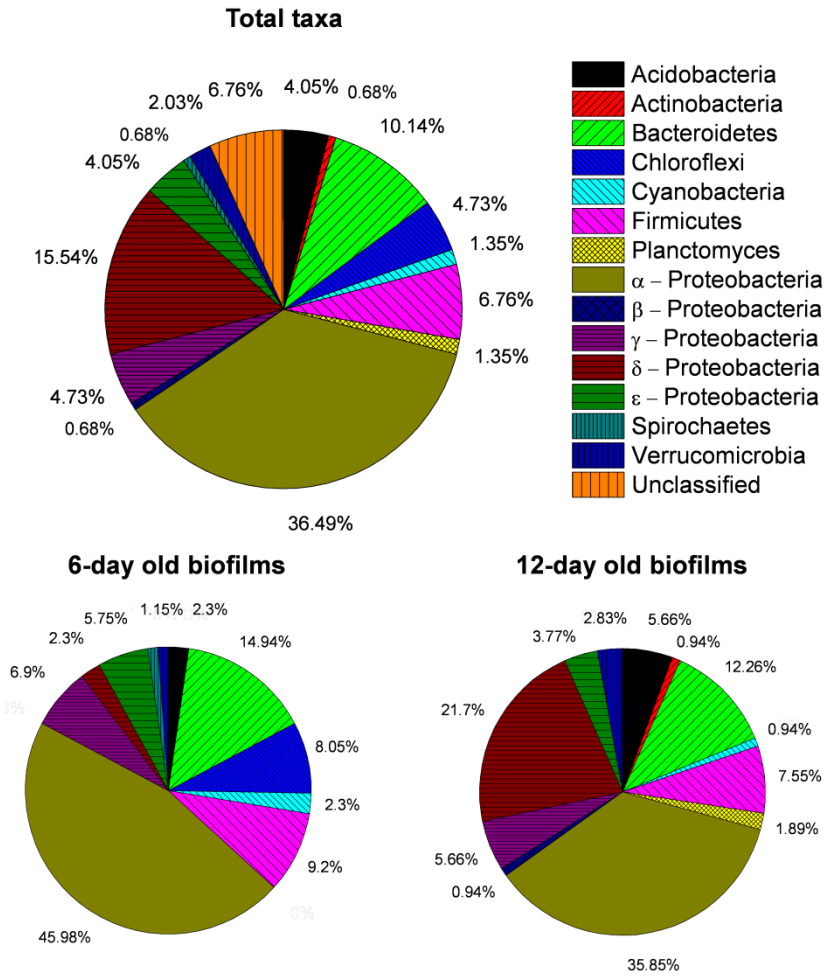

Figure 3.9 Diversity of taxa in biofilms on polystyrene in Hong Kong coastal waters (November 2007) using PhyloChip analysis (after Chung *et al*. 2010).

3.3.2.2 Diatoms

Diatoms (Bacillariophyceae, Ochrophyta) are a diverse group of eukaryotic algae, usually dominating the phytoplankton of nutrient-rich marine waters. Diatoms are major primary producers and occupy an important role in marine biogeochemical cycles. In addition to their

planktonic form, diatoms may occupy a wide variety of habitats such as sands in coastal beaches, the interstices on the bottom side of ice, living surfaces and can live heterotrophically in deep-sea sediments. The attachment of diatoms on surfaces has made them important fouling organisms that adhere on man-made substrates and along with bacteria, constitute a major problem to artificial structures immersed in the marine environment. A typical example of marine biofilm formed in a temperate estuary (Southampton, UK) over 3 weeks during the summer period is shown in **Figure 3.10**. This is the first time a three-dimensional, true colour (**Figure 3.10a**), marine biofilm is shown *in situ* using an optical 3D micro coordinate system providing more refined microscopic imaging of a fully hydrated biofilmed surface. Important information can be acquired on the biofilm surface topography, roughness and structure (**Figure 3.10b**) as well as biofilm thickness (**Figure 3.10c**). We believe that this rapid and non-invasive (no fixation or staining required) optical imaging technique, is ideal for the assessment of marine biofilms on artificial surfaces where samples can be processed within minutes after retrieval. It has been shown that, as with bacterial biofilms, the planktonic diatom community structure differs from the biofilm community, with pennate diatoms dominating the biofilms and centric diatoms the water column (Patil and Anil 2005 and included citations). Frequently identified fouling diatoms include the pennate genera *Navicula*, *Nitzschia*, *Cocconeis*, *Licmophora*, *Synedra*, *Amphora*, *Achnanthes*, *Bacillaria*, *Biddulphia* and the centric genera *Melosira*, *Fragilaria*, *Grammatophora*, *Rhabdonema*, *Berkeleya* (Railkin 2004). Settlement of marine periphytic algae on glass substrata in a tropical estuary in Singapore showed that the periphytic algal community comprised 30 microalgal species, dominated by diatoms (78 %), followed by Cyanobacteria (19 %), green flagellates (1 %), dinoflagellates (1 %) and other forms accounting for the remaining 1 % of the total cell counts. Diatoms such as *Skeletonema costatum* and *Thalassiosira rotula* dominated the assemblages, together with the marine Cyanobacteria *Synechococcus* sp. (Nayar et al. 2005). Measurements for silicate concentrations in the water column, water temperature, photosynthetically available radiation, pH and dissolved oxygen all have an important influence on the periphytic algal community, which can be negative or positive (Nayar et al. 2005). Similarly, among the biofilm diatoms on fibreglass and glass coupons in a monsoon-influenced tropical estuary, pennate diatom species belonging to the genera *Navicula*, *Amphora*, *Nitzschia*, *Pleurosigma* and *Thalassionema* were dominant (Patil and Anil 2005). The biofilms formed on these two substrata revealed significant differences in density and diversity, however, the species composition was almost constant. Additionally, diatom community structure in the biofilms

illustrated significant differences between seasons which were attributed to physicochemical and biological changes in the water column. An aquaculture study in Malaysia (Khatoon et al. 2007), showed that diatoms consisting of *Amphora, Navicula* and *Cymbella* were found to be most abundant on all the test substrates (bamboo pipe, plastic sheet, polyvinylchloride pipe, fibrous scrubber and ceramic tile) despite differences in the overall settlement densities. In addition, blue–green algae *Oscillatoria* were the next most important group while green algae were the least abundant. *Nitzschia*, *Cylindrotheca*, *Navicula* and *Amphora* sp. have also been identified in ten-day old biofilms developed on polystyrene Petri dishes immersed at the low intertidal zone in Port Shelter, Hong Kong, China (Chiu et al. 2008).

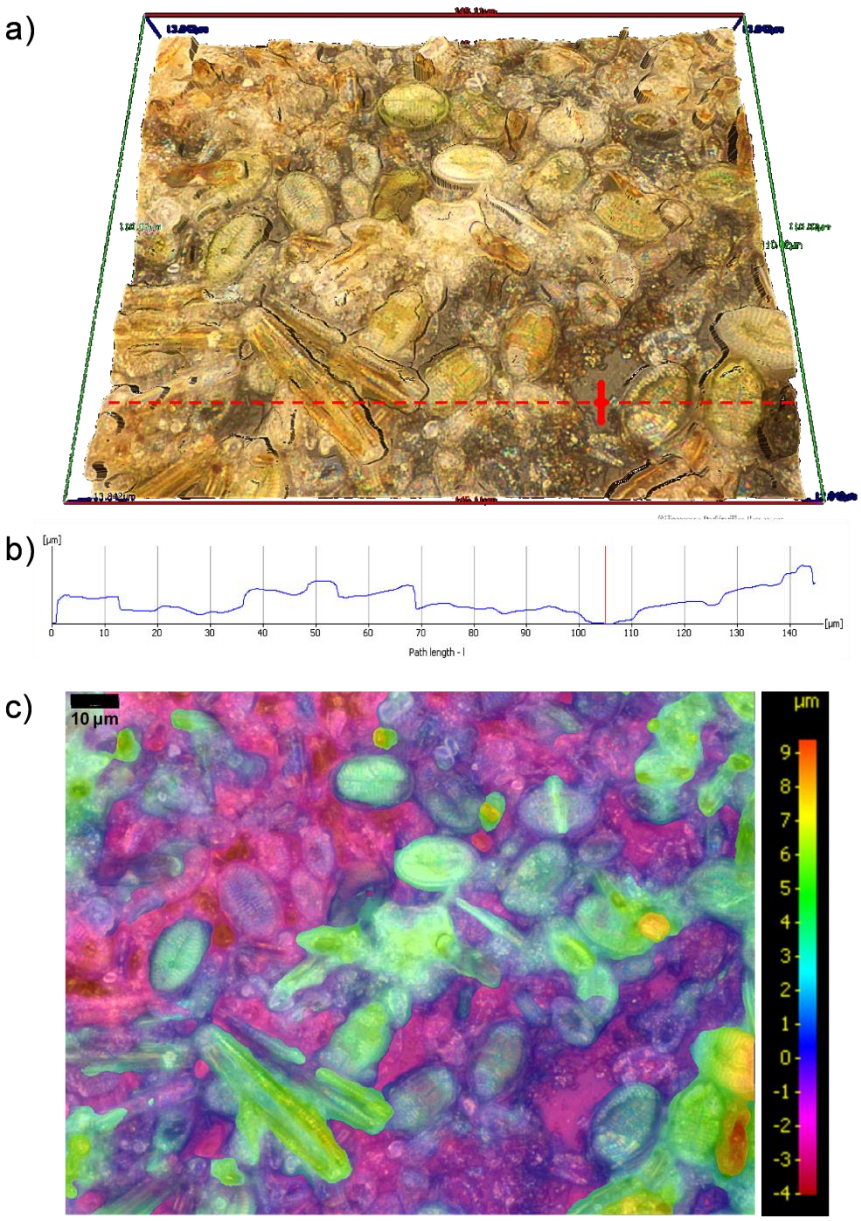

Figure 3.10 Alicona InfiniteFocus microscope images: a) a real colour 3D topography of a natural biofilm mainly composed of diatoms (*Amphora* sp. and *Navicula* sp.) on a panel immersed for three weeks (21st June – 11th July 2010) in Southampton Water, UK (1.0 mm × 1.5 mm, length by width), the red dashed line indicates the cross-section shown in b), b) cross-section showing the surface topography and c) biofilm thickness (µm).

3.3.3 Substrates with antifouling coatings

It is now reasonably well-established that different antifouling (AF) surfaces behave in contrasting ways with regard to the attachment and growth of marine fouling. The main focus of current research into AF surfaces or coatings that hinder fouling is associated with either

self-polishing coatings (SPC) with booster biocides or silicone fouling-release coatings (FRC) with hydrophobic properties based on physicochemical and mechanical effects.

Although FRCs inhibit most macrofouling, they fail to prevent colonisation of "slime" layers (biofilm) that are largely composed of diatoms and bacteria (Casse and Swain 2006, Molino and Wetherbee 2008). Diatoms especially have been found to persistently adhere to, and colonise, even the most fouling resistant of artificial surfaces (Anderson et al. 2003). There are a number of reports in the public literature showing that diatoms dominated biofilms adhere tenaciously to hydrophobic surfaces and do not release from FRCs even on vessels operating at high speed (>30 knots) (Anderson et al. 2003) and have been shown to significantly impact the performance of FRCs (Molino et al. 2009a,b).

Static and hydrodynamic seawater immersion testing of four commercial AF coatings, of which three were biocide based (tributyltin (TBT) self-polishing, copper self-polishing, and copper ablative) and one was a biocide free FRC, were performed in Florida (Casse and Swain 2006). After static immersions for sixty days, both Gram-positive (Actinobacteria and Firmicutes) and Gram-negative *(*α- and γ-*Proteobacteria*) bacteria were found on all coated surfaces using a culture dependant technique. The main two genera present during the static trials were *Micrococcus* and *Pseudomonas,* while bacterial total cell counts were found to be similar on all test surfaces (**Table 3.1 A**). Regarding diatom diversity, it was greatest on the copper ablative and lowest on the copper self-polishing surfaces. The dominant diatom populations found on all AF coatings during static trials were *Amphora*, *Synedra* and *Navicula* (**Table 3.1 A**). Following hydrodynamic immersion testing of the coatings, the biofilm diversity decreased and the dominant cultivable bacterium was *Micrococcus* (Cassé and Swain 2006, **Table 3.1 A**). Bacterial counts on all surfaces showed a substantial decrease after the dynamic testing and although the greatest cell count decrease was observed for the FRC, bacterial diversity was highest on that coating. For diatoms, *Amphora* was the dominant genus that remained attached to most surfaces with the exception of the copper ablative coating (Cassé and Swain 2006, **Table 3.1 A)**. *Achnanthes* was present on both the TBT self-polishing and copper ablative surfaces after static immersion but remained only on TBT self-polishing after hydrodynamic immersion. This probably reflects the resistance of *Achnanthes* to TBT but not to copper (Callow 1986).

Another study was conducted over three seasons in both temperate and tropical marine environments in Australia where three commercial coatings were tested: *i)* an FRC (Intersleek 700®), *ii)* a copper (I) oxide and zinc pyrithione SPC (Intersmooth®, BEA 360) and *iii)* a TBT

containing SPC (Super Yacht®, YBA 800). Overall, diatom biofilms colonised the FRC more rapidly when compared to biocidal SPC paints (sixteen day study in each season) (Molino et al. 2009a, **Table 3.1 B**). The extent of diatom fouling was greatest at the temperate site (high water temperature and reduced salinity due to an extensive influx of freshwater into the coastal region during the wet season). *Nitzschia* was the dominant genus, however, *Cylindrotheca*, *Licmophora*, *Amphora*, *Cocconeis* and *Toxarium* were also identified with no clear exposure site effect (Molino et al. 2009a, **Table 3.1 B**). When the pioneering colonisation of bacterial biofilms on the FRC was investigated, the coating displayed the quickest colonisation by bacteria, resulting in major modification of these coated surfaces within 2–4 days following immersion in the ocean (Molino et al. 2009b). It should be noted that Molino *et al*., identified their sampling technique (*i.e*. scraping the biofilm off the coated surface) to be limiting for taxonomic analysis, especially for surfaces with low diatom colonisation.

Table 3.1. Biofilm formation on AF coatings constructed using data from A) Casse and Swain 2006 and B) Molino et al. 2009 (it should be noted that where no diatoms were observed this may be as a consequence of the sampling technique)

A

Coatings	Bacteria – Static	Bacteria – Dynamic	Diatoms – Static	Diatoms – Dynamic
FR Biox L	M A Ps V	M Sta Str Ps	Am S F Na	Am
Sn-SPC Hempels 79051	M A Prs Ps	M	Am S Na Ac	Am S Ac
Cu-SPC Sea Quantum Classic	M Sta Str A Ps	M Str	Am S Na	Am S Na
Cu-Abl Interspeed 642	M Ps	M	Am S F Ac Na Ni	

Bacteria		Diatoms	
Gram-positive		*Achnanthes*	Ac
Micrococcus	M	*Licmophora*	L
Staphylococcus	Sta	*Nitzschia*	Ni
Streptococcus	Str	*Cylindrotheca*	C
Gram-negative		*Bacillaria*	Ba
Alcaligenes	A	*Amphora*	Am
Pseudomonas	Ps	*Cocconeis*	Co
Proteus	Pr	*Toxarium*	T
Vibrio	V	*Navicula*	Na
		Fragilaria	F
		Synedra	S

B

Coatings	SEASON: July/August – SITE: Tropical	July/August – Temperate	November/December – Tropical	November/December – Temperate	February/March – Tropical	February/March – Temperate
FR Intersleek 700	Ba Am	Ac L Ni Cy	Ni Am T Co	Ni Am T Co L Cy	L Ni T	L Ni Am Ac Na
SPC Intersmooth 360				Ni Cy		
SPC Super Yacht				Ni		

Field tests conducted in the cold seawater of the St. Lawrence Estuary (Canada) over two months were also designed to evaluate the efficiency of marine paints (Pelletier et al. 2009). Diatoms from the genus *Amphora* were dominant on cuprous oxide paints whereas the other commercial and natural product biocide containing paints displayed a high diversity of diatoms such as *Cocconeis* sp., *Fragilaria* sp., *Licmophora* sp., *Melosira* sp., *Navicula* sp., *Nitzschia* sp. in addition to *Amphora* sp. These observations confirm the resistance of this latter genus to copper toxicity. Interestingly, *Amphora* also appears to be resistant to the organic biocides Copper Omadine™ and Sea Nine®211.

A study has been performed on the bacterial composition of concretions on the USS Arizona, a national naval memorial located in Pearl Harbor (Hawaii), where the microbial community may be at a stable late stage. 16S rDNA clones indicated that the biofilms consisted of bacteria related to only three phyla: Firmicutes, Bacteroidetes, and Proteobacteria (α and γ). Among the *α-Proteobacteria*, two of the three clones clustered with sequences from the genus *Roseobacter*. These data could be coherent with dominance on non AF

surfaces but with a lower diversity that may result from residual AF paint on the hull (either copper or mercuric oxide based paints) (McNamara et al. 2009).

Published studies directly investigating the biofilm community on vessel hulls are very scarce. In a study conducted by Inbakandan et al. (2010), biofilms were collected from the bottom of a fishing vessel's hull docked at an Indian harbour. Among the 16 strains of culturable marine biofilm forming bacteria, representatives of the Firmicutes were dominant (56 %) compared to the high GC Gram-positive bacteria (19 %), *γ-Proteobacteria* (12 %), CFB group (6 %), and Enterobacteria (6 %). Interestingly, bacteria of the human body and the opportunistic pathogen *Proteus mirabilis* were also identified (Inbakandan et al. 2010). Considering in-service diatom communities, a study on 20 ships coated with SPC paints containing TBT and copper showed that *Amphora* sp. were the dominant species on all ocean-going vessels, whereas *Achnanthes*, *Amphiprora*, *Navicula* and *Stauroneis* were also observed in some cases. *Achnanthes* was not reported to be copper resistant (Callow 1986). Overall, there are relatively few published studies of marine biofilm communities and this limits the ability to directly evaluate the data due to the disparate sites, environmental conditions and substrates. In addition, diversity studies have mainly been based on culture-dependent techniques which can cause bias in community structure analysis. Increasingly studies are using molecular fingerprinting approaches (e.g. DGGE and terminal-restriction fragment length polymorphism T-RFLP) or FISH and consequently comparison between the structures of biofilm communities is possible, however, species level of identification is scarcely performed. Molecular techniques are used to a lesser extent to study eukaryotic microorganisms from biofilms, especially the autotrophic communities of diatoms (Webster et al. 2006) which were mainly identified to the genus level using optical microscopy. These identification limitations also prevent conclusive comparisons between the published studies. Thus, metagenomic approaches should be developed in order to better describe and understand the processes during biofilm development in the marine environment.

3.4 Biofilms and macro-fouling: a love / hate affair

Surface colonisation by marine organisms often signifies the most important step in the life history of a species as a shift from the planktonic to the benthic life style is crucial for survival. Marine organisms themselves suffer pressures from the settlement of foulers – a phenomenon often referred to as *epibiosis* (from the Greek *επί* = epi = on top and *βίος* = bio = life), see **Figure 3.11**. In highly productive areas of the ocean, such as reefs, coverage of the primary substrate – the sea bed – may be close to 100%. Fouling by secondary organisms can be detrimental to the settled organism, restricting access to light and nutrition, and increasing the probability of tissue damage and disease (Bryan et al. 1996). Widespread evidence suggests that chemical cues from marine organisms affect colonisation processes of secondary colonisers (reviewed by Harder and Yee 2009). Marine colonisation processes are broadly described as sequential steps with microbial biofilms preceding initial attachment. Biofilms are therefore, considered to be key mediators for the subsequent colonisation of macro-organisms. However, detailed information for any one system on the nature of such cues, their distribution *in situ*, and their effects on the demography of colonizers is rare (Steinberg and De Nys 2002). Understanding the role of microbial biofilms in chemical ecology would be substantially enhanced with greater knowledge of the bacterial species composition in the environment and their abundance (Steinberg et al. 2002). The laboratory and field methodologies used to assess the effect of biofilms on macrofoulers can be found in an extensive review by Wieczorek and Todd (1998). **Table 3.2** summarises the recently published literature on the effect of biofilm on macrofouler's settlement and/or larva metamorphosis with emphasis on the substrate used.

Figure 3.11 Wooden surface submersed in Southampton water, (UK) for 20 months with a complex biofouling community developed including coralline algae, tube worms, sponges, sea mats and sea weeds.

Table.3.2. Review of selected papers on the effect of marine biofilms on macrofouler's settlement and metamorphosis, +/- signifies the negative or positive effect of the biofilm on macrofouler's settlement and metamorphosis.

Substrate	Biofilms species	Macrofouler Phylum	Macrofouler species	Effect	+/-	Reference
Glass slide and polystyrene Petri dishes	*Deleya marina* (*Cobetia marina*, syn) *Alteromonas macleodii* *Pseudomonas fluorescens*	**Crustacea**	*Balanus improvises*	Settlement & metamorphosis	+/-	O'Connor and Richardson 1996
Glass Marble quartz cembonit	Natural biofilm: bacteria, diatoms, fungi, and protozoa		*Balanus amphitrite*	Settlement	-	Faimali et al. 2004
Polystyrene Petri dishes	Natural biofilms		*B. amphitrite*	Settlement	+	Qian et al. 2003
Polystyrene Petri dishes	*Micrococcus* sp., *Rhodovulum* sp., *Vibrio* and natural biofilm		*B. amphitrite*	Settlement	+/-	Lau et al. 2003
Polystyrene (low wettability) & glass (high wettability)	Natural biofilm		*B. amphitrite*	Settlement	+	Hung et al. 2008
Polystyrene Petri dishes	Natural biofilm		*B. amphitrite*	metamorphosis	+	Chiu et al., 2008
Polystyrene Petri dishes	Natural biofilm		*B. amphitrite*	Settlement	+/-	Wieczorek et al. 1995
Methacrylate (Plexiglass) disks	Natural biofilm		*B. amphitrite*	Settlement	-	Olivier et al. 2000
Polystyrene Petri dishes	Natural biofilm		*B. amphitrite*	Settlement	+/-	Wieczorek et al. 1995
Glass slides (under flow)	Natural biofilm		*B. amphitrite*	Settlement	+	Zardus et al. 2008
Polystyrene Petri dishes	Natural biofilm		*B. amphitrite* *Balanus trigonus*	Settlement	+	Lau et al. 2005
Rock chips	Natural biofilm		*Semibalanus balanoides*	Settlement & metamorphosis	+	Thompson et al. 1998
Polystyrene dishes	Natural biofilm		*B. trigonus*	No effect	N	Thiyagarajan et al. 2006
Polystyrene Petri dishes	*Pseudoalteromonas luteoviolacea,* *Cytophaga lytica* isolates and natural	**Annelida**	*Hydroides elegans*	Settlement & metamorphosis	+	Huang and Hadfield 2003

	biofilms					
Polystyrene Petri dishes	(UV-irradiated) Natural multi- and single-species biofilms		*H. elegans*	Settlement	+	Hung et al. 2005
Polystyrene Petri dishes	**Bacteria:** *Roseobacter sp., α*-subclass *Proteobacteria* isolates		*H. elegans*	Settlement		Lau and Qian 2001
Polystyrene Petri dishes	Natural biofilm		*H. elegans*	Settlement & metamorphosis	+/-	Unabia and Hadfield 1999
Glass slides	Natural diatom biofilm		*H. elegans*	Settlement	+/-	Harder et al. 2002
Polystyrene Petri dishes	Natural and controlled biofilms		*H. elegans*	Settlement	-	Huang et al. 2007
Polystyrene Petri dishes & borosilicate glass	Natural diatom biofilm		*H. elegans*	Settlement	+	Lam et al. 2003
Polystyrene Petri dishes	Natural biofilms		*H. elegans*	Settlement	+	Shikuma and Hadfield 2006
Glass slides with low, medium and high wettabilities	Natural biofilm		*H. elegans*	Settlement & metamorphosis	+	Huggett et al. 2009
Polystyrene Petri dishes	Natural biofilm extracts		*H. elegans*	Settlement & metamorphosis	+	Hung et al. 2009
Polystyrene Petri dishes	*Pseudoalteromonas* sp. Sf57 isolate (plus 9 differently pigmented mutants derived from the isolate)		*H. elegans*	Settlement	+/-	Huang et al. 2011
Polystyrene Petri dishes & granite rock	Natural biofilm		*H. elegans*	Settlement		Chung *et* al. 2010
Polystyrene Petri dishes	Natural biofilm		*H. elegans*	Settlement	+	Lau et al. 2005
Glass slides (under flow)	Natural biofilm		*H. elegans*	Settlement	+	Zardus et al. 2008
Slates- polished with 600 grade wet and dry emery paper	Natural biofilm		*Pomatoceros lamarkii*	Settlement	+	Hamer et al. 2001
Polystyrene Petri dishes	**Diatoms:** *Acnanthes sp., Amphora coffeaeformis, A. Tenerrima, Nitzschia constrica*	**Bryozoa**	*Bugula neritina*	Settlement	+	Dahms et al. 2004
Polystyrene Petri dishes	**Bacteria:** *Pseudoalteromonas sp.* PB-2 *Nitzschia frustulum*		*B. neritina*	Settlement	-	Dahms et al. 2004
Glass slides (under flow)	Natural biofilm		*B. neritina*	Settlement	0	Zardus et al. 2008

Polystyrene Petri dishes	*Deleya marina (Cobetia marina,* syn)		Natural bryozoan larvae	Settlement	-	O'Connor and Richardson 1996
Glass slides	γ-Proteobacteria isolates (*Pseudoalteromonas, Vibrio, Shewanella, Halomonas, Pseudomonas*)	**Chlorophyta**	*Enteromorpha* sp.	Settlement	+	Patel et al. 2003
Glass slides	Natural biofilm: diatoms and bacteria	**Mollusca**	*Mytilus galloprovincialis*	Settlement & metamorphosis	+	Bao et al. 2007
Supernatant (not substrate)	**Bacteria:** *Alteromonas colwelliana* *Vibrio cholerae (*596-B) *V. cholerae* (HTX)		*Crassostrea gigas*	Settlement & metamorphosis	+	Fitt et al. 1990
Ceramic tiles	Natural biofilm		*Crassostrea virginica*	Settlement	+	Campbell et al. 2011
Glass slides (under flow)	Natural biofilm	**Chordata**	*Phallusia nigra*	Settlement	+	Zardus et al. 2008

Biofilm composition and larval settlement are known to be affected by the physical properties of a substrate, such as colour (Satheesh and Wesley 2010), surface roughness (Kerr and Cowling 2003), wettability (Maki et al. 1992) as well as topography (Magin et al. 2010). However, only limited information is currently available on the interactions between the physical properties of a substrate, biofilm formation and subsequent larval settlement. It should be noted that the relationships between biofilms and macrofoulers have usually been studied by performing bioassays with a limited selection of algal or invertebrate species that are commonly cultured in laboratory and are of commercial interest.

Natural biofilms significantly increased adhesion strength of macrofoulers in most of the studies: for the ascidian *Phallusia nigra* (reported from the Mediterranean to Micronesia) (Zardus et al. 2008), the polychaete tubeworm *Hydroides elegans* (*e.g.* Huang and Hadfield 2003, Hung et al. 2005, Shikuma and Hadfield 2006, Zardus et al. 2008, Huggett et al. 2009), the serpulid *Pomatoceros lamarkii* (Hamer et al. 2001), several mussels (Bao et al. 2007, Campbell et al. 2011) and the barnacle *Balanus amphitrite* at one or more developmental stages (*e.g*. Qian et al. 2003, Hung et al. 2008, Chiu et al. 2008, Zardus et al. 2008). Maki and Mitchell (1985) presented evidence that larvae of another small tube-dwelling polychaete, *Janua brasiliensis*, are stimulated to settle and metamorphose by biofilm EPS, such as *Pseudomonas marina.* Related to algal species, Dillon et al. (1989) found enhanced settlement of *Enteromorpha* spores on mixed microbial biofilms. On the contrary, the widespread temperate and tropical bryozoan *Bugula neritina* appeared to be a relatively indiscriminate settler by the presence of natural or laboratory (including diatoms) biofilms (Dahms et al. 2004, Zardus et al. 2008).

The polychaete tubeworm, *H. elegans,* is one of the most studied species along with *B. amphitrite* (see **Table 3.2**). *H. elegans* is an early colonizer of newly submerged surfaces in the succession of macrofouling invertebrates, with a global distribution found mainly in tropical and subtropical bays and harbours (Shikuma and Hadfield 2006). The presence of a biofilm is a pre-requisite for larval settlement of *H. elegans* (*e.g*. Lau et al. 2005) and it was found that larval metamorphosis of this species was not affected by nutrient enrichment but predominately by the age of biofilms (Chiu et al. 2008).

When clean surfaces were tested (*i.e.* no biofilm present) *B. amphitrite* cyprid attachment was greatly affected by surface wettability with preferential settlement on hydrophilic surfaces (glass). However, the presence of aged biofilms (six days old) overrode

the negative effect of hydrophobic surfaces on cyprid attachment illustrating that surface wettability does not alter the positive effect of natural biofilms on barnacle larval attachment (Hung et al. 2008). The latter, thus, indicates that ideally test surfaces should be submerged for a sufficient duration to allow the biofilm and the macrofoulers to mature and reproduce (Shikuma and Hadfield 2006, Huggett et al. 2009, Chung et al. 2010). For instance, the biofilm age has been reported to influence ascidian larvae (Wieczorek and Todd 1998), coral larvae (Webster et al. 2004), mussel larvae (Bao et al. 2007), temperate or tropical barnacle cyprids (Wieczorek et al. 1995, Thompson et al. 1998, Faimali et al. 2004, Hung et al. 2008) as well as algal spores (Pattel et al. 2003).

Surface wettability is a factor known to affect both biofilm and larval settlement, thus, attempts have been made to investigate a successive relationship (*i.e.* surface wettability / biofilm formation / larval settlement) by Huggett et al. (2009). Surfaces were immersed with 6 different wettabilities (2 low, 2 intermediate and 2 high) for up to ten days and found that natural biofilm assemblages were not affected by surface treatments. Equally, larvae of the marine tubeworm *H. elegans* did not illustrate a preferential settling behaviour according to surface wettability, rather biofilm age (ten days old) was found to be the main attractant with older biofilms inducing higher larval recruitment. The non-preferential biofilm attachment on varying surface hydrophobicities was suggested to be due to adaptable attachment mechanisms often observed in bacteria (Shea *et al*., 1991). Four different substrates (marble, quartz, glass, and cembonit) and their effect on biofilm formation and subsequent *B. amphitrite* cyprid attachment were tested by Faimali et al. (2004). They found that cyprid attachment differed among the four substrates with glass being the least favourable while biofilms demonstrated the opposite preferences with glass being readily colonised. However, when cyprids were provided with the same substrates but colonised with biofilms, they found that biofilms inhibited cyprid attachment in an age dependent manner, *i.e.* older biofilms hindered settlement (Faimali et al. 2004). In a more recent study, extracts from biofilms and *H. elegans*'s larva attachment against two different substrates (granite rocks and polystyrene Petri dishes) was compared (Chung et al. 2010). It was found that biofilm community composition was modified by both age and substratum type, however, biofilm age appeared to be the main driving factor for changes in species composition. The biofilm extracts were bioassayed against *H. elegans*'s larval attachment and it was found that biofilm age was the only factor inducing settlement (Chung et al. 2010). Contradictory results, presented by Thompson et al. (1998), showed that *Semibalanus balanoides* cyprids metamorphosis and

settlement was enhanced by mature biofilms in field trials, however, laboratory tests did not support these findings. The settlement was reported to be predominantly influenced by the proximity of conspecifics and by traces of previous barnacle colonisation.

The primary colonization of submerged surfaces by *H. elegans* in Pearl Harbor was reported to be due to an increase in biofilm densities rather than a shift in dominant bacterial species assemblage (Shikuma and Hadfield 2006). The impact of bacterial densities on settlement has been reported in other tropical places for *H. elegans* by Huang and Hadfield (2003) and Huggett et al. (2009) as well as for *Enteromorpha* zoospores (Joint et al. 2000, Patel et al. 2003). Conversely, Chung et al. (2010), and to a lesser extend Lau et al. (2005), found no evidence of correlation of *H. elegans* settlement with bacterial densities. Similarly, the larval settlement of two *Balanus* species (*B. amphitrite* and *B. trigornus*) was unrelated to bacterial density or biomass (Lau et al. 2005). For larvae of *B. amphitrite* (Hung et al. 2007) or *H. elegans* (Huang and Hadfield 2003), induction of metamorphosis by biofilm bacteria shows no correlation with bacterial phylogenetic relationships. Similarly, the attachment of spores of *Enteromorpha* was strain, but not taxon, specific (Patel et al. 2003).

In general, very few studies report data that deal with the interactions between biofilm forming diatoms and macrofoulers. Among diatom strains isolated from natural biofilms, only 10% induced the larval settlement of *H. elegans*, compared to 31% and 59% that showed either weak or no inducement, respectively. The variability in larval settlement was not correlated with the density of diatoms in mono-specific films (Harder et al. 2002). Contrary to marine bacteria, diatom-induced larval settlement cues are more likely to be composed of polymeric components, such as EPS and not secondary metabolites (Lam et al. 2003). Chung et al. (2010) highlighted that although chemical cues are produced by several microbes in natural biofilms, the chemical profiles are likely to vary quantitatively and qualitatively over the period of biofilm development.

Overall, the presence of a biofilm has been shown to demonstrate contrasting effects on macrofouler settlement associated with both inhibitory and stimulating effects (see **Table 3.2**). These contradictory results may be due to differences in experimental procedures:

i) the low reproducibility inherent in experimental settlement assays for invertebrate larvae (Wieczorek and Todd 1998),

ii) field *vs*. laboratory based experiments, where laboratory conditions provide a controlled environment whereas field experiments are subjected to dynamic conditions such as seasonality (*e.g.* Lau et al. 2003),

iii) natural multi-species *vs*. mono-specific biofilms, where again it has been shown that biofilm community composition is season and time dependant (*e.g.* Bao et al. 2007), therefore it may induce different attachment responses to macrofoulers,

iv) different macrofouling species used within the various studies which do not facilitate direct data comparisons.

Similarly, the adhesion of macrofoulers may be facilitated by the presence of biofilms; however, this remains to be established, as this may result from a combination of physico-chemical and biological factors. The exact attachment behaviour of macrofoulers on a biofilmed substrate is yet to be discovered, *e.g.* whether larvae penetrate through the biofilm to adhere onto the surface or integrate their own adhesive with that of the biofilm in order to achieve a more persistent attachment (Zardus et al. 2008).

In this Section, we have attempted to summarise the literature concerning marine biofilms, the influence of composition and dynamics from two points of view: (*i*) substrates with and without antifouling capabilities and (*ii*) their influence on macrofouling. This review has revealed that despite two decades of intensive research we still remain largely ignorant of the fundamental mechanisms and dynamics involved during surface colonisation.

Often the presence of a biofilm is a prerequisite for macrofoulers settlement. However, the interaction between species should be coupled with the surrounding environmental parameters as it has been clearly demonstrated that they can affect both the biofilm and macrofoulers. The reviewed studies have explored both the impact of surface on biofilms and the subsequent larvae and spore settlement. As there is contradictory evidence regarding how surface properties directly control macrofoulers settlement, experiments should focus on the relationship between biofilm diversity and/or functions and settlement. Thus, overall questions that still require further attention include: the intra / inter species interactions, biofilm / environment interactions and biofilm / substrate interface interactions.

It is evident that marine biofilms are dynamic communities with extensive interactions between different species. Thus, a range of approaches need to be combined in biofilm research for better understanding of these complex communities. A current limitation within

biofilm research is the poor reproducibility of studies. Researchers from different test locations and groups perform biofilm studies in accordance with their own protocols, which leads to variations in the available data.

3.5 Bio-inspired / biomimetic approach for AF

The term biomimetics as the word signifies (from the Greek *βίος*=bio=life and *μίμησις*=mimesis=to imitate) is used to describe technologies that are inspired by nature. Aristotle once said "nature does nothing without purpose or uselessly" (384 BC - 322 BC*,* in *Politics)*. The examination of a biological system has often served as a model for numerous engineering-related applications in order to overcome the scientific challenges. In the same context, bio-inspired antifouling technologies illustrate a strong candidate to resolve the problem of biofouling in an environmentally friendly manner.

3.5.1 Natural Products (NPs)

In the marine environment, a wide variety of species illustrate antifouling abilities by several means, *e.g.* the use of chemical (*e.g.* Burns et al. 2003) and physical defences (*e.g.* Burns and Ilan 2003), symbiotic relationships between host (*e.g.* algae) and epibionts (*e.g.* bacteria) that prevent fouling. The impediment of biofouling in a natural way, as observed in marine organisms, has triggered the scientific interest and led to the examination of marine natural products as a possible route for a novel antifouling technology.

Nearly 20,000 natural products have so far been described that originate from marine organisms (Blunt et al. 2008). Since the early 1980s, a great number of marine natural products have been assayed against organisms implied in the biofouling process and several reviews dealing with their potential use as novel antifouling biocides have been realised (Davis 1989; Abarzua and Jakubowski 1995; Clare 1996; Omae 2003; Fusetani 2004). Natural antifouling products can be easily degraded chemically, photochemically and biologically and when incorporated in paint formulations, the overall antifouling effectiveness of the surface has been reported to diminish within a short period of time (Lewis 2002). Marine organisms are able to synthesise new compounds to maintain the antifouling effect, but such an option is not available to the paint formulator. However, Price et al. (1992), in an attempt to overcome these deficiencies, has used a method of microencapsulation and controlled release. According to this novel technique, microcylinders of copper or iron metal formed on a substrate of phospholipid have been utilised to deliver tetracycline (polyketide antibiotic),

isothiazolone antifouling agents and crude extracts of the sea pansy *Renilla*. It has been reported that microencapsulation enhanced the activity of the natural antifoulants, with metallic tubules providing heat and solvent stability and a barrier to light. It is therefore, well understood that although natural products used as biocides may be the answer to the problem of biofouling on ship hulls, the incorporation of the NP into the paint system has to be conducted in such manner in order to achieve a controlled release rate.

Sessile marine organisms (*e.g.* sponges, soft corals and seaweeds) as well as micro-organisms are known to elaborate chemical defence mechanisms against predation and epibiont growth (**Table 3.3**). The metabolites excreted might repel or inhibit fouling organisms and can act enzymatically by dissolving the adhesives, interfering with the metabolism of the fouling organisms, inhibiting the attachment, metamorphosis, or growth promoting negative chemotaxis, altering the surface of the organisms, or finally acting as biocides.

Table 3.3. Taxonomic distribution of 160 marine species from which potential antifouling natural products have been extracted [Data obtained from several sources: (Clare, 1996; Omae, 2003; Fusetani, 2004; Raikin, 2004; Chambers 2009).

Marine Organisms	Extracts with potential AF activity (%)
Parazoa	38.5
Algae	19.5
Cnidaria	17.95
Tunicates	7.05
Mollusca	7.05
Echinodermata	3.2
Bryozoa	2.6
Sea grass	1.95
Bacteria	1.95
Multi-phyla	0.25

Antifouling marine natural products have been classified according to their biosynthetic pathways into five main compounds: 1) terpenoids (isoprenoids), 2) steroids and saponins, 3) fatty acid-related, 4) bromotyrosine derivatives and 5) heterocyclic compounds. Lactones, furas and furanones are some examples of compounds that have shown multiple antifouling activities. Specifically, halogenated furanones from the Australian red alga *Delisea pulchra* have shown to exhibit antifouling properties (de Nys et al. 1998; Maximilien et al. 1998b; Dworjanyn et al. 1999; Dworjanyn et al. 2006). Interestingly, it was found that in *D.pulchra*

furanones are encapsulated within specialised glands located at the surface of the alga (Dworjanyn et al. 1999). These secondary metabolites were found to be released onto the algal surface at concentrations (from 10 to several 100 ng cm^{-2}, depending on the furanone) that largely reduced the settlement of eukaryotic and prokaryotic fouling organisms in both field and laboratory assays (Maximilien et al. 1998, Dworjanyn et al. 2002). Additionally, the degree of fouling attachment was negatively correlated with furanone levels present on the algal surface (Dworjanyn 2001). In the red alga of the genus *Laurencia*, the secondary metabolite terpenoid was found to be located in intracellular vesicles called *corps en cerise* (Young et al. 1980). Phlorotannins are polymers of phloroglucinols located in membrane-bound structures termed physodes (Ragan 1976); these can be found on the surface of the algal thallus and release the metabolites into the marine environment. Phlorotannins are known to exhibit antifouling (Wikstrom and Pavia 2004) and bacteriocidal (Nagayama et al. 2002) properties. At this point it must be emphasised that details on the localisation and presentation of most algal secondary metabolites are largely unknown. This lack of information impedes our knowledge on the possible ecological roles of these metabolites.

Secondary metabolites are complex molecules and the active compounds involved in inhibition have frequently been difficult to identify, posing this way, a problem in creating structural analogues for incorporation into antifouling coatings (Murthy et al. 2009).

3.5.1.1 Algal extracts

A wide spectrum of marine organisms is known to possess antifoulant metabolites; however, algae are an important and commonly assessed key source of potent antifouling natural product. Particularly, red algae (phylum: Rhodophyta) are known to exhibit antifouling properties (de Nys et al. 1995; Sudatti et al. 2008).

An important factor that contributes towards the exploitation of marine algae as natural resources against biofouling is that these organisms are cultivable, relatively easy to harvest and that the extract yield is relatively high. Hence, algal extracts represent cost effective alternative antifouling compounds and are an attractive source for a commercially viable product. Algae are often sedentary and thus act as a biomimetic solution for static ship operational profiles. Some algae can tolerate exposure out of the marine environment (*e.g.* during low tides) and a ship's hull would mimic this exposure/immersion at the waterline of the splash zone.

In the current research project, a model red alga species, *Chondrus crispus*, has been used as a model natural product extract since it was found by previous studies to exhibit antifouling properties (Nylund and Pavia 2003, Hellio et al. 2004a, Chambers 2011). The choice of phylum was based on the literature and the specific species (*C. crispus*) on the availability of previous bioassays on this organisms where it was shown that extracts of *C. crispus* revealed promising inhibitory activities on the germinating spores of fouling microalgae (Hellio et al. 2002). Furthermore, *C. crispus* extracts have been found to hinder diatoms from the genus *Amphora* (Jackson 1991). The ethanolic extract of *C. crispus* has been reported to be non-toxic to sea urchin larvae (Hellio et al. 2000) and show no toxic effects on lysosomal and mitogenic activities against mouse fibroblast even up to concentrations of 1000 µg mL^{-1} (Hellio et al. 2004). In experiments carried out at the University of Southampton (Chambers 2009) the crude ethanol extract was used in its entirety which provided a mixture or 'cocktail' approach to harnessing any antifouling properties. This was done to achieve a broad spectrum activity as opposed to using specific constituents that have activity to resist specific fouling species. A whole cell extraction of potential natural product sources is a classic method though there are reservations on the extracts ecological relevance to the organism (Nylund et al. 2007). In the current work, a dried source of *C. crispus* was used, since analysis of the dried source algae allows examination of potential 'off-the-shelf' as well as economically viable natural product solutions. Experiments showed that the isolated extracts had a good antifouling efficacy (≥ 25

µg L^{-1}) against key marine fouling bacteria and microalgae (Chambers et al. 2011). The goal with crude extracts of *C. crispus* was to see how this compound could function by direct incorporation into a paint matrix as part of a full antifouling system. The extract was incorporated into a CDP and its activity was limited to 6-10 weeks in Southampton Water immersion trials, thus a potential way forward would be to examine the extract in a controlled binder technology such as a laboratory designed SPC (Chambers 2011). In contrast, *C. crispus* dried extract was found to enhance marine microbial activity, potentially acting as a nutritional source for the species tested (Cox et al. 2010).

The brown alga *Bifurcaria bifurcata* is another species with antifouling properties which was provided by the University of Toulon (MAPIEM) for the needs of the current EDA collaborative project (ACWS). The choice of *B. bifurcata*, commonly found along the North East Atlantic shores, was made due to its rich array of linear diterpenes in ether extracts (Combaut and Piovetti 1983; Valls et al. 1986; Semmak et al. 1988; Hougaard et al. 1991a; Hougaard et al. 1991b; Valls et al. 1993a; Valls et al. 1993b; Valls et al. 1995; Culioli et al. 1999; Culioli et al. 1999b; Culioli et al. 2000; Hellio 2001; Culioli et al. 2002). Hellio et al. (2001) isolated a series of extracts and linear diterpenes from *B. bifurcata* and found promising levels of antifouling activities. Marechal et al. (2004) found that crude extracts of *B. bifurcata* had an antifouling effect against two marine bacteria, *Cobetia marina* and *Pseudoalteromonas haloplanktis* and cypris larvae of the barnacle *Balanus amphitrite*. The antifouling activity varied on a seasonal base with increased levels during the summer months.

3.5.1.2 Terrestrial extracts / NPs

In the 1980s, terrestrial plants were explored as a source of AF compounds (Omae 2003), but were superseded by investigations on marine organisms in the 1990s. Recently, terrestrial natural products, pharmaceuticals, and enzymes have been recognized as important sources of non-toxic antifoulants this was extensively reviewed by Qian et al. 2009. In the current research project two terrestrial NPs were chosen according to previous studies illustrating promising antibacterial activity, usnic acid and juglone (*e.g.* Francolini et al. 2004 and Wright et al. 2007, respectively).

Usnic acid, **(I)** is a yellow pigment that exists in two enantiomeric forms (+)-usnic acid and (-)-usnic acid, depending on the projection of the angular methyl group at the chiral 9b position. While designated an acid, the molecule contains no carboxylic acid (-COOH) groups.

However, the -OH groups all have some acidic character, with the -OH at position 3 being the most strongly acidic (pK_a 4.4) due to an inductive effect of the keto group (Sharma 1966). The solubility of usnic acid in pure water is <0.01 g / 100 mL (Stark 1950) but will be higher in seawater (pH 8) owing to ionisation of the –OH groups. Crude lichens have been used in folk medicine since ancient times to treat various medical conditions. One biologically active secondary metabolite identified in lichens of several species including *Usnea* and *Cladonia* is usnic acid [2,6-diacetyl-7,9-dihydroxy-8,9b-dimethyl-1,3(2H,9bH)-dibenzo-furandione].

Juglone [5-hydroxy-1,4-naphthalenedione] **(II)** occurs naturally in all parts of the black walnut (*Juglans nigra*) tree, especially the nut husks and roots. Juglone is an inhibitor of respiration which deprives other plants of the energy needed for metabolic activity, and plants grown near black walnut trees exhibit symptoms such as foliar yellowing, wilting, and eventual death (Dana 2001). Juglone is used in consumer products such as herbal medicines and hair dye formulations although it is potentially toxic to humans (National Institutes of Health 1999). A related US patent (Cutler 2000) claims solutions of juglone or its derivatives in organic solvents as additives for removing zebra mussels and quagga mussels from water intake pipes and various other underwater hard surfaces.

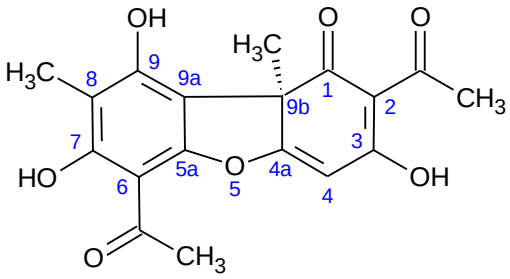

(I) Usnic acid

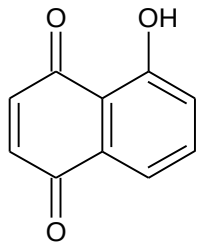

(II) Juglone

3.5.2 Topography/surface texture

It is now well-established that surface topography and texturing can affect biofouling attachment (reviewed by Salta et al. 2010, Scardino et al. 2011). Increasing evidences illustrate that modified surfaces using topographies and texturing mimicking marine organisms appear to be promising. To avoid epibiosis, marine organisms have developed surface textures that appear to be almost foul-free such as whale skin (Baum et al. 2002), mussel/bivalve surfaces (Scardino and de Nys 2004), crabs and eggshell casings (Bers and Wahl 2004). Bioinspired surfaces were developed by the AMBIO project (Advanced Nanostructured

Surfaces for the Control of Biofouling), such as sol-gel coatings with nanoparticle inclusions, and nanoscaled self-assembled surfaces (Callow and Callow 2009). Sharklet AF™ is a commercial product that exploits the shark's skin, *i.e.* mimicking its ridged platelet structures (Carman et al. 2006). Chlorophyta spores cannot attach on surfaces with topographic features separated by size scales smaller than that of the spore (Carman et al. 2006; Schumacher et al. 2007) resulting in 86 % reduction in *Ulva* spore attachment (Carman et al. 2006). Generally, it has been proposed that when the texture is wider than the fouler, choice is the main driving mechanism for settlement (Scardino et al. 2008). In a recent publication, several micro-topographic patterns including: *i*) pillars, *ii*) ridges, *iii)* triangle/pillars, *iv*) Sharklet AF™ and *v*) recessed Sharklet AF™ were engineered (in PDMSe) and tested against *Ulva* spores and the marine bacterium *C. marina* (Magin et al. 2010). The results showed a negative linear correlation of normalized, transformed attachment density for both organisms with increase in surface roughness. Encouraging results were obtained when more complex, wrinkled hierarchical structures remained almost clear (diatom settled between ridges on the smallest size scale) for almost 1 year (Efimenko et al. 2009).

A substantial number of publications have investigated the textured surface of mollusc shells with a review highlighting the following (in order of importance) 5 parameters that illustrate good AF efficacy: *i*) low fractal dimension, *ii*), high skewness of both roughness, *iii*) waviness profiles, *iv*) higher values of isotropy and *v*) lower values of mean surface roughness (Scardino et al. 2009a,b, 2011). It has to be noted that, although micro-topographic and textured surfaces appear to be promising for AF purposes, rarely these technologies/strategies are as effective as the organism *in situ*, indicating that additional parameters contribute towards an AF activity during the organism's life time. Importantly, it was highlighted that these technologies are usually targeting a limited number of taxonomic groupings, for instance coatings that inhibit macrofoulers (*e.g.* algae, barnacles and mussels) may not be active against biofilms. Scardino and de Nys (2011) primarily focused on the effect of surface modifications on macrofoulers, however, they noted that microbial biofilms can modify and/or mask the surface topographies/properties and they went on to state the need to control these complex biofilm communities.

Chapter 4

4. Growth under different culture media and protocol optimisation

4.1 Introduction

The initial growth conditions play a key role in cell biology, since the environment will affect the physiology and therefore the growth and kinetic response of an organism to a treatment. Importantly, the marine environment is very dynamic with physico-chemical factors influencing biological processes (*e.g.* see **Section 3.3.1**). The differences between artificial sea water (ASW) and natural sea water (NSW) compositions may vary greatly due to naturally occurring nutrient seasonality observed in the sampled NSW, plus variable salinity and pollutant levels, at the sampling location. For laboratory-based assays, ASW is generally considered to provide greater controllability over the aforementioned water properties and it was therefore decided to conduct a series of tests comparing the different experimental media, *i.e.* NSW *versus* ASW and the levels of carbon typically used in bacterial bioassay testing. The sterilisation procedure was also assessed in the current experiments *i.e.* media autoclaved *versus* sterile filtered. This was done for two main reasons: 1) autoclaving ASW (without peptone) produced precipitates in the solution and 2) preliminary experiments illustrated a significant change in the medium's pH where it was found that the solution became more acidic after autoclaving. The overall lay-out of this chapter can be seen in **Figure 4.1**.

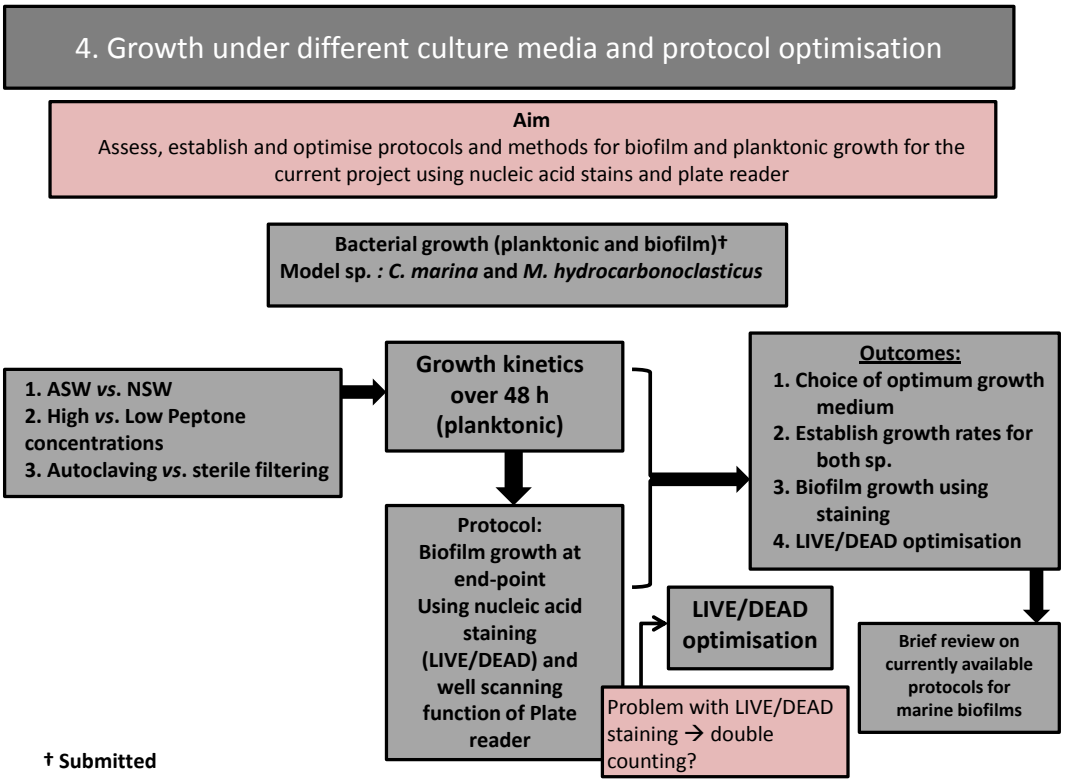

Figure 4.1. Flow chart on Chapter 4 lay-out.

4.2 Material and methods

4.2.1 Microtiter assays and the multidetection plate-reader

The experimental system, whose most common format is often referred to as the microtiter plate assay, is a high-throughput method used to monitor several biofilm parameters such as attachment and/or growth to an abiotic surface. Essentially, the bacteria are exposed to numerous experimental treatments (*e.g.* natural products) and the cell response is detected utilising a multidetection plate-reader. Common detection modes for plate-reader assays include absorbance (optical density, OD), fluorescence intensity (relative fluorescence units, RFU), luminescence, time-resolved fluorescence and fluorescence polarization. For the scope of this work, a plate-reader provides qualitative and quantitative data of biofilm attachment and growth utilising absorbance and fluorescence intensity.

A typical optical path for plate-readers is illustrated in **Figure 4.2**. The light source for the BMG Labtech plate reader is a xenon flash lamp, which is becoming increasingly common in fluorescence instruments. The desired excitation wavelength is selected using a monochromator. A unique feature is the mirror with hole to transmit the excitation. The fluorescence, which occurs in all directions, is directed toward the detector optics by the same mirror. Typically, the microplate is moved to position each well within the observation path by an x-y scanning stage. Some plate-readers include a second mirror under the microplate (well plate) to facilitate cell-based assays or absorption measurements on a large number of samples (Lakowicz 2006).

Luminescence differs from fluorescence since the light emitted by the samples is due to a chemical or biochemical reaction. In this case, the optical system consists in a light-tight reading chamber, and photomultiplier tube (PMT) detector measuring the light emitted by the samples. Typical applications include luciferase-based gene expression assays, cell viability and cytotoxicity assays based on the luminescent detection of ATP.

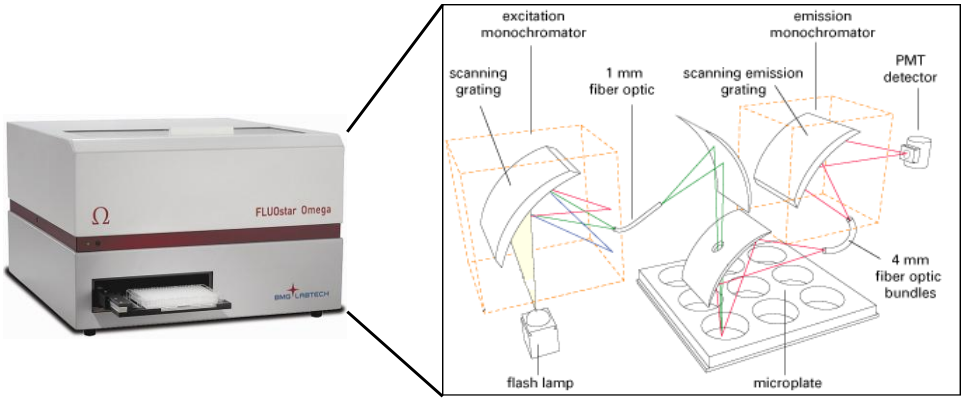

Figure 4.2. The optical path for a multidetection plate-reader (modified from Lakowicz , 2006).

4.2.1 Marine bacteria species

The marine biofilm forming species utilised in this work were *Cobetia marina* (ATCC 25374) and *Marinobacter hydrocarbonoclasticus* (ATCC49840). Both species have previously been used as models in studies on initial attachment of marine bacteria to surfaces (*e.g.* Ekblad et al. 2008, Akesso et al. 2009, D'Souza et al. 2010).

C. marina is a Gram-negative, slightly halophilic, aerobic species. Its morphology is characterised as rod-shaped cells that are 1.6 – 4.0 µm in length and 0.8 – 1.2 µm in diameter, which occur singly and in pairs. Most strains are motile by means of 2 – 5 polar peritrichous flagella. Colonies are round, bright, smooth and cream-pigmented (Difco Marine Agar) (Bauman et al. 1972, Bauman et al. 1983).

M. hydrocarbonoclasticus is a Gram-negative, halotolerant, aerobic, rod-shaped bacterium isolated from Mediterranean seawater (Gulf of Fos, France) near a petroleum refinery. It grows in NaCl concentrations of 0.08 to 5.5 M and uses various hydrocarbons as the sole source of carbon energy (Gauthier et al. 1992). This non-spore-forming species actively grows in marine broth reaching 2 - 3 µm in length and 0.3 – 0.6 µm in diameter. On marine agar, young colonies are circular, with diameters of 1 – 2 mm, smooth, convex, and white, with regular edges. Following one week incubation, colonies expand to 2 – 4 mm in diameter and become rosy-beige coloured without diffusible or fluorescent pigments (Gautier et al. 1992). Cells are motile, possessing a single unsheathed polar flagellum in media with NaCl concentrations of 0.6 – 1.5 M, and non-motile in media of low (≤ 0.2 M) or high (≥ 1.2 M) NaCl.

4.2.2 Growth conditions

Marine bacteria species are commonly cultured in marine broth which includes peptone (P), a carbon source recommended for ATCC species, in either sterilised natural sea water (NSW) or artificial sea water (ASW). Both species were revived from the original lyophilate and stored as frozen stock (cryopreservation) aliquots in Sea Salts (S9883, Sigma, see **Table 4.1**) plus 18 g L^{-1} peptone, abbreviated as SSP (D'Souza et al. 2010), with 10% glycerol added and preserved at -80 °C.

Table 4.1. Composition of the artificial sea water (ASW).

Main constituents	Concentration (mg L^{-1})
Chloride	19290
Sodium	10780
Sulphate	2660
Magnesium	1320
Potassium	420
Calcium	400
Carbonate/bicarbonate	200
Strontium	8.8
Boron	5.6
Bromide	56
Iodide	0.24
Lithium	0.3
Fluoride	1.0
Total trace metals	0.5

Marine Agar: For the initial culture, the cryopreserved vile was thawed and a sterile inoculation loop was immersed in the thawed suspension to transfer bacteria that were streaked to isolation (or plated out) on freshly prepared marine agar plates (Difco, Marina Agar 2216) where 55.1 g were added in deionised water (18 MΩ cm resistivity) (**Figure 4.3 A, B**). Stock of agar plates were sealed with parafilm and kept at 4 °C for up to 10 days before use. Marine agar subcultures were then placed in a cooled incubator (Binder KB115, Jencons-WDR) at 28 °C. Young colonies were formed within 42 h after incubation. Subcultures were conducted by transferring individual colonies on new marine agar plates once a week. The latter was repeated for up to eight subcultures after which new cryopreserved cells were used. All the above were conducted under sterile conditions (*i.e.* under a laminar flow cabinet).

Broth medium: To grow the bacteria in broth, ASW (35 g L^{-1}) was sterile filtered through a 0.2 µm pore size filter (Steritop™ Millipore® Filter Units). Bacteriological peptone was added

at a concentration of 18 g L^{-1}. The resultant medium was abbreviated SSP, *i.e.* sea salts with peptone. The choice of peptone concentration in the medium was decided following pilot assays testing two different concentrations (9 g L^{-1} and 18 g L^{-1}) in order to establish good bacterial growth. The final decision of 18 g L^{-1} was based on results maintained from the pilot assays with the additional advantage of common use of experimental procedures between this work and TNO, The Netherlands, as this is TNO's standard growth medium recipe. Results of bacterial growth in different peptone concentration are presented in **Section 4.3**.

Batch cultures in SPP were achieved by using a sterile inoculation loop to transfer a single colony from the marine agar into the media (**Fig. 4.3 B and C**). The batch culture was then incubated at 28 °C under agitation (100 RPM). In order to obtain an exponentially growing culture at the required OD_{595} of 0.2, approximately 12 h of grow were required (usually this is achieved overnight).

Cryopreserved bacterial can also be directly added in the marine broth, however, this is not recommended as adding the step of plating out cells on agar, potential contamination can be visually observed.

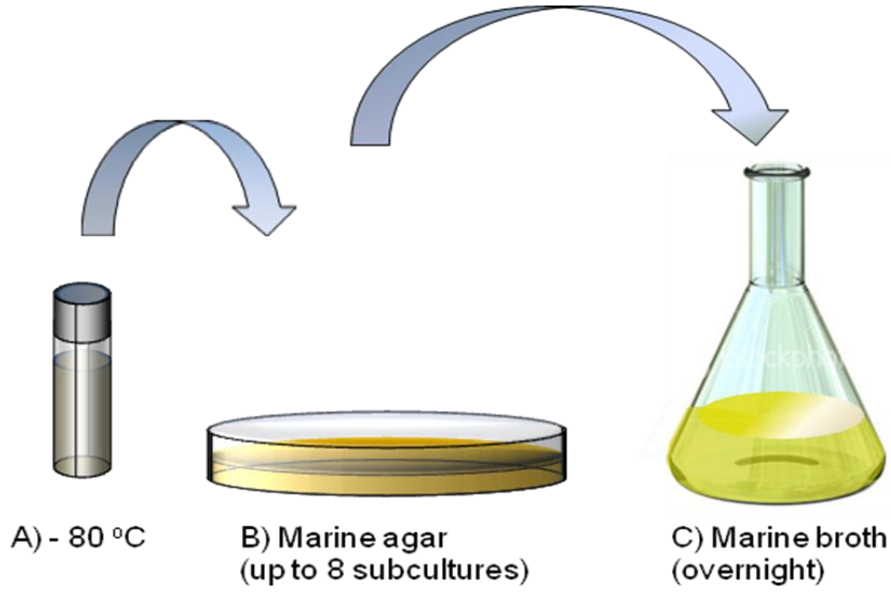

Figure 4.3. Typical bacterial culturing procedures: A) bacterial cryopreserved stock at –80 °C, B) streak to isolation of bacteria from thawed stock on marine agar plates, and C) inoculating individual colonies from the marine agar into the marine broth to obtain a batch culture.

4.2.3 Choice of media: planktonic growth

Both *M. hydrocarbonoclasticus* and *C. marina* were kept at 28 °C in SSP under agitation overnight. The cultures were washed in order to avoid any medium carry over using the following steps: 40 mL of the overnight cultures were placed into 50 mL centrifuge tubes and the cells were centrifuged at 4000 rpm for 8 minutes at 6 °C. Once the cells were centrifuged down, creating a pellet at the bottom of the centrifuge tube, the supernatant (medium) was disposed and sterile phosphate-buffered saline pH 7.2 (PBS, P5368 Sigma Aldrich) was introduced. The cells were then re-suspended (using a vortex mixer) in PBS and re-centrifuged.

The sterilisation procedure was also assessed in the current experiments *i.e.* media autoclaved *versus* sterile filtered through 0.2 µm pore size (Steritop™ Millipore® Filter Units). NSW was collected from Southampton Water, UK, in May 2010 and GF/F filters were used to remove coarse particulates prior to the sterilisation procedures.

Wells of a 96-well plate (optical bottom plated with polymer base, black, Nunc™) were conditioned by the addition of 190 µL of the experimental media 1 h before bacterial inoculation. Following the well conditioning, 10 µL of washed cells were inoculated into the wells to achieve a final volume of 200 µL per well. Seven different experimental media were tested as outlined in **Table 4.2**.

Table 4.2. Experimental media for *C. marina* and *M. hydrocarbonoclasticus*. ASW = artificial sea water, NSW = natural sea water, P = peptone, H = high concentration (18 g L^{-1}) and L = low concentration (9 g L^{-1}).

Water	Peptone conc. (g L^{-1})	Sterilisation	Acronym
ASW	18	Autoclaved	ASWPH (or SSP)
ASW	9	Autoclaved	ASWPL
ASW	0	Autoclaved	ASW
ASW	18	Filtered (0.2 µm)	ASWPH
NSW	18	Filtered (0.2 µm)	NSWPH
NSW	9	Filtered (0.2 µm)	NSWPL
NSW	0	Filtered (0.2 µm)	NSW

Five replicas for each treatment were performed. Likewise, four replicas of un-inoculated wells were also taken to assess for possible procedural contamination and background signal. Cell growth experiments were performed for a total duration of 42 h at 28 °C and absorbance at λ = 595 nm (OD_{595}) was measured using a multidetection plate-reader

(FLUOstar Omega, BMG LABTECH, Offenburg, Germany). The optical density (OD_{595}) was measured every 15 minutes. The software used was Mars Data Analysis Software, Version 2.00 (Omega, BMG LABTECH).

4.2.4 Choice of media: biofilm growth

To quantify biofilm growth at the end point of the growth kinetics, the media in the 96-well microplates were removed and each well was individually washed (by pipetting) twice with ASW in order to remove any planktonic cells. After the washing steps, the biofilm was stained with FilmTracer™ LIVE/DEAD® Biofilm Viability Kit (Molecular Probes) which was prepared according to manufacturer's instructions and the plates were stored in the dark at 28 °C for 20 minutes. It has been reported in various studies that the LIVE/DEAD technique may often result in the production of artefacts, such as the non-specific binding of Propidium Iodide (PI) and the simultaneous presence of both stains that have been shown to result in double counting of cells as dead and live (Stocks 2004, Biggerstaff et al. 2006, Berney et al. 2007a), as observed in the current work. Therefore, here were present the Syto9 data to illustrate the overall biofilm biomass.

Following the incubation period, the wells were again washed twice with ASW to remove the excess stain. Finally, 100 µL of ASW were added to the wells to prevent biofilm dehydration during the measurements. The multidetection plate-reader was utilised for direct end point measurements (relative fluorescence units, RFU) to allow high-resolution analysis of fluorescence intensity which was conducted using λ_{EX} = 475 nm and λ_{EM} = 520 nm.

In addition, the well scanning capability of the plate-reader was used for visualizing biofilm in individual wells allowing identification of heterogeneous biofilm structures. Each well, was scanned to produce an image of the biofilm formation (scan matrix dimension: 30 × 30 equivalent to a resolution of 213 µm × 213 µm, scan width 6 mm). The main advantage of the imaging utility is the direct observation of biofilm formation *in situ*, which was sufficiently sensitive to identify biofilm features, as well as the plethora of sampling points within the well, providing this way, a very accurate measurement representative of the entire well. Although well scanning is not specifically designed to replace the direct microscopic observations, an initial and rapid observation of the biofilm structure can be achieved.

4.2.5 LIVE/DEAD kit optimisation for the plate-reader

As mentioned in **Section 4.2.4**, the double counting of bacterial cells as both dead and live was observed. In order to optimise the protocol and achieve a more realistic representation of the stained cells, validation assays were designed. Overnight cultures of *C. marina* were washed according to **Section 4.2.3** and inoculated in black 96-well plates where OD_{595} measurements were taken. The plate was then incubated for 1 h to allow attachment (at 28 °C). The full experimental design and matrix can be seen in **Figure 4.4**. Following the 1 h incubation, the media (ASW) were removed and in half of the biofilmed wells the killing factor was introduced, *i.e.,* 1 % VIRKON (X2, X4, and X6); ASW was added in the remaining biofilmed wells (X7-X10), see **Figure 4.4**. The well plates were then incubated for 30 min. Again, the wells were emptied and gently washed with ASW twice. The nucleic acid stains from the LIVE/DEAD kit were inoculated as shown in **Figure 4.4**. All treatments were replicated six times. As control in the experimental design, a column of unstained bacteria was present (Sample X4) in order to account for any potential autofluorescence deriving from the cells.

Following the plate-reader measurements at the end-point, epifluorescence microscopy (EVOS*fl*, AMG, Westover Scientific, Inc.) using the standard GFP and RFP LED light cubes (λ_{EX}: 370 nm – λ_{EM}: 525 nm and λ_{EX}: 531 – λ_{EM}: 593 nm, respectively) where images from the build-in camera were taken from each well in order to verify and/or compare results between the two techniques (*i.e.* plate-reader and microscopy). Image analysis was conducted using ImageJ (Biophotomics) where images were turned into stacks and transformed into a binary, *i.e.* either 0 or 255.

1. Inoculate washed cells and measure OD

Well plate Lay-Out

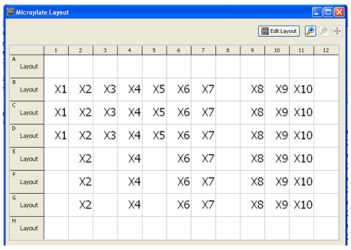

Where: X2,X4,X6-X10 inoculated with bacteria

2. Incubate for 1 hr → Measure OD

3. Kill with 1 % VIRKON →
X2, X4, and X6

4. Incubate for 30 min

5. Measure OD

6. Wash inoculated wells and add stains:
X2: Syto9
X4: PI
X6: Both stains (L/D)
X7: Syto9
X8: PI
X9: Both stains (L/D)
Uninoculated wells: X1, X3 and X5 with Syto9, PI and L/D, respectively.

Test Matrix

Treatment	Sample	Stains	Filter Set 1		Filter Set 2		Filter Set 3	
			Excitation (nm)	Emission (nm)	Excitation (nm)	Emission (nm)	Excitation (nm)	Emission (nm)
Killed	X1	S9	475-10	520 620	485 540	510 610	485 544	510 610
Killed	X2	PI	475-10	520 620	485 540	510 610	485 544	510 610
Killed	X3	Both	475-10	520 620	485 540	510 610	485 544	510 610
Live	X5	S9	475-10	520 620	485 540	510 610	485 544	510 610
Live	X6	PI	475-10	520 620	485 540	510 610	485 544	510 610
Live	X7	Both	475-10	520 620	485 540	510 610	485 544	510 610
Just Bacteria	X4	None	475-10	520 620	485 540	510 610	485 544	510 610

Measurements

Figure 4.4. Schematic of the LIVE/DEAD optimisation experiments.

4.2.6 Statistical analysis

Differences in OD_{595} and RFU values between experimental and controls were assessed by applying one-way ANOVA. To establish the homogeneity of variances, Levene's test of equal variances was applied. Where homogeneity of variances was not met, the non-parametric Kruskal-Wallis test was applied. All conclusions are based on a 5 % level of confidence ($p < 0.05$). Statistical analysis was performed using SPSS software (version 17.0).

4.3 Results and Discussion

4.3.1 Planktonic growth

The initial growth conditions play a key role in cell biology, since the environment may affect the physiology and therefore the growth and kinetic response of an organism to a treatment. Growth rates and doubling times for *C. marina* and *M. hydrocarbonoclasticus* are shown in **Table 4.3**. Overall, when comparing like for like peptone concentrations for the two different sea waters types (*i.e.* ASW *vs*. NSW), no significant differences in cell growth were found. Therefore it was concluded that using ASW as an alternative to NSW is acceptable to avoid seasonal, and day to day, variability in chemistry and nutrients. Regarding the peptone levels for the two waters, it was found that the high peptone concentrations (ASWPH, 18 g L^{-1}) promoted higher bacterial growth when compared to the low concentrations (ASWPL, 9 g L^{-1}). Specifically, for *C. marina* the growth rate was significantly higher for ASWPH when compared to ASWPL ($p < 0.022$), ASW ($p < 0.001$). Similarly, for *M. hydrocarbonoclasticus* the media with high peptone concentrations (ASWPH) illustrated the best growth performance (ASWPL, $p < 0.001$ and ASW $p < 0.001$). Also, when comparing the sterilization procedures conducted on the ASW media, *i.e.* filtered *vs.* autoclaved, no significant difference in growth for both species was found. In the literature, autoclaving is routinely used as a medium sterilisation method for bacterial growth, however, due to measurable changes in the medium's chemistry (pH ~8.1) following autoclaving, the use of filtration was decided to be the most appropriate procedure for the purpose of this work.

Table 4.3. Growth rates and doubling times for both species, *M. hydrocarbonoclasticus* and *C. marina*, during exponential growth phase using absorbance λ= 595 nm (OD_{595}) where ASWPH = Artificial Sea Water Peptone High, ASWPL = Artificial Sea Water Peptone Low, ASW = Artificial Sea Water, FASWPH = Filtered Artificial Sea Water Peptone High, NSWPH = Natural Sea Water Peptone High, NSWPL = Natural Sea Water Peptone Low and NSW = Natural Sea Water.

Species		ASWPH	ASWPL	ASW	FASWPH	NSWPH	NSWPL	NSW
M. hydro	Growth rate (h^{-1})	0.115 ± 0.008	0.091 ± 0.006	0.022 ± 0.010	0.113 ± 0.007	0.109 ± 0.009	0.090 ± 0.002	0.013 ± 0.002
	Doubling time (h)	6.03 ± 0.39	7.59 ± 0.52	35.66 ± 14.80	6.11 ± 0.36	6.35 ± 0.53	7.63 ± 0.22	53.38 ± 8.41
C. mar	Growth rate (h^{-1})	0.079 ± 0.004	0.072 ± 0.002	0.055 ± 0.006	0.075 ± 0.002	0.073 ± 0.002	0.075 ± 0.002	0.06 ± 0.010
	Doubling time (h)	8.77 ± 0.47	9.54 ± 0.30	13.77 ± 2.25	9.21 ± 0.31	9.39 ± 0.30	9.15 ± 0.27	11.29 ± 2.51

4.3.2 Biofilm growth

In **Figure 4.5**, the degree of *C. marina* biofilm formation within the various media after 42 h incubation can be seen. In good agreement with the planktonic growth data, this species formed similar biofilms at the same peptone concentrations for both ASW and NSW. Again, consistent with the cell growth assays, lower biofilm growth is observed for the treatments without any carbon source (*i.e.* no peptone). In comparison to the growth rates (**Table 4.3**), there is generally good correlation between the test media / sterilisation and the biofilm formation, which demonstrates a good level of bioassay consistency for the ASW and NSW measurements.

In contrast to *C. marina*, *M. hydrocarbonoclasticus* shows an interesting difference in behaviour when comparing planktonic cells to biofilm growth. As seen in **Table 4.3**, although the lowest planktonic growth was found to be in ASW and NSW (no peptone), biofilm formation was highest in NSW when compared to the rest of the media. This may be due to an almost instantaneous switch from plankton to biofilm forming phenotype. This switch may have been triggered by low or absent carbon source concentrations 'obligating' the cells to adopt a survival strategy, *i.e.* to form a biofilm. Biofilms are more tolerant of external threats such as biocides, antibiotics and overall unfavourable environmental conditions, when compared to the planktonic cells. Therefore, it can be suggested that NSW triggered the switch from planktonic to biofilm mode due to unfavourably low nutrient concentrations found in this medium. The NSW is likely to contain organic nutrients, which are naturally occurring in coastal waters, thus providing a source of nutrition that could possibly supply sufficient energy for the initial biofilm formation. The ASW did not trigger the same response since no organic nutrients are present.

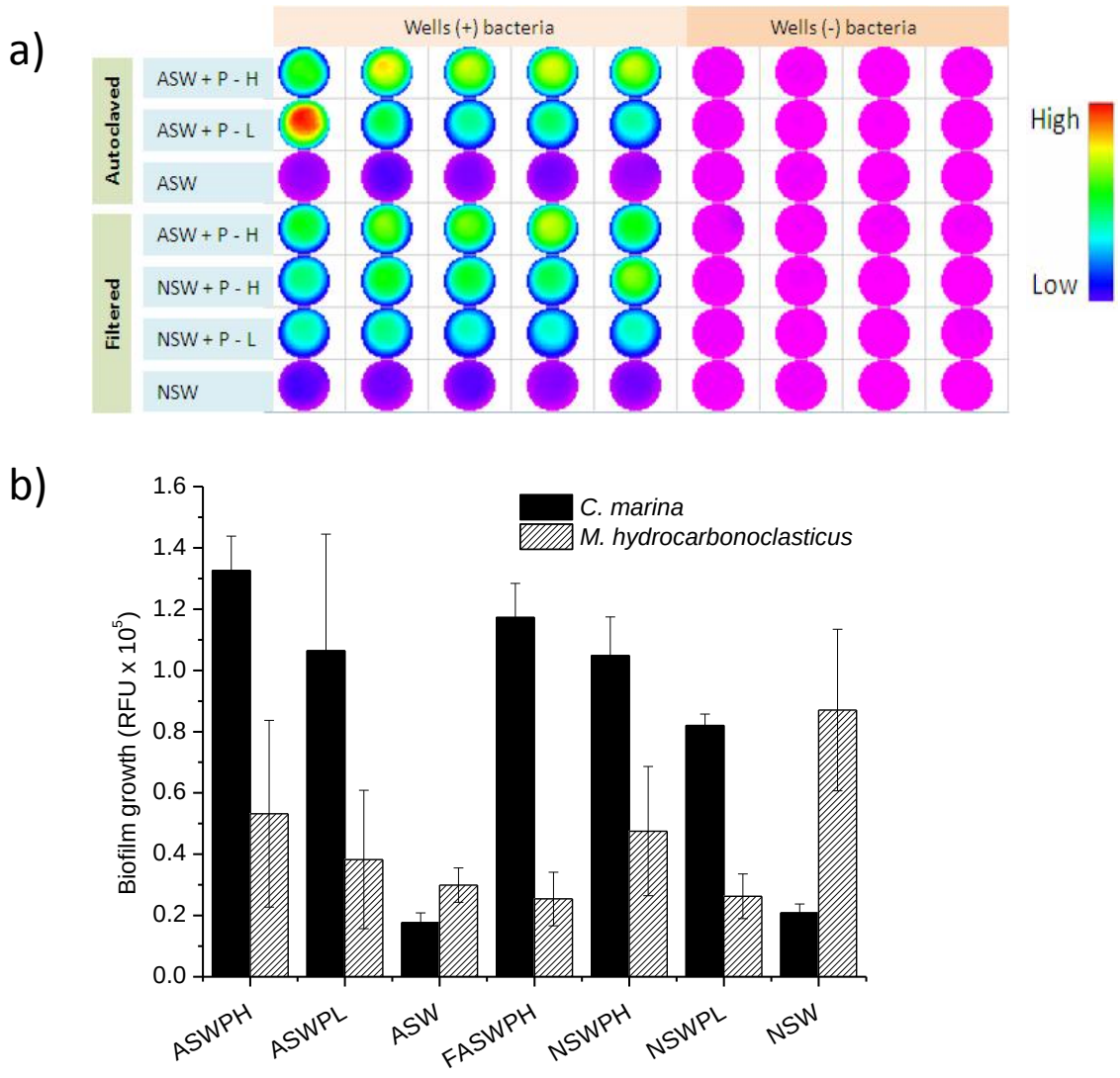

Figure 4.5. a) Example of the well-scanning imaging of *C. marina* biofilm formed after 42 h on the 96-well plate surface as a function of fluorescence intensity at λ_{EM} = 520 nm (live bacteria) and b) the biofilm formation after 42 h in different media for species *C. marina* and *M. hydrocarbonoclasticus*. Syto9: λ_{EX} = 485 nm, emission λ_{EM} = 510 nm. Error bars ± STDEV.

4.3.3 Comparing *M. hydrocarbonoclasticus* and *C. marina*

For the planktonic cell growth kinetics (**Section 4.3**) *M. hydrocarbonoclasticus* and *C. marina* showed a similar response to both ASW and NSW at all peptone and non-peptone media. In general, cell ODs were found to be high in peptone-containing media and low in no-peptone media (ASW and NSW) for both species. Differences in growth rates between the

species were found, with *C. marina* growing faster. When comparing growth in ASW and NSW, *C. marina* showed higher ODs in just ASW (~0.6) as opposed to *M. hydrocarbonoclasticus* (~0.2) at the end point (42 h) indicating that planktonic cells of *C. marina* grow better in this medium (ASW). For biofilm growth after 42 h, the two species showed very different responses especially when grown in NSW without peptone. This suggests that *C. marina* and *M. hydrocarbonoclasticus* have different physiological adaptations to dramatic changes of the surrounding environmental conditions (from high peptone to no peptone containing media) with *C. marina* readily forming biofilm at high peptone concentrations as opposed to *M. hydrocarbonoclasticus* which grew the largest biofilm in just NSW.

These pilot experiments illustrated crucial differences in biofilm formation and growth between the two species. This is of importance since greater variety in inter-specific biofilm response to environmental stimuli may be proved useful in assessing antifouling / anti-biofilm strategies. By assessing the effect of an AF product against species with different responses, greater insights on the product's efficacy / mode of action can be inferred.

Overall, NSW and ASW media appear to give comparable data for both species and at all experimental conditions (also **Section 4.3**). Therefore, the use of ASW for laboratory-based experiments combines the necessary controlled environment but also importantly it closely simulates the natural growth conditions observed in NSW (with and without peptone). Thus, the ASW media and filtered sterilisation will be used in all future bioassay work associated within the wider EDA project.

4.4.2 LIVE/DEAD kit protocol optimisation

One of the most popular approaches for assessing AF and overall antimicrobial activity of a compound against biofilms is the use of nucleic acid stains that depend on cellular integrity. The most commonly used commercial kit LIVE/DEAD Bac*Light* contains two stains: 1) SYTO9, a green fluorescent intercalating membrane permeable stain and expected to stain all cells and 2) propidium iodide (PI), which is membrane impermeable and is known to stain cells with compromised membranes (Stewart and Franklin 2008). It is argued (by the manufacturers) that PI has a stronger affinity for nucleic acid and that, when stains are present within the cell, SYTO9 is displaced from the nucleic acid and the cells fluoresce in red. The advantages of this technique for assessing bacterial viability include: *i)* prompt data acquisition (within 1 h), *ii)* spatial resolution of live/dead cells within the biofilm (something that colony

forming units –CFUs cannot achieve), *iii)* identification of viable non-culturable cells, *iv)* localisation of cell-membrane integrity at the single-cell level and *v)* simple to use and commercially available (Stocks 2004; Stewart and Franklin 2008). Disadvantages of this technique have also been reported by various studies with the most common being the production of artefacts, such as the non-specific binding of PI and the simultaneous presence of both stains that have been shown to result in double counting of cells as dead and live (Stocks 2004; Biggerstaff *et al.* 2006; Berney *et al.* 2007a). For instance, PI may interfere with phosphates in buffers (manufacturer's instructions, FilmTracer™ LIVE/DEAD® Biofilm Viability Kit), which was indeed observed in the current work. This artefact was resolved by staining a sufficient number of controls (without bacteria) the readings of which were subtracted from the experimental replicas.

The choice of optimal filters to measure signals from the two stains, *i.e.* S9 and PI, is therefore crucial to ensure data reliability, since often the recommended filters (by the manufacturer and/or the literature) may not be suitable for all bacterial species. In **Figure 4.6** the fluorescence intensity from attached bacteria stained with the LIVE/DEAD components (separately and mixed) can be seen.

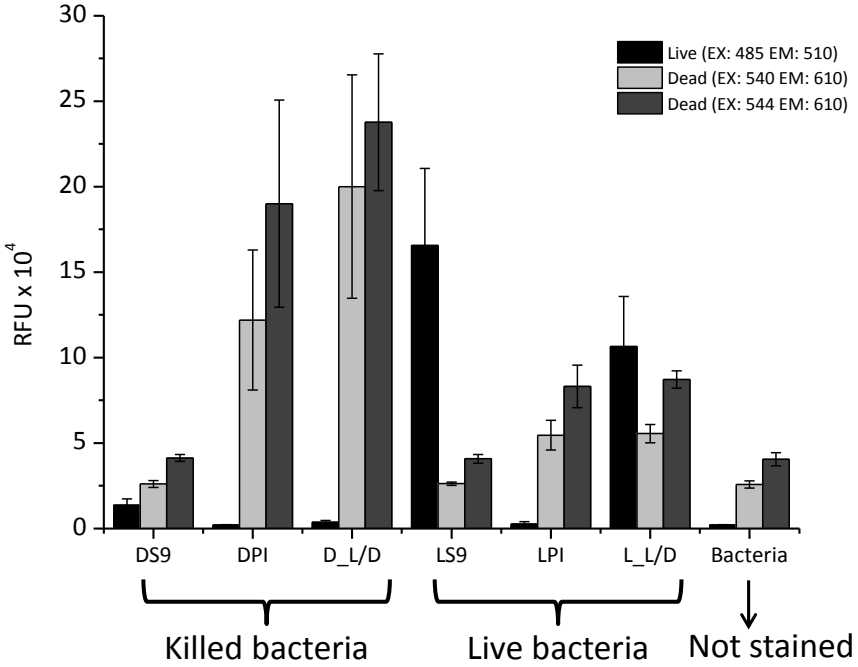

Figure 4.6. Plate-reader measurements at different excitation and emission wavelengths to assess biofilm viability where DS9, DPI and D_L/D signify 'killed' bacteria and stained with S9, PI and the LIVE/DEAD mixture (S9 and PI), respectively. Similarly, LS9, LPI and L_L/D signify the same combinations but this time bacteria are not killed. Units: Relative Fluorescence Units (× 10^5). Error bars ± STDEV.

For the 'killed' bacteria stained with S9, low intensity was received from the "live" wavelengths (λ_{EX} 485 nm, λ_{EM}: 510 nm) while, some signal was emitted from the "dead" wavelengths (λ_{EX}: 540 and 544 nm, λ_{EM}: 610 nm). However, when compared to the control i.e. not-stained bacteria, the intensity at the "dead" wavelengths are comparable, which indicates that the signal resulted from minor autofluorescence of the cells themselves. For the "killed" bacteria stained with just PI, both "dead" excitation/emission filters gave high signals while negligible signal was emitted from the "live" filters. The same was observed for the "killed" bacteria stained with the LIVE/DEAD (S9/PI) mixture (**Figure 4.6**). These results show that the filter sets sample the true signals from "killed" cells and there is neither overlapping of the readings between the two stains nor double counting.

For the "living" cells stained with just S9, increased signal was received at the "live" wavelengths while from the "dead" wavelengths, similar amount of intensities as the ones found on the non-stained cells (and "killed" stained with S9) was observed. As for the "living" bacteria stained with just PI, the two "dead" excitation filters produced slightly different results with the λ_{EX} = 544 nm illustrating higher values when compared to the λ_{EX} = 540 nm (almost no signal from the "live" wavelengths was observed). The same was observed for the "living" cells stained with the LIVE/DEAD kit (*i.e.* higher intensity values for the 544 nm compared with the λ_{EX} = 540 nm).

Additionally, following plate-reader sampling, epifluorescence microscopy was employed to verify the obtained data (**Figure 4.7**). It is clear that there is good correlation between the two techniques (r^2 = 0.933). From the results obtained using the LIVE/DEAD assay, it was decided that the filters for assessing biofilm toxicity will be, λ_{EX} / λ_{EM}: 485 nm / 510 nm, and 540 / 610 nm for the LIVE and DEAD, respectively.

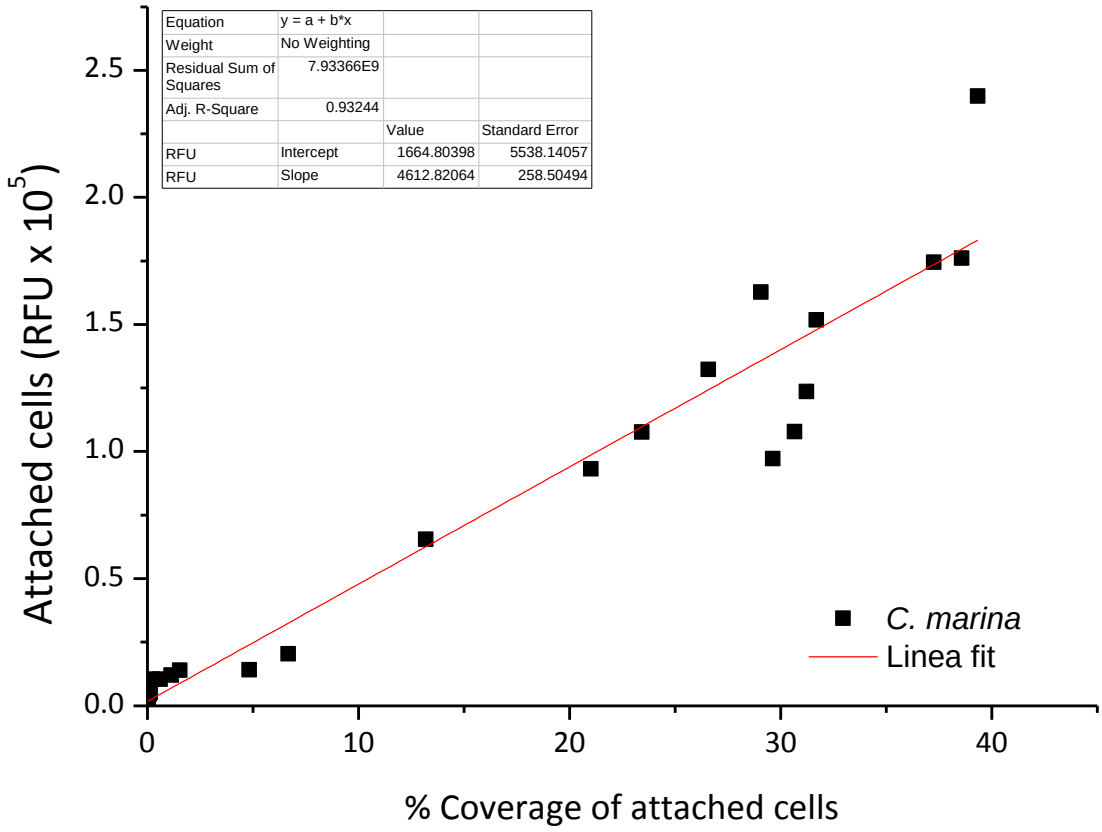

Figure 4.7. LIVE/DEAD kit evaluation using two techniques, where *y-axis* data obtained from the plate-reader as a function of fluorescence intensity (RFU) and *x-axis* same data obtained from epifluorescence microscopy where ImageJ analysis was utilised to calculate the percentage biofilm coverage on the 96-well plates.

4.4 Protocol review and summary

4.4.1 Staining techniques

Crystal violet (CV) staining is also a commonly used method (*e.g.* Staflien et al. 2006 2007) for bacterial biomass quantification. First described by Christensen et al. (1985), CV is a basic dye which binds to negatively charged surface molecules and polysaccharides in the EPS matrix (Li et al. 2003). Therefore, if biofilm viability needs to be addressed, CV is not suited to evaluate killing of biofilm cells, as it stains both live and dead bacterial cells as wells as the matrix (EPS) (Pitts et al. 2003). An alternative stain frequently used for assessing adherent bacteria is DAPI (4',6-diamidino-2-phenylindole) which binds to the AT-rich regions of double stranded DNA of vital and dead cells (Schwartz et al. 2003).

Although both CV and DAPI staining are frequently used in AF for assessing biofilm adhesion and overall formation, these stains require fixation of the cells. Fixation results in cell shrinkage while it is more time consuming as it requires more incubation steps. In contrast, Syto9 and PI are performed on living cells, typical incubation time is very short (~20-30 min), fluorescence measurements are conducted *in situ* and very importantly, uncompromised versus compromised cells can be distinguished.

4.4.2 Plate-reader technology

The use of multidetection plate-readers for quantifying bacterial biofilms has been increasingly used for AF studies. The assessment of planktonic and biofilm bacterial growth is frequently conducted using 96-well plates since the high well numbers facilitate the study of several molecules, with varying concentrations simultaneously and with a sufficient number of replication, verifying this way the experimental repeatability (Briand 2009). An additional advantage of the 96-well plate experiments is the use of small quantities of the test-molecule (maximum working volume in each well: 200 µL) which is crucial when assessing the AF efficacy of NPs that are often found to produce very small yields once extracted. Also, the sensitivity of the plate-reader has been proven to be sufficient for measuring fluorescence signals from as young as 1 h old biofilms, making the use of 96-well plates in corroboration to the plate-reader, a high-through put powerful platform for AF experiments.

Screening biofilm attachment and growth using the plate-reader provides a high throughput method to obtain quantitative data, however, in order to verify and/or calibrate

cell numbers or biofilm formation, direct microscopic observations are necessary. Typically, epifluorescence and CLS microscopy is used to acquire both quantitative and detailed qualitative information such as biofilm thickness, surface coverage, morphology and often EPS (*e.g.* Hall-Stoodley et al. 2004). Despite all the aforementioned advantages that microscopy provides, it can be a slow and not adapted for screening purposes assessment method (Leroy et al. 2007). Therefore, a combination of the two different methods, *i.e.*: 1) plate-reader as a high throughput screening technique and 2) microscopy for verification and a detailed data acquisition of samples of interest, is ideal for AF assays. In addition, plate-reader data can be calibrated against epifluorescence microscopy or flow-cytometry. Flow cytometry is a technique which permits the characterisation of individual cells in populations, in terms of distributions in their properties such as DNA content, protein content, viability, enzyme activities (Berney et al. 2007b).

4.4.3 Protocols: general literature observations

In **Sections 4.5** and **4.6**, the protocols for bacterial growth and biofilm formation were presented. The ASW chosen for bacterial growth simulated the average world sea water salinity, 35 (35 g/kg). In studies where ASW is used, as opposed to NSW, salinities range between 38-40 (*e.g.* Stafslien et al. 2006, Stafslien et al. 2007, D'Souza et al. 2010), which we believe is not representative of real sea water conditions. Also, in a high-throughput methodology developed for fouling-release coating screening, biofilms were washed using deionised water prior staining with CV to remove planktonic cells (Staflien et al. 2007). Generally, Gram-negative marine bacteria experience physiological stress and may even undergo cell lysis on transfer from seawater to low ionic environments, *i.e.* deionised/distilled water (*e.g.* De Voe and Oginsky 1969; Gauthier et al. 1992). Thus, the choice of deionised water as washing medium is not appropriate for the purpose of AF bioassays that investigate attachment patterns (attachment might be significantly influenced by the addition of deionised water).

Chapter 5

5. Antifouling performance against marine bacterial attachment for three natural products: *Chondrus crispus* extract, usnic acid and juglone

5.1 Brief introduction

In the current chapter, three NPs were investigated for their AF performance against two model biofilm forming bacteria (*Cobetia marina* and *Marinobacter hydrocarbonoclasticus*). Crude extracts of the red seaweed *Chondrus crispus* is the marine natural product tested while the terrestrial natural products are the pure compounds (+)-usnic acid and juglone. The terrestrial products chosen for their AF potential, have previously demonstrated antibacterial properties, however, their activity against marine species is reported for the first time in this current work.

The objectives of this work were firstly to develop a new bioassay to allow a rapid *in situ* assessment of newly attached bacteria using microtiter plates combined with nucleic acid staining and plate reader technology. Despite the frequent use of nucleic acid staining in medical settings, there is sparse application of such methodologies for the evaluation of marine biofilms. Secondly, to use this novel bioassay approach for the evaluation and/or screening of two NPs as environmental friendly compounds and one crude extract from a marine source that could potentially be used as natural anti-biofilm agents. The investigation demonstrates the proof-of-concept for a rapid assessment method that has the potential to be used for a broad range of anti-biofilm studies, where the initial attachment is of primary importance.

5.2 Materials and methods

5.2.1 Natural products

Dried commercially available *C. crispus* (Carrageen, supplied by Carraig Fhada Seaweed, Ireland) was used for preparing natural product extracts according to Chambers et al. (2011). A 50 g sample of the dried seaweed was soaked in 500 mL of absolute ethanol (Fisher AR Grade) for 15 minutes. This rendered the seaweed brittle as any remaining traces of water were extracted, so that the fronds were more easily and uniformly crushed. The crushed seaweed in absolute ethanol (Fisher AR Grade) was then finely pulverised using a Silverson high shear lab mixer. A general purpose disintegrating head utilising firstly a coarse screen, followed by a fine high shear screen was used. Disintegration was carried out for approximately 5 minutes at speeds of up to 5,000 rpm, taking care not to let the ethanol temperature rise above 35 °C. This produced a seaweed particle size of approximately ≤ 1 mm. The suspension was left to macerate for 30 minutes with occasional stirring, and then filtered under vacuum through a 0.2 µm glass filter (Whatman Anodisc 47). The filtered ethanolic seaweed extract was then evaporated to dryness using a rotary evaporator (Buchi Rotavapor R-210) at below 35 °C.

The following final extraction steps were conducted according to a method reported by MAPIEM (Personal Communication). Toluene solvent (Fisher AR Grade) was added to the green/brown residue. This solvent readily dissolved the bulk of the material leaving a small amount of white insoluble residue which was discarded. The toluene was then removed from the combined washings under vacuum using the rotary evaporator at a bath temperature of ≤ 35 °C. The residual solvent-extracted product was a dark greenish-brown semi-solid residue designated, *C. crispus* toluene, CCT. The ^{1}H NMR spectrum of *C. crispus* was recorded in chloroform-d (Sigma-Aldrich, 99.96 atom % D) using a Bruker DPX400 NMR spectrometer at 400 MHz.

Both juglone and usnic acid were purchased from Sigma-Aldrich® (AR grade, catalogue numbers H47003 and 329967, respectively). The current work has only investigated the (+)-usnic acid form.

5.2.2 Marine bacteria species and culture conditions

The marine biofilm forming species used in this study were *Cobetia marina* (ATCC 25374) and *Marinobacter hydrocarbonoclasticus* (ATCC49840). The culture conditions have been detailed in **Chapter 4** (**Section 4.2.2**).

5.2.3 Attachment Bioassays

The 96-well microplates (optical bottom plated with polymer base, black, Nunc ™) were inoculated with 200 µL of ASW for 1 h prior to bacterial inoculation in order to condition the wells. The choice of ASW as experimental medium was chosen as several studies have demonstrated that initial attachment is triggered by starvation conditions in the surrounding environment, such as the oceans and low nutrient waters (*e.g.* reviewed by Brading et al. 1995). After 1 h, the wells were emptied and 199 µL of the prepared bacteria (washed according to the previous section and re-suspended in ASW at OD_{595} = 0.2) were inoculated at each well. In order to fully dissolve the natural products (NPs), 100 % dimethyl sulfoxide (DMSO) was used as solvent to produce a stock solution of 40,000 ppm while serial dilutions in DMSO (100 vol. %, all percentages by volume) followed to give the final concentrations listed in **Table 5.1**. The NP concentrations used in the current study are comparable with those reported in the antifouling literature, typically in the order of 1 ppm to 1000 ppm (Fay et al. 2010, Camps et al. 2011). A 1 µL aliquot from each NP stock solution was added to the wells to result in a final well volume of 200 µL. Using the NP dissolved in a small volume (1 µL) of DMSO was found to be the preferred option as it allowed a very low final DMSO concentration (0.5 %) in the wells. DMSO can be bacteriostatic at high concentrations of 12.5-20% (*e.g.* Jacob et al. 1964, Wood and Wood 1975), therefore the lower its concentration, the lower the risk of bacterial toxicity due to this solvent, rather than the NP itself. Control wells containing no NP validated that 0.5 % of DMSO did not affect bacterial attachment.

Table 5.1. Natural products (NP) used to assess bacterial attachment where, JUG = juglone, UA = usnic acid, CCT = *C. crispus* toluene soluble. Units: ppm = µg mL^{-1}.

NP	Concentration (ppm)
CCT	0.1, 5, 10, 20, 50, 100, 200
UA	0.1, 5, 10, 20, 30, 40
JUG	0.1, 5, 10, 20

Each NP concentration was replicated 5 times and with 3 wells containing NPs but no bacteria (blanks). Controls included: bacteria in ASW and bacteria in ASW plus 0.5 % DMSO. Following bacteria inoculations and NP additions, the 96-well plates were incubated for 1 h at 28 °C under static conditions. The attachment assays were carried out for 1 h so as to reduce any effect of crowding and aggregation of bacterial cells and to prevent 3D biofilm formation (D'Souza et al. 2010).

After the incubation time, OD_{595} measurements were taken to establish the planktonic growth and no significant differences were found between the treatments ($p \leq 0.05$). Then all suspensions in the 96-well plates were removed and each well was individually rinsed (by pipetting) twice with ASW in order to remove any planktonic cells. Staining with FilmTracer™ LIVE/DEAD® Biofilm Viability Kit followed (as discussed in **Section 4.2.4**), to achieve bacterial attachment quantification. In addition, the well scanning capability of the microplate reader was used for visualizing newly attached biofilms/bacteria in individual wells allowing identification of heterogeneous biofilm structures and their distribution (*e.g*. whether there is marked attachment on the well walls, which is often considered an issue in well plate assays). Each well, was scanned to produce an image of the newly attached formations (scan matrix dimension: 30 × 30 equivalent to a resolution of 213 μm × 213 μm, and a scan width of 6 mm). The main advantage of the imaging utility is the direct observation of biofilm formation *in situ*, which was sufficiently sensitive to identify biofilm features, providing in this way a measurement which is representative of the entire well. The percentage of attachment reduction ($R\%$) was determined by the following expression:

$$R\% = \left(\frac{(Con - Exp)}{Con} \right) \times 100 \qquad [5.1]$$

Where, *Con* = control (*i.e.* no compound added) and *Exp* = experimental (*i.e.* with compounds).

5.2.4 Statistical analysis

Differences in OD_{595} and RFU values between experimental and controls were assessed by applying one-way ANOVA. To establish the homogeneity of variances, Levene's test of equal variances was applied. Where homogeneity of variances was not met the non-parametric Kruskal-Wallis test was applied. Statistical analysis was performed using SPSS software (version 17.0). Differences were considered statistically significant for $p < 0.05$.

5.3 Results and Discussion

Generally, screening assays for novel AF compounds are separated into two categories; toxicity and AF assays (Dahms and Hellio 2009). Toxicity is examined using the Lethal Concentration 50 (LC_{50}) where the concentration to kill 50 % of the organisms is used an indicator of the compound's acute toxicity. Another routinely used assay is the Effective Concentration 50 (EC_{50}) where 50 % of the organisms are affected when administrated in a concentration response manner. Increasingly, there is evidence that active compounds affect organisms at non-toxic concentrations (Maximilien et al. 1998b), hence, the necessity for more insightful AF testing. In future AF assays should also focus on the mechanisms by the organisms, for instance biological, chemical, physical and behavioural, that facilitate their initial attachment / adhesion / colonization onto a surface (Briand 2009, Dahms and Hellio 2009)).

Recently, few bioassays have reported the use of plate-readers (microtiter plate assays) in conjunction with stains to measure biofilm inhibition of adhesion and/or growth within an antifouling context (Leroy et al. 2008, D'Souza et al. 2010, Camps 2011). Frequently, the use of crystal violet (CV) is used to quantify total biofilm biomass on antifouling surfaces (Stafslien et al. 2006, 2007a,b,c). CV is a basic dye which binds to negatively charged surface molecules and polysaccharides in the EPS (Christensen et al. 1985, Li et al. 2003). Although this is a rapid and reproducible technique to assess biofilm growth, the analysis is conducted by colorimetric means where acetic acid is used to extract the CV retained by the biofilm. Also, CV could possibly stain particulates deriving from the paint or any material tested. Nucleic acid stains such as DAPI (Leroy et al. 2008, Camps et al. 2011) as well as Syto13 (D'Souza et al. 2010) are recently being employed to assess biofilm adhesion and growth. The use of DAPI requires cells fixation (formaldehyde) and the addition of EtOH to achieve the stain's solubilisation at the final stage where the plate reader is used to measure the fluorescence intensity obtained from the solution (*e.g.* Leroy et al. 2007). Both CV and DAPI staining require fixation of the cells which often results in cell shrinkage while it is more time consuming as it requires more incubation steps (*e.g.* Hannig et al. 2010). Thus, any information on the biofilm structure or colonisation patterns and/or morphotypic variation of the biofilm is lost.

In this current study, the attached bacteria were stained with the nucleic acid stain Syto9 and the *in situ* non-intrusive quantification was determined for the newly attached biofilms (on the well bottom). The use of the well-scanning function of the plate reader allowed the highest possible sampling resolution (213 × 213 μm) in each well, thereby (*i*)

providing a highly representative quantification of the attached cell clusters and (*ii*) facilitating the identification of biofilm structural features and attachment patterns. For instance, studies conducted on biofilm adhesion on FR-coatings (Stafslien et al. 2007b), demonstrated that although the overall biofilm biomass did not change between the FR coatings and the control, visual observations illustrated that biofilm had significant surface coverage reduction on the FR coatings (the biofilm retracted). This demonstrates the necessity of *in situ* (and spatial) quantitative measurements in order to assess potential anti-biofilm effects. Also, the time scales of most published adhesion bioassays typically range from a minimum of 3 h to a maximum of 24 h (Leroy et al. 2008, D'Souza et al. 2010, Camps 2011). In this study, the initial attachment was evaluated within 1 h which was found to be sufficient to allow quantification, thus demonstrating the high sensitivity of the method.

5.3.1 *Chondrus crispus* extracts and bacterial attachment

The ^{1}H NMR spectrum indicates a high content of aliphatic carbon chains with features typical of fatty acid esters (triglycerides) and a small amount of unsaturation (see **Figure 5.1**). However, the analysed sample consists of a crude mixture of compounds to which it is not possible to assign any specific chemical structure. No signals were observed at chemical shifts (δ) above 8 ppm, indicating a lack of free carboxylic acid groups (δ > 10 ppm). Fresh *C. crispus* has been shown to contain high levels of polyunsaturated fatty acids (Trevor 1989) so the apparent lack of unsaturation could result from the extended air drying process that the seaweed has been subjected to.

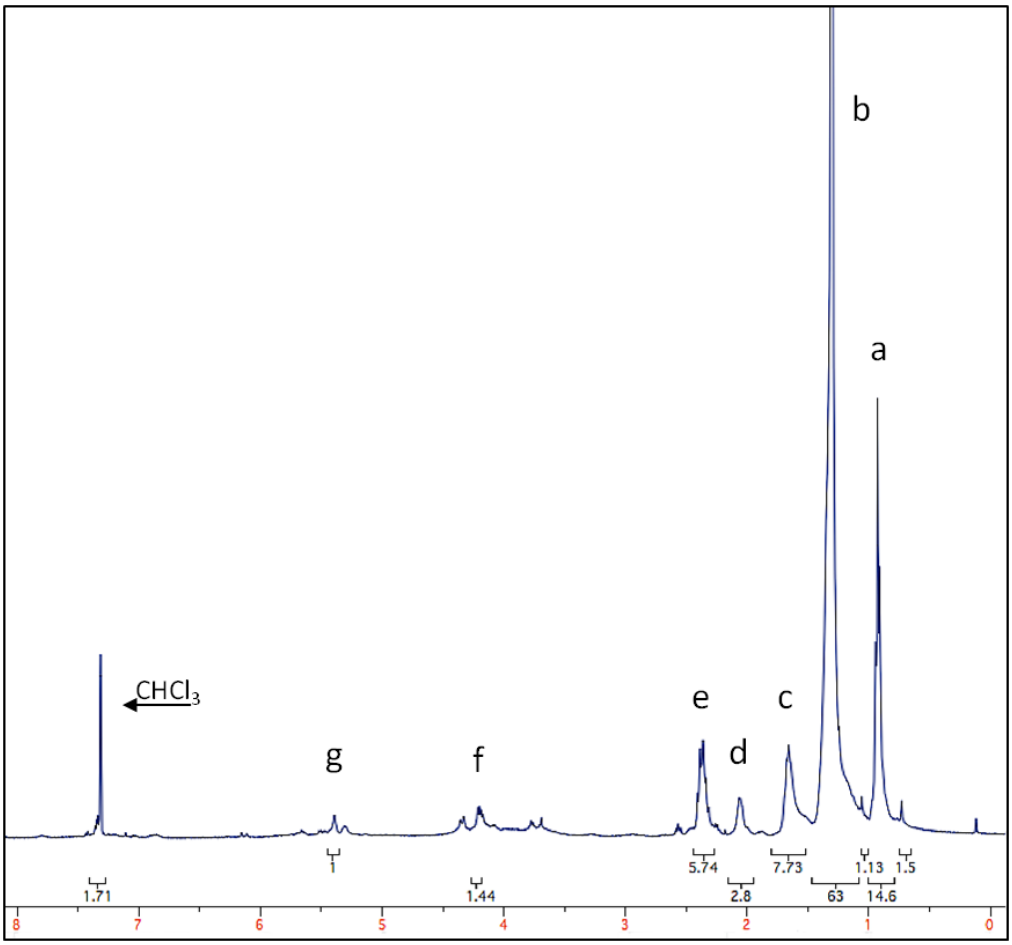

Figure 5.1. ^{1}H NMR spectrum of the *C. crispus* organic extract.

Major peak assignments (Guillén 2002) referenced to $CHCl_3$ at δ = 7.28 ppm are:

a	0.896	-C**H**$_3$
b	1.272	-(C**H**$_2$)n-
c	1.625	-OCO-CH$_2$-C**H**$_2$-
d	2.027	-C**H**$_2$-CH=CH-
e	2.331	-OCO-C**H**$_2$-
f	4.168	-C**H**$_2$-OCOR
g	5.360	-C**H**=C**H**-

Triglycerides are not known to exhibit marked AF effects therefore any anti-biofilm activity observed could be due to constituents of the crude extract not identifiable from this spectrum.

Figure 5.2a shows the attached biofilm in the individual wells (only one replica shown here) and their spatial distribution with respect to NP concentrations. There appears to be an edge effect where the fluorescence signal (signified by purple-blue colours) appears to be low at the well edges, indicating less bacteria attachment; while most of the signal is deriving from the centre of the wells in a circular-elliptical manner for both species. Overall, for the *C. crispus* extract – CCT– attachment of *M. hydrocarbonoclasticus* was significantly increased when exposed to the CCT concentration of 20 ppm ($p < 0.001$). However, there was significant reduction when *M. hydrocarbonoclasticus* was exposed to the higher CCT concentrations of 100 ppm and 200 ppm ($p < 0.001$ and $p < 0.016$ respectively; **Figure 5.2b**). For *C. marina*, attachment was significantly higher at low CCT concentrations, *i.e*. 0.1 ppm, 5 ppm, 10 ppm and 20 ppm ($p < 0.010$, $p < 0.002$, $p < 0.001$ and $p < 0.001$, respectively; **Figure 5.2b**). However, at the higher concentrations of 50 ppm, 100 ppm and 200 ppm, attachment was significantly inhibited ($p < 0.010$, $p < 0.020$ and $p < 0.031$, respectively; **Figure 5.2b**). Although the overall accumulation for *C. marina* was reduced at high CCT concentrations, a dose response was not observed, suggesting that this species was only affected by CCT concentrations between 20 ppm to 50 ppm and above (**Figure 5.2b**). The overall maximum attachment reductions were 35 % and 50 % for *M. hydrocarbonoclasticus* and *C. marina*, respectively (**Figure 5.2c**).

The reverse concentration response of enhanced *M. hydrocarbonoclasticus* and *C. marina* attachment at low CCT concentrations (**Figure 5.2**), may be explained by the presence of hydrocarbons and fatty acids typically found in seaweeds, such as *C. crispus* – that may have been used by both species as sole carbon source (Bauman et al. 1972, Gauthier et al. 1992) – potentially leading to biofilm proliferation. In nature, the nutrient concentrations within the biofilm may become depleted due to consumption and diffusion (*e.g*. Riber and Wetzel 1987, Burkholder et al. 1990), to overcome this limitation, epiphytic bacteria can consume algal exudates, while the algae may benefit from the recycling of nutrients performed by the bacteria, including carbon (*e.g*. Wetzel 1993). This beneficial mutual relationship between bacteria and the algae is reported to result in a high bacterial activity (Haack and McFeters 1982, Kirchman et al. 1984, Neely and Wetzel 1995). Interestingly and in agreement with the current work, Cox et al. (2010) have also recently reported that a methanolic *C. crispus* crude extract enhanced both Gram-negative and Gram-positive bacterial growth of *Listeria monocytogenes*, *Salmonella abony*, *Enterococcus faecalis* and *Pseudomonas aureginosa*.

The AF efficacy of *C. crispus* crude extracts has been previously reported (*e.g.* Hellio et al. 2000b, Hellio et al. 2004, Cox et al. 2010, Chambers et al. 2011), however, the active

components have yet to be identified as the various NP extracts were not fully fractionated and assessed. Tannins are found in *C. crispus* extracts (Cox et al. 2010) and these are known to act against fouling organisms, such as barnacles (*e.g.* Stupak et al. 2003). An alternative antimicrobial mechanism has previously been proposed by Sullivan and Ikawa (1973), who isolated and purified the enzyme hexose oxidase from *C. crispus* (Sullivan and Ikawa 1973, Hansen and Stougaard 1997, Savary et al. 2001). Hexose oxidase is a copper-containing glycoprotein that catalyzes the chemical reaction (Equation 5.2):

$$\text{D-glucose} + O_2 \rightleftharpoons \text{D-glucono-1, 5-lactone} + H_2O_2 \qquad [5.2]$$

Metal component analysis of the enzyme has shown a copper content of 0.11 %, *i.e.* equivalent to 1100 ppm. Copper is known to be toxic to a variety fouling organisms (*e.g*. Howell et al. 2009) therefore it may be hypothesised that the presence of hexose oxidase in *C. crispus* could negatively affect *M. hydrocarbonoclasticus* because of its copper content. Also, the enzymatic generation of hydrogen peroxide (H_2O_2) has been shown to have a promising AF efficacy (Kristensen et al. 2010, Olsen et al. 2010). However, in this current study, the use of toluene as a solvent would possibly limit the enzyme extraction.

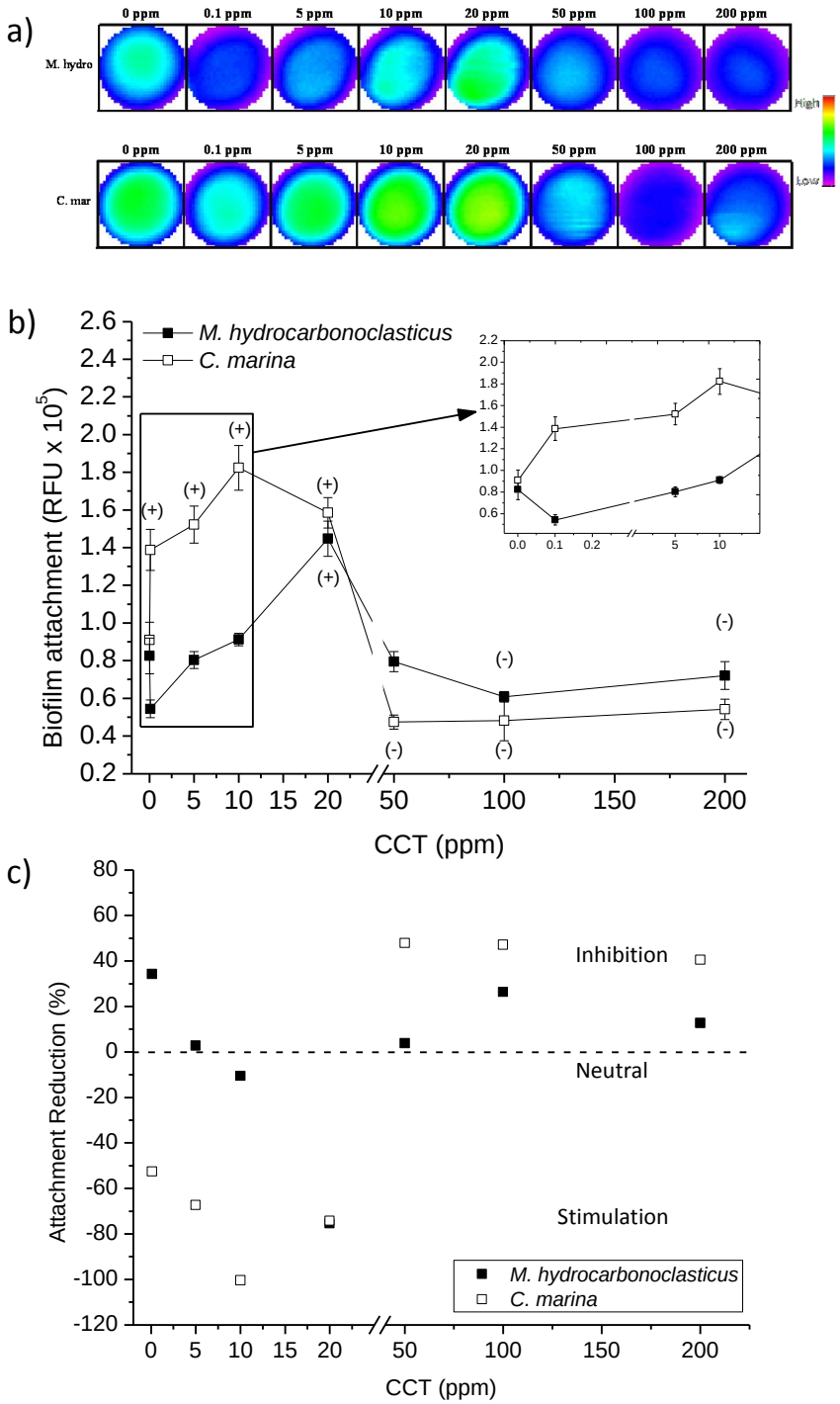

Figure 5.2. The performance of *C. crispus* on *C. marina* and *M. hydrocarbonoclasticus* biofilm accumulation where: (a) is the well scan images of individual wells (scan matrix dimension: 30 × 30 equivalent to a resolution of 213 µm × 213 µm, scan width 6 mm); (b) end point fluorescence intensity (Units: relative fluorescent units, RFU). Positive / negative (+/-) symbols indicate significant increase (+) or decrease (-) in attachment of the species when compared with the control at 95% confidence intervals. Syto9: λ_{EX} = 485 nm, λ_{EM} = 510 nm. Error bars ± STDEV; (c) attachment reduction according to RFU values, as a percentage of the control (0 %, dashed line), where negative values indicate increased attachment and positive values inhibition.

Overall, these results suggest that CCT can act as both an attachment promoter, as well as an inhibitor depending on the NP concentration. This is supported by recently published studies where it was reported that at high concentrations, antibiotics eradicate bacteria, while at low concentrations biofilm formation is induced (*e.g*. Hoffman et al. 2005, Linares et al. 2006); this phenomenon is often termed as a hormetic response within the medical and toxicological context (*e.g.* Calabrese 2001).

5.3.2 Usnic acid and bacterial attachment

The well scans in **Figure 5.3a** show more prominent localised bacterial features especially for *M. hydrocarbonoclasticus* indicating patchy attachment patterns at 0 – 10 ppm concentrations. For *C. marina*, bacterial attachment is localised mainly at the centre of the well and radiates out towards the edges (**Figure 5.3a**). Overall, the bacterial attachment bioassays demonstrated that *M. hydrocarbonoclasticus* was not affected by the addition of usnic acid at the low concentrations of 0.1 ppm, 5 ppm, 10 ppm and 20 ppm. However, bacterial attachment was significantly inhibited in a concentration response manner by usnic acid at concentrations 30 ppm and 40 ppm ($p < 0.022$ and $p < 0.001$, respectively; **Figure 5.3b**). The highest usnic acid concentration caused the highest attachment reduction (65 %) of all NPs tested in the current study for *M. hydrocarbonoclasticus* (Figure 4c). The effect of usnic acid on marine bacteria has not been reported previously. According to the literature, this compound is mostly active against Gram-positive species with little evidence of antimicrobial efficacy against Gram-negative bacteria (Lauterwein et al. 1995). The current results illustrate the first evidence of the effect of usnic acid on bacterial attachment for the Gram-negative marine bacterium *M. hydrocarbonoclasticus*. For *C. marina*, no inhibitory effect was observed (**Figure 5.3**), rather an enhancement at almost all concentrations with an up to 110 % increase in attachment for 0.1 ppm to 10 ppm (**Figure 5.3c**). These contradictory results between species emphasize the importance of including a range of different bacterial species for AF screening purposes.

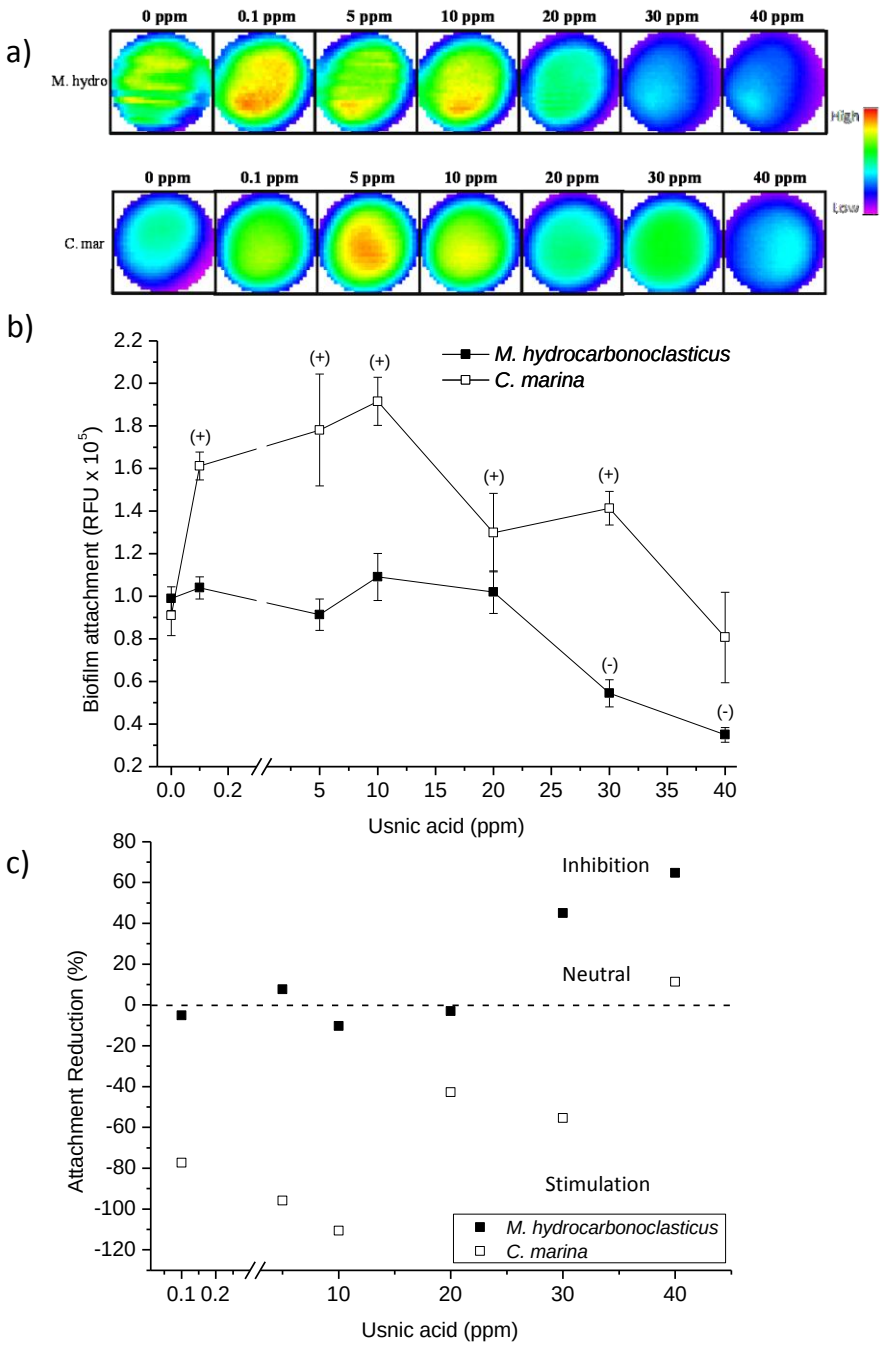

Figure 5.3. The performance of usnic acid on *C. marina* and *M. hydrocarbonoclasticus* attachment where: (a) is the well scan images of individual wells (scan matrix dimension: 30 × 30 equivalent to a resolution of 213 µm × 213 µm, scan width 6 mm); (b) end point fluorescence intensity (Units: relative fluorescent units, RFU). Positive / negative (+/-) symbols indicate significant increase (+) or decrease (-) in attachment of the species when compared with the control at 95% confidence intervals. Syto9: λ_{EX} = 485 nm, λ_{EM} = 510 nm. Error bars ± STDEV; (c) attachment reduction according to RFU values, as a percentage of the control (0 %, dashed line), where negative values indicate increased attachment and positive values inhibition.

Usnic acid is a secondary lichen metabolite that possesses antimicrobial activity against a number of planktonic Gram-positive bacteria (*e.g*. Ingólfsdóttir 2002) as well as antiviral activity. Although the mechanism of action of usnic acid against bacteria is still unknown, experimental evidence has illustrated that its antiviral activity is due to its ability to inhibit RNA transcription (Campanella et al. 2002). (+)-Usnic acid and its isomer (-)-usnic acid have been shown to be active against clinic isolates of *E. coli* and *E. faecium* (MIC: 16 ppm) and clinical isolates of methicillin- or muporicin-resistance *Staphylococcus aureus* (MIC: 16 ppm, Lauterwein et al. 1995). In the same study, it was shown that both isomers exhibited profound activity against pathogenic anaerobic Gram-negative *Bacteroides* sp. (MIC: <16 ppm) and anaerobic Gram-positive bacteria (*Clostridium* MIC: 4 ppm and *Propionibacterium* sp. MIC: 2 ppm). Also, Francolini et al. (2004) reported an MIC of 32 ppm for *S. aureus* while the Gram-negative *Pseudomonas aeruginosa* showed an MIC at 256 ppm. In the same study, the effect of usnic acid (loaded on a polymer) on initial bacterial attachment using flow cells was assessed for *S. aureus* and *P. aeruginosa*; it was found that this NP did not affect biofilm formation for *P. aeruginosa*, however it significantly affected biofilm morphology (shape and thickness), indicating that the molecule may have interfered with signalling pathways. The usnic acid did not prevent initial attachment of *S. aureus*, however, this species exhibited a different response of high cell mortality and therefore significant biofilm reduction.

5.3.3 Juglone and bacterial attachment

In **Figure 5.4** the performance of juglone is shown to give a clear concentration response effect inhibiting *M. hydrocarbonoclasticus* attachment at 5 ppm, 10 ppm and 20 ppm ($p < 0.007$, $p < 0.005$ and $p < 0.004$, respectively; **Figure 5.4a and 5.4b**). The well scans for M. hydro illustrate uniform attachment patterns, with the exception of bacteria at the highest juglone concentration (20 ppm), where attachment can be characterised as slightly clustered (**Figure 5.4a**). Similarly, *C. marina*'s attachment was significantly reduced by juglone in a concentration response manner at 10 ppm and 20 ppm ($p < 0.050$ and $p < 0.035$, respectively; **Figure 5.4b**). At the lowest juglone concentration (0.1 ppm) there is an increase in attachment (although not statistically significant) for both species. Overall, at the highest concentrations, this NP inhibited attachment by about 45 % and 55 % for *M. hydrocarbonoclasticus* and *C. marina*, respectively (**Figure 5.4c**). The current study reports, for the first time, the use of juglone against marine biofilm forming bacteria, and illustrates an activity against bacterial

attachment. In the context of AF strategies against marine biofilms, juglone appears to be a promising compound which will be further investigated.

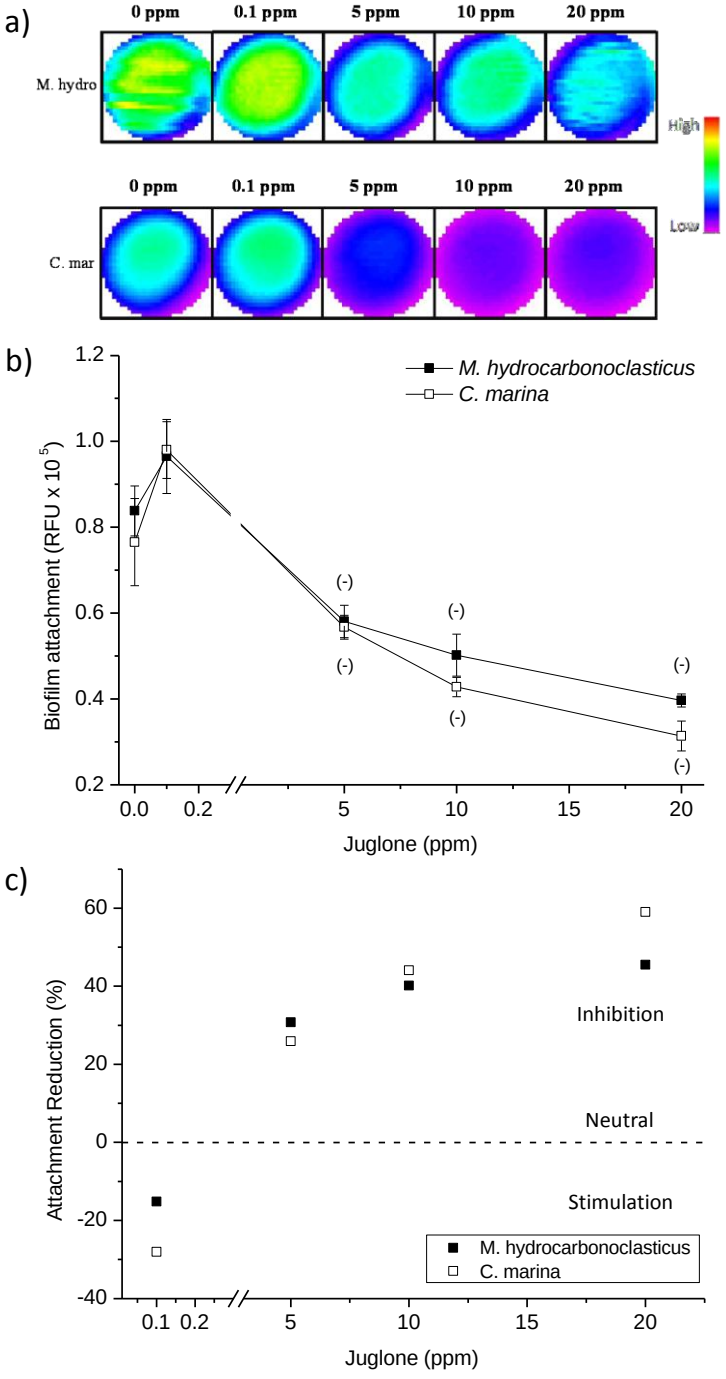

Figure 5.4. The performance of juglone on *C. marina* and *M. hydrocarbonoclasticus* attachment where: (a) is the well scan images of individual wells (scan matrix dimension: 30 × 30 equivalent to a resolution of 213 µm × 213 µm, scan width 6 mm); (b) end point fluorescence intensity (Units: relative fluorescent units, RFU). Positive / negative (+/-) symbols indicate significant increase (+) or decrease (-) in attachment of the species when compared with the control at 95% confidence intervals. Syto9:

λ_{EX} = 485 nm, λ_{EM} = 510 nm. Error bars ± STDEV; (c) attachment reduction according to RFU values, as a percentage of the control (0 %, dashed line), where negative values indicate increased attachment and positive values inhibition.

Juglone is related to the naphthoquinone family of organic compounds and occurs naturally in the leaves, roots, husks, and bark of the walnut family, particularly the black walnut tree (*Juglans nigra* L.). Juglone is widely reported to be growth-stunting to many plants types where it exerts an allelopathic effect by inhibiting specific enzymes needed for metabolic function (Soderquist 1973). Such quinone type compounds have been widely identified and used as anticancer, antibacterial or antimalaria drugs, and also as fungicides and herbicides (reviewed by O'Brien 1991). Additionally, herbal preparations derived from juglone extracts have been used as hair dyes and skin colorants in addition to being applied topically for the treatment of acne, inflammatory diseases, ringworm, fungal, bacterial, or viral infections. Their therapeutic effect has been attributed to quinone cytotoxicity (Inbaraj and Chignell 2004). The overall toxicity mechanism of naphthoquinones has still not been clearly established, especially for prokaryotes. However, in general, juglone is classified as a strong redox cycler with high potential to react with oxygen and its reactive species. Therefore, it interferes with vital cell processes such as respiration, photosynthesis, cell division, and membrane transport (Bertin et al. 2003, Chobot and Hadacek 2009).

The antimicrobial activity of naphthoquinones has been reported in several studies (*e.g*. De Haan and Charles 1969, Riffel et al. 2002, Tran et al. 2004, Wright et al. 2007, Jeon 2009). Juglone has been shown to act against the marine bioluminescent species, *Vibrio fischeri* and the dinoflagellate *Glenodinium folieaceum* (Wright et al. 2007). Using the Lumitox® assay for *V. fischeri* (where reduction of bioluminescence is linked to the inhibition of cellular activity as a decreased rate of respiration), juglone exhibited bactericidal activity at concentrations as low as 0.005 ppm. In another study, the same naphthoquinone (5 hydroxy-1, 4-napthoquinone) extracted from the heartwood of *Caesalpinia sappan* exhibited a good antibacterial performance against the intestinal Gram-positive bacterium, *Clostridium perfringens* (Lim et al. 2007).

In addition, two commercially available biocides (diuron and tolyfluanid) were tested against biofilm formation of two marine species, namely *Pseudoalteromonas* sp. and *Vibrio vulnificus* (Fay et al. 2010) and it was found that the biocides inhibited cell attachment at concentrations of 10 ppm. These inhibitory concentrations are slightly higher from the anti-

biofilm effect of juglone found in the current work (5 ppm), illustrating this way, the good potential of this compounds as alternative to currently prohibited biocides (such as diuron and tolyfluanid).

5.3.4 Physico-chemical parameters of the two terrestrial compounds

A compound's solubility in water needs to be known. Most frequently, this parameter is estimated by means of quantitative structure/activity relationships based on the log octanol-water partition coefficient (log K_{ow}). It is an important parameter used in the assessment of environmental fate and transport of organic chemicals because the octanol phase is a surrogate for the lipid phase or organic carbon content of the environmental compartments. For comparison, the physical chemistry parameters relating to solubility for the two terrestrial compounds and five organic antifouling biocide molecules that are approved under the Biocidal Products Directive 98/8/EC were calculated using the online version of ACD/Labs Algorithm Version: v5.0.0.184 (see **Table 5.2**), (https://ilab.acdlabs.com/iLab2/).

Table 5.2. Calculated Physico-chemical parameters for NPs used in the current work and approved commercial biocides.

Parameters	Usnic acid	Juglone
Solubility[1] (ppm)	420*	160*
LogP[2]	2.29 (RI = 0.63)	1.85 (RI = 0.88)
pKa1[3]	5.3 ± 0.8	9.5 ± 0.4
pKa2[3]	9.0 ± 0.9	
pKa3[3]	12.0 ± 0.9	
LogD at pH 8.2	-0.65	1.83

Parameters	Tolylfluanid	Dichlorfluanid	DCOIT (SeaNine™)	Cybutryne
Solubility[1] (ppm)	39	58	63	390
LogP[2]	3.58 (RI = 0.82)	3.32 (RI = 0.80)	4.59 (RI = 0.62)	3.45 (RI = 0.75)
pKa1[3]	-5.06 ± 0.5	-5.37 ± 0.5	-6.09 ± 0.6	4.12 ± 0.1
pKa2[3]	-16.79 ± 0.7	-16.89 ± 0.7		-2.55 ± 0.2
pKa3[3]				
LogD at pH 8.2	3.58	3.32	4.59	3.45

[1] in pure H_2O; [2] (AB/LogP v2.0); [3] ACD Labs algorithm. *the calculated solubility for both NPs (in deionised water) appears to be much higher than observed in the current work and in the literature (e.g. Kristmundsdottir et al. 2005). The solubility of usnic acid in water is highly dependent on pH which may not have been controlled in practical studies.

LogP (also referred to as log K_{ow}) is the logarithm of the partition coefficient of the unionised compound between octanol and water phases at equilibrium. LogD is the logarithm of the distribution coefficient of an ionisable compound between octanol and water phases at defined pH values. The pKa parameter is the negative logarithm of the acid dissociation constant. Calculated logD values for juglone and usnic acid over the pH range of 0 – 12 are plotted in **Figure 5.5**. Partitioning of juglone into the water phase is low below pH 9, while the more easily ionized usnic acid increasingly enters the water phase at pH > 5. At seawater pH (average seawater pH 8.2) usnic acid is predominately partitioned into the water phase, while juglone remains in the octanol phase. For polystyrene microtiter plates adsorption of lipophilic organic substances on to the well walls will occur depending on the logP and/or logD values. Generally, it is considered that chemicals with a logP of greater than 3 should be regarded as problematic within microtiter assays depending on the stability of the concentration over the experimental timescales (Reidl and Altenburger 2007, Schreiber et al. 2008). Although both NP compounds have logD values at pH 8.2 lower than 3 (-0.65 and 1.83 for usnic acid and juglone, respectively), there is greater potential for juglone to have adsorbed on to the well surfaces to some extent, changing the concentration within the ASW.

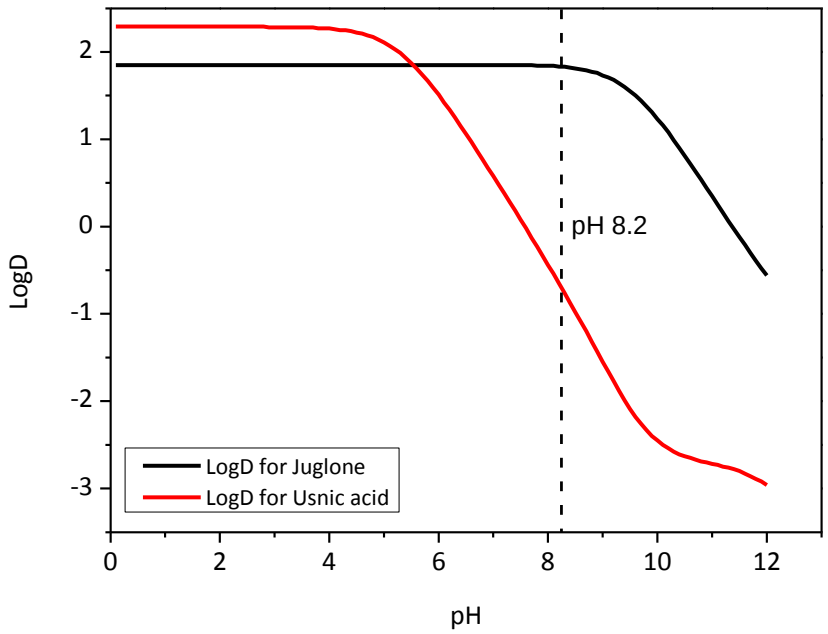

Figure 5.5. LogD values for juglone and usnic acid, where the dashed line signifies the pH value at 8.2 (average sea water pH).

The logP of 1.83, indicating a higher degree of hydrophilicity for juglone than for the commercial biocides, suggests that it has a lower potential for bioaccumulation and adsorption to sediments following release into the marine environment as reported by Wright et al. (2007). In addition, the persistence of juglone has been shown to be dependent on the sterile status and light / dark conditions, for instance a half-life of 12.7 h in sterile illuminated estuarine water *vs*. 87 h in non-sterile and dark conditions. By contrast, previously used commercial biocides such as Diuron and Irgarol have half-lives of 14 and 250 days, while their logP values are 2.8 – 3.95 and 2.8, respectively (Thomas 2001, Thomas and Brooks 2010). LogP, although it does not take pH into account, is often used as a relative indicator of the tendency of an organic compound to adsorb into marine sediments. Juglone, with a relatively low logP value, is known to have limited bioaccumulation and short half-life (Comber et al. 2002, Wright et al. 2007) and thus it could therefore be considered an appropriate candidate compound for AF coatings. From an effective AF perspective, if usnic acid were to be incorporated into a coating and released, due to its low logD the leachant would predominantly exist in the aqueous phase leading to rapid dispersion and dilution in the marine environment. Whereas, juglone with a higher logD, may exist at relatively higher local concentrations at the coating surface resulting in a greater potency. It would therefore be a more effective NP candidate for AF coatings (Comber et al. 2002).

5.4. Summary

The current work has investigated the AF performance of 3 NPs by developing a methodology combining a systematic and high-throughput approach, in conjunction with a more detailed assessment into initial bacterial attachment. The toluene soluble part of *C. crispus* (CCT) was found to inhibit bacterial attachment at concentrations of 50 ppm - 200 ppm for *C. marina*, and 100 – 200 ppm for *M. hydrocarbonoclasticus*. However, low CCT concentrations appeared to have promoted *M. hydrocarbonoclasticus'* attachment, suggesting an alternative activity of this extract in a concentration dependant manner. Usnic acid was found to be active against *M. hydrocarbonoclasticus* deterring biofilm attachment at concentrations 30 and 40 ppm, while *C. marina* was not inhibited by this natural product. The best anti-biofilm performance was observed for the terrestrial pure compound juglone. This NP inhibited both *M. hydrocarbonoclasticus's* and *C. marina's* attachment, in a concentration response manner, at concentrations as low as 5 ppm to 20 ppm.

The use of nucleic acid staining facilitated the *in situ* quantification of attached bacteria which has only recently been adopted within the AF context. Also, we used the imaging/scanning capability of the microplate reader for the novel application of visualising biofilms on surfaces allowing identification of biofilm features as well as their spatial distribution. In addition to existing AF bioassays against marine biofilms, such as assessing planktonic (through absorbance -OD- measurements) and biofilm (by eye or CV staining) growth, this study has explored: *i*) the use of fluorescent labelling of targeted biofilm components (DNA and extracellular *e*DNA) which are cell activity-specific; and *ii*) a comprehensive rapid procedure (*in situ* 1 h assays). Analogous with clinical studies, this work has demonstrated for the first time a hormetic response using NP compounds against marine bacteria. The assay developed in the current study is simple, fast and perfectly suitable for high-throughput quantification of bacteria attachment in a microtiter plate.

Chapter 6

6. Assessing biofilm formation on NP-containing coatings

6.1 Introduction

As previously discussed biofouling is a surface related phenomenon and as such it is essential to investigate the relationship between fouling organisms and the water/substrate interface. Thus, this study has incorporated NPs into model systems, in order to assess the effect of NP-containing coatings on biofilm formation. The main components of commercial AF coatings include a binder and the biocide, which are increasingly expected to have a lifetime of typically up to 5 years with a controlled and stable release rate (see **Figure 6.1**). Laboratory screening of AF coatings containing novel NPs has often been largely unexplored mainly due to difficulties in assessing their AF activity over short experimental timescales (typically for only a maximum of a few days). One of the most important factors in biocide AF coating performance is the control of the biocide release rates to persist over several years. Therefore, for laboratory based experiments, assessing NPs that have been incorporated into a coating, activity should be tested over longer time periods (*e.g.* 48 h) to provide greater understanding of the NPs release rates.

As shown previously in **Section 5**, the usnic acid, juglone and *C. crispus* crude extract all demonstrated an antifouling efficacy against marine biofilm attachment, although the extent and the mechanism the NPs activity appeared to be species specific. For this reason, the current investigation will focus on biofilm growth on NP-coated surfaces. This has been achieved by the development of a novel bioassay protocol that has allowed the *in situ* observation of biofilm formation and growth, generating both quantitative and qualitative data. Specifically, this chapter is separated in two sections (**Figure 6.2**) where, although initial method development gave promising results several limitations were identified (Section 6.2) which were further addressed by optimising the method (**Section 6.3**).

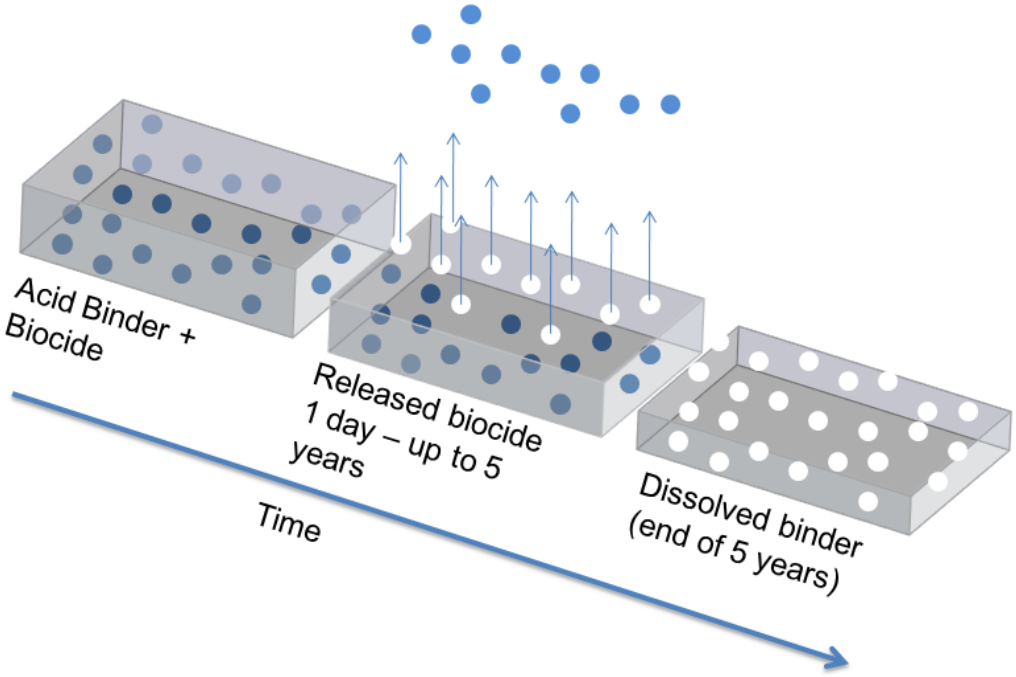

Figure 6.1. Schematic of a biocide based AF coating comprised of a binder (rectangular) and biocide (blue circles). The biocide is released with time (up to 5 years) leaving a dissolved binder at the end (note: the AF coating thickness is decreasing with time).

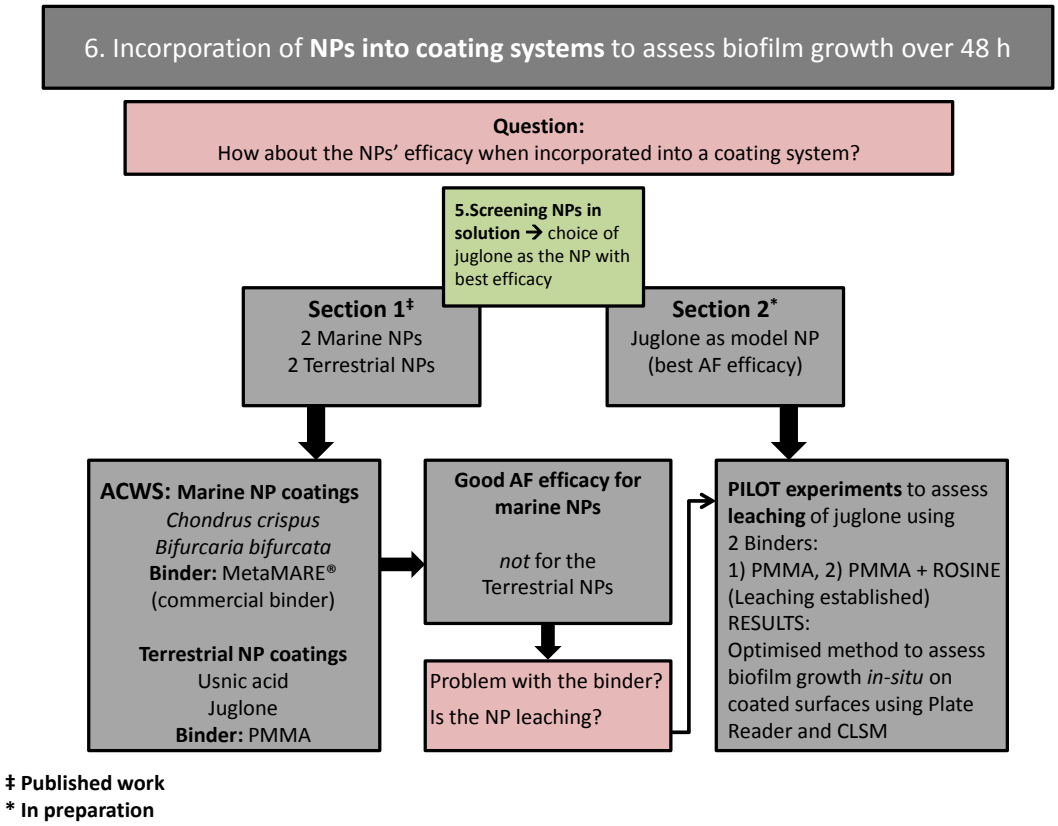

Figure 6.2. Schematic summarising Chapter 6 lay-out and structure.

6.2 Experiment 1

6.2.1 Materials and Methods

6.2.1.1 Test surfaces

Polycarbonate coupons (thickness: 3.5 mm, diameter: 13.5 mm) were cleaned and rinsed with 70 % EtOH prior to coating. Two coating formulations were applied with four different NPs listed in **Table 6.1**. Two binders were used for each formulation, polymethylmethacrylate (PMMA) and Metamare B175™. PMMA is used as a model inert binder (Silence et al. 1995) as it is frequently utilised in submerged man-made materials (*e.g.* marine sensors), while Metamare B175™ is a commercially available binder used in marine paint formulations. Metamare B175™ is an acrylic resin which enables the erosion of the film over long periods.

For the extraction of *C. crispus,* the procedures are discussed in detail in **Chapter 5.** *Bifurcaria bifurcata* was prepared by **MAPIEM**; when extracted with diethyl ether this species showed an extraction yield of between 2.5 and 3.0 % of the algal dry weight. This yield was obtained after only one extraction process by maceration of the algal material in solvent over several days. For comparison, the extraction yield of the *Cystoseiracea* (in particular species belonging to *Cystoseira*) did not exceed 1.0 %. In this study, however, ethanol has been used instead of diethyl ether. A sole extraction by maceration lasting only 12 h gave a yield of 0.9 % (Maréchal et al. 2004). The terrestrial natural compounds, juglone and (+)-usnic acid were purchased from Sigma-Aldrich® (H47003 and 329967, respectively).

Polymer solutions for coatings were supplied (Metamare B175™, a blend of rosin and acrylic polymer in xylene, solid content 60 wt. %) or prepared (PMMA Mw ~ 120,000, Aldrich) by dissolving solid polymer (30 wt. %) in toluene solvent (laboratory reagent grade, low in sulphur, Fisher Scientific) under constant stirring. Dissolution of PMMA was facilitated by heating the mixture of polymer powder and toluene at 50 ˚C in a reaction flask fitted with a reflux condenser and stirring with a paddle stirrer at 60 rpm. NPs were dissolved in the polymer solutions at ambient temperature by placing the mixtures in glass laboratory bottles and rotating these on a laboratory roller mixer (Stuart SRT6D) until dissolved. TiO_2 pigment (10 wt. %, based on the dried coating) was dispersed into the polymer/biocide solution using a Silverson L4RT high shear lab mixer for 5 minutes at 2,000 rpm with no dispersing screen fitted.

The amount of compounds in some experimental formulations is given by volume (Table 6.1) since it is common practice in the coatings industry to quantify the amounts of pigments and other ingredients in paints by the volume fraction they occupy in the dried paint film rather than their weight fraction in the formulation. This is because the properties of paint films such as water uptake, hardness, etc., are highly dependent on the relative volumes of the different ingredients. Most physical properties of a paint film undergo a dramatic change when the volume of pigment exceeds a certain level known as the Critical Pigment Volume Concentration (Asbeck and Loo 1949). This is the volume content of pigment at which the individual pigment particles come into direct contact with each other.

In order to produce a uniform coating layer the following procedures were followed: **1)** a paper reinforcement ring was adhered on the coupon to allow a defined circle (diameter of 5.7 mm) of the coupon to be exposed for the coating application, **2)** 500 mL of each paint formulation was then placed atop each coupon and a draw bar was used to create a uniform layer within the ring, and **3)** the ring was removed to give a circular coating with an average thickness of 50 µm, **Figure 6.3**. Toluene was added to facilitate the coating application. Once the coating formulations were applied on the polycarbonate coupons, they were left to dry at room temperature for several days.

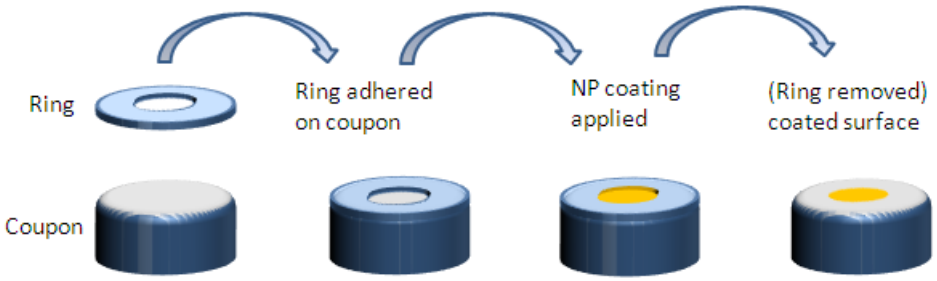

Figure 6.3. Schematic of the application of NP coatings on the polycarbonate coupons.

Following drying, the coupons were sterilised carefully by immersion in 70 % EtOH – the coated surface remained exposed to air (*i.e.* only the sides and bottom of the coupons were immersed into the EtOH solution). To sterilise the coated part of the coupons, these were exposed to UV radiation for 10 min.

Table 6.1. Paint formulations (according to the two binder compounds) used on polycarbonate coupons, NP = Natural product, MTM = Metamare B175™, PMMA = polymethylmethacrylate

Formulations	Composition			Active Compound Concentration (µg/g)	Sample Abbreviation
	Binder (80 wt. %)	**Pigment (10 wt. %)**	**NP (10 wt. %)**		
Formulation 1	MTM	TiO_2	*Bifurcaria bifurcata*	100,000	BB
	MTM	TiO_2	*Chondrus crispus*	100,000	CC
	MTM	TiO_2	None (control)	0	CON
Formulation 2	**Binder (95 vol. %)**	**Pigment**	**NP (5 vol. %)**		
	PMMA	None	(+)-Usnic acid	61,500	UA
	PMMA	None	Juglone	61,500	JUG
	PMMA	None	None (control)	0	CON

6.2.1.2 Bacterium species and growth conditions:

The marine bacterium *Pseudoalteromonas sp.* NCIMB 2021 was used in this experimental work (due to initial experiments conducted with the species previously). *Pseudoalteromonas sp*., originally isolated by Fletcher and Floogate (1973), is Gram-negative rod-shaped biofilm forming aerobe with single polar flagella, but these are only present when in planktonic state. This species has been used in several studies of attachment properties and mechanisms (*e.g.* Fletcher and Loeb 1979, Rasmussen and Ostgaard 2003). Bacterial growth conditions were discussed in detail in **Section 4.2.2**.

6.2.1.3 Experimental set-up

A clear 24-well plate (Nunclon™ D Multidishes, Sigma-Aldrich D7039) was used as a vessel containing the polycarbonate coupons bearing the NP coatings (**Figure 6.4 top**). There were two replicas for each NP with one un-inoculated control to account for possible contamination and background signal from the coating each self (**Figure 6.4 bottom**). Each coupon was glued on the bottom of the wells using a very small drop of Dow Corning marine silicone and left to dry. The coupons were then fully immersed in 700 µL of sterile filtered ASW and left for 1 h to allow surface conditioning. A 50 µL aliquot of freshly grown (log-phase) bacterial suspension was then inoculated into the wells and the 24-well plate was stored in dark under static conditions for 24 h at 28 °C. At the end of the experiment (24 h later), 100 µL (in duplicate) of the suspended culture from each well was transferred into a 96-well plate (Optical Bottom Plates, 96-Well, Nunclon™Δ) to measure the planktonic growth using absorbance at 620 nm (**Figure 6.5**). The remaining bacterial suspension in the 24-well was

pipetted out and the coupons were gently washed twice using PBS, leaving only the attached bacteria on the coupon surface.

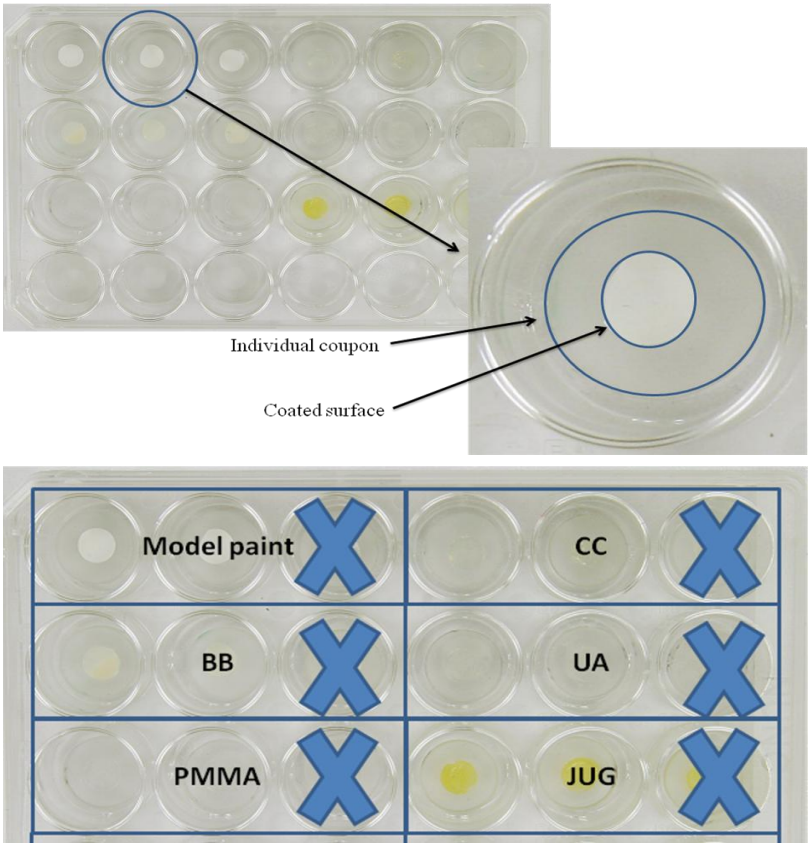

Figure 6.4. ***Top image*****: top view of the experimental 24-well plate with a close up on the individual polycarbonate coupon positioned in a well.** ***Bottom image*****: experimental set up of the NP-coated coupons where ✖ = uninoculated (no bacteria) blank coupons.**

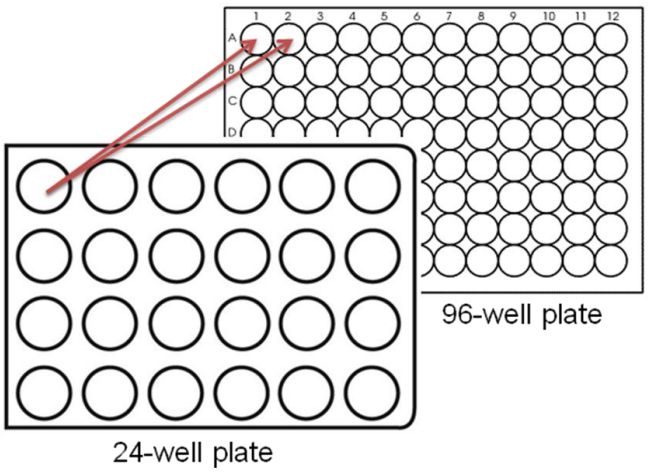

Figure 6.5. Schematic of the well plate set-ups for measuring *Pseudoalteromonas* sp end-point OD_{620} (96-well plate) following a 24 h incubation (24-well plate).

6.2.1.4 Staining

A fluorescent staining method using the LIVE/DEAD *Bac*Light Bacterial Viability Kit (Molecular Probes) was performed to assess biofilm growth and viability. Details on stain preparation are given in **Section 4.2.4**. An aliquot of 60 µL of the LIVE/DEAD mastermix was added to each experimental surface. The plate was then incubated for 20 minutes in the dark at 28 °C. The stain volume was found to be sufficient for covering the coated surface and keeping the sample hydrated throughout the incubation period (**Figure 6.6**). At the end of the incubation period, the coupons were gently rinsed with ASW to remove excess stain. Finally, 700 µL of ASW was added in order to keep the samples (and subsequently the biofilms) hydrated during the data acquisition time. Each well, containing the natural product coating, was scanned to produce an image of the biofilm. This technique provided the opportunity to observe live and dead bacteria in biofilms directly on the coated surfaces using a 30 × 30 well scanning matrix. The software used was Mars Data Analysis Software, Version 2.00 (Omega, BMG LABTECH, Offenburg, Germany).

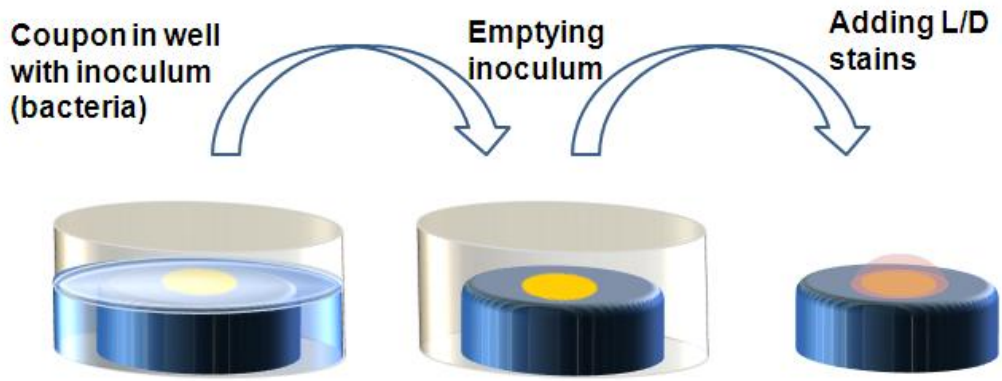

Figure 6.6. Schematic of the individual coupon within a well, illustrating the staining (LIVE/DEAD) droplet positioned atop the coated surface.

6.2.1.5 Confocal laser scanning microscopy (CLSM) and image analyses

Microscopic Image acquisition was performed on a Leica TCS SP2 AOBS (Leica Microsystems, France) laser-scanning confocal laser microscope (LSCM). The coatings did not show marked signs of autofluorescence. CLSM allowed the simultaneous 3D monitoring of PI and SYTO9 dyes. The excitation wavelength used for S9 was λ_{EX}: 480 nm and the emitted fluorescence was collected in the range of λ_{EM}: 500 to 600 nm. The red fluorescent nucleic acid

stain PI was excited at λ_{EX}: 488 nm and the emitted fluorescence was collected in the range of λ_{EX}: 650 to 700 nm. Images were made via a ×63 Leica water immersion objective. Simulated 3D fluorescence projections, vertical cross-sections through the biofilms and deconvolution using Wiener filter were generated using the LSCM 3D package of the Leica SP2 software. Biofilm surface coverage and thickness were calculated using ImageJ (MacBiophotonics ImageJ, USA) where CLSM images were converted into a binary system (0 or 1) and the covered areas (with biofilm) were quantified.

6.2.1.6 Statistical analysis

Differences in OD_{620} and RFU values between experimental (CC, BB, UA and JUG) and control (PAINT, PMMA) were assessed by applying one-way ANOVA. To establish the homogeneity of variances, Levene's test of equal variances was applied. All conclusions are based on 5 % level of confidence ($p < 0.05$). Statistical analysis was performed by using SPSS version 17.0.

6.2.2 Results and discussion: Experiment 1

To date there are only a limited number of reports found in the published research literature on laboratory assessment for antifouling paints and their effect on bacterial attachment and/or biofilm growth. In this study, NP-containing coatings were applied to polycarbonate coupons, placed in a 24-well plate and then inoculated with the marine biofilm forming bacterium *Pseudoalteromonas sp.* for 24 h.

Well scans on the coatings can be seen in **Figure 6.7a**, where the clear increased biofilm formation is evident on the control of Formulation 1 (*i.e*. MTM + TiO_2). Specifically, high fluorescence intensity represented by yellow and red colours is mainly located on the top-left side of the coating in a circular manner. On the contrary, low signal is emitted from the rest coatings signified by dark blue indicating a low biofilm formation. This technique provided the opportunity to observe bacteria directly (*in situ*) on the coated surfaces (**Figure 6.7a**). Extracting the data from **Figure 6.7a**, the fluorescence intensity emitted by the bacteria at wavelengths of 520 nm (Syto9) can be seen in **Figure 6.7b**. For the Formulation 1, biofilm formation was significantly higher for the control (MTM containing coupon) when compared to both the *C. crispus* (CC) – and *B. birfucata* (BB) – containing coupons at $p = 0.004$ (for both).

These data suggest that biofilm occurred on the MTM control, while the NP coatings appeared to inhibit biofilm growth (**Figure 6.7**). This implies that the marine NPs were readily present into the wells and active over 24 h resulting in biofilm growth arrest.

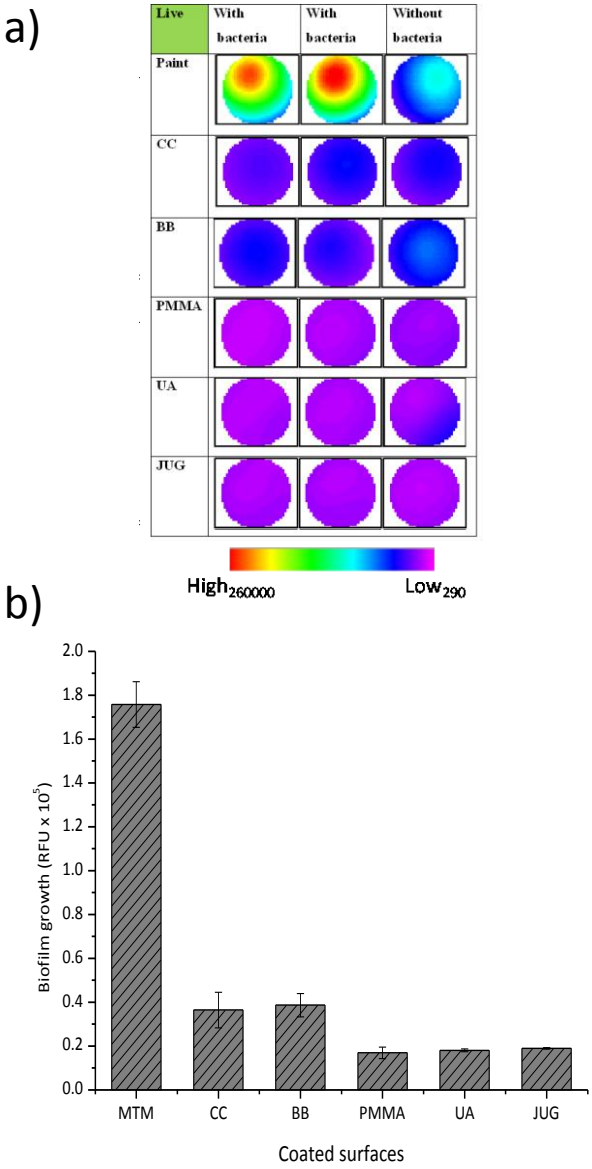

Figure 6.7. Biofilm growth of *Pseudoalteromonas* sp. on the NP coatings as a function of fluorescence intensity (RFU), at λ_{EM} = 520 nm (live bacteria) where a) well-scanning imaging of the species with each pixel corresponding to a numerical value of a 30 × 30 matrix and b) the averaged data from the well scans. Formulation 1: MTM = Metamare B175™ + TiO_2, CC = *Chondrus crispus* + Metamare B175™ + TiO_2, BB = *Bifurcaria bifurcata* + Metamare B175™ + TiO_2. Formulation 2: PMMA = poly(methyl methacrylate), UA = usnic acid + PMMA, JUG = juglone + PMMA. Error bars ± STDEV.

For Formulation 2, the data obtained do not suggest any significant difference in biofilm growth between the control (PMMA) and the NPs (UA and JUG, **Figure 6.7b**). Although these NPs (UA and JUG) have previously been shown to have good efficacy against bacterial attachment (UA was found to have species specific activity, see **Chapter 5**), the current results do not illustrate the same activity. One explanation for this outcome is that *Pseudoalteromonas* sp. is not affected by these NPs. Another possible explanation is the use of PMMA which is a rather hydrophobic binder (Silence et al. 1995) and therefore it may hinder deliver/release of the NP into the aqueous solution. In addition to the latter notion, both UA and JUG are relatively water insoluble (in comparison to marine NPs) which may suggest that PMMA is not the ideal delivery/binder system for water insoluble products, resulting in a slow-eluding coating system. Contact angle measurements, illustrated an increase in hydrophobicity of the PMMA (67.5°) film with the addition of usnic acid (85-90°).

Figure 6.8 shows a biofilm colonized polycarbonate surface compared to a clean surface. CLSM is useful for biofouling studies since it allows the 3D imaging of fully hydrated living biofilms on spatial scales relevant to the single cell level up to large biofilm clusters. In addition, specific stains can be used to view the biofilm slime and physically quantifying biofilm thickness, volume and surface area coverage.

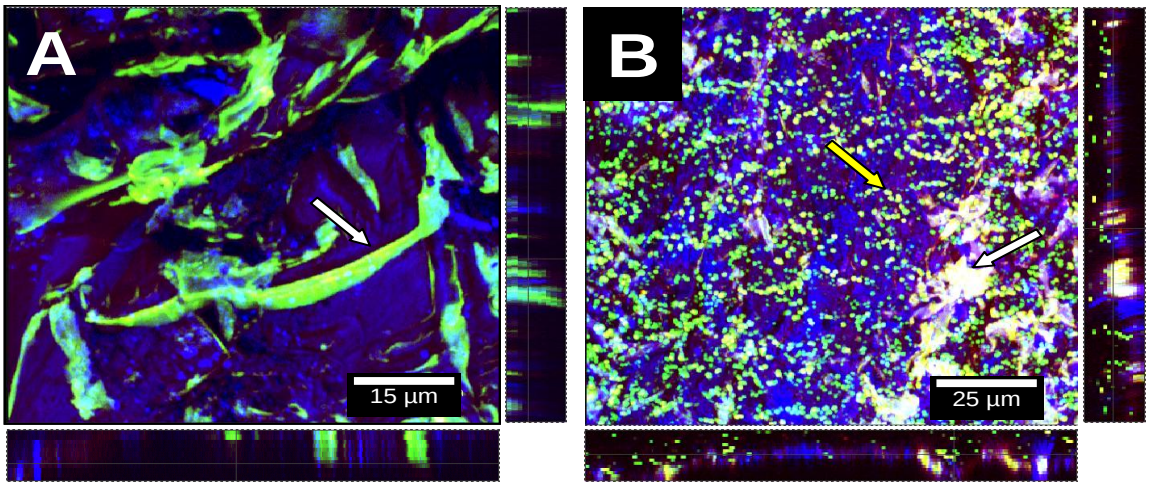

Figure 6.8. Confocal microscopy images of (A) a clean polycarbonate coupon and (B) a polycarbonate coupon with bacteria that are stained with nucleic acid Live/Dead stains, attached to the surface. The white arrow indicates autofluorescing signal from the material and yellow arrow is pointing at bacteria.

Lastly, it has been observed that when PMMA was applied onto a surface it resulted in a smooth film (Dennington, personal communication). This might have influenced bacterial

adhesion as microtopography is considered to play a key role in attachment mechanisms (reviewed by Salta et al. 2010). When comparing the results between the two Formulations it is clear that there is very different response in biofilm growth (**Figure 6.7)**. This may have resulted from differences in: *i*) the nature of the products, *i.e.* marine (CC and BB, Formulation 1) *vs*. terrestrial (UA and JUG, Formulation 2) and/or ii) the binder used in each formulation, *i.e.* Metamare B175™ (Formulation 1) *vs*. PMMA (Formulation 2). The use of two different binder systems (i.e. Metamare B175™ and PMMA) was decided, since Metamare B175™ would not be included in future experiments. The exact composition of Metamare B175™ could not be disclosed due to product confidentiality; therefore, the use of a simpler and controlled system, such as PMMA, was decided to be the preferred binder for future experiments. PMMA is a common material used in orthopaedic surgery as part of bone cement and antibiotics are often incorporated into these cements, where subsequent elution produces high local concentrations of antibiotic while simultaneously minimising systemic toxicity (Hanssen and Spangehl 2004, Zalavras et al. 2004, Mori et al. 2010) . A major characteristic of currently available antibiotic cements is that an initial burst of antibiotic elution occurs within 24 to 48 h, with poor subsequent sustained release (Kuechle et al. 1991, Méndez et al. 2002, Virto et al. 2003, Lewis 2009) Similarly, in the current study, a burst elution when NPs are incorporated into PMMA cannot be excluded, however, more experimental work is required in order to measure the leaching of the NP with time. The 24-48 h leaching window observed for antibiotics would be ideal for AF bioassays as biofilm growth can easily be supported within that time scale. Biofilm-mediated released rates of biocides have been previously proposed as the bacterial extrapolymeric matrix has shown to bind metals such as copper (Bashkar et al. 2006) and potentially affect the diffusion rate of the compound and consequently control its release rate (Howell 2009). **Figure 6.9** shows the optical densities (OD_{620}) and establishes that planktonic growth did not differ significantly between the wells containing the experimental coatings.

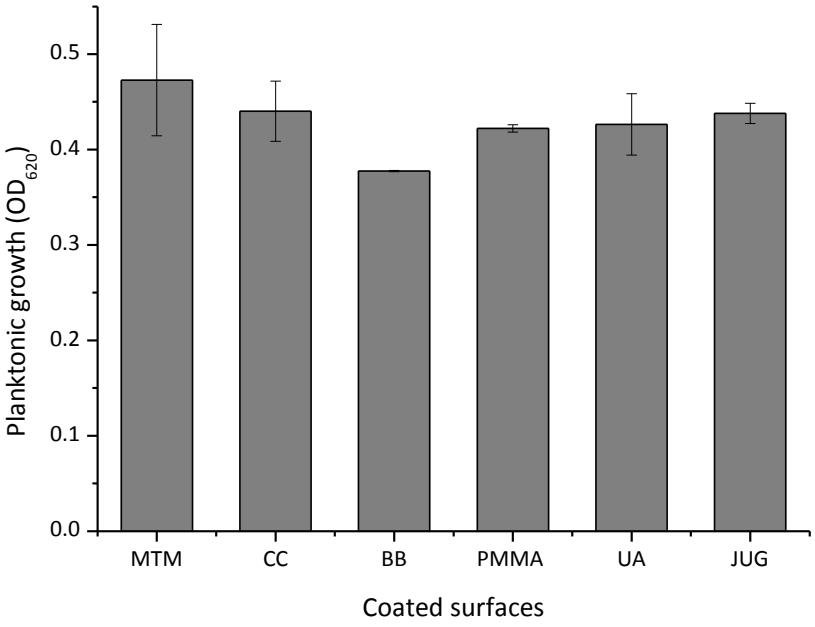

Figure 6.9. OD_{620} measurements (planktonic growth) of *Pseudoalteromonas* sp. within wells containing NP bearing coatings. Formulation 1: MTM = Metamare B175™ + TiO_2, CC = *Chondrus crispus* + Metamare B175™ + TiO_2, BB = *Bifurcaria bifurcata* Metamare B175™ + TiO_2. Formulation 2: PMMA = poly(methyl methacrylate), UA = usnic acid + PMMA, JUG = juglone + PMMA. Error bars ± STDEV

6.2.2.1 Limitations for Experiment 1

The limitations observed during the protocol development include: the autofluorescent signal deriving from the polycarbonate coupons, interfering with CLSM analysis (**Figure 6.9**) and possibly fluorescence spectroscopy (plate reader) readings. The use of glass coupons is considered necessary for generating reproducible and repeatable bioassays. Adhesion between the coating film and the glass might be an issue (see **Chapter 7, Section 7.2.2.2**), therefore treatments (*e.g.* silanization or lapping) of the glass surfaces will be attempted, assuring this way, good linkage between the two materials (PMMA and glass). Also, a positive control will be included in future coupon experiments, *i.e.* using a common booster biocide such as cuprous oxide (Cu_2O) to facilitate data interpretation.

As previously discussed within **Chapter 3**, the NP/biocide leaching rates also depend on flow conditions, *i.e.* a dynamic flow is expected to increase the NP's diffusions rate within the film and therefore elude faster. Future experiments will include a dynamic flow by incubating the 24-well plates under agitation with the aim to increase NPs leaching rates. Additionally, a

second binder will be added to the experimental matrix: *i.e*. a binder with higher solubility in sea water, that will facilitate a faster (for the purpose of the current experimental work, where coatings are assessed within few hours) and more controlled release rate of the compound through binder dissolution due to the surrounding environmental conditions (sea water slightly alkaline pH 8.2) (Lewis 2002).

6.3 Experiment 2

The acknowledged limitations of the initial coupon experiments (Experiment 1, previous **Section 6.2**) lead to a series of optimisation procedures in order to achieve readily reproducible and reliable methods for the identification of AF efficacy of biocide-containing coatings against biofilm formation. Briefly, this was achieved by: *i*) changing the coated substrate (to glass) in order to avoid autofluorescence and achieving good adhesion between coating and glass, *ii*) testing two binder systems, *iii*) establishing and quantifying leaching of the NP, *iv*) adding a positive control to the experimental matrix (Cu_2O coated surfaces) to allow direct comparison and evaluation between the commercially established booster biocide and the experimental (NP), *v)* extending the experimental time to 48 h and *vi*) using a more sophisticated coating procedure (spin coating) in order to produce reproducible coatings. The experimental procedures in the current Section addressed all issues/problems/limitations observed in the previous Section.

6.3.1 Materials and Methods

6.3.1.1 Test surfaces

Glass coupons (thickness: 3.5 mm, diameter: 13.5 mm) were lapped using a lapping machine (Kemet 15 Diamond Flat Lapping / Polishing machine, Kemet International Ltd, UK) with diamond micro-particles size 25 μm for 20 minutes to produce rough surfaces. This was done to improve adhesion between the smooth glass surface and the PMMA-based coatings, which was previously observed to be poor. The glass coupons were then cleaned with 100 % acetone, followed by 70 % EtOH. Each coupon was permanently numbered (using a diamond cutter) and weighted. The coupons were then rinsed again with 70 % EtOH under sterile conditions (*i.e*. laminar flow hood) and placed in sterile Petri dishes.

Polymer solutions for the coatings were prepared (PMMA and rosin) by dissolving solid polymer (30 wt. %) in toluene solvent (laboratory reagent grade, low in sulphur, Fisher Scientific) under constant stirring. Rosin (gum rosin, Aldrich) dissolved rapidly in toluene under mild agitation at ambient temperature, while dissolution of PMMA was slower and was facilitated by heating the mixture of polymer powder and toluene at 50 ˚C in a reaction flask fitted with a reflux condenser and stirring with a paddle stirrer at 60 rpm. To make the 80:20 wt./wt. PMMA:rosin polymer blend solutions of each polymer having the same solid content

(30 wt. %) were mixed in this weight ratio. Juglone and Cu_2O were dissolved in the polymer solutions at ambient temperature by placing the mixtures in glass laboratory bottles and rotating these on a laboratory roller mixer (Stuart SRT6D) until dissolved. Details on composition of the coating formulations applied are listed in **Table 6.2**.

For the coating application, a spin-coating machine was used to achieve a uniform layer with predictable and reproducible thicknesses (see **Figure 6.10**). Specifically, the settings for the spin coating were as follows: Acceleration: 2000 rpm, speed: 7500 rpm, Time: 1 min, Paint viscosity: 500 mPa (castor oil). To maintain the viscosity toluene was used as a solvent. Following the spin coating procedure, the coupons were placed in sterile Petri dishes where they were transferred under sterile conditions (laminar flow hood) to allow evaporation/drying (for 4 days). Following drying, the coupons were carefully immersed into 70 % EtOH – the coated surface was exposed to air (*i.e.* only the sides and bottom of the coupons were immersed into the EtOH solution).

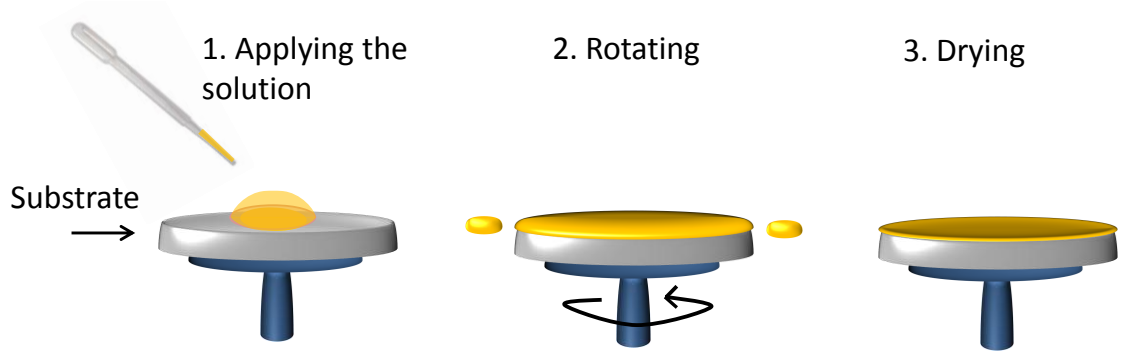

Figure 6.10. Spin-coating procedure.

Table 6.2. Paint formulations used on glass coupons, JUG = juglone, ROS = rosin, PMMA = polymethylmethacrylate. Blanks: uninoculated, *i.e.* there was no bacteria present. *AC = Active Compound

Formulation	(+/-) Bacteria	Composition						Active Compound Concentration (µg/g)	Coating Thickness (µm)	No. of coupons
		(wt. %)			(vol. %)					
		AC*	PMMA	ROS	AC*	PMMA	ROS			
Experimental	1. JUG + PMMA +ROS	6.25	75	18.75	5	76	19	62,500	15.03 ± 4.2	12
	2. JUG + PMMA	6.15	93.85		5	95		61,500	14.78 ± 4.2	12
Biocidal	3. Cu_2O + PMMA + ROS	68.91	24.87	6.22	30	56	14	689,100	7.87 ± 3.0	12
	4. Cu_2O + PMMA	68.55	34.45		30	70		685,500	4.45 ± 0.7	12
(-)ve control	5. PMMA + ROS	80	20		80	20		0	3.91 ± 0.7	24
	6. PMMA	100			100			0	3.81 ± 0.6	24

6.3.1.2 Pilot assay – Leaching Rates

As discussed in the previous section (Experiment 1), the use of PMMA as an inert binder could have limited the release of the NP, therefore, the addition of rosin was decided to be included since it is a common ingredient in paint formulations. The matrix of these paints must contain a resinous material sufficiently soluble in sea water to maintain adequate leaching of the toxin, but not so soluble as to result in the rapid deterioration of the film. Rosin is commonly used for this purpose since its solubility appears to be within the limits required (*e.g.* Atta et al. 2006).

In order to assess the leaching/release of juglone from the current experimental paint matrix, a pilot assay was conducted where the coated coupons were assessed for 48 h under agitation (to aid release) without bacterial inoculation. The experimental matrix consisted of the Coatings 1, 2, 5, and 6, see **Table 6.2**.

The coupons were transferred in a clear 24-well plate (Nunclon™ D Multidishes, Sigma-Aldrich D7039) and 1 mL of filtered (0.2 μm) ASW was added in each well. To avoid water evaporation over the experimental time (48 h), parafilm was used to seal the lid of the 24-well plate. Parafilm is a known material that allows gas exchange, *i.e*. CO_2 and O_2, but minimizes evaporation. The plate was then incubated in the dark at 28 °C (Cooled incubator) under 100 rpm agitation. Each coating formulation was replicated six times.

To establish calibration curves for juglone, the compound was dissolved in 100 % DMSO, as discussed in **Chapter 5** (**Section 5.2.3**) where serial dilutions of 64, 32, 16, 8, 4, 2, 1, and 0.5 ppm were prepared in filtered ASW. The serial dilutions were then inoculated in a 96-well plate (eight replicas) and the UV-Vis absorbance spectrum function of the plate reader was utilised over a scan wavelength range of 200 to 700 nm at a 2 nm resolution.

6.3.1.3 Experimental set-up

The marine bacterium *C. marina* was used in this experimental work. Growth conditions can be found in **Chapter 4**.

The coated glass coupons were treated as discussed in **Section 6.2.1** (*i.e.* rinsed with 70 % EtOH) and placed in a clear 24-well plate (Nunclon™ D Multidishes, Sigma-Aldrich D7039). The experimental set-up can be seen in **Figure 6.11**. Before bacterial inoculations, 0.95 mL (1 mL for the blanks) of SSP was added to achieve conditioning of the coatings, for 1 h. In order

to account for any autofluorescence from the coated coupons (and correct for any non-biological signal), all 48 coupons were scanned at the LIVE/DEAD wavelengths (*i.e*. Live: λ_{EX} = = 485 nm and λ_{EM} = 510 nm, Dead: λ_{EX} = 540 nm and λ_{EM} = 610 nm, excitation and emission, respectively) in the absence of SSP and bacteria, see **Figure 6.12.**

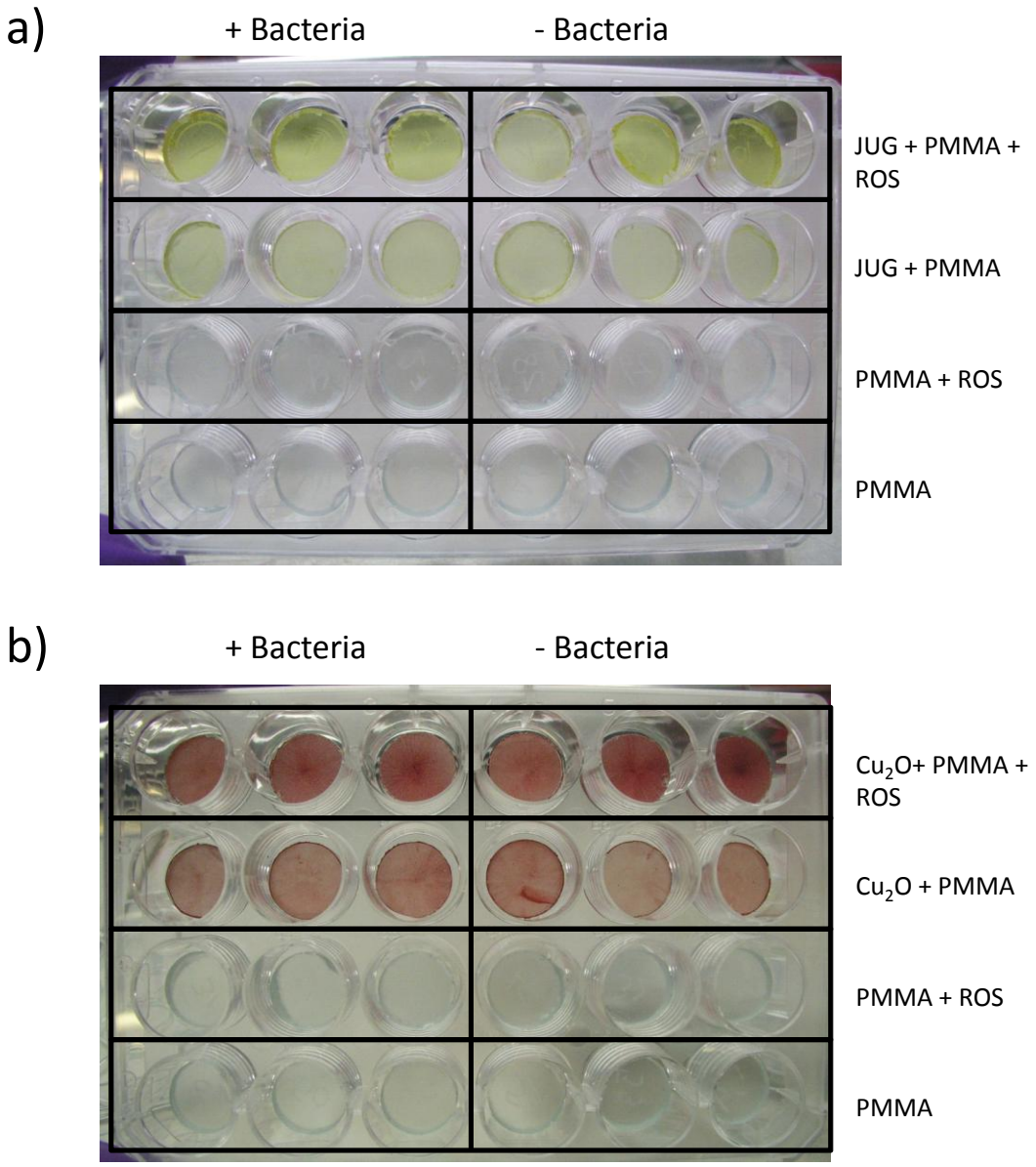

Figure 6.11. Coupon experimental set-up with coatings (right labels) containing: a) juglone and b) Cu_2O. (+) bacteria = wells where bacteria will be inoculated and (-) wells where no bacteria will be added serving as blanks. JUG = juglone, ROS = rosin, PMMA = polymethylmethacrylate

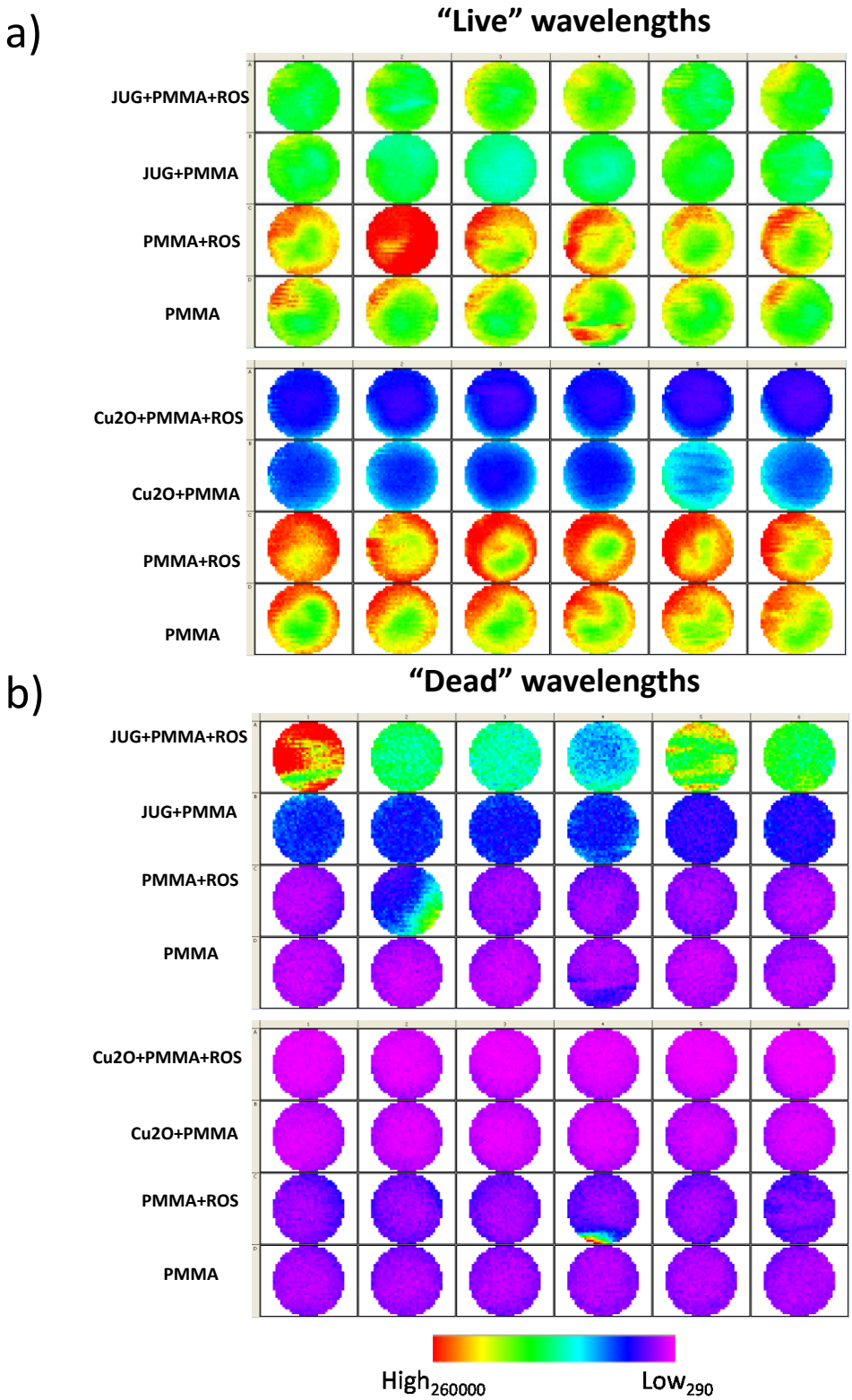

Figure 6.12. Well scanning (30 x 30 matrix) of the coated coupons before bacterial inoculations where: a) is the "Live" wavelengths (λ_{EX} = 520 nm) and b) the "Dead" wavelengths (λ_{EX} = 620 nm). JUG = juglone, ROS = rosin, PMMA = polymethylmethacrylate

Following the well-scanning measurements, 50 μL of overnight culture of *C. marina* (OD_{595} 0.2) grown in SSP, were inoculated in the experimental wells (**Figure 6.11**). The two 24-well plates were then sealed with parafilm and placed in dark at 28 °C under agitation (100 rpm).

Following a 48 h incubation, the plates were removed from the incubator and placed under the laminar flow hood. Sterile tweezers (70 % EtOH) were used to remove the coupons from the wells (tweezers were sterilized for each coupon to avoid cross-contamination) which were gently rinsed with filtered ASW using a pipette (1 mL), and placed in a new sterile 24-well plate. Then 1 mL of filtered ASW was introduced into the wells to avoid coupon/biofilm dehydration. The remaining solutions in the empty-experimental 24-well plate were transferred to 96-wells plates as shown previously in **Figure 6.4** and OD_{595} measurements followed, to establish planktonic growth. In addition, 5 μL from each well were inoculated on Marine Agars to check differences in colony growth (in addition to the OD measurements).

Fluorescence end-point measurements were made on the rinsed coupons at the LIVE/DEAD wavelengths to account for changes on the autofluorescence signal over the 48 h incubations. The coupons were then stained with LIVE/DEAD as outlined in **Section 6.2.1.3,** with the only difference that coupons were fully immersed using 500 μL of the stains in the 24-wells. Following the 20 m incubation period, coupons were gently rinsed with ASW to remove excess stains and transferred in a new sterile 24-well plate. Fluorescence end point and well scanning measurements (30 × 30 matrix, six flushes per sampling point were taken) were then taken.

6.3.1.4 Microscopy and Image analysis

In all experiments, images were acquired from random positions in the central part of the coupons.

CLSM image acquisition

Confocal microscopy was performed using a Leica TCS SP2 AOBS (Leica Microsystems, France) laser-scanning confocal microscope. The excitation wavelength used for S9 was 480 nm, and the emitted fluorescence was collected in the range of 500 to 600 nm. The red fluorescent nucleic acid stain PI was excited at 488 nm, and the emitted fluorescence was collected in the range of 650 to 700 nm. Images were collected through a ×63 Leica water

immersion objective and acquired at 0.502 µm intervals down through the biofilm, and therefore the number of images in each stack varied according to the thickness of the biofilm. For each Coating (1-6, see **Table 6.2**) at least two replicas (coupons) were samples with at least three stacks, *i.e*. $n = 6$ (in some cases $n > 10$), were taken.

CLSM image analysis

CLSM images were analysed by the computer program COMSTAT (Heydorn et al. 2000). A fixed threshold value and connected volume filtration was used for all image stacks. In-house MATLAB (MathWorks) scripts were used to obtain data from CLSM images. Features calculated by COMSTAT in the current study:

Bio-volume. The bio-volume is defined as the number of biomass pixels in all images of a stack multiplied by the voxel size $[(\text{pixel size})_x \times (\text{pixel size})_y \times (\text{pixel size})_z]$ and divided by the substratum area of the image stack. The resulting value is biomass volume divided by substratum area ($\mu m^3\ \mu m^{-2}$). Bio-volume represents the overall volume of the biofilm, and also provides an estimate of the biomass in the biofilm (Heydorn et al. 2000).

Thickness distribution and mean thickness. This function locates the highest point (µm) above each (*x*,*y*) pixel in the bottom layer containing biomass. Hence, thickness is defined as the maximum thickness over a given location, ignoring pores and voids inside the biofilm. The thickness distribution can be used to calculate a range of variables, including biofilm roughness and mean biofilm thickness. Mean biofilm thickness provides a measure of the spatial size of the biofilm and is the most common variable used in biofilm literature, probably because of its simple interpretation and the fact that it can be measured without the use of CSLM and image analysis software (though not as precisely), (Heydorn et al. 2000).

6.3.1.5 Minimum inhibitory concentration (MIC), 50 % effective concentration (EC_{50}) and minimum bactericidal concentration (MBC) for juglone

MIC: *C. marina* was grown in SSP overnight. MICs were conducted in 96 well plates (optical bottom plated with polymer base, transparent, Nunc™) and bacterial growth was monitored at OD_{595}. Juglone serial dilutions were prepared according to Andrews (2001). Solvent used: 0.5 % DMSO final concentration in each well. The following dilutions were tested: 64, 32, 16, 8, 4, 2, 1 and 0.5 ppm. Each dilution was replicated five times while un-inoculated wells for each concentration served as controls and were replicated three times. Measurements were taken

every 15 minutes for 24 h at 28 °C. MIC was determined at the lowest concentration of juglone at which there was no growth (Andrews 2001). The EC_{50} was determined at the concentration where 50 % of bacterial growth was affected by juglone.

MBC: Following the 24 h experimental period for the MICs, 5 µL from each well (in triplicates) were transferred on marine agar (Difco, Marina Agar 2216) to establish the MBCs. Each concentration tested for bacterial growth without the inhibitor (juglone) was replicated three times. The marine agars were then incubated for 24-48 h at 28 °C. Where bacterial colonies were not formed, the MBC was established.

6.3.1.6 Statistical analysis

Differences between experimental and controls (for both plate-reader and CLSM data) were assessed by applying one-way ANOVA. To establish the homogeneity of variances, Levene's test of equal variances was applied. Where homogeneity of variances was not met, the non-parametric Kruskal-Wallis test was applied. All conclusions are based on 5 % level of confidence ($p < 0.05$). Statistical analysis was performed by using SPSS version 17.0 and Minitab version 16.

6.3.2 Experiment 2: Results and Discussion

6.3.2.1 Determination of juglone leaching

To establish the extent of juglone leaching from the two formulations (1: JUG + PMMA + ROS and 2: JUG + PMMA), tests were performed in filtered ASW over a duration of 48 h. This was undertaken in order to determine whether the NP compound actually leached from the coated surfaces, and if so, to quantify the concentrations within the well fluid volumes.

Juglone Calibration

Figure 6.13a shows the UV-vis spectra for juglone serial concentrations in ASW between 0 (zero) ppm and 64 ppm. A peak can be clearly seen at a wavelength of 520 nm, which was utilised to construct a calibration plot (see **Figure 6.13b**). The linear regression (R^2 = 0.9915) will be used to determine the unknown juglone concentrations during the leaching tests.

a)

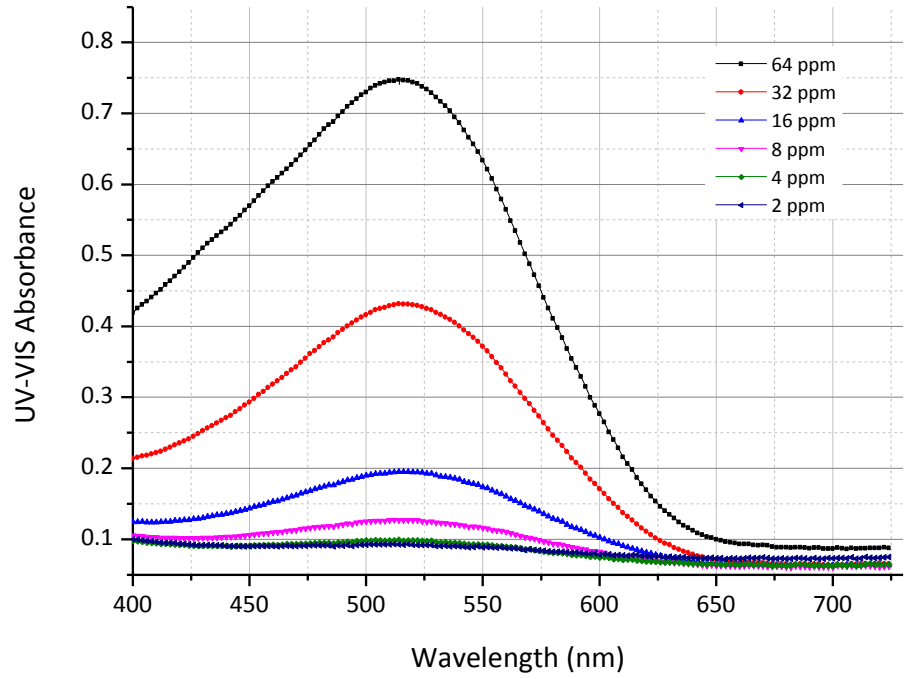

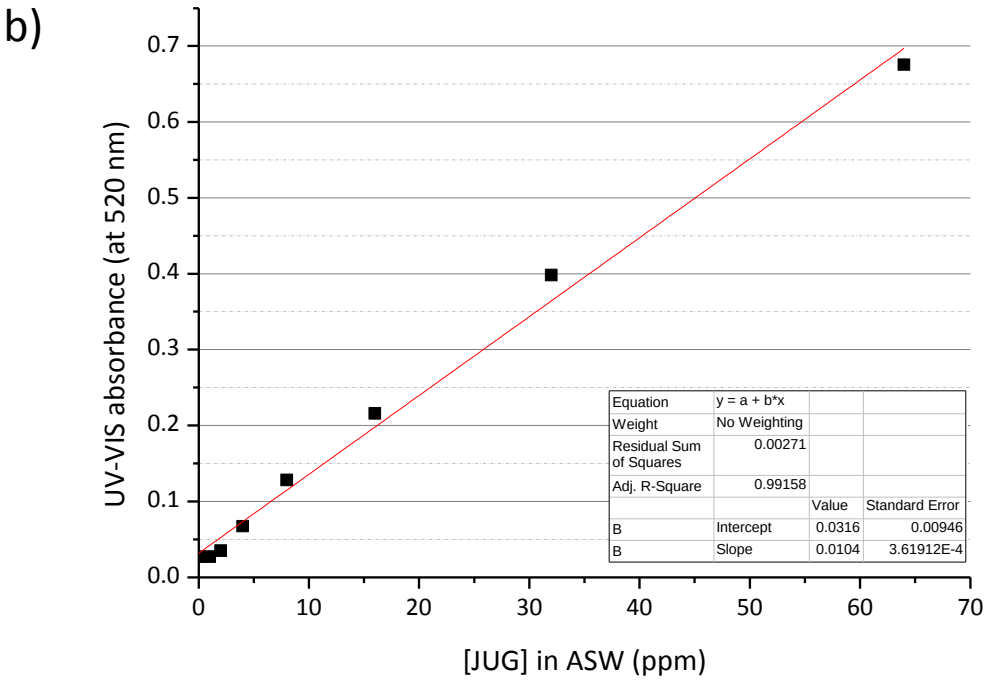

Figure 6.13. a) UV-Vis spectra for the serial juglone dilutions in ASW and b) the calibration plot for the juglone concentrations between 1 to 64 ppm.

Juglone leaching after 24 and 48 h

During the ASW immersion of the coating formulations two sampling points were taken at 24 h and 48 h. Overall, juglone leaching from both coating formulations was detected at concentrations ranging from 1.70 to 1.99 ppm after 24 h, and 1.96 to 2.35 ppm after 48 h, for Coating 1 (JUG + PMMA + ROS) and Coating 2 (JUG + PMMA), respectively, **Table 6.3**. The concentrations obtained will be dependent on the extent of water phase / well wall / coating surface partitioning and the juglone's half-life, see Chapter 5. It must be noted that the aim of this assay was to establish whether juglone leaching occurs from the coatings. Overall, it can be concluded that most of juglone leached at 24 h for both coatings

Table 6.3. Leaching of juglone from coated surfaces where Coating 1 = JUG + PMMA + ROS and Coating 2 = JUG + PMMA. Each coating was replicated six times, ± STDEV, Significance assessed using 1-Way ANOVA.

Coating	24 h - ppm	48 h - ppm	Thickness (µm)	*p*-value
Coating 1	1.70 ± 0.20	1.96 ± 0.21	14.95 ± 2.02	$p < 0.05$
Coating 2	1.99 ± 0.36	2.35 ± 0.35	19.57 ± 6.05	NS
p-value	NS	$p < 0.04$		

6.3.2.2 MIC, EC_{50} and MBC for juglone

The growth inhibiting activity of juglone was examined and was found to have strong inhibition against *C. marina* was at 16 ppm, while the EC_{50} was found to be at 5 ppm, see **Figure 6.14.** This comes in good agreement with data obtained from the attachment bioassays shown in **Chapter 5** (attachment was negatively affected for *C. marina* at 5 ppm in 1 h long experimental time). The minimum bactericidal concentration (MBC) for *C. marina* was also found to be at 16 ppm.

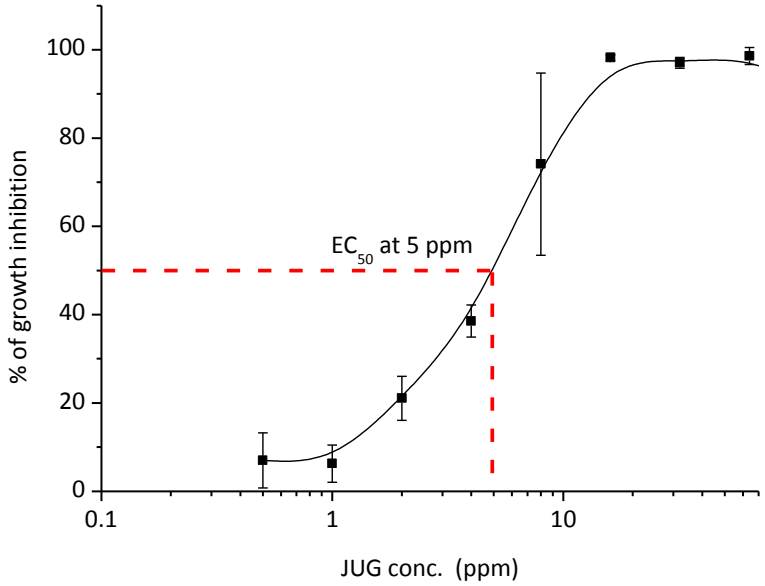

Figure 6.14. Inhibition of growth for *C. marina* (Absorbance, OD_{595}) in the presence of juglone at concentrations 64, 32, 16, 8, 4, 2, 1 and 0.5 ppm (*x*-axis). Error bars ±STDEV.

6.3.2.3 Assessing biofilm growth on AF coatings using the microplate reader

For the first time, the *in situ* evaluation of biofilm growth was achieved through the use of a plate reader on coated surfaces utilising nucleic acid staining. Due to the almost complete absence of "dead" cells (PI stained) the two components of the LIVE/DEAD kit have been plotted separately (**Figures 6.15 and 6.16**). In **Figure 6.15**, the effect of each formulation on biofilm attachment and growth is shown (Syto 9). Overall, a clear difference in biofilm growth is apparent for both experiments (*i.e.* juglone and Cu_2O-containing coatings), with PMMA and PMMA + ROS (controls) acquiring significantly higher growth (p = 0.004).

Within the different formulations (*i.e.* JUG + PMMA + ROS *vs*. JUG + PMMA; PMMA + ROS *vs*. PMMA; and Cu_2O + PMMA + ROS *vs*. Cu_2O + PMMA) no significant difference in biofilm growth was found. However, between coatings with the same binder a significant effect was

found for the ones with the combination of PMMA + ROS, *i.e*. growth was significantly higher in the (-)ve controls (PMMA + ROS) when compared to the experimental (JUG + PMMA + ROS) and the biocidal coating (Cu_2O + PMMA + ROS) with $p = 0.042$ and $p = 0.003$, respectively. For the PMMA-containing coatings (*i.e*. rosin was not present), no significant difference in biofilm growth was observed for both juglone- and Cu_2O- containing coatings (*i.e.* the JUG + PMMA *vs*. PMMA and Cu_2O + PMMA *vs*. PMMA). This indicates that PMMA alone as a binder was not performing as well as the one with the rosin additive. The release assays in **Section 6.3.2.1** have demonstrated that when PMMA was used as the sole binder most of the measured concentration was found to be released within the first 24 h. On the other hand, the combination of PMMA + ROS illustrated a more controlled release with the juglone concentration accumulating throughout the test duration, *i.e*. reaching higher values at 48 h. Although in the current experiments the juglone concentrations (released from the coatings) were not measured, it can be assumed that a similar response occurred since the coatings were nominally identical. As discussed previously in **Chapter 5**, it is important to consider the partitioning coefficient of juglone as well as its half-life, since these will influence the compound's concentration both in the solution and at the coating / biofilm interface. Thus, the juglone 'burst effect' from the PMMA coating may have resulted in a rapid release of the compound from the coating during the first 24 h which would then be dispersed and diluted in the well solution during the remaining 24 h, thereby lowering the anti-biofilm potency (relatively short half-life). The rosin addition may have allowed greater availability of the compound at the coated surface throughout the 48 h (constantly being released), potentially resulting in a better anti-biofilm performance.

When the juglone-containing coatings (*i.e.* Experimental: JUG + PMMA + ROS and JUG + PMMA) were compared against the Cu_2O-containing coatings (*i.e*. biocidal: Cu_2O + PMMA + ROS and Cu_2O + PMMA) no significant difference in biofilm growth was found. Therefore, it can be concluded that the juglone-containing coatings performed similarly as those containing the booster-biocide (the Cu_2O-containing), indicating a clear anti-biofilm activity against *C. marina*.

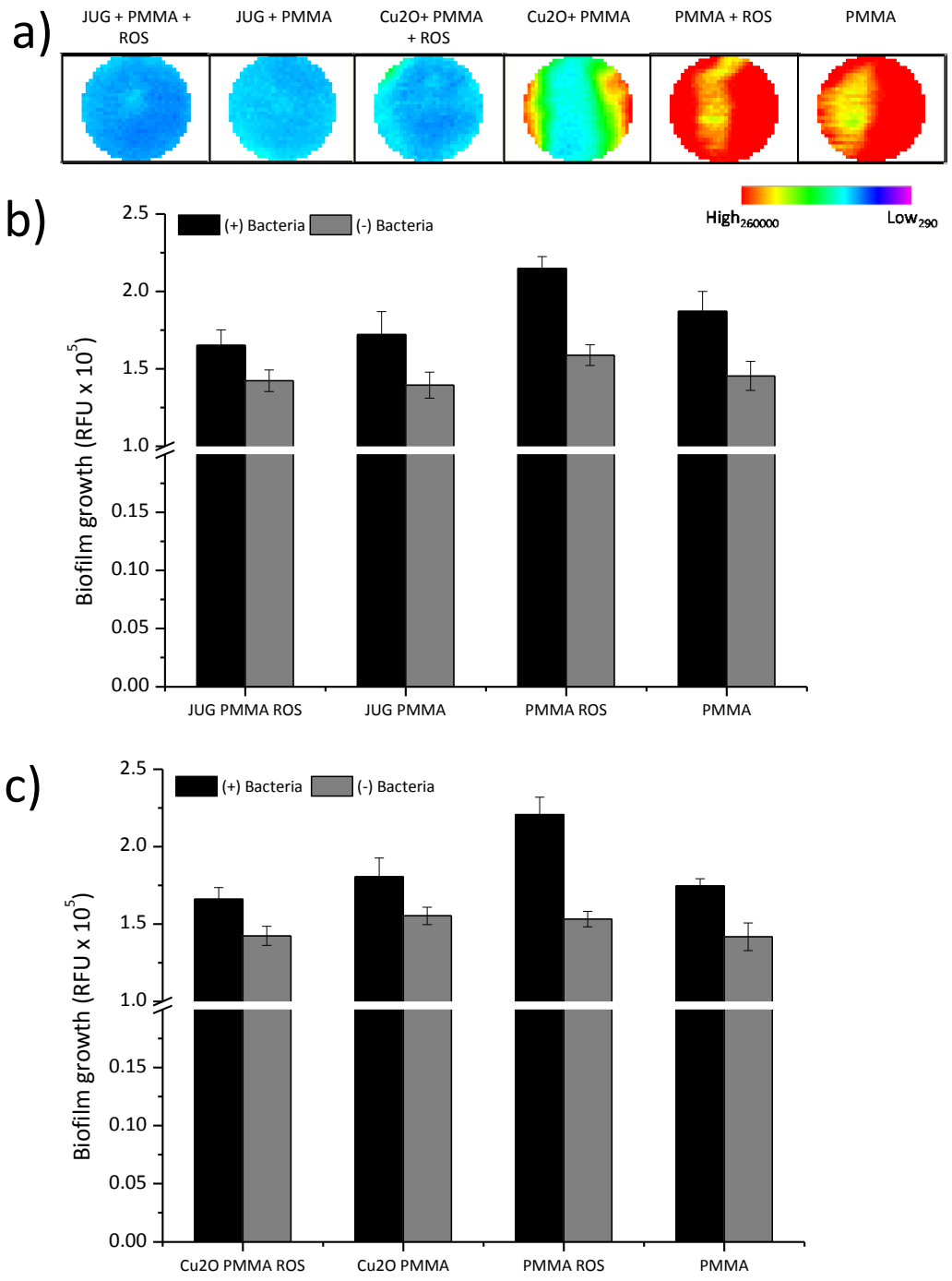

Figure 6.15. Biofilm growth/adhesion using LIVE/DEAD (Syto9) nucleic acid staining on coated coupons *Experimental*: JUG + PMMA + ROS, JUG + PMMA, *biocidal*: Cu_2O + PMMA + ROS, Cu_2O + PMMA and *(-)ve control*: PMMA + ROS, PMMA, where: a) well-scanning (213 × 213 µm scanning matrix), b) plotted fluorescence signals from Experimental and (-)ve control and c) plotted fluorescence signals from *biocidal* and (-)ve controls. RFU: Relative Fluorescence Units, ± SE, *n* = 6 (replicated twice).

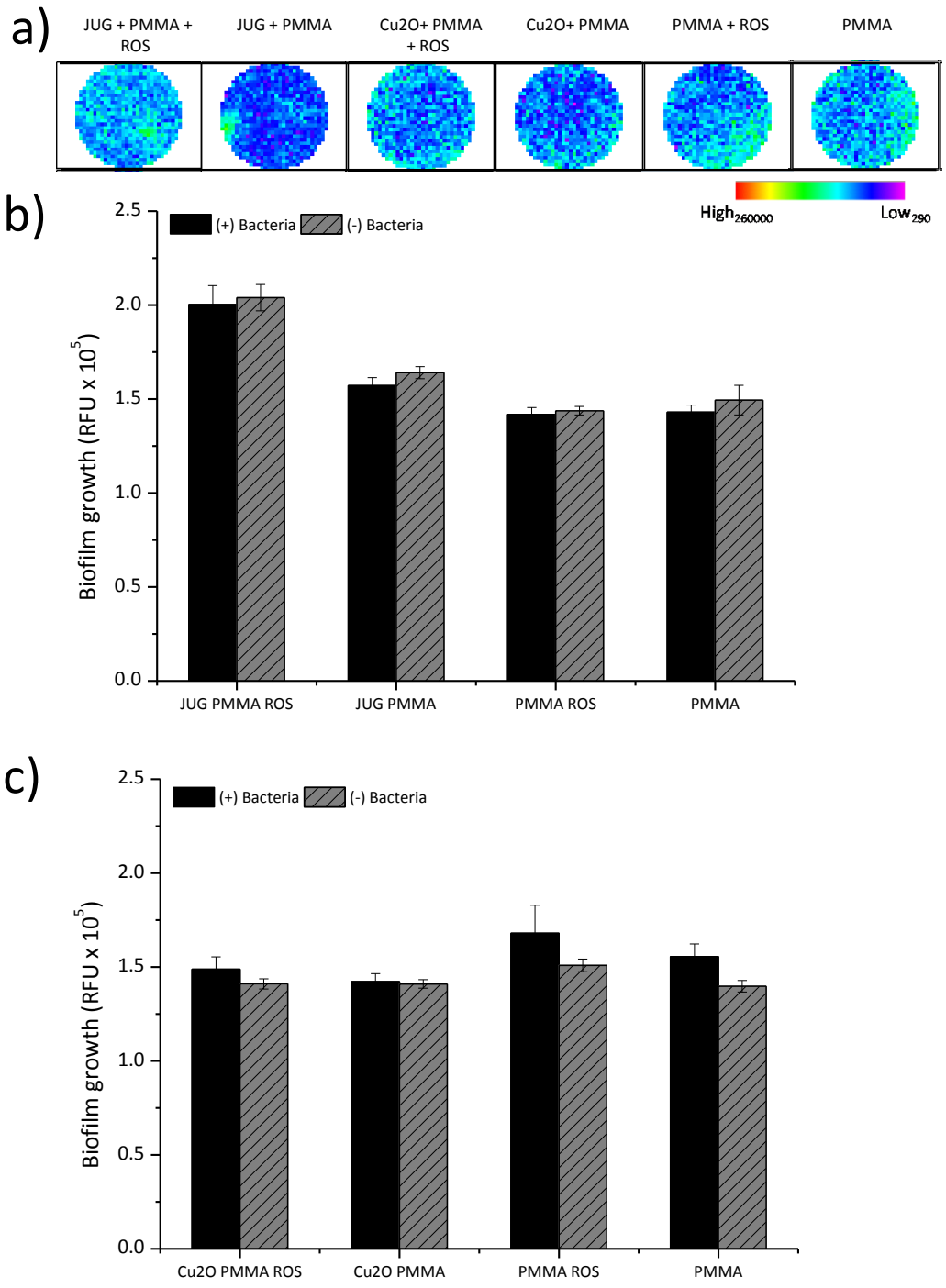

Figure 6.16. Biofilm growth/adhesion using LIVE/DEAD (PI) nucleic acid staining on coated coupons *Experimental*: JUG + PMMA + ROS, JUG + PMMA, *biocidal*: Cu_2O + PMMA + ROS, Cu_2O + PMMA and *(-)ve control*: PMMA + ROS, PMMA, where: a) well-scanning (213 × 213 µm scanning matrix), b) plotted fluorescence signals from Experimental and (-)ve control and c) plotted fluorescence signals from *biocidal* and (-)ve controls. RFU: Relative Fluorescence Units, ± SE, *n* = 6 (replicated twice).

As discussed in **Section 6.3.1.3**, before bacterial inoculations the coatings were found to auto-fluoresce at the LIVE/DEAD wavelengths using the well-scanning function of the plate reader. This was confirmed by epifluorescence microscopy at the experimental end-point using the same wavelengths as the ones for the plate reader where localised fluorescing surface features were present, see **Figure 6.17**. This explains the overall high RFU values found across the various experiments. For this reason in **Figure 6.18** the signals derived from the blank coatings (*i.e*. no bacteria) have been subtracted.

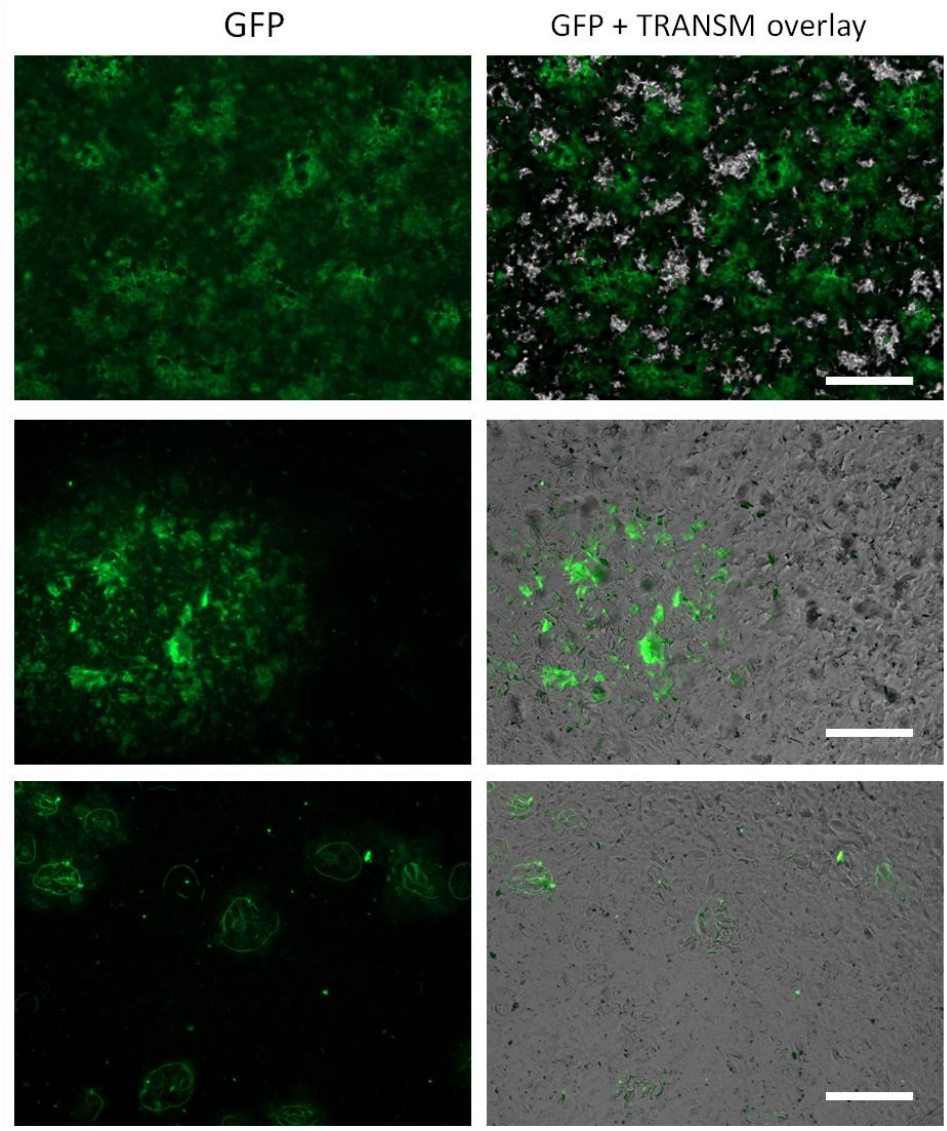

Figure 6.17. Epifluorescence and transmitted microscopy of blank coatings (no bacteria) at the end point (48 h) where, *Top*: Cu_2O + PMMA + rosin, *Middle*: PMMA and *Bottom*: PMMA + Rosin. Scale bars = 100 µm.

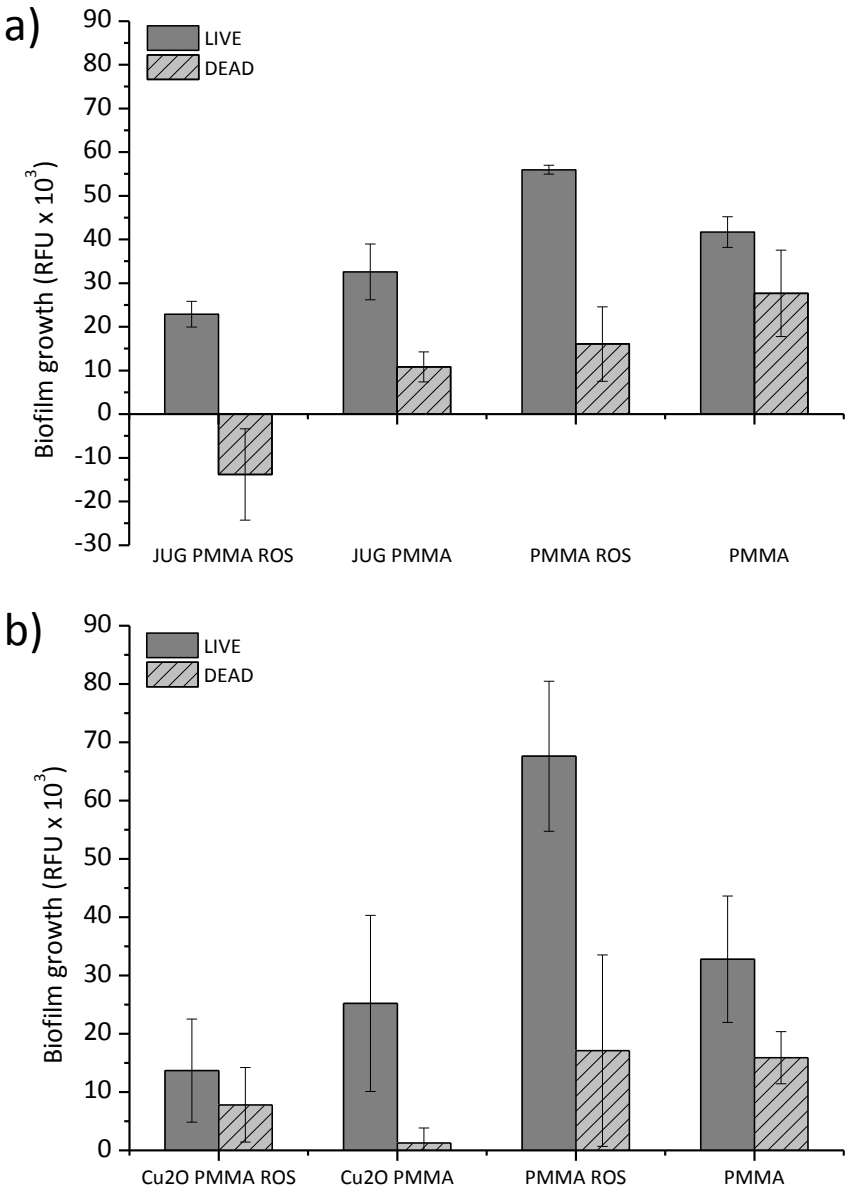

Figure 6.18. Biofilm growth at 48 h where the blanks have been subtracted for both stain wavelengths (LIVE/DEAD). Error bars ± SE.

6.3.2.4 Planktonic growth

The planktonic growth measured at the 48 h end-point within the wells can be seen in **Figure 6.19.** Interestingly, no significant difference was found in planktonic growth within the wells containing the different coatings. This suggests that only biofilm attachment was affected by the juglone- and Cu_2O-containing coatings, while these data also agree with findings on planktonic growth from Experiment 1 (**Section 6.2.2**), where only biofilm formation

was inhibited. Agar growth experiments did not show any differences between treatments, confirming this way, that planktonic growth was not affected.

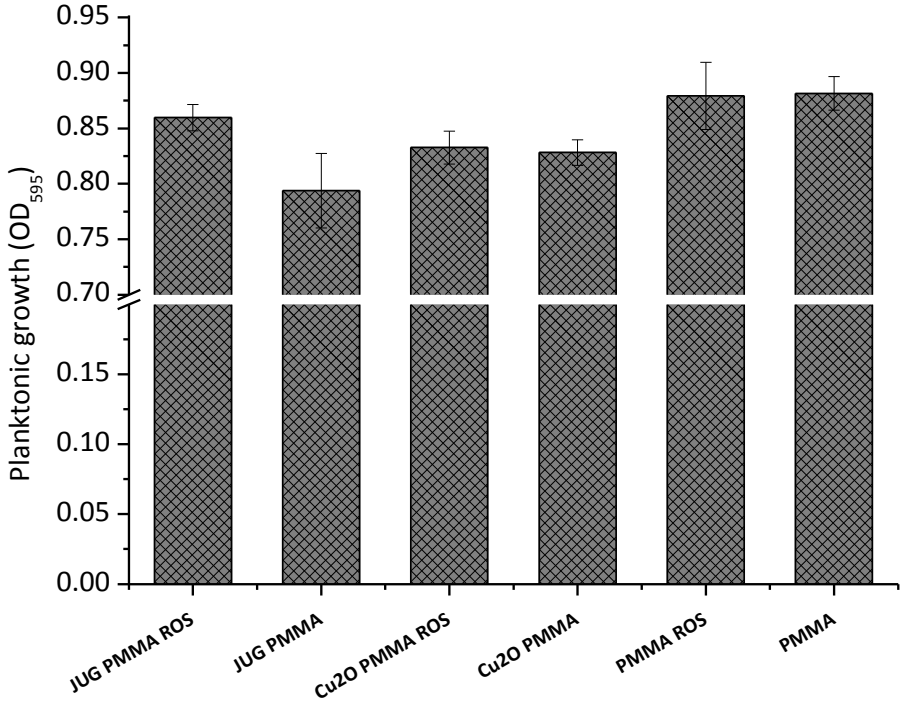

Figure 6.19. Planktonic growth of *C. marina* at the experimental end-point (48 h), as a function of OD_{595}, taken from wells containing the coated surfaces as indicated in the *x*-axis. Error bars ± SE.

Visual examination of the Cu_2O-containing wells illustrated interesting observations, as seen in **Figure 6.20**. In the wells where the Cu_2O-containing coupons were incubated, the solutions were coloured blue in the uninoculated-with-bacteria wells (- bacteria), especially for the Cu_2O + PMMA + ROS coupons. The latter verifies the "hypothesis" that the addition of rosin would enhance the leaching of compounds into the well solutions. The colour change may be attributed to oxidation of the Cu_2O into Cu^{2+} ions, typically characterised by blue (*e.g.* Lincoln et al. 2003, Ogden and Beer 2006).

On the other hand, the wells containing the same coupons but inoculated with bacteria did not demonstrate a colour change. This suggests that a bacteria-Cu_2O interaction may have occurred. Indeed, some marine biofilm bacteria, such as *Marinobacter* sp. have been shown to have Cu^{2+} binding capabilities (Bhaskar and Bhosle 2006). It has been observed that adhered bacterial cells visualised on copper-based surfaces have been associated with copious amounts of extracellular mucilage (Dempsey 1981, Molino et al. 2009a). Specifically for *C. marina,* it has been shown that this species in batch culture has copper binding abilities that reach 16.8 μg

mg^{-1} (Ford et al. 1987, Bhaskar and Bhosle 2006). EPS generally contains high molecular weight compounds with charged functional groups and possess both adsorptive and adhesive properties. Due to the presence of charged moieties, EPS ideally serves as a natural ligand source providing binding sites for the charged particles and/or molecules including metals (Decho 1990). The higher affinity of EPS towards copper might assist in the immobilization of copper in the natural environment, thereby protecting the cells from copper toxicity, as suggested by Bhaskar & Bhosle, 2006 (also, Kazy et al. 2002, Teitzel and Parsek 2003).

Overall, there is good agreement in the literature suggesting that when exposed to copper (or other heavy metals) the bacterial phenotype preferred is the biofilm due to the high EPS binding ability, as opposed to a planktonic state. However, in most cases copper is dosed in the solution resulting in highly toxicities, thus influencing the bacterial layer in the liquid-biofilm interface (*e.g.* Teitzek and Parsek 2003). In the present work Cu_2O is incorporated within a coating therefore, the initial bacterial attachment is likely to be directly affected during the colonisation process. Indeed biofilm formation was not apparent in the current work, rather a unicellular layer on the surface was only present (**next Section**, **Figure 6.23**). Within the well, a concentration gradient of Cu_2O leaching into the solution would be expected, with higher Cu_2O (or Cu^{2+}) concentrations closer to the coating-liquid interface. This may explain two phenomena: (*i*) the lack of biofilm on the surface and (*ii*) the presence of planktonic bacteria within the well column (no significant difference when compared to the controls). Additionally, the lack of dead (PI-stained) cells indicates that the concentration of Cu^{2+} was not sufficiently high enough to be toxic to *C. marina*.

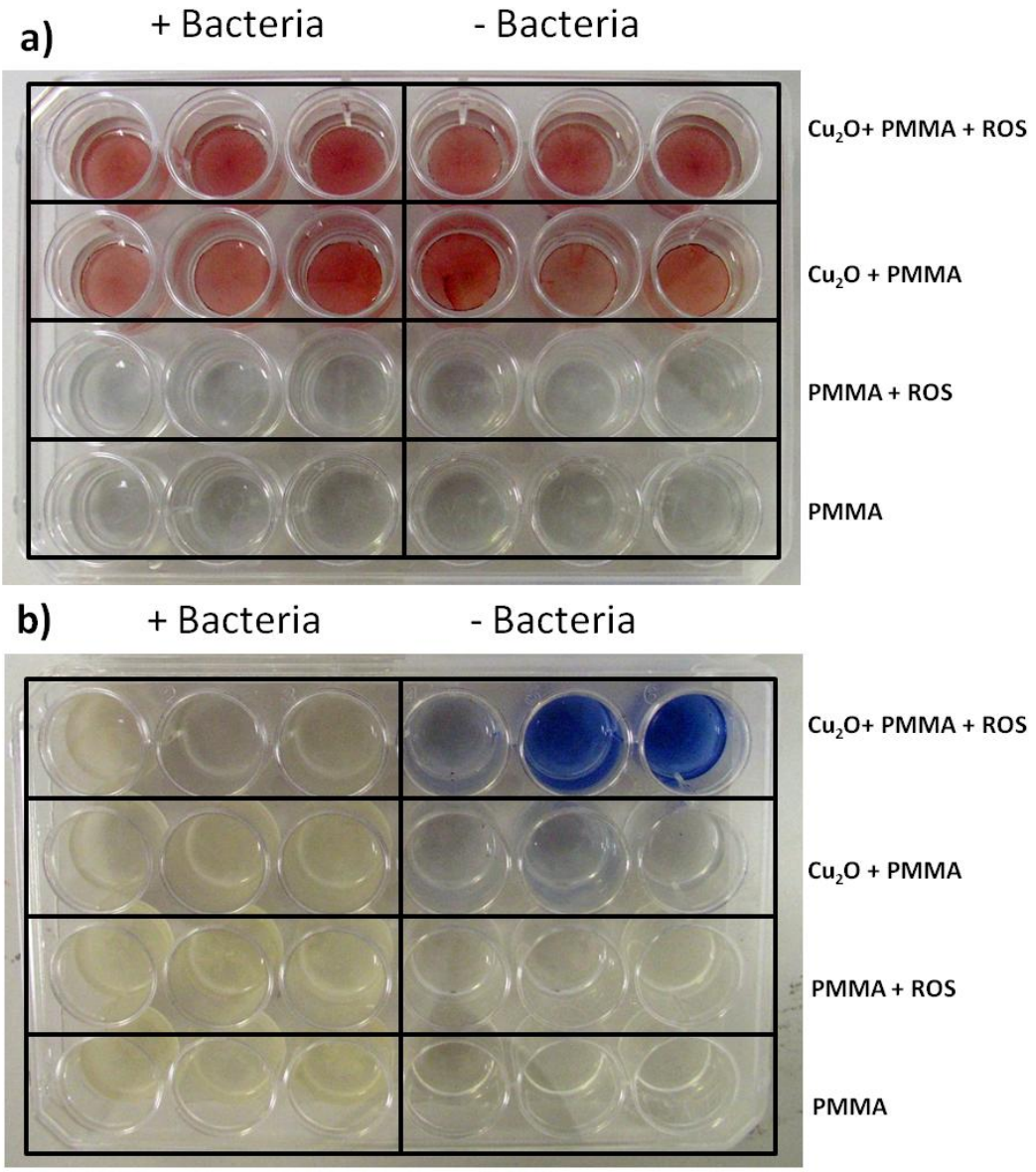

Figure 6.20. Pictures of the 24-well plate at the experimental end-point (48 h) where: a) the Cu_2O-containing coatings and (-)ve Controls and b) the solutions remained following coupon removal. Note the differences in blue-colouration in the solutions from the blanks (- bacteria).

6.3.2.5 Biofilm morphology

Data analysis from the CLSM using COMSTAT was undertaken in order to: (*i*) confirm the plate reader results; (*ii*) allow the direct comparison between the two techniques and (*iii*) to utilise the high resolution of the CLSM to assess the biofilm microstructures that formed on the various coatings. **Figures 6.21** to **6.23** show the CLSM images obtained from 3D stacks associated with the experimental, (-)ve and biocidal control formulations, respectively. The experimental (JUG + PMMA + ROS, JUG + PMMA) are characterised by single and/or chains of cells with an apparent lack of EPS, **Figure 6.21**. Conversely, for the (-)ve control coatings (PMMA + ROS and PMMA) clear biofilm structures can be seen, especially on the PMMA + ROS where a thick and relatively homogenous biofilm is formed, while on the PMMA control, evidence of clustered cells and EPS is also apparent, however to a lesser extent (when compared to PMMA + ROS), see **Figure 6.22**. For the biocidal (*i.e.* Cu_2O + PMMA + ROS and Cu_2O + PMMA), no biofilm formation can be seen and the cell morphology appears to be different with maybe few rod-like cells and more undefined shaped particles, leading to doubts as to whether these are bacterial cells. Indeed, in the previous **Section** (**6.3.2.5**) epifluorescence microscopy on blank Cu_2O coatings (without bacteria) showed fluorescing structures (see **Figure 6.17**), and therefore, any by-products deriving from the coating material cannot be excluded as being the structures seen in **Figure 6.23**.

Specifically, there was a significant effect (p = 0.000) on biofilm growth between the coatings containing PMMA + ROS (JUG + PMMA + ROS *vs*. Cu_2O + PMMA + ROS *vs*. PMMA + ROS) which was associated with both higher thickness and biovolume (p = 0.000 for both parameters) found on the (-)ve controls (PMMA + ROS). These results agree well with the data obtained from the plate reader. The same significant effect (p = 0.002) of the (-)ve controls on biofilm morphology was also observed for the JUG + PMMA *vs*. Cu_2O + PMMA *vs*. PMMA, *i.e.* greater biofilm thickness and biovolume (p = 0.001 and p = 0.002, respectively) were found on the PMMA coatings. This effect was not evident for the plate reader data.

Table 6.4. Biovolume and maximum biofilm thickness of *C. marina* found on coated surfaces by COMSTAT analysis. JUG = juglone, PMMA = poly(methyl methacrylate), ROS = rosin.

Formulations	Coatings	Max. thickness (μm)	Biovolume ($\mu m^3\ \mu m^{-2}$)
Experimental	1. JUG + PMMA + ROS	12.3 ± 0.6	0.09 ± 0.04
	2. JUG + PMMA	12. 5 ± 2.3	0.04 ± 0.02
(-)ve Control	3. PMMA + ROS	33. 5 ± 5.2	8.60 ± 2.17
	4. PMMA	23.0 ± 2.0	1.10 ± 0.49
biocidal	5. Cu_2O + PMMA + ROS	10. 9 ± 0.6	0.01 ± 0.00
	6. Cu_2O + PMMA	9.8 ± 0.7	0.01 ± 0.00
P_{KW} value	1 *vs.* 3* *vs.* 5	p = 0.000	p = 0.000
P_{KW} value	2 *vs.* 4* *vs.* 6	p = 0.001	p = 0.002
P_{KW} value	1 *vs.* 2	NS	NS
P_{KW} value	3 *vs.* 4	p = 0.043	p = 0.005
P_{KW} value	5 *vs.* 6	NS	NS

± SE, $_{KW}$ = Kruskal-Wallis, starred coatings (*) signify those that contribute to the effect.

As observed with the plate reader measurements, the CLSM data also confirmed the absence of "dead" cells. This implies a non-toxic effect of the coatings on biofilms, and therefore, only inhibition of attachment and growth, however, the almost complete lack of "dead" cells still remains to be fully understood. As already discussed in **Chapter 5,** the overall toxicity mechanism of naphthoquinenes has still not been clearly established, especially for prokaryotes, however, the potential interference of juglone (which is a strong redox cycler with high potential to react with oxygen and its reactive species) on cell division and membrane transport (Bertin et al. 2003, Chobot and Hadacek, 2009) may account for the overall inhibition of biofilm growth on juglone-coated surfaces found in the current work.

The use of CLSM was found to be informative on various additional biofilm characterisation parameters corroborating / adding to the less sensitive but high throughput analysis by the plate reader. Overall, there was good consistency between the two techniques underlining a good anti-biofilm performance of the juglone containing coatings. The few discrepancies between the two datasets may be attributed to the nature of the measurement methods, *i.e*. CLSM uses laser light which provides better controllability since emitted wavelengths can usually be optimised to limit overlapping of the coatings' auto-fluorescence and the nucleic acid stains.

This assay was designed for the rapid evaluation of AF coatings on biofilm attachment and/or initial formation. The experimental time scale was extended to 48 h (as opposed to 1-2 h, as shown in chapter 5) due to the nature of the coatings, *i.e*. biocide-release. As explained in the previous section, the use of PMMA as a binder is beneficial due to its inert nature (and biodegradable), but also, the majority of the compound's release has been shown to take place within the first 24-48 h (burst effect), therefore it was necessary to extend the experiment appropriately. A successful AF technology against biofouling should be able to last for more than five years in order to be economically viable. However, testing in the lab cannot be achieved over such expended time-scales. The main aim is to test whether an AF technology is effective against initial biofilm formation and as such, the methodology developed in the current study illustrated good AF efficacy within the desired time-scales. As discussed in **Chapter 3,** AF technologies are now focusing on no-release-biocide based coatings due to acknowledged problems with legislation approvals, shifting attention towards FRCs and/or non-leaching ("tethered") biocide coatings (Kugel et al. 2011), as well as topographically modified surfaces (Scardino et al. 2011). For such technologies, AF activity is aimed to have an immediate response towards fouling, therefore testing for initial attachment at short time scales would be appropriate. Thus, the methodology developed in the current study would be ideal for assessing initial biofilm processes, such as attachment and formation, making this method directly comparable to field trials/realistic scenarios.

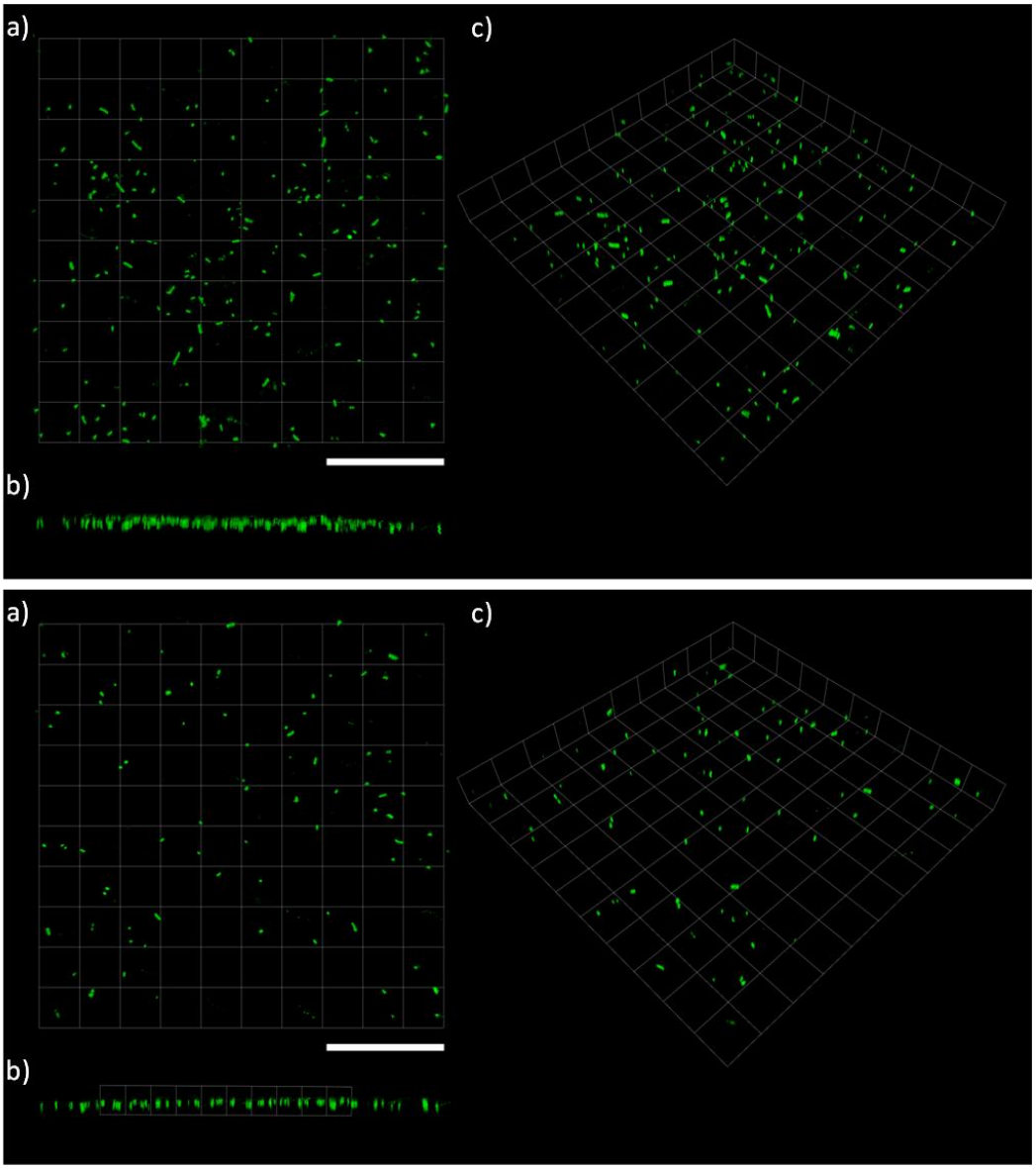

Figure 6.21. CLSM microscopy on LIVE/DEAD stained *C. marina* on the coated surfaced at the end-point (48 h), where *Top*: JUG + PMMA + ROS, *Bottom*: PMMA + ROS and a) top view, b) side view and c) 3D view. Each scare on the grid: 37.65 µm^2, scale bars: 112 µm.

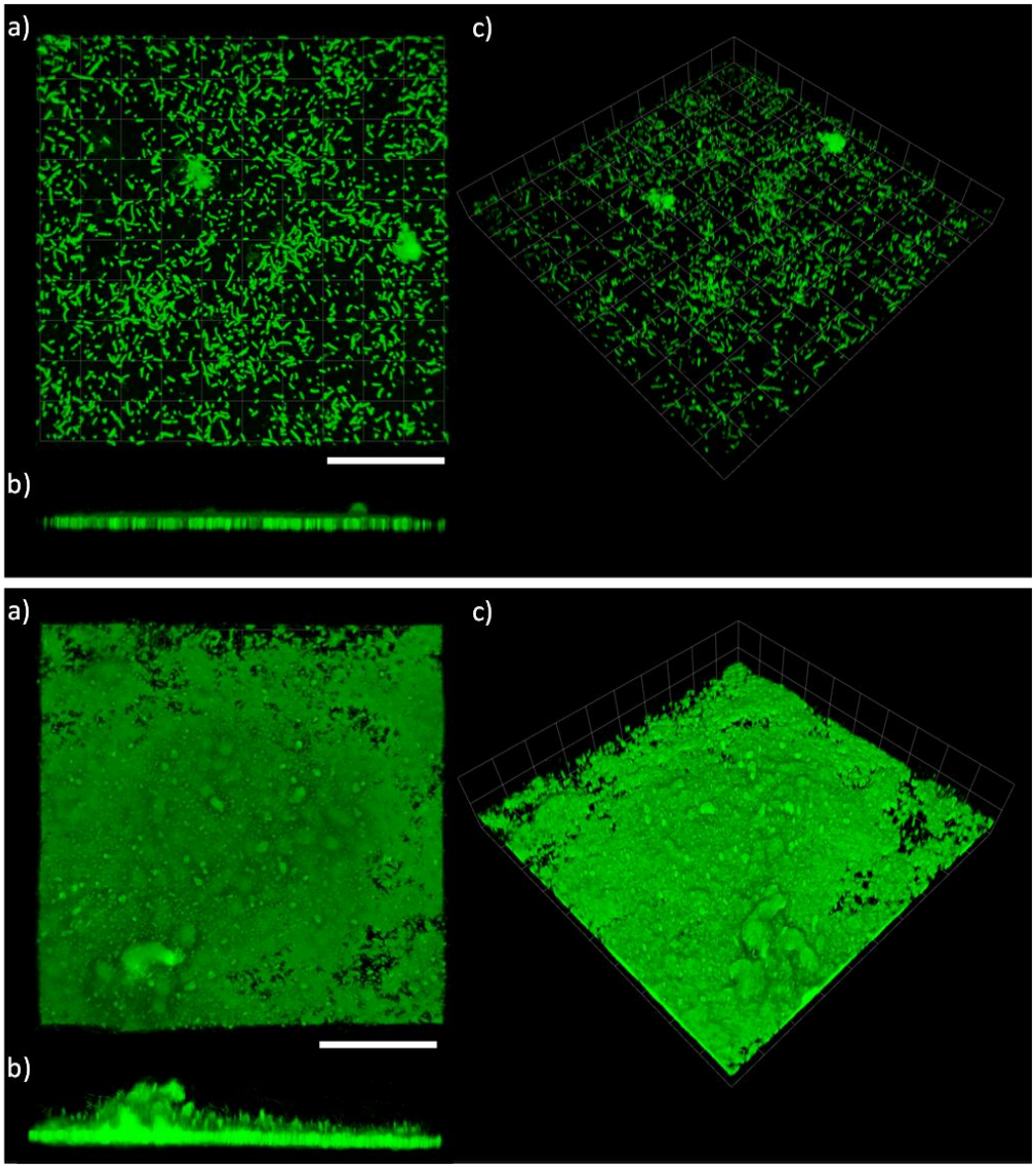

Figure 6.22. CLSM microscopy on LIVE/DEAD stained *C. marina* on the coated surfaces at the end-point (48 h), where *Top*: PMMA + ROS, *Bottom*: PMMA and a) top view, b) side view and c) 3D view. Each scare on the grid: 37.65 µm^2, scale bars: 112 µm.

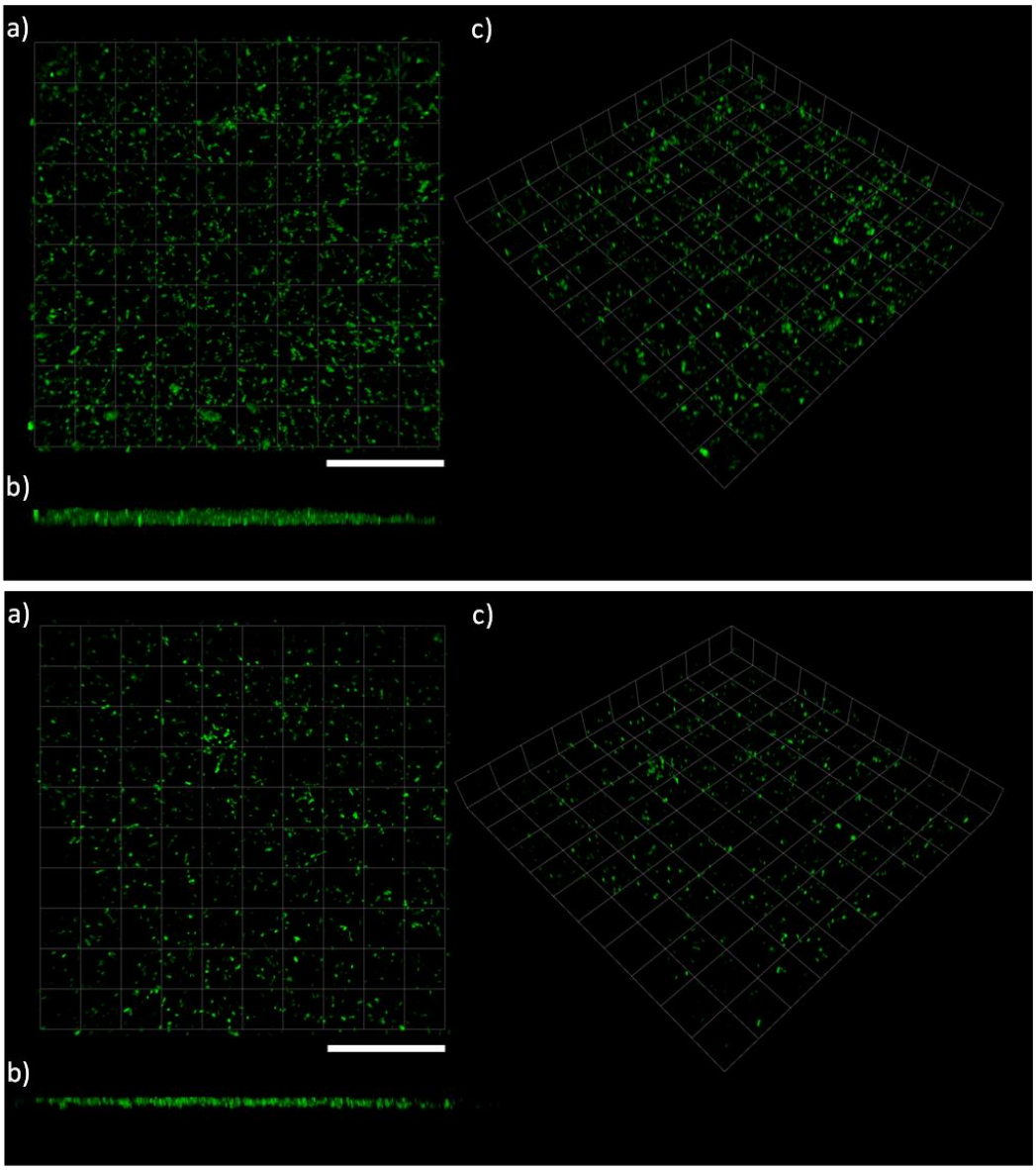

Figure 6.23. CLSM microscopy on LIVE/DEAD stained *C. marina* on the coated surfaces at the end-point (48 h), where *Top*: Cu_2O + PMMA + ROS, *Bottom*: Cu_2O + PMMA and a) top view, b) side view and c) 3D view. Each scare on the grid: 37.65 µm^2, scale bars: 112 µm.

6.4 Summary

The development of a novel bioassay that assessed NP-containing coatings against marine biofilms was achieved.

- **Experiment 1:**

Marine NP-coatings containing *C. crispus* and *B. bifurcata* demonstrated good AF activity against *Pseudoalteromonas* sp. the terrestrial NP-coatings (*i.e.* usnic acid and juglone) did not illustrate AF activity against *Pseudoalteromonas* sp. Differences between the two formulations may be attributed to: *i*) the choice of binder, *i.e.* the inert PMMA (formulation 1) *vs*. the erodible Metamare B175™ and/or *ii*) selective activity of marine products against *Pseudoalteromonas* sp. over the terrestrial NPs.

- **Experiment 2:**

The protocol was optimised in terms of: *i*) ideal experimental binder, *ii*) establishing juglone leaching from the coating, *iii*) *in situ* biofilm quantification directly on the coated surfaces using two different techniques, *i.e.* the commercial and high-throughput plate reader and the highly sensitive CLSM, both of which gave consistent results.

Juglone exhibited good AF efficacy, significantly inhibiting biofilm formation when incorporated into a coating giving comparable results with the commercially available booster biocide Cu_2O.

There was no apparent decrease in planktonic growth between the experimental (juglone containing coatings) and the controls ((-)ve controls: just the binder, biocidal: binder + Cu_2O) indicates that only biofilm formation was inhibited (very few compromised cell present). However, more physiological studies are necessary to conclude on the compound's effect on the cell's biology.

Chapter 7

7. Screening of NPs under different flow conditions using three flow cell systems

7.1 Introduction

There has been a shift in the understanding of the bacterial biofilm structures from that of a homogeneous layer of cells embedded in a matrix to a much more complex heterogeneous arrangement (Stoodley et al. 1999). This change has been driven by the use of flow cell devices and high resolution confocal microscopy that has allowed the observation of fully hydrated biofilms. It is now widely appreciated that biofilms consist of cell clusters separated by interstitial voids and channels (Lawrence et al. 1991, Caldwell et al. 1992, de Beer et al. 1994, Massol-Deya et al. 1995, Moller et al. 1998). It was determined that water could flow through these channels (Stoodley et al. 1994) and facilitate the mass transfer of nutrients to biofilm bacteria (de Beer and Stoodley 1995, de Beer et al. 1996). In addition to mass transfer, the biofilm structure will influence, as well as being disturbed by, the hydrodynamics (interfacial drag of a two-phase system) within a flowing system, which will consequently affect detachment (Kwok et al. 1998) and energy losses (Lewandowski and Stoodley 1995, Stoodley et al. 1998, 1999). Detailed knowledge of biofilm structure allows for a better understanding of how developing biofilms are influenced by the surrounding environment and allows better interpretation of biofilm processes, both of which are important in order to control biofilms in industrial situations. Thus, it is the goal of this present study to document and quantify the influence of hydrodynamics and anti-biofilm NPs on the development and structure of a model biofilm-forming bacterium using *in situ* microscopic monitoring and image analysis.

This chapter will focus on three studies that aimed at exploring the feasibility of assessing NP performance and biofilm attachment under controlled hydrodynamic conditions. As previously discussed in **Chapter 6**, within AF technologies the importance of assessing NP

modified surfaces is crucial in order to understand the nature of bacterial inhibition. However, there is only sparsely available published research on the performance of coatings with incorporated NPs and subjected to hydrodynamic flow conditions.

As explained earlier, biofilms constitute complex aggregations of cell clusters with channels running between them where convective flow can facilitate the supply oxygen and nutrients inside the biofilm (Stoodley et al. 1994). This clearly has significant importance in the case of biofilms growing on AF coatings, since not only will these channels transport nutrients from the surrounding water into the biofilm, but they will also assist in the transport of biocides from the AF coated surface through the biofilm to the surrounding water.

This Chapter is separated into three Sections (overall structure is shown in **Figure 7.1**) where three flow cell systems were employed for the assessment of bacterial attachment in the presence and/or absence of NPs:

Study 1: NPs incorporated into a coating system under one shear stress: the *FC81* system.

Study 2: NPs in solutions under two different shear stresses: the *BioFlux* system.

Study 3: Design, fabrication and assessment of a microfluidic device for initial biofilm formation: the *Ship-on-a-Chip* system, which may allow evaluation of NPs in solution as well as into a coated system under four different shear stresses similar to a vessel's *in-service* conditions: the *Ship-on-a-Chip* system.

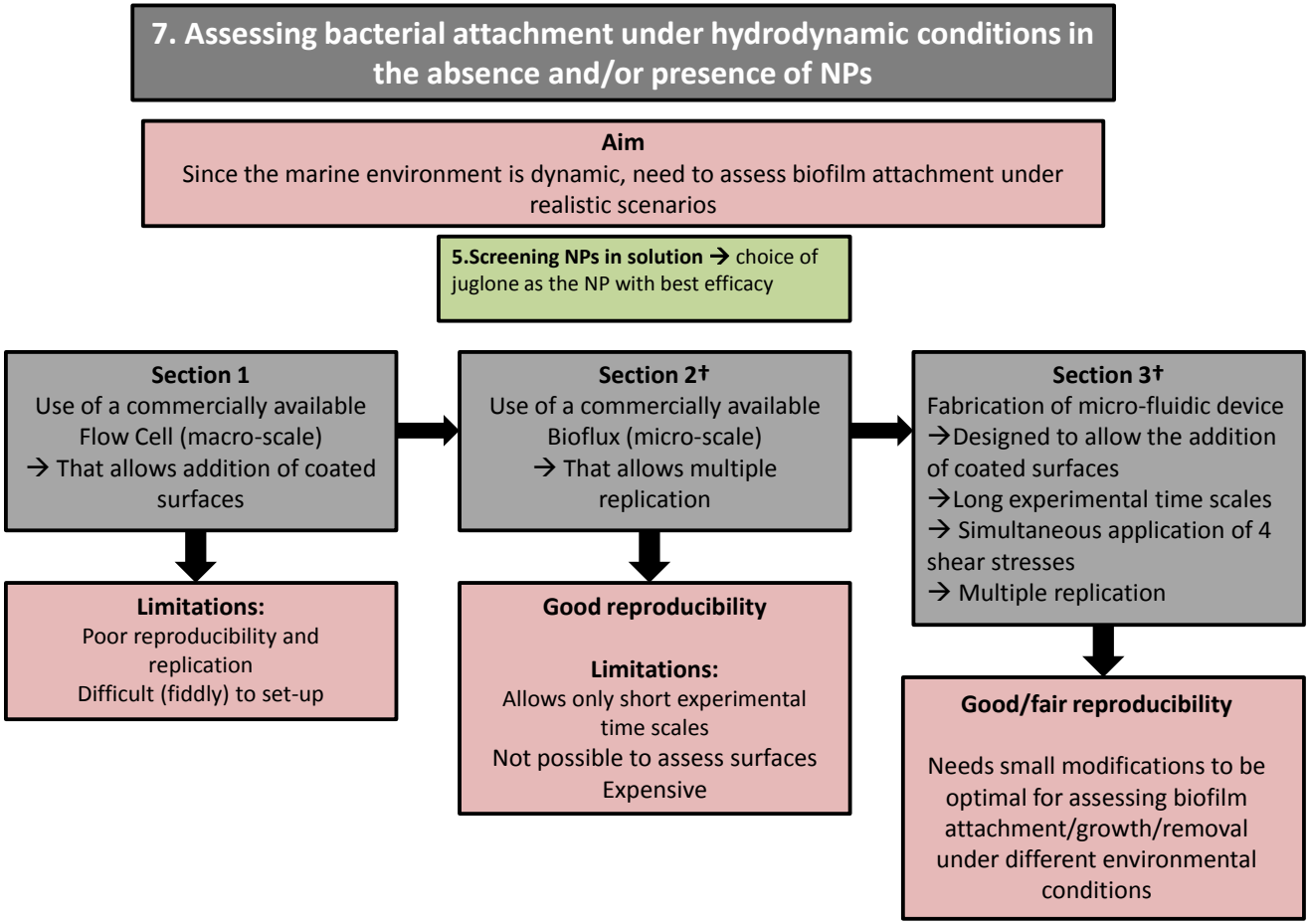

Figure 7.1. Schematic illustrating the lay-out of Chapter 7. The crosses (†) represented submitted work.

7.2 Study 1: Screening of an NP-containing coating system and subjected to flow conditions

7.2.1 Materials and methods

7.2.1.1 Test surfaces

Standard glass microscope coverslips (24 mm × 66 mm; VWR, USA) were cleaned with 100 % EtOH and coated with PMMA incorporating 10 % usnic acid (Sigma-Aldrich). The control surface was just PMMA only. In order to produce a thin uniform film, toluene was added and the resultant film thickness was about 100 µm. Once the coating treatments (PMMA only and PMMA + usnic acid) were applied to the glass coverslip, they were left to completely dry at room temperature for several days. Contact angle measurements of the experimental surfaces were performed in order to characterise their hydrophilic / hydrophobic behaviour (Dennington, Personal communication):

PMMA contact angle: 67.5° (hydrophilic)

PMMA + usnic acid contact angle: 85 - 90° (hydrophobic)

7.2.1.2 Biofilm flow cell system

To observe biofilm morphology, the coated glass slides were incorporated into a closed-cycle flow cell system (**Figure 7.3**). The flow cell (FC81, BST, Bozeman, MT, USA), consisted of a single channel machined into a polycarbonate body sealed with a glass coverslip observation window with channel dimensions of 50 mm × 12.6 mm × 1 mm (length by width by height). The flow cell was connected to a peristaltic pump (Masterflex; Cole Palmer, Niles, Ill, USA) by silicone rubber tubing (1.3 mm internal diameter) in order to provide continuous flow of ASW. Calibration of the peristaltic pump can be seen in **Figure 7.2**. The flow system was first sterilized in an autoclave and then flushed with 70 % EtOH for 15. Three washes followed with sterile-filtered (0.22 µm) deionised water (18 MΩ m purity water) for a total of 1 h. The experimental surfaces were then inserted under sterile conditions (laminar flow hood) and the complete assembled system was flushed with sterile filtered ASW for 1 h to allow conditioning of the chamber and stabilisation of the flow. A magnetic stirrer was used to prevent cell settlement at the bottom of the bottle and also to keep the culture aerated. The flow rate was

set to be 1.2 mL min^{-1}, the wall shear stress was calculated to be 9.52 × 10^{-3} Pa by using Equation 7.1 for rectangular chambers (Bacabac et al. 2005):

$$\tau_w = \frac{6\mu Q}{bh^2} \qquad [7.1]$$

where τ_w = wall-shear stress (Pa), Q = measured volumetric flow rate (m^3 s^{-1}), μ = fluid dynamic viscosity (kg m^{-1} s^{-1}), b = width of the channel (m), and h = distance between plates (m).

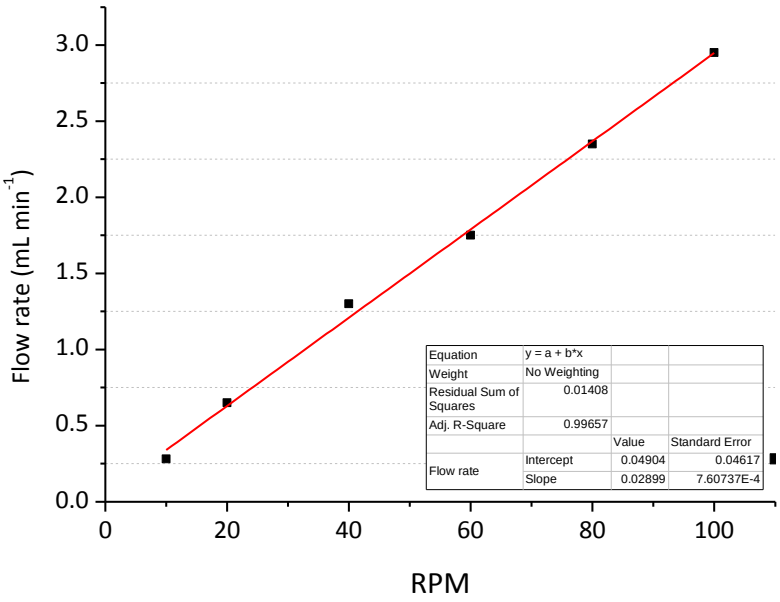

Figure 7.2. Peristaltic pump calibration with a linear fit to determine flow rates. A graduated cylinder was used to collect the water and measure the fluid volume pumped during a fixed time interval.

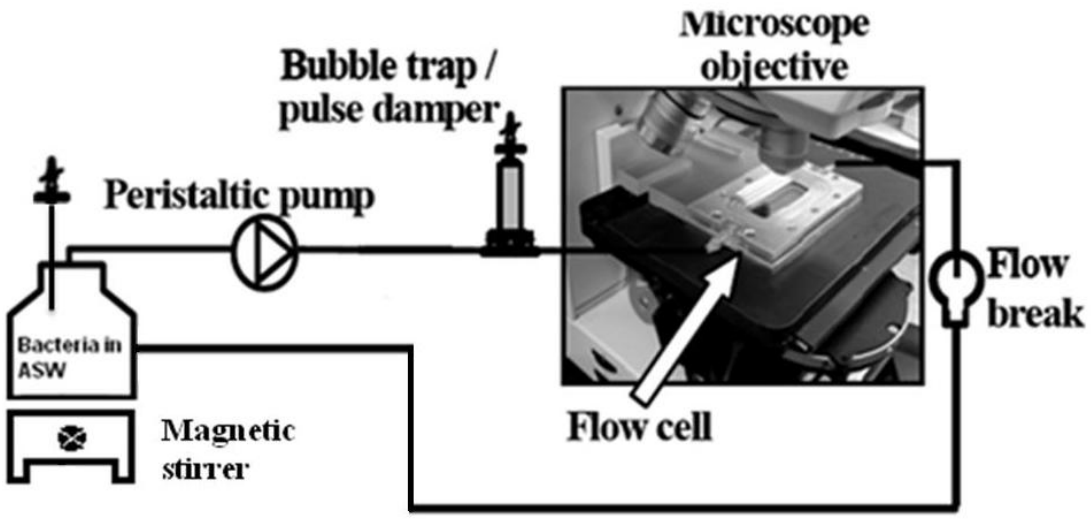

Figure 7.3. Schematic of the FC81 flow cell, closed loop and microscope set up (adapted from Stoodley and Warwood 2003).

7.2.1.3 Attachment bioassay

The marine bacterium *C. marina* was used in this experimental work. Growth conditions can be found in **Chapter 4**. Overnight bacterial suspensions were washed in order to avoid any medium carry-over according to methods described in **Section 4.2.3**. Following OD_{595} measurements (OD_{595}:0.2), the bacteria were added in the closed-cycle flow cell system using a sterile syringe (5 mL).

For each treated surface the following steps were undertaken. After 1 h of bacterial exposure, the flow cell was disconnected from the tubes and transferred under a sterile environment where it was disassembled. The experimental surfaces were then gently washed with ASW using a 1 mL pipette to remove detached bacterial cells. The surfaces were then stained using the FilmTracer™ LIVE/DEAD® Biofilm Viability Kit (Molecular Probes) and incubated at 28 °C for 20 minutes (see **Section 4.2.4** for details). After the incubation period, the test surfaces were rinsed using ASW to remove excess stains and placed into petri dishes containing ASW to avoid dehydration. The petri dishes were then sealed with parafilm and stored at 4 °C overnight for CLSM analysis.

7.2.1.4 Confocal Laser Scanning Microscopy (CLSM) analysis

Image acquisition was performed on a Leica TCS SP2 AOBS (Leica Microsystems, France) confocal laser-scanning microscope (CLSM). The characterisation of biofilms on polymer films (PMMA) containing usnic acid. The PMMA did not show any signs of autofluorescence. LSCM allowed the simultaneous 3D monitoring of PI and SYTO9 dyes. The excitation wavelength used for S9 was λ_{EX} = 488 nm, and the emitted fluorescence was collected in the range of λ_{EM}: 500 to 600 nm. The red fluorescent nucleic acid stain PI was excited at λ_{EX} = 594 nm, and the emitted fluorescence was collected in the range of λ_{EM}: 650 to 700 nm. Images were collected through a ×63 Leica water immersion objective. Simulated 3D fluorescence projections, vertical cross-sections through the biofilms and deconvolution using Wiener filter were generated using the LSCM 3D package of the Leica SP2 software. Biofilm surface coverage and thickness were calculated using ImageJ (MacBiophotonics ImageJ, USA) where CLSM images were converted into a binary system (either 0 or 1) and the biofilm covered areas were quantified.

7.2.1.5 FC81 Computational Fluid Dynamic simulations

In order to validate the theoretical value of shear stress (**Equation 7.1**), a three-dimensional numerical model of the FC81 flow cell was designed. The three-dimensional geometries of the flow cell were created with a CAD software Gambit 2.4.6 (Simmetrix Inc., USA), shown in **Figure 7.4**.

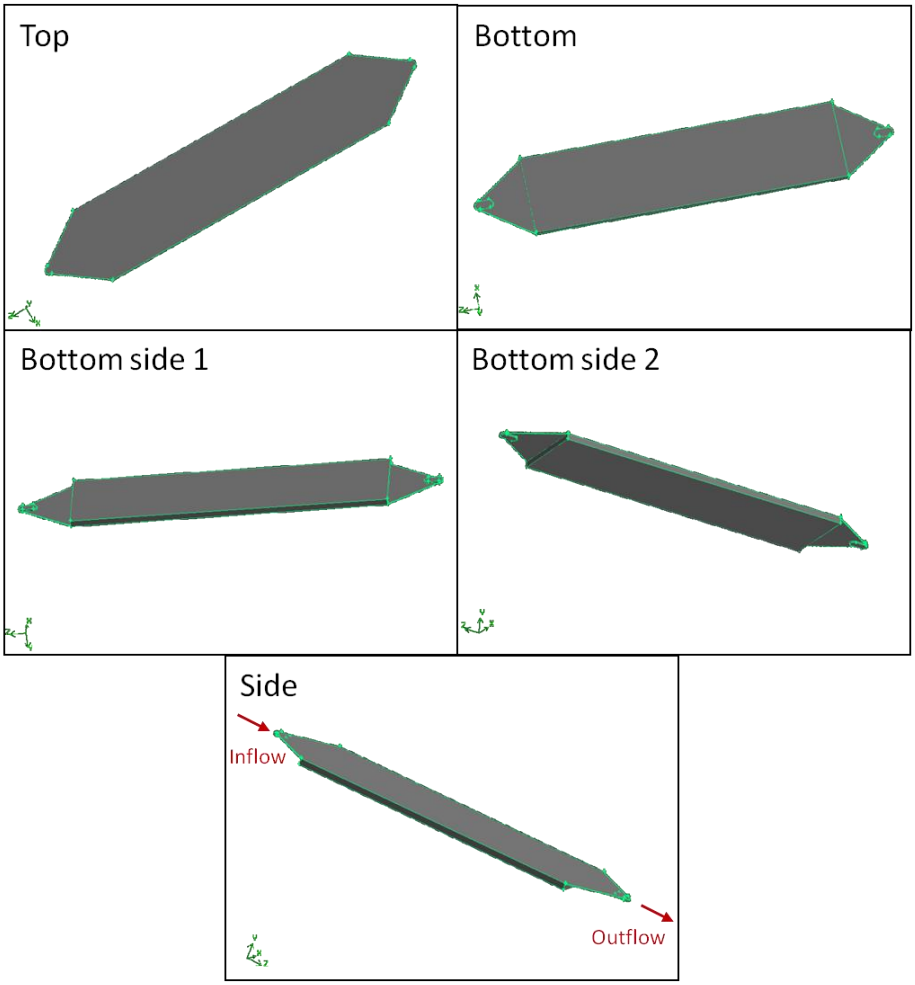

Figure 7.4. Modelled geometry of the flow cell chamber created using CAD software Gambit 2.4.6.

***Meshing*:**

The computational domain was discretized using Gambit 2.4.6 with a stair-step meshing scheme. The stair-step meshing scheme creates and meshes a faceted volume with a shape that approximates the volume to be discretized. All the mesh elements present in the created faceted volume are cubic hexahedra of uniform size.

Total number of elements: 300560

Element size: 0.1 mm

***Assumptions*:**

The following assumptions were made:

- The size of the mesh is subjected to a compromise between a fine mesh density and the computational cost.
- Fluids are considered single phase incompressible.

- A steady flow condition is applied at the device inlet.
- Constant pressure (equal to 101325 Pa) was imposed at downstream outlet boundary.
- No slip boundary condition at channel walls.
- Constant temperature (20 °C).

Viscosity and density of sea water at 20 °C were used to evaluate the boundary conditions. Specifically, the dynamic viscosity was set at 0.00108 kg m^{-1} s^{-1} (Pa s), while the density was set at 1025 kg m^{-3} (National Physical Laboratory, 2012).

Computational procedure:

ANSYS Fluent 12.0 computational fluid dynamic package, which utilizes the finite volume method for spatial discretization, was used to solve three-dimensional, single phase, conservation equations for mass and momentum (Navier-Stokes equation).

7.2.2 Results and discussion

7.2.2.1 Wall-shear stress characterisation of the flow cell (FC81)

Figure 7.5 shows the modelled velocity field within the FC81 flow chamber. Specifically, **Fig 7.5(A)** represents the contour of the velocity magnitude on a cross section perpendicular to the main flow direction. As expected, by the imposition of the non-slip boundary conditions, the velocity is higher in the central region of the chamber and lower at the walls. In **Figure 7.5(B)** the velocity profile is reported which is characterized by a steep gradient in the near-wall region and a relatively uniform profile in the central region. These features are typical of laminar flow through a square-section channel with a high aspect ratio.

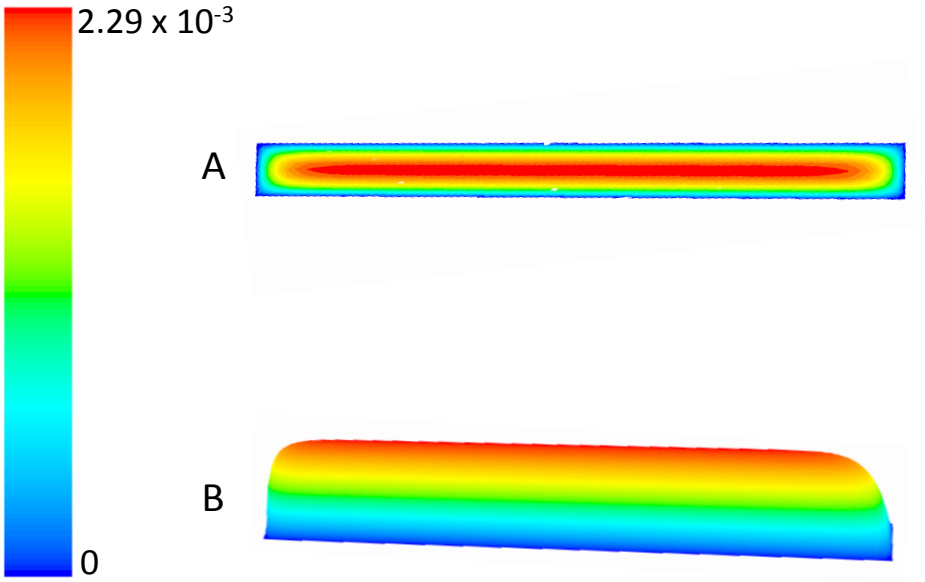

Figure 7.5. (A) The velocity field profile on a cross-section in the middle of the channel and perpendicular to the flow direction (units: m s^{-1}) and (B) three-dimensional velocity profile within the flow chamber, units: m s^{-1}. The velocity has been calculated on a cross-section perpendicular to the flow direction (*z*).

Figure 7.6(A) shows the contour of the wall-shear stress on the coverslip. The wall-shear stress is defined using Equation 7.2.

$$\tau_w = -\mu \frac{dv}{dy}\bigg|_{y=0} \qquad [7.2]$$

where μ is the dynamic viscosity of the working fluid and dv/dy is the velocity gradient, in respect to the y-coordinate perpendicular to the flow direction (the no-slip condition means that the speed of the fluid at the wall (relative to the boundary) is zero). It can be seen that a relatively homogeneous distribution of shear stress is achieved on the plate, apart from localised effects at the entrance and outlet regions (*i.e.* entrance and exit of the flow). A lower shear stress at the corners may also be induced by flow recirculation (**Figure 7.6B**). A plot of the shear stress along a line taken in the middle of the glass coverslip is shown in **Figure 7.6(B)** (from the red dotted line), illustrating a rather uniform wall-shear stress at approx. 8.8×10^{-3} Pa. This value is reasonably consistent with the theoretical value which was calculated to be 9.5×10^{-3} Pa (**Equation 7.1**).

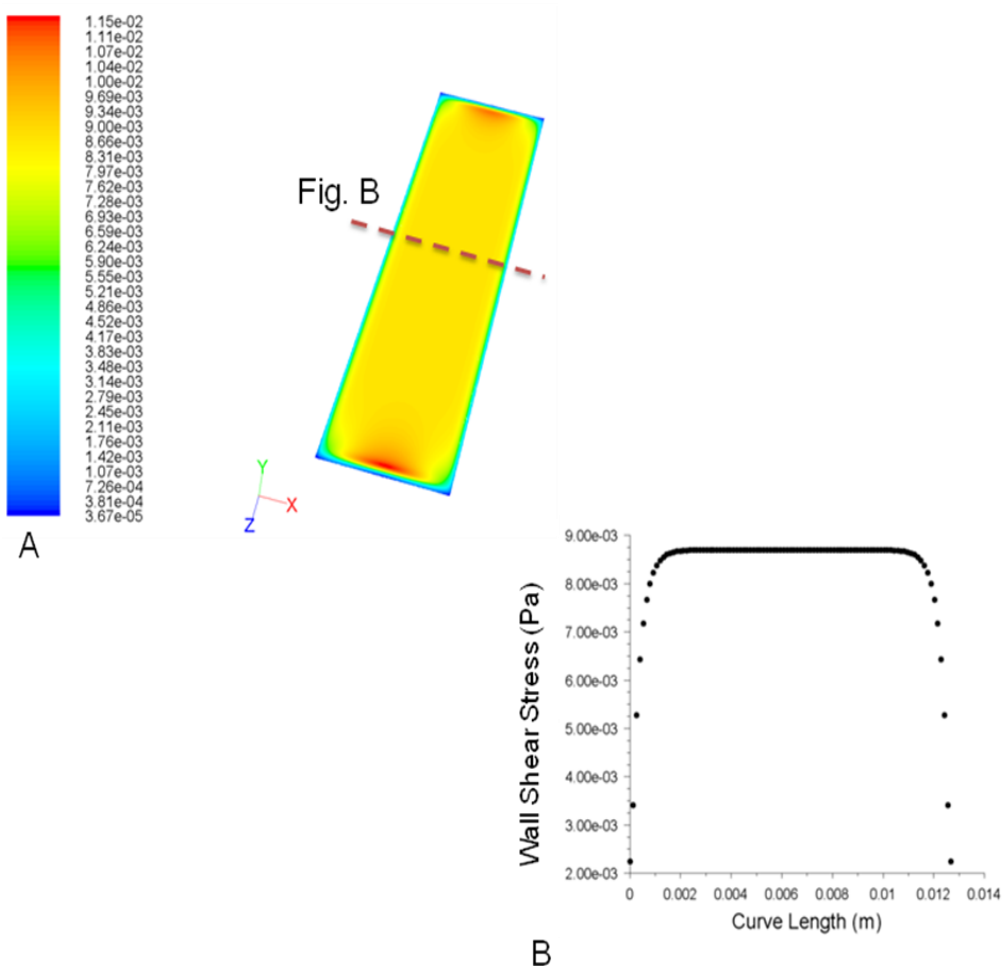

Figure 7.6. (A) Wall-shear stress field across the entire coverslip surface. (B) Plot of the wall-shear stress along a line (red dashed line in A) taken at the centre position of the glass coverslip (A). Units: Pa.

7.2.2.2 NP-coatings and *Cobetia marina* attachment under flow conditions

The FC81 flow cell system was utilised to evaluate the attachment of *C. marina* on a NP-containing surface under controlled flow hydrodynamics. In **Figure 7.7** CLSM images show the differences in biofilm structures between the NP-containing (10% usnic acid + PMMA) and the control surfaces (PMMA only). It is clear that biofilm clusters are formed on the control surface while, on the NP-containing surface a mono-layer formation and individual single cells are evident at the coating interface. The biofilm viability does not appear to be influenced, since both the live *vs*. dead cells are of equal proportion between the control and the NP-containing surfaces. Additionally, a decreased biofilm thickness was observed for the NP containing surface (**Figure 7.8**). Although statistically significant differences in biofilm thickness and surface coverage between the control and the NP-containing surface were not found (**Figure 7.9**), the structural variability between the two substrates suggests an effect of the NP on biofilm attachment. The usnic acid effect on biofilm morphology may be indicative of interference of this molecule with signalling pathways that have been previously observed by Francolini et al. (2004) for *P. aureginosa*. The current results are preliminary as they have not been replicated and the microscopic fields were only three for each experimental surface. This was due to incompatibility of the glass with the coating which was found to be detaching from the substrate (glass) a few hours after the experiments. The limitations and future work on flow cell experiments will be discussed in **Section 7.4.**

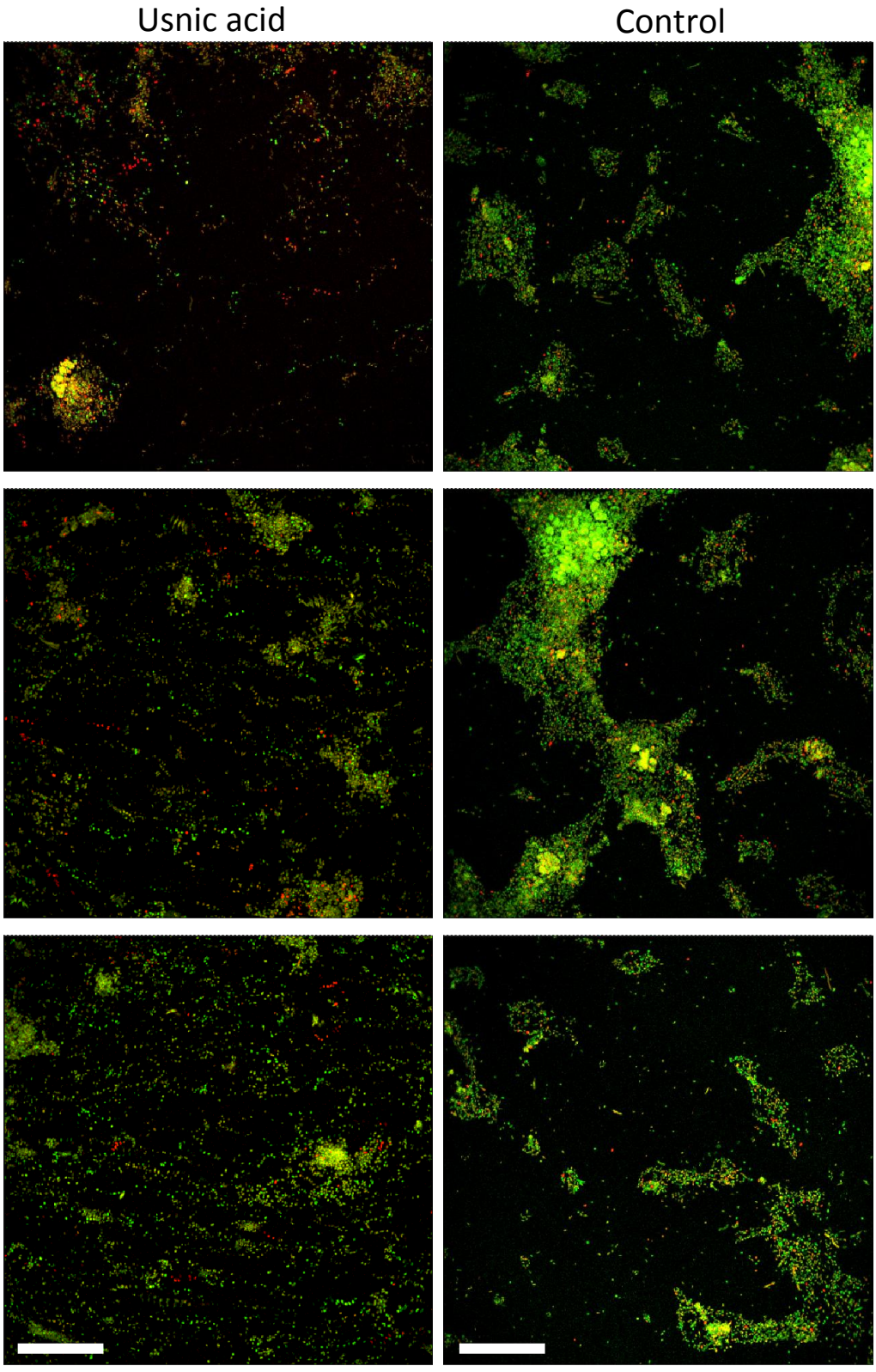

Figure 7.7. CLSM images showing the influence of NP-containing coating (10 % usnic acid + PMMA, *left images*) on *C. marina* biofilm formation in the FC81 flow cell with a flow of 1.2 mL min^{-1} at 25 °C in an ASW medium. Control surface was PMMA only (*right images*). Scale bar = 50 µm.

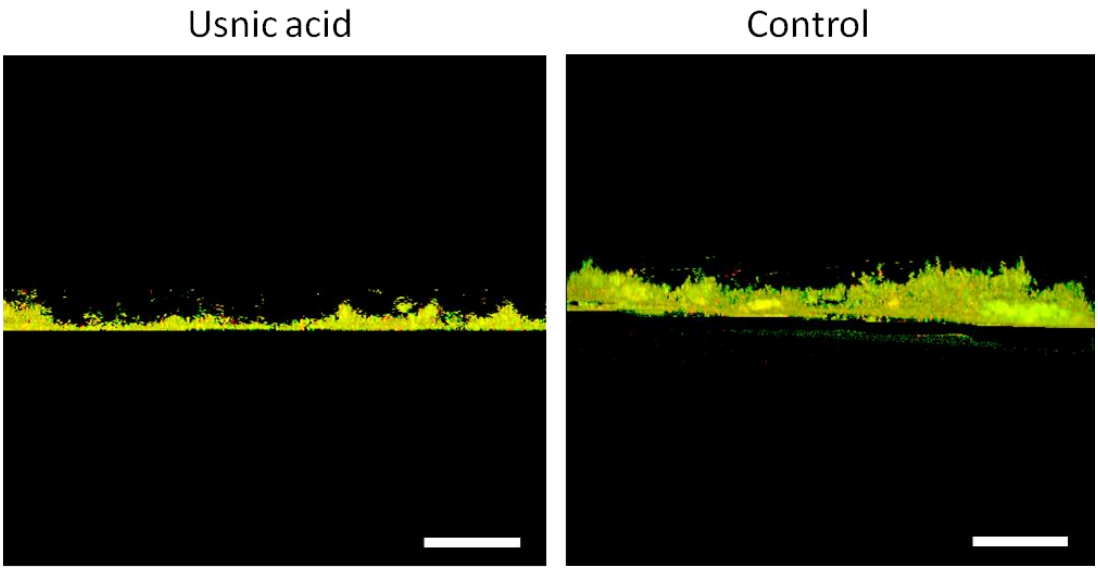

Figure 7.8. CLSM images showing the influence of NP-containing coating (10% usnic acid + PMMA, left image) on *C. marina* biofilm thickness in the FC81 flow cell with a flow of 1.2 mL min^{-1} at 25 °C in an ASW medium. Control surface was PMMA only (right image). Scale bar = 50 µm.

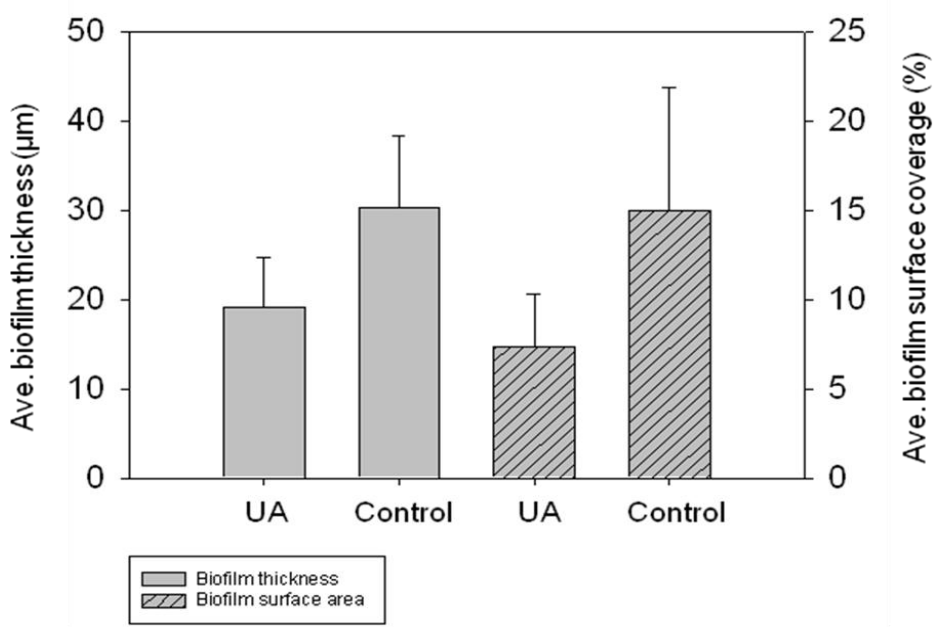

Figure 7.9. Influence of the NP (10% usnic acid + PMMA) on biofilm thickness and surface coverage by *C. marina* in the FC81 flow cell with a flow of 1.2 mL min^{-1} at 25 °C in ASW (Control = PMMA only).

In **Chapter 5**, the effect of usnic acid in solution was investigated against *C. marina* where the results demonstrated that it did not inhibit attachment for this species. However, the negative effect on biofilm morphology when the NP was incorporated into a coating system and subjected to hydrodynamic conditions, illustrate that interactions between bacteria and the NP may not be as straightforward as previously thought. Therefore, the corroboration of AF assays that answer different questions such as: (*i*) NP toxicity, (*ii*) effect of NP on biofilm attachment, growth and physiology and (*iii*) hydrodynamic effects on biofilm attachment, growth and physiology, should be coupled and included in future assessments in order to gain more insightful information about the nature of NP activity against biofilms.

Regarding the hydrodynamic effects on biofilms, Rieu et al, (2008) compared two growth models (static and dynamic flow-cell) for the food pathogen *Listeria monocytogenes* and found that both biofilm structure and spatiotemporal gene expression were greatly affected. It has been proposed that biofilms arranged their internal structures according to the flow velocities at which they are formed in order to control: (*i*) nutrient transport rates and (*ii*) the mechanical elasticity to withstand the shear stress of the surrounding water (Beyenal and Lewandowski 2002). Remarkably, it was suggested that the internal architecture rearrangement satisfied the second goal at the expense of nutrient transport (Beyenal and Lewandowski 2002).

A common challenge in AF assays is the direct assessment of a biocide-containing (in our case NP-containing) coating against marine biofouling. This is largely due to difficulties in measuring and controlling the biocide release rate in dynamic testing with acknowledged problems by the ASTM and ISO release rate methodologies (Howell, 2009). Since biofilms can regulate nutrient and oxygen uptake by diffusive and structural mechanisms (Stoodley *et al.* 1999), NPs/biocides released from a surface may also fall within the same regulatory system. Biofilm-mediated released rates of biocides have been previously proposed as the EPS has shown to bind metals such as copper (Bhaskar and Bhosle 2006) and potentially affect the diffusion rate of the compound and consequently control its release rate (Howell 2009). A good example is the decrease in release rate of about 70 % of TBT when bacteria were inoculated and attached on a TBT SPC coating (Mihm and Leob 1988). One possible explanation was proposed by Liermann et al. (2000) who suggested that exudates from the biofilm could reduce a coating's pH therefore, increasing Cu_2O dissolution and thus release rates. It has been observed that adhered bacterial cells visualised on copper-based surfaces

have been associated with copious amounts of extracellular mucilage (Dempsey 1981, Molino et al. 2009).

In general, the interactions between biofilms and AF coatings remain largely unexplored and any attempt to investigate this relationship would provide invaluable insights on biofilm-mediated biocide release rates.

7.2.3 Summary

- The effect of a NP-containing surface (PMMA plus UA) under flow conditions against *C. marina* attachment was tested for the first time.

- It was found that the UA containing surface had an effect on biofilm with reduced thickness and surface coverage when compared to the control (PMMA).

- Specifically, *C. marina*'s attachment patterns were structurally different between the two experimental surfaces *i.e.* evidence of initial biofilm formation on the control (biofilm clusters) while on the NP surface single cells.

- Although when in solution, usnic acid did not illustrate evidence of AF activity on *C. marina*'s attachment (**Chapter 5**), the current preliminary results indicate that when this NP is incorporated into a coating system and subjected to flow → attachment was negatively affected.

- Protocol/methodology limitations were identified and future improvements include the design and construction of a novel micro-fluidic cell that will allow better experimental replication using a range of controlled hydrodynamic scenarios representative of the natural/real conditions *i.e.* experienced by the biofilms when attached on a ship's hull during movement (15 knots) and docked (1.2 knots – tidal speed), see **Section 7.4.**

- In this study, a three-dimensional model of the FC81 flow cell has been determined for the first time. With this knowledge of the wall-shear stress within the experimental flow cell chamber, a more complete understanding on what shear forces the biofilm experiences has been established for these experimental conditions. In addition, simulating the flow will further result in cell's layout optimisation to avoid localised phenomena such as flow recirculation in the chamber corners.

7.3 Study 2: NPs in solutions under two different shear stresses using a commercial system

7.3.1 Brief introduction

This study assessed natural product AF performance of an isolated compound from a terrestrial source – juglone – against the biofilm forming bacterium, *Cobetia marina*. Novel protocols/bioassays were developed to test the *in situ* AF efficacy of the natural product on attached bacteria utilising a commercially available microfluidic system. Hydrodynamic conditions using microfluidic channels have been uniquely utilised to assess marine AF in terms of biofilm attachment and growth under controlled hydrodynamic regimes similar to tidal flows within ports and dockyards (*e.g.* up 1.2 m s^{-1}, Green Rhino Energy, 2012). These bioassays were corroborated using a suite of microscopy techniques, epifluorescence and confocal laser scanning microscopy, in order to compare biofilm structures in the presence and absence of the juglone.

The majority of biofilm studies previously reported have involved the use of macro-scale reactors (Meyer et al. 2011). More recently, there have been increased efforts to study bacterial biofilms in a microfluidic setting. Microfluidic systems provide several advantages, including inexpensive fabrication, highly parallel throughput, small size, and tight control over the microenvironment for cell culture. One such device is the BioFlux System. Microfluidic devices are ideally suited to study biofilms since they allow the creation of biological niches by providing relevant fluidic conditions such as physiological flow velocities and low fluid-to-cell volume ratios, and by maintaining stable temperature profiles over long periods of time (*e.g.* Richter et al. 2007). The control of these parameters is vital because they determine stress-related cellular signalling levels known to influence cellular behaviour (Park and Shuler 2003).

7.3.2 Materials and methods

7.3.2.1 Test species

The marine bacterium used for the dynamic assays was the biofilm forming species, *Cobetia marina* (ATCC 25374). Bacteria were grown in SSP, according to **Chapter 4** (**Section 4.3.2**).

7.3.2.2 Microfluidic flow system (BioFlux™)

High-throughput screening of under-flow biofilm observations (*e.g.* formation and viability) requires a device that permits development of multiple biofilms with controlled flow rates and determination of various parameters in real time. For this reason, the BioFlux System was produced (**Figure 7.10a,** BioFlux System device, Fluxion Biosciences, South San Francisco, CA, USA) where controlled shear stresses are applied on microfluidic channels integrated into microtiter well plates (Benoit et al. 2010). The use of a standard well-plate format (**Figure 7.10b**) allows compatibility with plate readers and multichannel pipettors, while the plate can also be examined microscopically (Benoit et al. 2010). The microfluidic channels are generated using photolithography etched micro-patterned silicon wafers as a mold for polydimethylsiloxane, which forms the sides and roofs of the channels (channel dimensions: 70 µm depth and 370 µm width). The bottom of the channels consists of a standard 180-µm coverslip glass, which allows microscopic observations to be made. The channels connect pairs of microtiter wells; one well of each pair is the inlet well from which fresh medium is pushed by pneumatic pressure through the channel into the outlet well, which holds the waste medium (**Figure 7.11c).** The microfluidic channels are $1/10^{th}$ the size of conventional flow cells, which permits laminar flow at a wider range of flow rates and results in uniform biofilm growth in the entire channel. The system includes an air compressor and electropneumatic regulators to deliver precisely controlled pressure to each channel via a manifold that interfaces with individual wells of the microtiter plate. The 24-well plates are pre-sterilized and do not require assembly or tubing connections, which minimizes the possibility of contamination. The wall-shear stress (Pa) is controlled by the associated software (BioFlux™ 200, Fluxion Biosciences Inc., Ver. 2.4.0.0), Benoit et al. (2010).

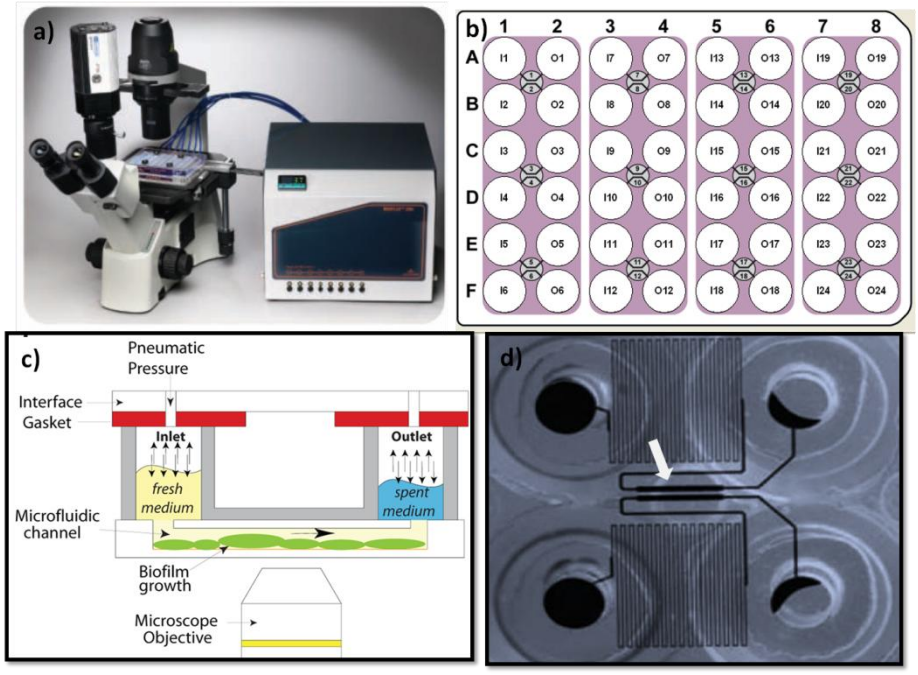

Figure 7.10. a) The BioFlux™ 200 System for live cell assays under controlled shear flow, b) schematic of the modified 48-well plate with 24 independent channels connecting pairs of wells, c) diagram illustrating the inlet and outlet wells containing fresh and waste media where pneumatic pressure applied to the top of the inlet well pushes fresh medium through the channels and, d) close-up of the microfluidic channel (white arrow).

7.3.2.3 Attachment and growth assays

Initially, the microfluidic channels were conditioned with SSP for 60 min prior to bacterial inoculation. Bacterial inoculation was performed using the "outlet" well to prevent contamination of the "inlet" well by pumping in the reverse direction for a few seconds. Overnight cultures of *C. marina* were grown in SSP as explained in **Chapter 4**. Following bacterial OD measurements (OD_{595} = 0.2) twelve microfluidic channels were inoculated by applying a shear stress of 0.1 Pa from the inlet wells through the channels to the outlet wells. The flow rate was sufficient to prevent back-contamination of the inlet wells. Bacteria were left under gravitational flow for 30 minutes to enable attachment (25 °C). Three separate experiments were conducted: following the incubation period, in each experiment, three channels were inoculated with juglone (0.1, 5 and 5 ppm), and three channels were the controls (0.5 % DMSO). The experimental set-up details can be seen in **Table 7.1**. In order to assess biofilm viability at the end-point, freshly prepared LIVE/DEAD stains were used (FilmTracer™ LIVE/DEAD® Biofilm Viability Kit, Molecular Probes). The stains were pumped

through the channels (shear stress: 0. 07 Pa) for 20 minutes in the dark (25 °C), which were then rinsed with ASW for 10 minutes (0.07 Pa).

As shown in **Table 7.1**, for the attachment assays two different shear stresses were applied for one main reason: the higher shear stress (0.3 Pa, 279 µL h^{-1}) was applied because it is similar to tidal flows within ports and dockyards (*e.g.* up to 1.2 m s^{-1}). However, one of the main limitations of the BioFlux™ device is that it supports only a small quantity of media (up to 1 mL), therefore the higher the shear stress used, the faster the media reservoir will be exhausted. For this reason, it was decided to apply the high shear stress (0.3 Pa) for 2 h, which was then followed by a second lower shear stress (0.07 Pa), in order to achieve an extension of the experimental time. The choice of 0.07 Pa (65 µL h^{-1}, equivalent to 697 µm s^{-1}) was decided upon previous studies (*e.g.* Benoit et al. 2010). To avoid risk of biofilm detachment, the high shear stress was decided to be applied first – allowing biofilm acclimation to higher flow. The specific juglone concentrations (*i.e.* 0.1, 5 and 20 ppm) were chosen to accommodate direct comparisons with data obtained from the static attachment bioassays where these concentrations were assessed (**Chapter 5**).

Table 7.1. Experimental set-up and parameters for attachment and growth assays for 0.1, 5 and 20 ppm juglone concentrations. Flow channels (replicas) per treatment: six.

Action/Steps	Time (h)	Shear Stress (Pa)	Microscopy
Microfluidic channel conditioning	1	0.1	-
Attachment Assay			
Bacteria attachment	0.5	0	TRANSM
JUG inoculation[1,2,3]			
Flow 1	2	0.3	Time lapse*
Flow 2	2	0.07	Time lapse*
End Point	4	0	TRANSM
L/D staining	0.3	0.07	Epifluorescence and CLSM
Growth Assay			
Bacteria attachment	0.5	0	TRANSM
	1.5	0.07	
JUG inoculation (20 ppm)			
Flow 1	13	0.07	Time lapse*
End Point	13	0	TRANSM

TRANSM – Transmission microscopy; CLSM – Confocal laser scanning microscopy
***Time lapse were recorded at 1 image 20 s^{-1}.**
[1] 20 ppm, [2] 5 ppm and [3] 0.1 ppm

7.3.2.4 Image acquisition and analysis

In all experiments, CLSM images were acquired from random positions in the central line of the flow channels, at a distance of at least 50 μm from the inlet and outlet.

CLSM image acquisition: The excitation wavelength used for S9 was λ_{EX} = 488 nm, and the emitted fluorescence was collected in the range of λ_{EM}: 500 to 600 nm. The red fluorescent nucleic acid stain PI was excited at λ_{EX} = 594 nm, and the emitted fluorescence was collected in the range of λ_{EM}: 650 to 700 nm. Images were collected through a ×63 Leica water immersion objective and acquired at 0.502 μm intervals down through the biofilm, and therefore the number of images in each stack varied according to the thickness of the biofilm. CLSM was conducted only on the biofilms formed under the juglone concentration of 5 ppm, since transmitted and epifluorescence microscopy illustrated that the other two concentrations (0.1 and 20 ppm) gave extreme effects, *i.e.* none and high attachment inhibition, respectively. Three stacks were acquired from each flow chamber giving a total of *N* = 9 per treatment.

CLSM image analysis: CLSM images were analysed by the COMSTAT software (Heydorn et al. 2000). A fixed threshold value and connected volume filtration was used for all image stacks. A MATLAB script was used to count attached cells from the CLSM images. The features calculated by COMSTAT in the current study, include: (*i*) bio-volume, (*ii*) thickness distribution and mean thickness (explained in **Section 6.3.1.4**) and (*iii*) the area occupied by bacteria in each layer (this is the fraction of the area occupied by biomass in each image of a stack). The substratum coverage is the area coverage in the first image of the stack, *i.e.* at the substratum. Substratum coverage reflects how efficiently the substratum is colonized by bacteria of the population and provides the vertical distribution of the biofilm (from deeper to outer regions of the biofilm).

Transmitted and epifluorescence image acquisition: Transmitted and epifluorescence microscopy was performed using the EVOS *fl* microscope (Advanced Microscopy Group, Bothell, WA) and the following $\lambda_{EX}/\lambda_{EM}$ wavelengths were used : GFP (470/525 nm) and RFP (531/593 nm). Images for both epifluorescence and transmission were captured using a ×10 objective.

Transmitted and epifluorescence image analysis: Biofilm surface coverage was calculated using ImageJ (MacBiophotonics ImageJ, USA) where both transmission and epifluorescence images were converted into a binary system (either 0 or 255) and covered areas (with biofilm)

were quantified. In order to evaluate the ratio of change between the treatments with time and shear stress, the data were normalised with their controls at time zero using the following equation:

$$N\% = \left(\frac{(t_0 - t_{2,4})}{t0} \right) \times 100 \quad [7.3]$$

Where N = change (%), t_0 = time zero and $t_{2,4}$= at times 2 and 4 h, respectively.

7.3.2.5 Statistical analysis

Differences in percentage coverage values between experimental datasets were assessed by applying one-way ANOVA. To establish the homogeneity of variances Levene's test of equal variances was applied. Where homogeneity of variances was not met, the non-parametric Kruskal-Wallis test was applied. All conclusions are based on 5 % level of confidence ($p < 0.05$). Statistical analysis was performed by using SPSS version 19.0 and Minitab version 16.

7.3.3 Results and discussion

For the first time, the direct observation of the juglone influence on newly attached marine biofilms (grown over 30 minutes) and the evolution of the AF effects with time (4 and 14 h) were assessed *in situ*.

7.3.3.1 Biofilm attachment and behaviour using time lapse, *in-situ* measurements:

Initially, time lapse microscopy was used to analyse the behaviour of attaching cells at an early stage in biofilm formation. Overall, time lapse imaging of *in situ* attachment/accumulation under two different shear stresses illustrates a clear difference between the control and the juglone treated flow channels, which is mostly evident after 2.5 h, at which point the shear stress is lower (0.07 Pa), **Figure 711**. Interestingly, the juglone treated biofilm clusters formed under the high shear stress of 0.3 Pa (**Figure 7.11a**), showed a morphological difference when compared to the controls, *i.e.* denser clusters can be seen when exposed to juglone (darker in colour).

The high temporal resolution of biofilm formation, acquired during time lapse imaging allowed the direct observation of biofilm performance (**Figures 7.12**) under the influence of juglone (5 ppm). Specifically, during the high shear stress, biofilm accumulation did not change over the 2 h period for both treatments. However, once the shear stress was lowered to 0.07 Pa, the control demonstrated a marked increase in growth/accumulation while no change was observed for the juglone treated biofilms. This can be explained by the fact that at high shear forces the biofilm morphology is generally defined by denser, more compact clusters while at low shear forces biofilm architecture differs with clusters being more “fluffy” and projected filamentous structures and/or towers (Picioreanu et al. 2001, **Figure 3.8** in **Chapter 3**). The latter is characterised by larger voids/pores within the biofilm (with higher visco-elasticity) that are known to facilitate mass transfer of nutrients (Stoodley et al. 1994). Also, these filamentous structures are considered to create a higher surface to area ratio, and therefore could allow higher diffusion of nutrients in the biofilm.

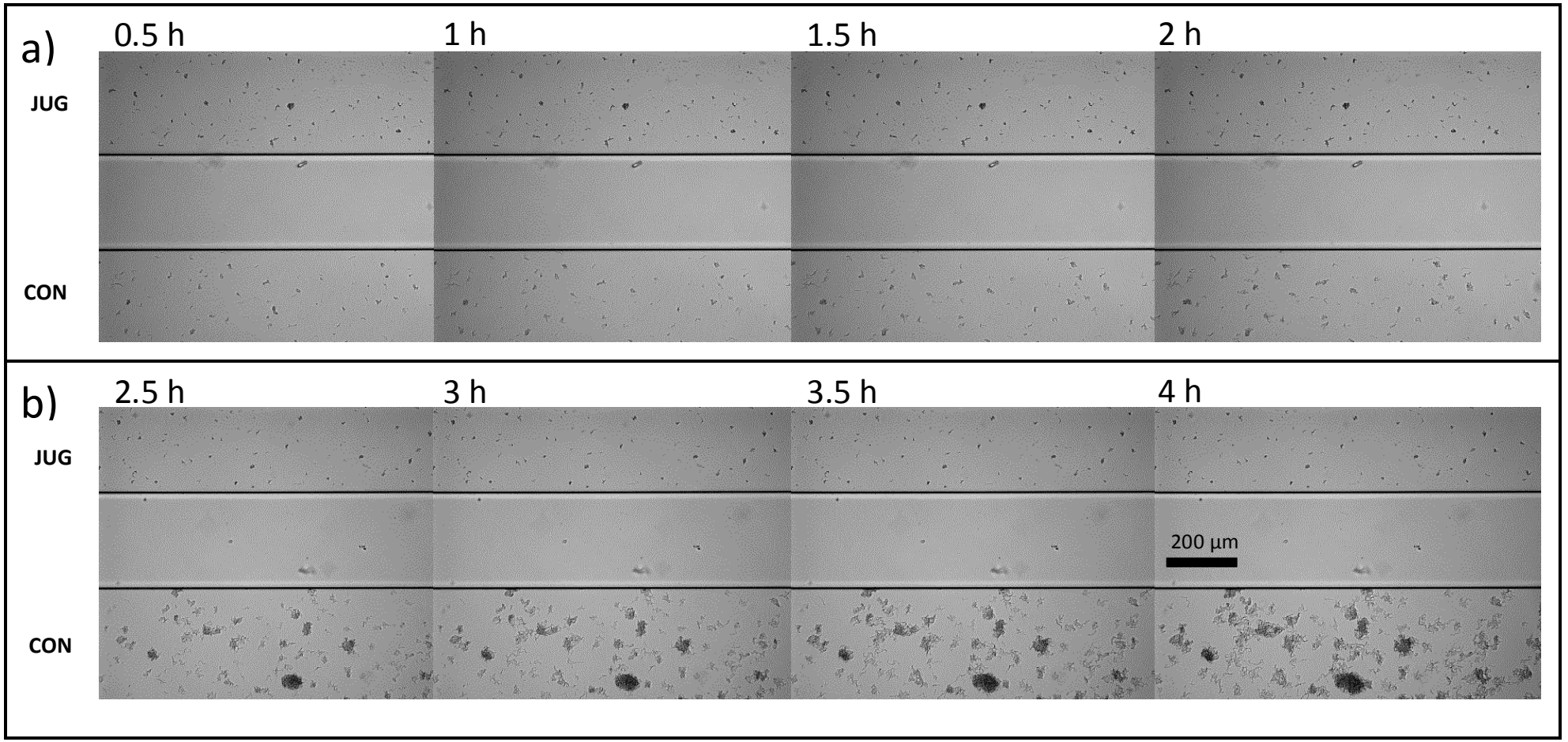

Figure 7.11. Time lapse images of *C. marina* at 30 minutes intervals over a total of 4 h, where: a) grown under 0.3 Pa and b) grown under 0.07 Pa. In both (a,b) *TOP* channel contains 5 ppm juglone (JUG) and *BOTTOM* is the control channel (CON, SSP plus 0.5 % DMSO).

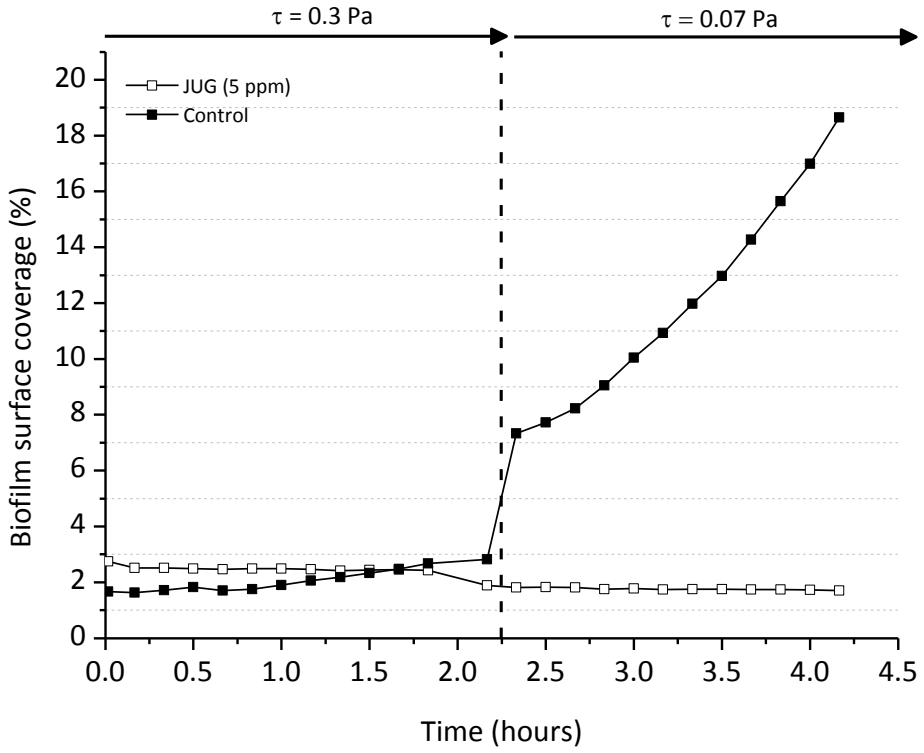

Figure 7.12. Hydrodynamic testing of *C. marina* biofilm attachment and growth in the presence and absence of 5 ppm juglone.

In **Table 7.2**, all the end-point measurements are summarised between the juglone treated biofilms and the controls, at time 0 (zero) h (no flow), 2 h (0.3 Pa) and 4 h (0.07 Pa). Overall, for the lowest juglone concentration at 0.1 ppm, no significant difference was found when compared to the control with time and shear stress. With increasing juglone concentrations, *i.e.* 5 and 20 ppm, biofilm formation / attachment was hindered significantly at 2 h (0.3 Pa) and 4 h (0.07 Pa). Specifically, for the biofilms inoculated with 5 ppm of juglone, following 2 h of exposure under flow characterised by a shear stress of 0.3 Pa, the surface coverage was significantly lower ($p < 0.001$). Also, when comparing the controls, there was an expected significant increase in biofilm formation / growth with time ($p < 0.001$), while comparisons between the juglone treated biofilms did not yield statistical differences with time. In order to evaluate the ratio of change between the treatments with time and shear stress, the data from **Table 7.2** were normalised with their controls at time-zero, see **Figure 7.13**. The main trend seen in **Figure 7.13** is that the higher percentage of change with time was found for the biofilms treated with 5 ppm juglone when compared to the control.

Table 7.2. Juglone treated (0.1, 5 and 20 ppm) and untreated (control) *C. marina* surface area coverage (%) at three different time points: 0 h (no flow), 2 h (0.3 Pa) and 4 h (0.07 Pa), respectively. Error bars ± SE. NS = not significant ($p > 0.05$).

Biofilm surface coverage (%)	Sample no.			Time: 0 h τ = 0 Pa	Time: 2 h τ = 0.3 Pa	Time: 4 h τ = 0.07 Pa	*P* value
Control 1	17	17	23	1.06 ± 0.11	4.94 ± 0.42	21.70 ± 1.05	$p_{KW} < 0.001$
0.1 ppm	18	17	23	1.34 ± 0.15	5.7 ± 0.40	19.78 ± 0.88	$p_{KW} < 0.001$
p value				NS	NS	NS	
Control 2	9	10	12	1.40 ± 0.11	3.66 ± 0.20	15. 16 ± 0.75	$P_{KW} < 0.001$
5 ppm	9	10	12	1.94 ± 0.19	2.37 ± 0.12	2.07 ± 0.08	NS
p value				$p_A < 0.028$	$p_A < 0.001$	$p_{KW} < 0.001$	
Control 3	9	8	10	1.47 ± 0.13	4.00 ± 0.91	11.57 ± 1.12	$p_{KW} < 0.001$
20 ppm	9	8	10	0.62 ± 0.13	1.20 ± 0.21	1.00 ± 0.16	NS
p value				$p_A < 0.001$	$p_{KW} < 0.021$	$p_{KW} < 0.006$	

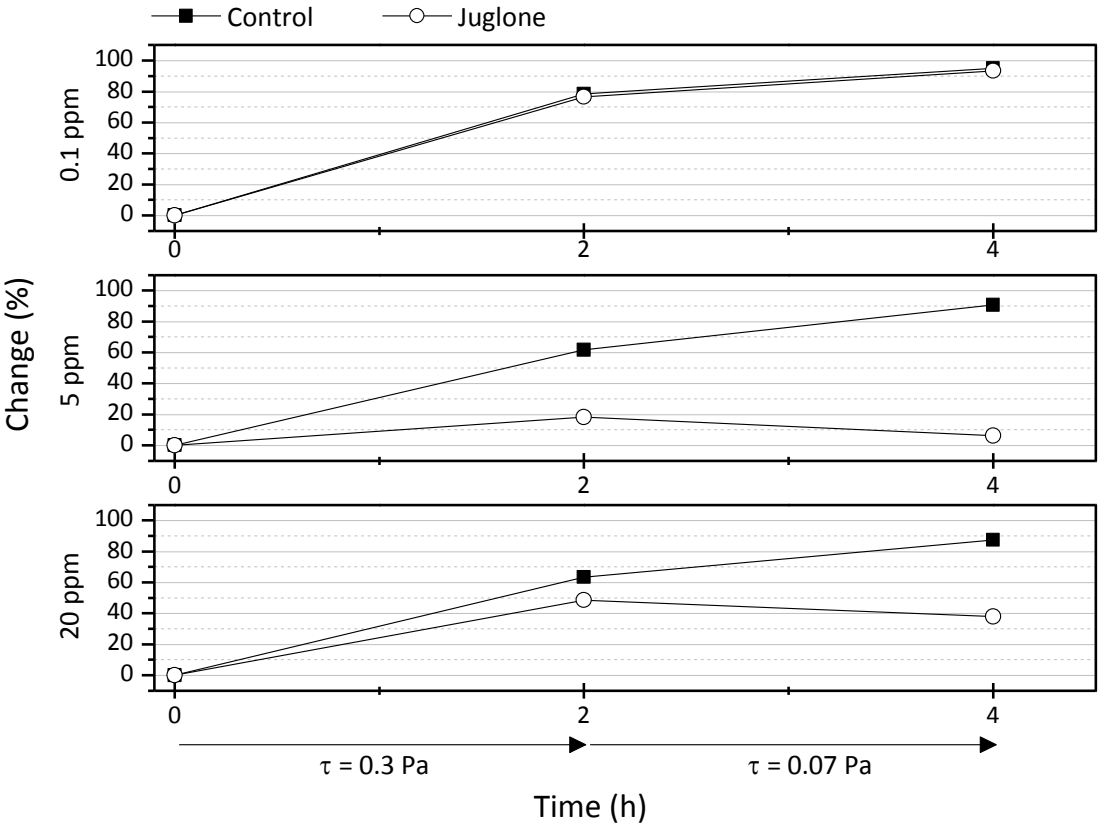

Figure 7.13. Change in biofilm attachment (%) with time and shear stress, treated with different juglone concentrations (0.1, 5 and 20 ppm).

7.3.3.2 Toxicity

Toxicity analysis can be seen in **Figure 7.14**, where an example of two channels containing *C. marina* biofilms (control *vs*. juglone at 5 ppm) stained with the LIVE/DEAD kit is shown. In the control flow channel, large biofilm clusters can be seen stained with S9 indicating intact cells and to a much lesser extent stained with PI, indicating compromised cells (**Figure 7.14a)**. In contrast, for the juglone (5 ppm) containing flow channels, the markedly smaller biofilm clusters are mostly stained with PI, indicating that most of the cells are compromised (**Figure 7.14b**). Specifically, in **Figure 7.15** the percentage of stained with S9 and PI biofilms are plotted for all three juglone concentrations, *i.e.* 0.1, 5 and 20 ppm. The low juglone concentration (0.1 ppm) significantly increased both live and dead biofilms ($p < 0.005$ and $p < 0.011$) when compared to the controls, **Figure 7.15a**. The higher juglone concentrations had a significant inhibitory and toxicity effect, as live cells are merely present in both treatments, 5 ppm ($p < 0.001$ for both S9 and PI) and 20 ppm ($p < 0.001$ for both S9 and PI), **Figure 7.15(b,c)**. These results clearly demonstrate that juglone has a deleterious effect on *C. marina*. Also, there is good consistency with the static attachment results (**Chapter 5**) where the microplate reader was used for high throughput screening of juglone and S9 data gave the same hormetic response, with the low concentration (0.1 ppm) enhancing attachment and the higher concentrations (5 and 20 ppm) significantly inhibiting it.

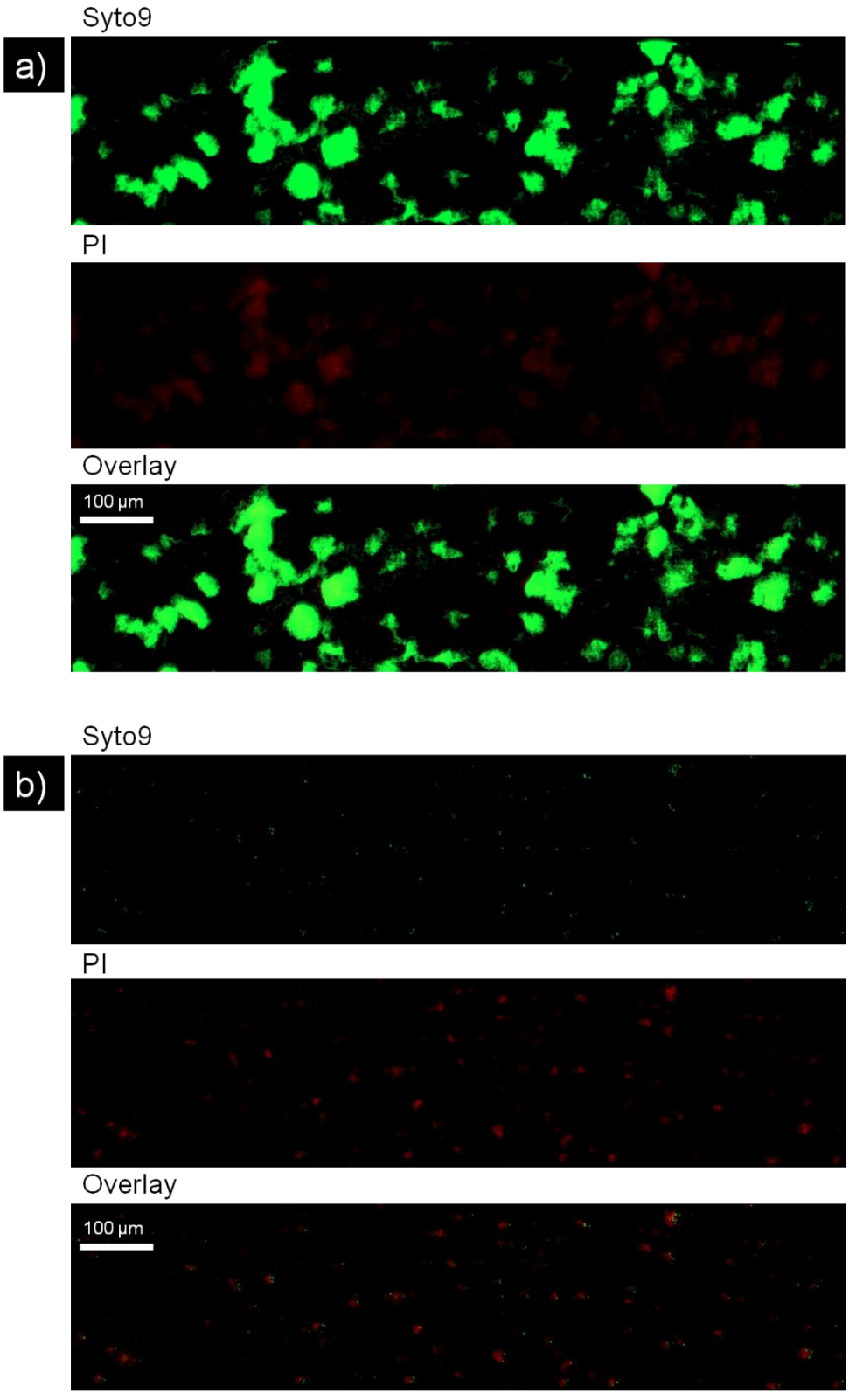

Figure 7.14. Epifluorescence microscopy: Example channels containing *C. marina* biofilms stained with the Live/Dead kit where, a) is the control (SSP + 0.5 % DMSO) and b) juglone at 5 ppm.

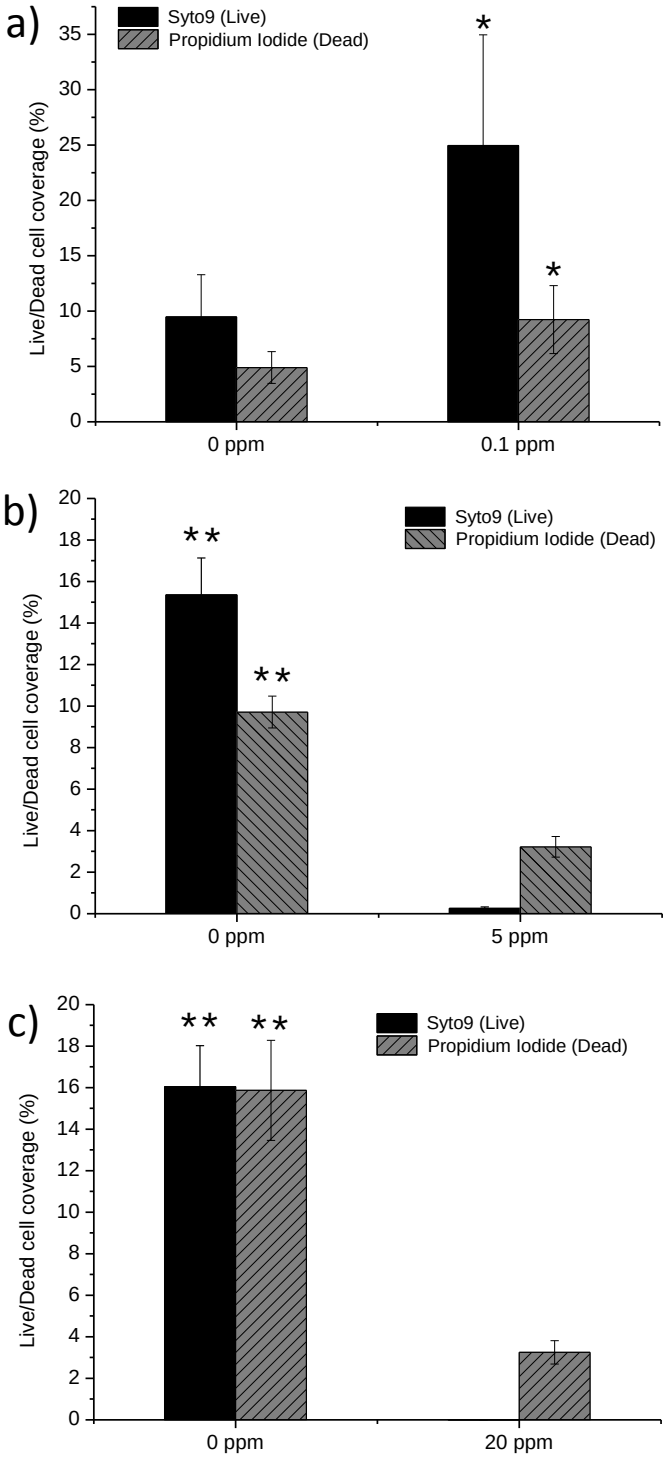

Figure 7.15. Quantitative data derived from epifluorescence microscopy to assess juglone toxicity for *C. marina*'s attachment on the chambers containing juglone at concentrations of a) 0.1 ppm, b) 5 ppm and c) 20 ppm. Error bars: ± STDEV. Single star (*) $p < 0.05$, (**) $p < 0.001$

7.3.3.3 Biofilm structure / morphology

Flow cell images (from CLSM-acquired images) were quantified for four properties of biofilm development using COMSTAT: maximum thickness, biovolume, surface to volume ratio and area occupied by bacteria in each layer (Heydorn et al. 2000, Colvin et al. 2011). Juglone affected each property of *C. marina* biofilms by decreasing both the maximum thickness and biovolume and increasing the surface to volume ratio (**see Table 7.3**). Markedly smaller and fewer colonies were formed after 4 h under flow in the presence of juglone when compared to the control, as illustrated in **Figure 7.16**, where a representative data set of thickness is shown using MATLAB from build-in COMSTAT codes. Specifically, the averaged control biofilm maximum thickness was found to be 30.6 μm which was significantly higher than the juglone treated one at 11.4 μm ($p < 0.001$), while the average biovolume was again significantly higher in the control at 2.07 $\mu m^3 \mu m^{-2}$ when compared to the juglone treated biofilms, 0.09 $\mu m^3 \mu m^{-2}$ ($p < 0.001$). Also, a significantly higher averaged ($p < 0.033$) surface to volume ratio value was found for the juglone treated biofilms (1.26 μm^2 μm^{-3}) when compared to the control (1.04 μm^2 μm^{-3}).

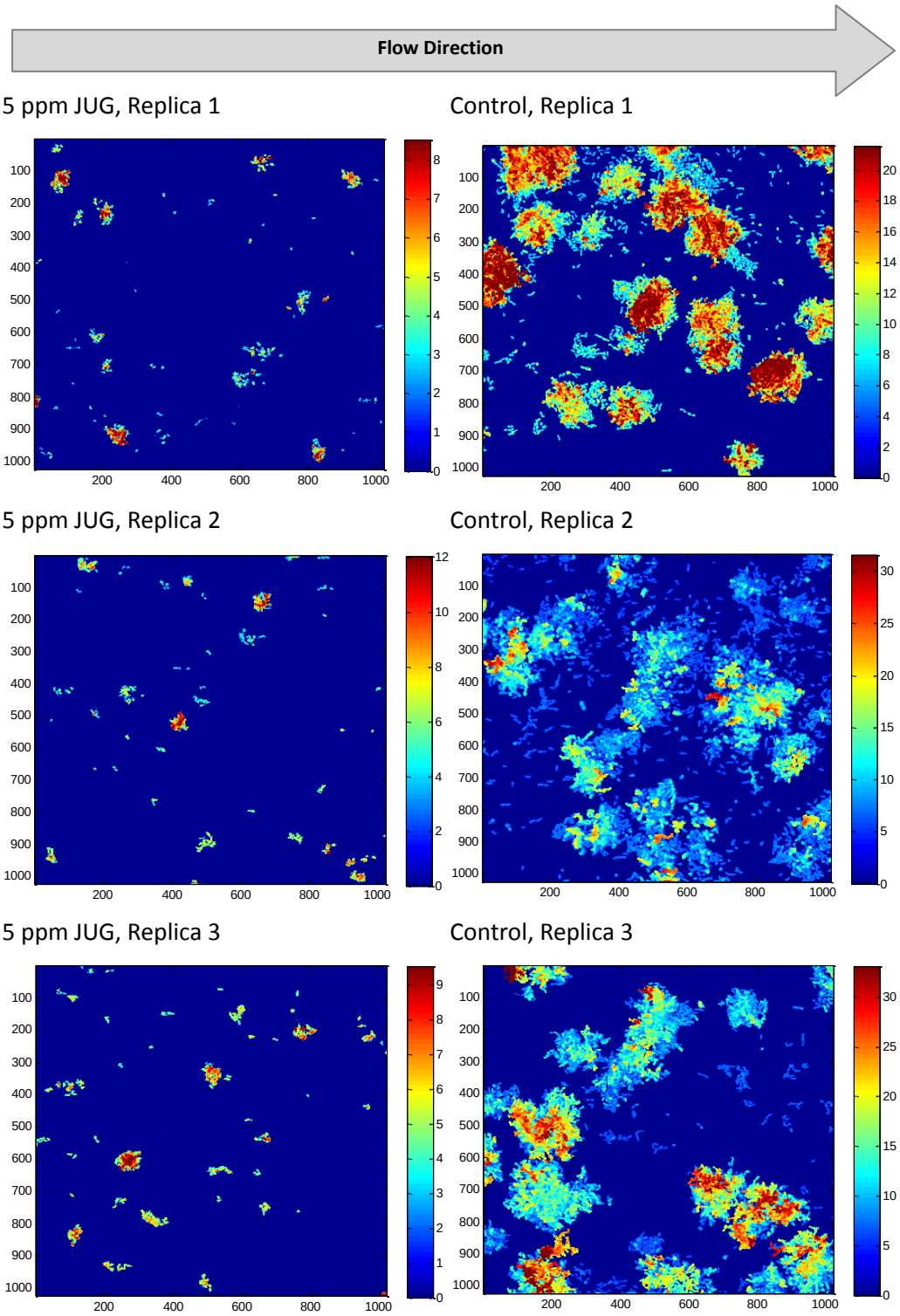

Figure 7.16. Intensity map reflecting biofilm thickness (scale: µm). Each replica represents a separate flow channel, and while more 3D stacks were acquired for each channel, here only one per channel is shown to avoid repetition. COMSTAT analysis performed using MATLAB.

Table 7.3. Maximum thickness, biovolume and surface-to-volume ratio of *C. marina* biofilms (average from 3 channels per treatment and 3 view points for each, *n* = 9 per treatment) where *A* is one-way ANOVA (parametric) and *KW* is Kruskal-Wallis (non-parametric).

Treatment	Max. thickness (μm)	Biovolume (μm^3 μm^{-2})	Surface to volume ratio (μm^2 μm^{-3})
Control	30.6 ± 3.09	2.07 ± 0.26	1.04 ± 0.06
Juglone (5 ppm)	11.4 ± 1.52	0.09 ± 0.01	1.26 ± 0.05
P value	$p_A < 0.001$	$p_{KW} < 0.001$	$p_A < 0.033$

The vertical distribution of bacterial accumulations from the glass surface to the fluid phase was also calculated from the CLSM stacks as explained before (**Section 7.3.1.4**), Jeon et al. 2009. **Figure 7.17** shows the spatial distribution (in the *y*-dimension) of biofilms grown in the absence and presence of juglone (5 ppm). For the juglone treatments, of the total 1.5 % bacterial surface coverage, the cell distribution was greatest within the first 2-3 μm of the overall 9 μm thick biofilm exhibiting a structure with bacteria distributed at the base of the colony/cluster. Conversely, the control biofilms demonstrated a typical mushroom-like morphology with most of the bacterial surface coverage (total of ~23 %) being between 5 and 7 μm, while the base of the cluster was comprised of approximately 10 % bacterial coverage. These differences in morphology between the control and juglone treated biofilms indicate that there was a morphotype response of *C. marina* biofilms in an attempt to prevent more juglone transport (or diffusion) into the cluster. Indeed, the complex three-dimensional biofilm architectures, such as mushroom like structures, may promote higher nutrient supply, through diffusion or transport (Picioreanu et al. 2000) especially at the basis of the biofilm which is comprised of the initial colonizing cells. Thus, in order to counter-act the supply of the toxic NP (in this case, juglone) the biofilm could potentially change its morphology by not forming a mushroom-like structure.

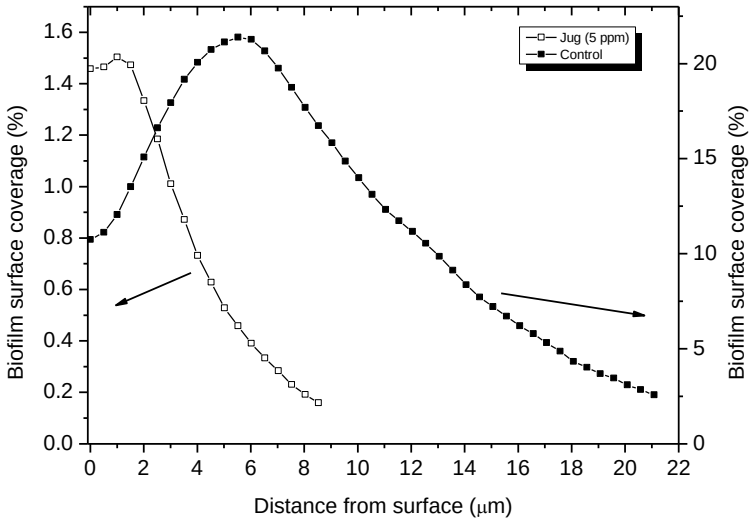

Figure 7.17. An example profile of *C. marina* biofilm distribution grown under flow conditions in the absence and presence of juglone (5 ppm).

7.3.3.4 Growth in the presence of juglone under controlled shear stress

Time lapse imaging of *C. marina* biofilm formation grown in a high juglone concentration (20 ppm) over 13 h can be seen in **Figure 7.18**. *C. marina* was left to attach for 2 h prior to juglone inoculation, establishing this way an initial biofilm formation, as opposed to the attachment assays where bacteria where left to attach for 30 min. The time lapse imaging illustrates that for the first two hours no marked differences between the juglone treated and the control biofilms were observed. This indicates that juglone did not act as fast against already formed biofilms, when compared to the attachment experiments where differences were observed from the first few minutes. However, after 2 h of continuous flow of juglone, almost complete detachment of the young biofilms was observed (**Figure 7.18**), while new biofilm formation appeared to be impeded for the following 6 h after which, a monolayer of attached bacteria started to form. The overall marked difference in biofilm surface coverage between the control and juglone containing channel with time can be seen in **Figure 7.19**.

Interestingly, cells exposed to juglone demonstrated an elongated morphology especially after the first 2 h (where the already existing biofilms were detached). A higher resolution image at 8 h of juglone inoculation clearly illustrates filamentous structures of the cells (**Figure 7.20**). Similar phenotypic changes have been reported previously for biofilm forming species such as *Pseudomonas aeruginosa*, where elongated cells resulted from nutrient depletion (Steinberg et al. 2002). It was suggested that bacteria elongate in order to have higher surface to area

ratio and therefore increase nutrient uptake, to avoid starvation (Steinberg et al. 2002). A recent study by Yoon et al. (2011) reported significant cell elongation of anaerobically grown *P. aeruginosa* due to endogenously produced metabolic nitric oxide. They postulated that cell elongation is likely to be caused by a defective cell division. Since cell-to-cell contact is an important determinant for biofilm formation and can be facilitated by an enlarged cell surface (Yoon et al. 2011), it can be hypothesised that cell elongation can be viewed as a response to environmental stress. Therefore, this phenotypic change of the cells triggered by the addition of juglone may be viewed as an adaption of bacteria responding to their local environment. It has to be noted, however, that more studies are needed to elucidate such conclusions.

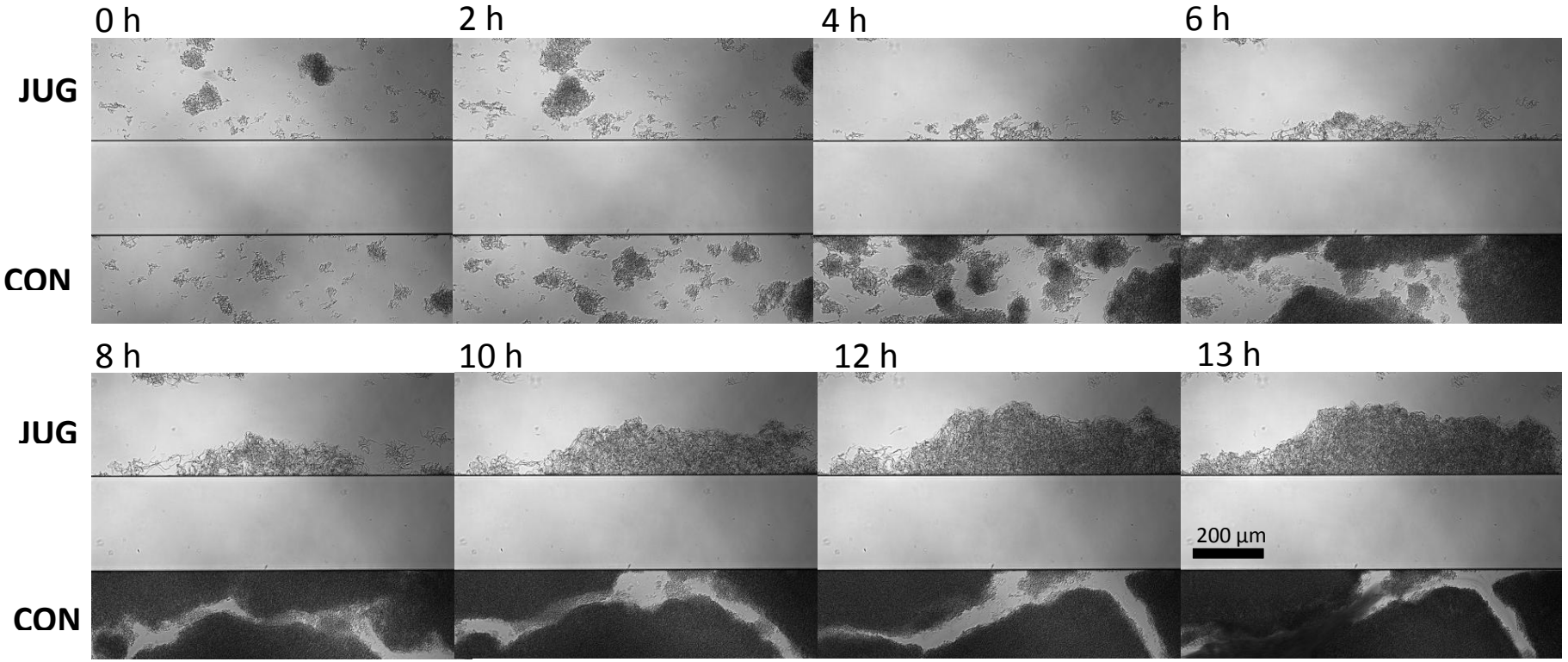

Figure 7.18. Time lapse imaging of *C. marina* under 0.07 Pa at 2 h intervals over a total of 13 h, where *TOP* channel contains 20 ppm juglone and *BOTTOM* is the control channel (SSP plus 0.5 % DMSO).

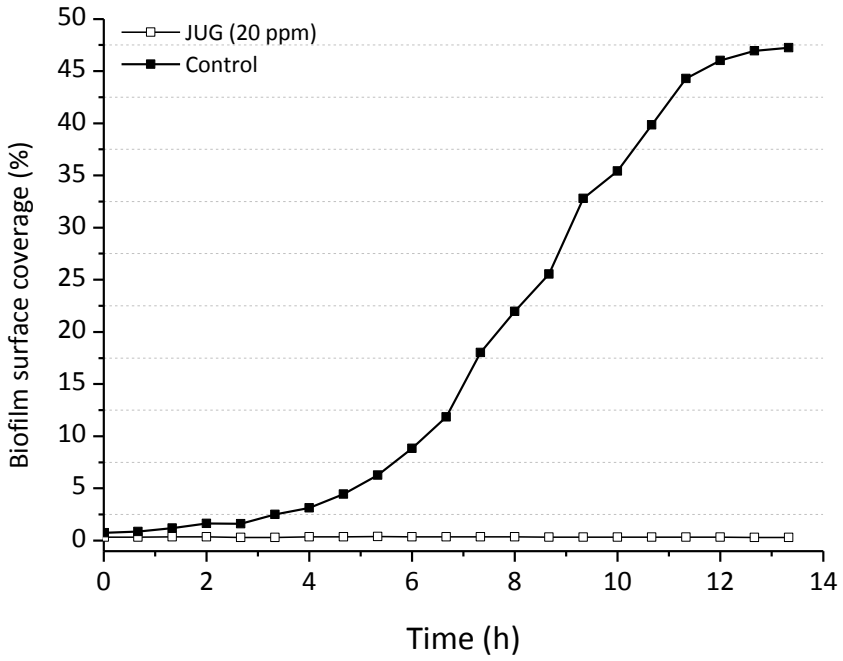

Figure 7.19. Hydrodynamic testing of *C. marina* biofilm growth in the presence and absence of 20 ppm juglone at 0.07 Pa over 13 h.

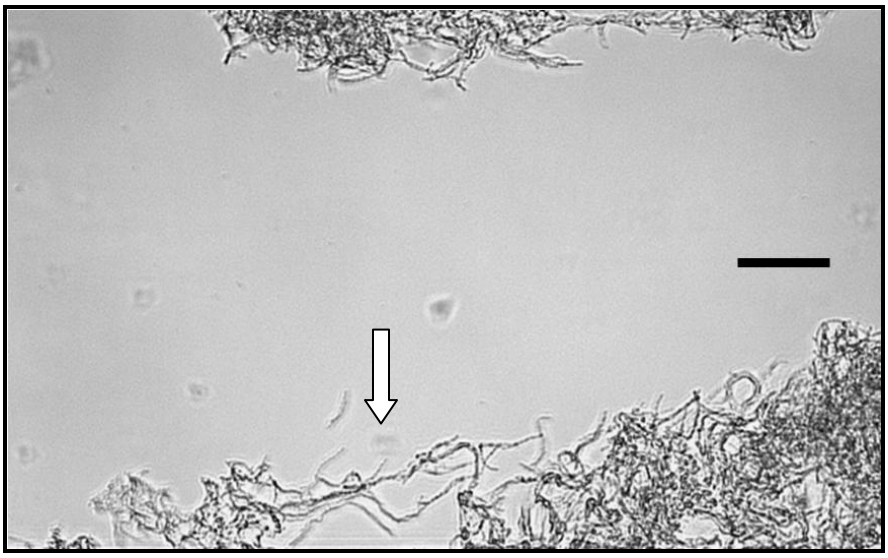

Figure 7.20. Close-up of newly attached *C. marina* after being exposed to juglone (20 ppm) for 8 h, illustrating elongated filamentous structures (white arrow). Scale bar = 50 µm.

7.4 Study 3: Ship-on-a-Chip, designing fabricating and testing a new microfluidic device

This investigation has developed a method for studying bacterial adhesion by using a custom-built microfluidic device with six parallel non-connected stepped channels (ship-on-a-chip, SoC). The design allows investigation of bacterial behaviour under a range of shear stresses (in this study the following shear stresses were applied: 0.03, 0.060, 2.15 and 4.30 Pa) equivalent to those associated with marine platforms. For each shear stress, a large number of cells are analysed, providing statistically relevant data within a single experiment. The new SoC microfluidic device enables in-depth analysis of biofilm processes such as attachment / detachment by utilising real-time video-microscopy and end-point CLSM. The device offers the possibility to analyse bacterial adhesion-associated processes under well-defined shear stresses within the same experiment.

The design was guided also by the necessity to construct a microfluidic device that should include other important features:

1) the ease to assemble and disassemble;
2) the option to sterilize all components;
3) good optical properties to facilitate microscopy analysis;
4) the possibility to change the substrate to facilitate direct observations of biofilm attachment (*i.e.* glass, NP-coated glass, paint-coated glass, etc.).

In order to meet all these requirements, the microfluidic SoC device was specifically designed with a modular assembly in four parts as shown in **Figure 7.21**, where the dimensions and design of each of the four parts are illustrated.

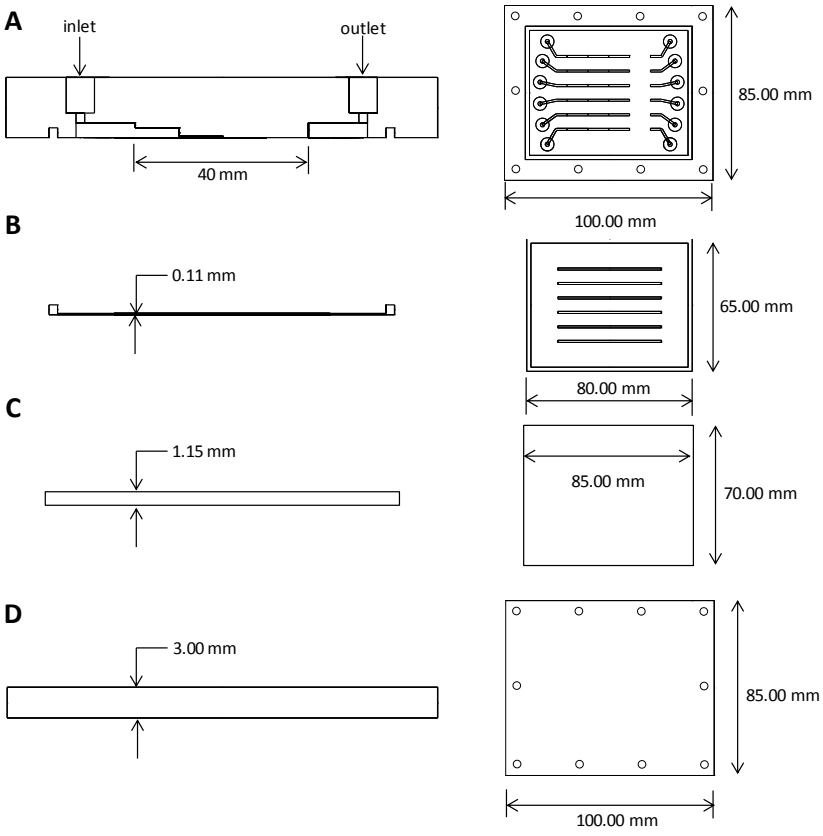

Figure 7.21. The SoC microfluidic device used for bacterial attachment studies. The cross-section (left) and top view (right) of the four parts of the assembly are shown together with their dimensions: (A) top plate; (B) gasket; (C) substrate; (D) base plate.

A detailed description of the optimisation, design and fabrication of the SoC device can be found in the **APPENDIX A7.1**. To briefly summarise, the optimisation process through computational fluid dynamics (CFD) modelling let to the fabrication of the SoC device which was specifically designed to consist of:

(1) a top-plate which contains on one side, the six channels in parallel with three chambers of depth 1.89, 0.30 and 0.04 mm, while on the other side the connection ports (six inlets and six outlets) with ¼-28 flat-bottom thread;

(2) a gasket containing through cuts that, when aligned with the channel in the top plate, formed the fourth channel geometry and hence defined the final chamber depths;

(3) a glass substrate plate which represents the surface where the biofilm attaches and;

(4) a base-plate manufactured from PMMA.

The device is assembled and held in place by means of screws, passing through the holes drilled at the edges of both the top and base plates.

7.4.2 Materials and methods

7.4.2.3 The SoC system (set-up)

In **Figure 7.22** a summary of the modelled shear stresses within the SoC, as well as the final SoC channel dimensions is shown (as determined in Appendix A7.1). **Figure 7.23** shows the actual SoC experimental set-up. A peristaltic pump (Watson-Marlow series 323S) was used at a flow rate of 0.5 mL min^{-1}, while calibration was conducted according to **Section 7.2.1.2**. In **Table 7.4** the experimental parameters (derived from the CFD simulations, see APPENDIX A7.1) within the chambers are shown (*i.e.* the shear stresses, *Re* and speed in knots). The reservoir contained freshly prepared media (SSP) and aeration was achieved through a sterile tube entering the reservoir allowing air exchange with the environment. A 0.22 μm sterile filter was adjusted at the end of the tubing to prevent contamination from the surrounding environment during the aeration processes. Differences in air-pressure within the medium reservoir created by the flow-through system, allowed air "bleeding" in the media. The SSP volume in the reservoir and recycling loop was ~ 500 mL. A damper was used to eliminate the pulsation of the flow and produce a linear flow (see Figure **7.23**). The various components were connected by silicon rubber tubing (Masterflex, 3.1 internal diameter).

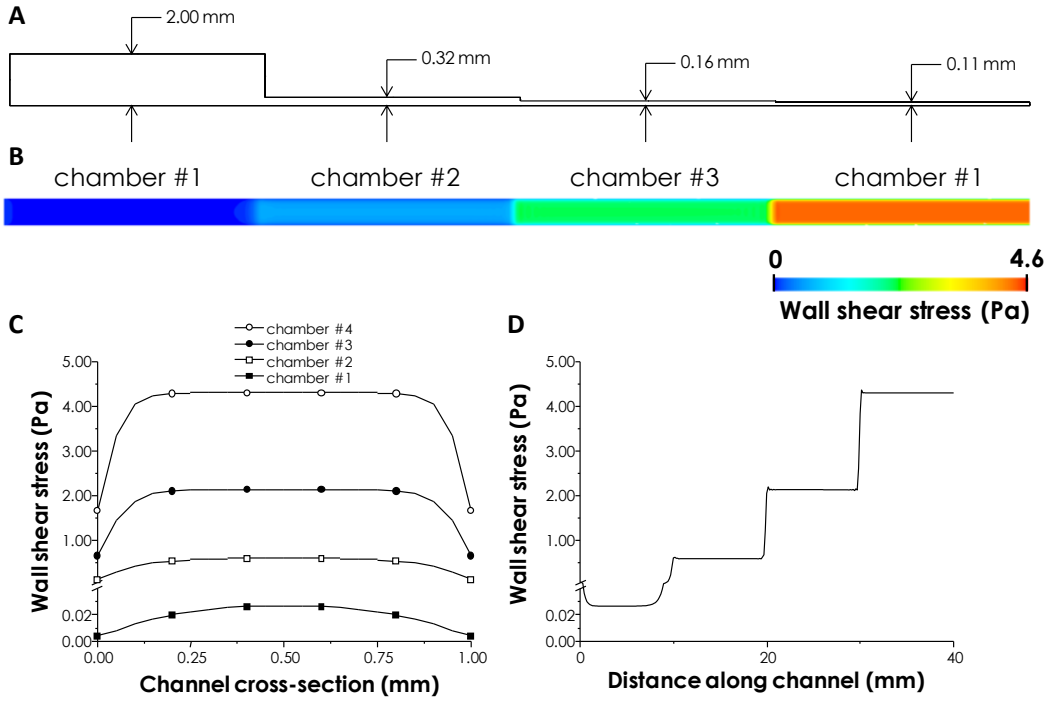

Figure 7.22. (A) Schematic of the microchannel showing the dimensions of the four micro-chambers. The flow field modelling within the channel used a flow rate of 0.5 mL min^{-1} at the inlet. (B) Colour map of the modelled wall-shear stress on the substrate surface. (C) The wall-shear stress along the cross section has been determined at the middle length of each chamber section. (D) Wall-shear stress at different positions along the channel, computed at half-width length of the channel sections showing the characteristic stair-like increase of the wall-shear stress (from APPENDIX 7A).

Table 7.4. The selected flow rate of 0.5 mL min^{-1}, resulted in the following parameter matrix. The *Re* in each channel was up to 14.*25, i.e.* the flow is characterised as laminar (1 knot = 0.514 m s^{-1}). See APPENDIX A7.1.

Wall shear stress (τ_w)			
shear 1 (Pa)	shear 2 (Pa)	shear 3 (Pa)	shear 4 (Pa)
0.03	0.60	2.15	4.30
Reynolds numbers			
Re 1	Re 2	Re 3	Re 4
5.27	11.98	13.63	14.25
Velocity (ASTM standards REF)			
v1 (knots)	v2 (knots)	v3 (knots)	v4 (knots)
0.72	1.75	2.24	3.18

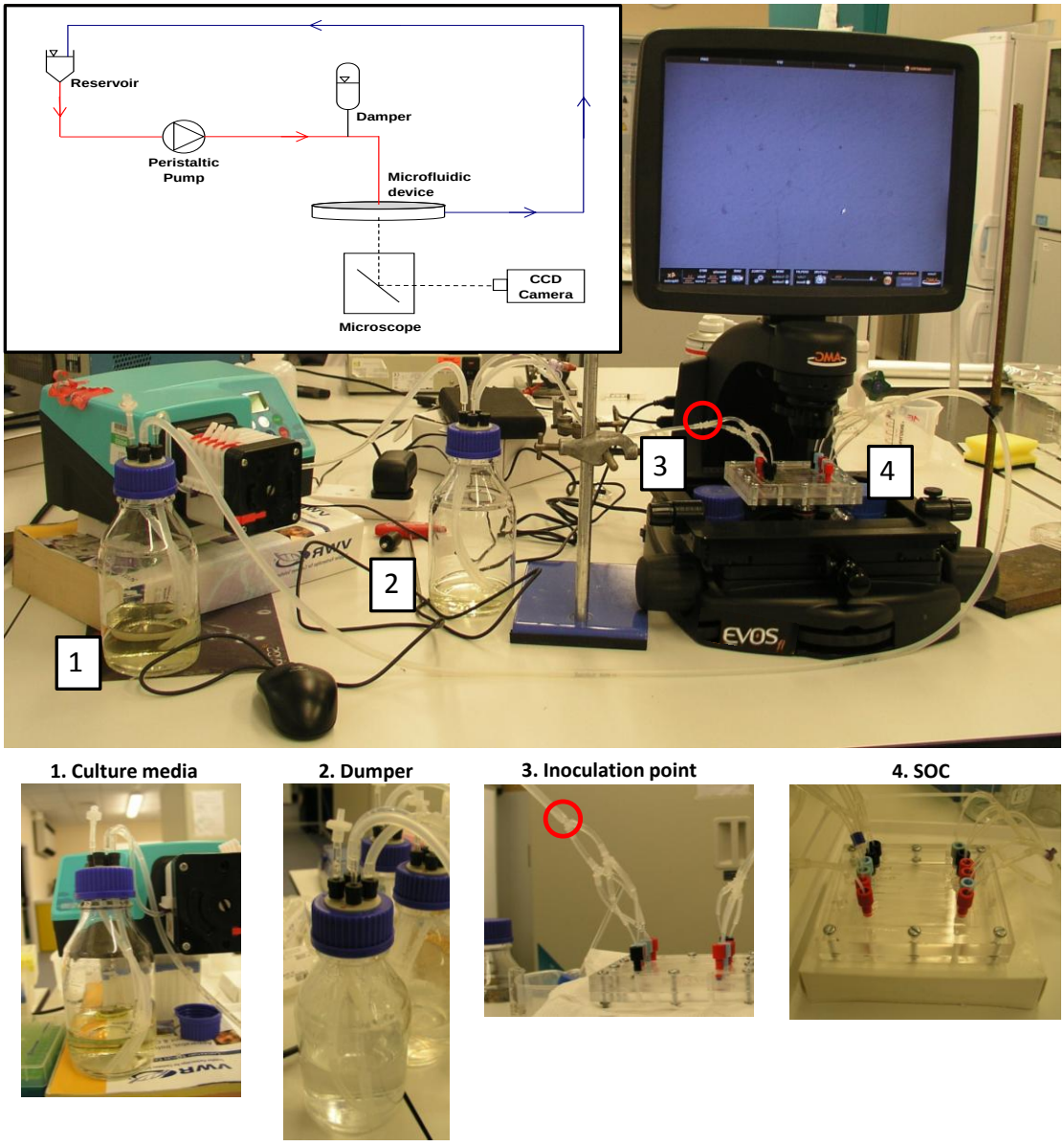

Figure 7.23. Schematic illustrating the SoC system, closed-loop and microscope set-up. Top left insert is a diagram showing the flow direction and associated components.

7.4.2.4 Bacterial attachment tests

An overnight culture of *C. marina* was grown in SPP as previously explained in **Chapter 4** (**Section 4.3.2**) with a measured OD_{595} of 0.2. The total experimental time was decided to be 4 h, in order to comply with the commercial system exploited in the previous **Section 7.3**. Prior to bacterial inoculation, the SoC system was sterilised by flowing 70 % EtOH for 15 min by means of flow. Three washes followed with sterile-filtered (0.22 µm) deionised water (18 MΩ

m purity water) for a total of 1 h. Finally SSP medium was flown through for 1 h to allow conditioning of the chambers and stabilisation of the flow. A sterile syringe (5 mL) was used to inoculate *C. marina* at the inoculation point (see **Figure 7.23**) while the SoC device was placed under the microscope using the ×20 transmitted objective lens (EVOS*fl*, AMG, Westover Scientific, Inc.). Images were taken using the microscope's built-in camera where triplicates in each flow cell were taken for all channels at time zero (t_0) resulting in N = 48. Following the t_0 measurements (images), time lapse images were taken manually every 10 min focusing in one channel in triplicates for all four chambers (*i.e.* four shear stresses), N = 12 images per sampling time. At the end point, *i.e.* at 4 h, images for all chambers were taken in order to allow direct comparison with the time zero data (n = 48). Following image sampling, the flow was stopped and clamps were used in either side of the tubing to ensure static conditions. Freshly prepared stains from the LIVE/DEAD kit were then introduced into the channels using a sterile syringe through the inoculation point and clams were removed to allow initiation of flow. The SoC was then kept in the dark for 20 min under gravitational flow, to allow sufficient staining. The stains were then flushed by initiating the flow for a total of 10 min. CLSM image acquisition and processing were conducted as described in **Section 7.3.1.4**. Images were taken at the centre of each chamber (from total two channels) where at least three stacks were obtained, *i.e.* a maximum total of six stacks per chamber.

7.4.3 Results and discussion

7.4.3.3 Spatiotemporal variation of biofilm formation in the SoC

The experimentally obtained time lapse curves of *C. marina*'s initial biofilm formation can be seen in **Figure 7.24.** The attachment/attaching behaviour of *C. marina* under the lower shear stresses of 0.03 and 0.6 Pa (**Figure 24a and b**) can be described as sigmoidal (typically characterised by an initial lag phase), followed by logarithmic growth and finally reaching stationary phase. Bacteria exposed to the second lower shear stress (0.60 Pa), however, appear to have a relatively prolonged lag phase when compared to biofilms under 0.3 Pa. Overall, under the two shear stresses of 0.03 and 0.60 Pa, bacterial attachment/growth appears to reach a steady state at the experimental end-point. *C. marina*'s initial biofilm formation under the higher shear stresses (2.15 and 4.30 Pa), is characterised by an exponential growth response where the stationary phase was not reached (**Figure 24c and d**). Although more data with time and at greater resolution would provide a clearer picture of potential different biofilm formation responses due to increasing shear stresses, the current data illustrate promising distinctive initial growth patterns between the four shear stresses. The differences in the kinetic behaviour of newly attached biofilms, demonstrating a steady state under 0.03 and 0.60 Pa (**Figure 7.24a** and **b**), may be explained by a the overlying slow velocity of the fluid causing nutrient transfer limitations (Stoodley et al., 1999); this may lead to a rapid depletion of the nutrients adjacent to the surface, while, the accumulation of toxic metabolites and waste products may also affect the biofilm's growth (Caldwell et al. 1992).

The initiation of the logarithmic growth phase varies across the four shear stresses. Specifically, with increasing shear stress bacteria appear to respond by increasing delay in entering the log phase, *i.e.* at 55, 125, 135 and 155 min for 0.03, 0.6, 2.15 and 4.30 Pa, respectively. The extended lag phase in biofilm kinetics for most of the observed shear stresses could be attributed to a possible adaptation period necessary for cell acclimation from an almost static to a hydrodynamic environment.

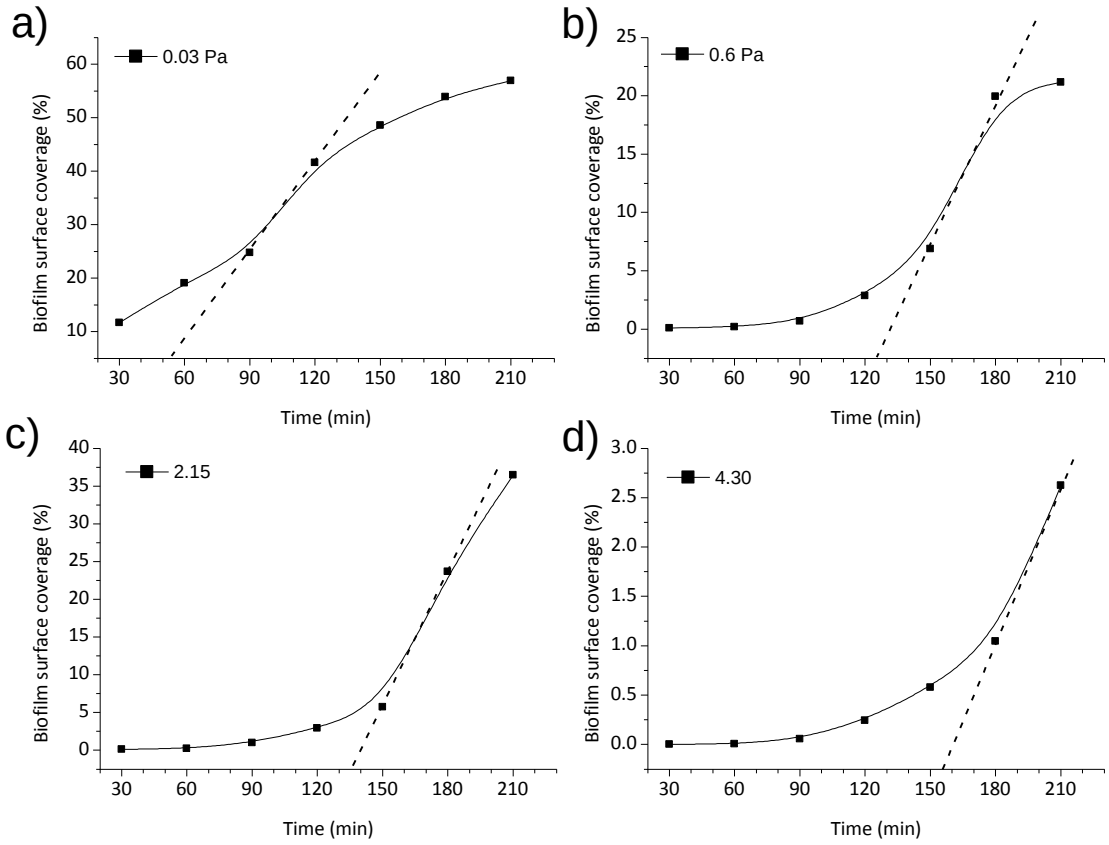

Figure 7.24. Hydrodynamic testing of *C. marina* attachment and initial biofilm formation with time, under 4 different shear stresses where a) 0.03 Pa, b) 0.60 Pa, c) 2.15 Pa and d) 4.30 Pa. Dotted lines illustrate the exponential growth phases. In APPENDIX A7.2 the chamber images where the time-lapse data were obtained, can be seen,

In **Figure 7.25** the surface coverage of bacteria under the four shear stresses after 30 and 210 min (3.5 h, end-point) averaged for all four replicas, can be seen. Following 30 min under hydrodynamic exposure, bacterial attachment was significantly higher at 0.03 Pa when compared to the remaining shear stresses ($p < 0.001$). However, when comparing biofilm formation at the end point across the four shear stresses, there appears to be a transition point beyond which biofilm formation is significantly lower. Specifically, no significance in biofilm surface coverage was found between 0.03 and 0.60 Pa, however, under 2.15 and 4.30 Pa biofilm formation was significantly lower (0.03 Pa *vs.* 2.15 and 4.30 Pa, $p < 0.001$ and $p < 0.001$; 0.60 Pa *vs.* 2.15 and 4.30 Pa, $p < 0.007$ and $p < 0.001$). For attachment, faster flow would bring more cells into contact with the surface due to better mixing but the sticking efficiency may be reduced because of higher shear (Stoodley et al. 1999).

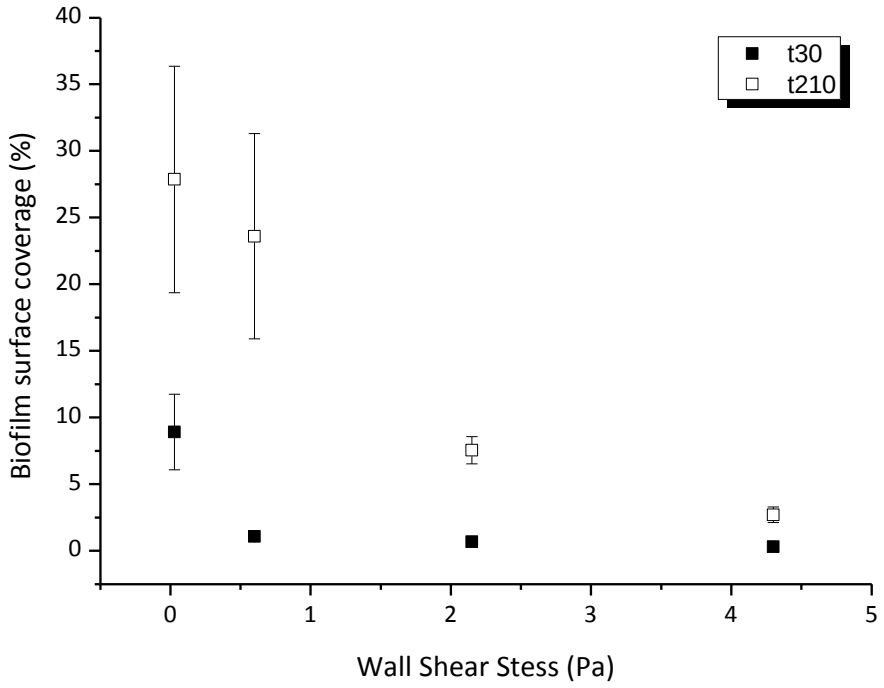

Figure 7.25 ***C. marina*'s surface coverage (%) after 0.5 h (t30) and 4 h (t210) for the four shear stresses, *i.e.* 0.03, 0.60, 2.15, and 4.30 Pa. Error bars ± STDEV.**

7.4.3.4 Morphological variation of biofilm formation in the SOC

The three-dimensional images obtained from CLSM stacks are illustrated in **Figures 26 & 27**. It is clear that there is distinct difference in morphology between biofilms grown in low (0.03 and 0.6 Pa) and high (2.15 and 4.30 Pa) shear stress. Specifically, at the low shear stresses (**Figure 7.26**) river-like passages/channels appear to have formed while when comparing the overall morphologies, biofilms formed under 0.03 Pa exhibit a more homogenous/smooth texture when compared to the ones exposed under the 0.6 Pa that appear to be comprised of more distinct interconnected patches. On the contrary, under the higher shear stresses (2.15 and 4.30 Pa), *C. marina* exhibited clustered formations with patchy and relatively rounded colonies (**Figure 7.27**).

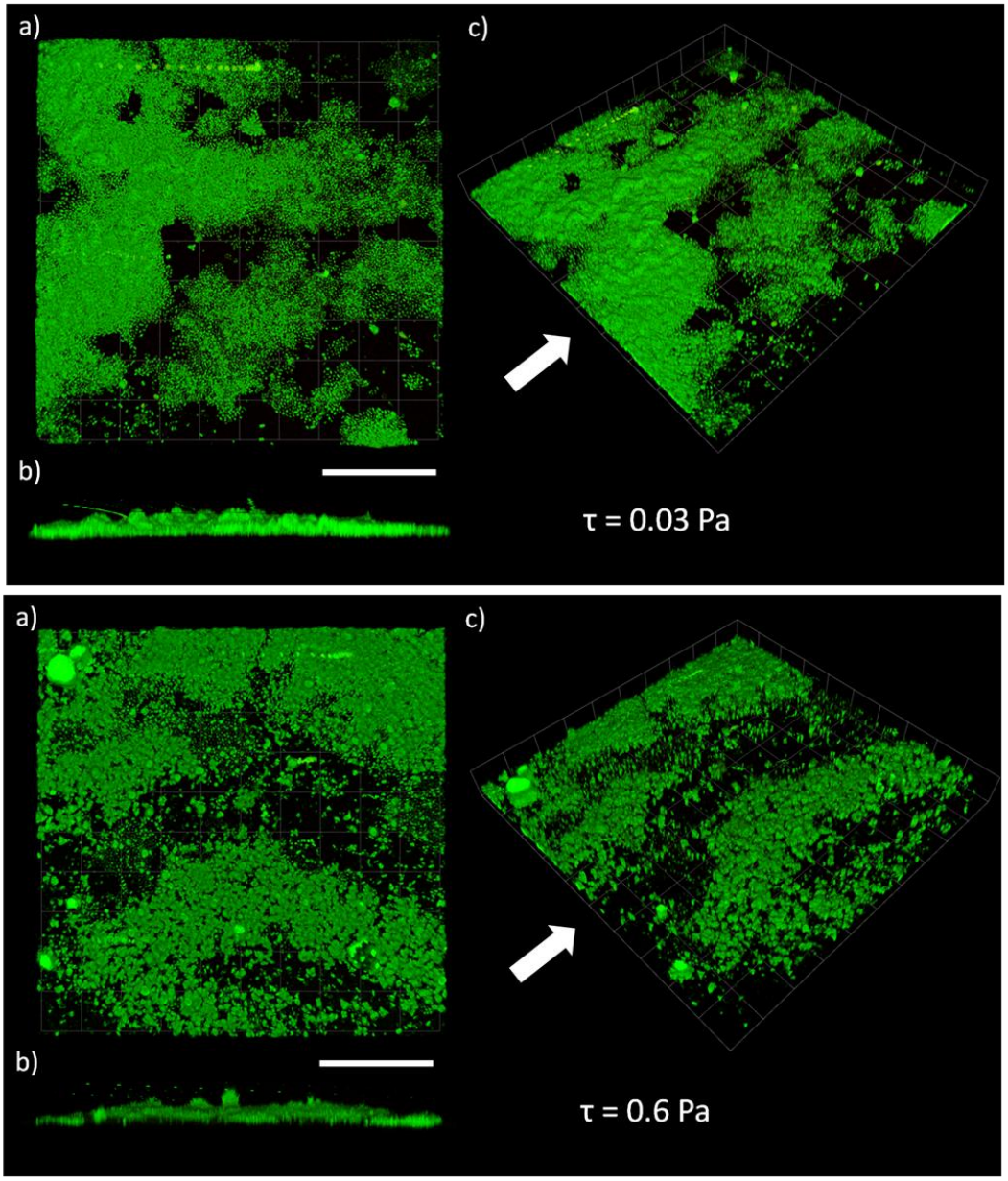

Figure 7.26. CLSM microscopy on LIVE/DEAD stained *C. marina* grown under different shear stresses at the end-point (4 h), where *Top*: 0.03 Pa, *Bottom*: 0.60 Pa and a) top view, b) side view and c) 3D view. Each scare on the grid: 37.65 µm^2, scale bars: 112 µm, white errors illustrate the direction of the flow.

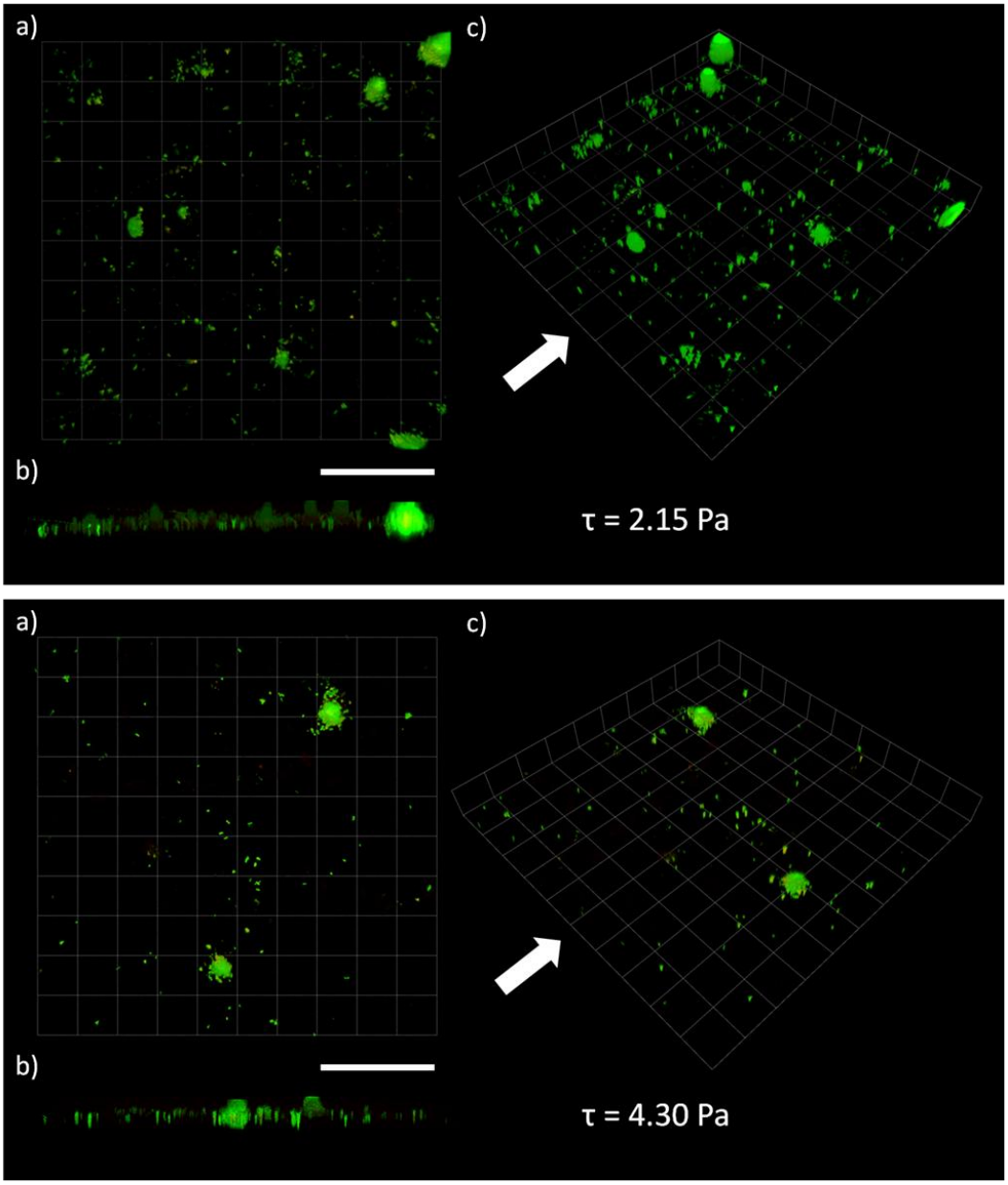

Figure 7.27. CLSM microscopy on LIVE/DEAD stained *C. marina* grown under different shear stresses at the end-point (4 h), where *Top*: 2.15 Pa, *Bottom*: 4.30 Pa and a) top view, b) side view and c) 3D view. Each scare on the grid: 37.65 µm^2, scale bars: 112 µm, white errors illustrate the direction of the flow.

Data obtained using the 3D CLSM images confirm the differences in morphological variation among biofilm clusters exposed to increasing shear stresses, as seen using transmitted microscopy. Higher data resolution allowed for the quantification of additional parameters such biofilm thickness, biovolume, surface to volume ratio and vertical distribution

of biofilm biomass. As seen in **Figure 7.28**, biofilm formation at the end point is markedly different between shear stresses, where especially profound differences in morphology can be seen between the two low shear stresses (0.03 and 0.60 Pa) and the high ones (2.15 and 4.30 Pa). The initial formation of a biofilm layer can be seen in both low shear stresses while internal pores/voids are present in the biofilm developed under 0.03 Pa (**Figure 7.28a**).

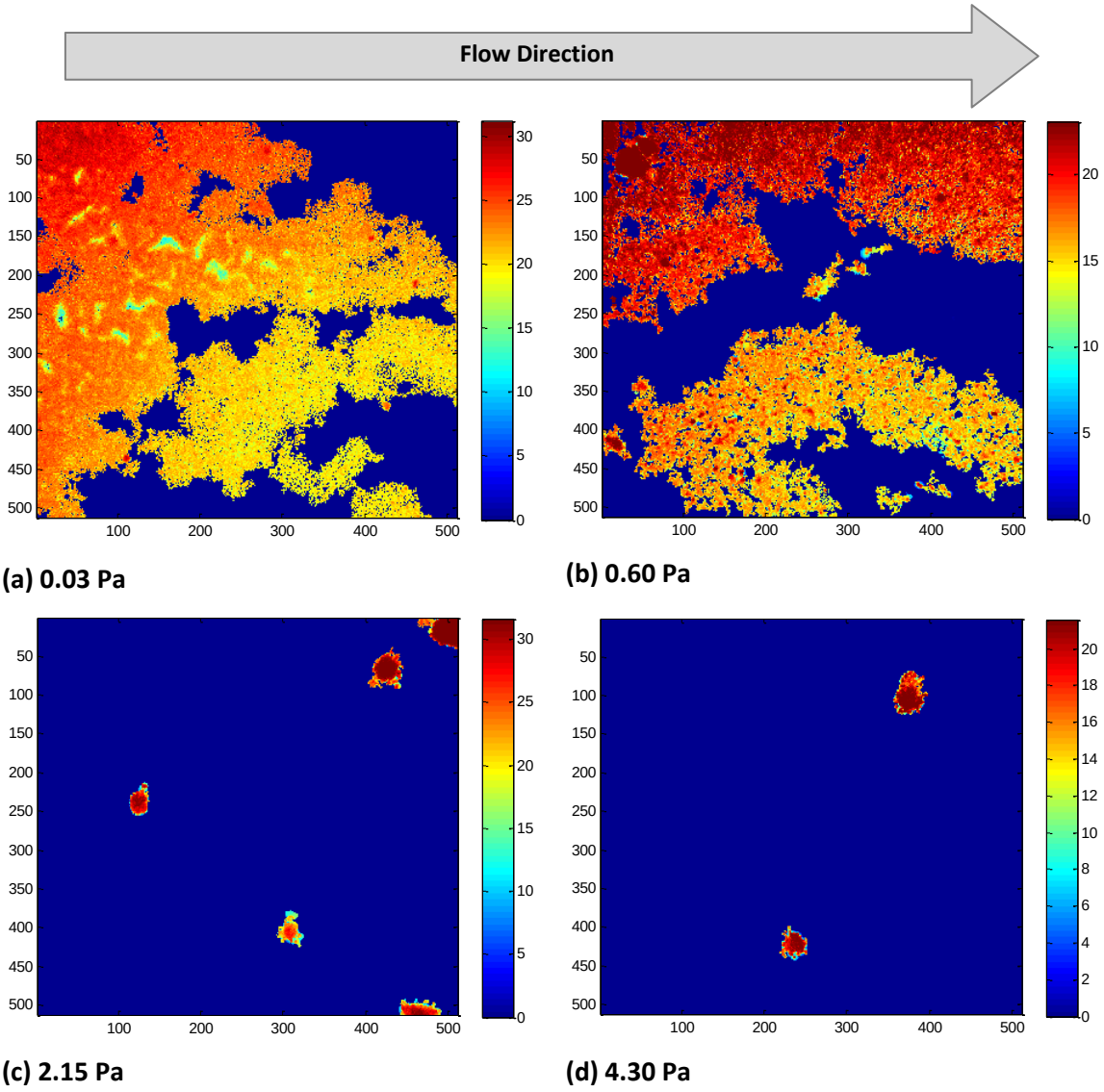

Figure 7.28 Intensity map reflecting biofilm thickness (scale: µm). Each image represents a flow chamber for each shear stress. COMSTAT analysis performed using MATLAB.

Biofilm maximum thickness was found to be significantly different with shear stress ($p < 0.006$); Bonferroni post-hoc analysis revealed that exposure under the highest shear stress (4.30 Pa) produced significantly thinner biofilms when compared to biofilms exposed to 0.03

and 2.15 Pa ($p < 0.006$ and $p < 0.05$, respectively), while no significant difference was found between 0.3 and 0.6 Pa, see **Table 7.5** and **Figure 7.29**. Additionally, there was a significant effect of shear stress on biofilm biovolume ($p < 0.038$). Post-hoc comparisons showed that the effect was mainly between the lowest shear stress (0.03 Pa) and the two higher shear stresses (2.15 and 4.30 Pa, $p < 0.050$ for both) (**Table 7.5 and Figure 7.29**). For surface to biovolume ratio, there is an apparent decrease with increasing shear stress (**Figure 7.29**), however, no significance was found, see **Table 7.5**.

Table 7.5. Maximum thickness, biovolume and Surface to volume ratio of *C. marina* under the four different shear stresses by COMSTAT analysis. ± SE, $_{KW}$ = Kruskal-Wallis, $_{A}$ = 1-Way ANOVA.

Shear stress	Max. thickness (μm)	Biovolume ($\mu m^3\ \mu m^{-2}$)	Surface to volume ratio ($\mu m^2\ \mu m^{-3}$)
0.03 Pa	31.7 ± 2.3	6.4 ± 4.4	0.9 ± 0.2
0.6 Pa	23.0 ± 3.0	3.8 ± 3.0	0.7 ± 0.4
2.15 Pa	27.4 ± 4.0	0.23 ± 0.10	0.6 ± 0.02
4.30 Pa	18.2 ± 3.5	0.09 ± 0.02	0.4 ± 0.12
p value	$p_A < 0.006$	$p_{kw} < 0.038$	NS

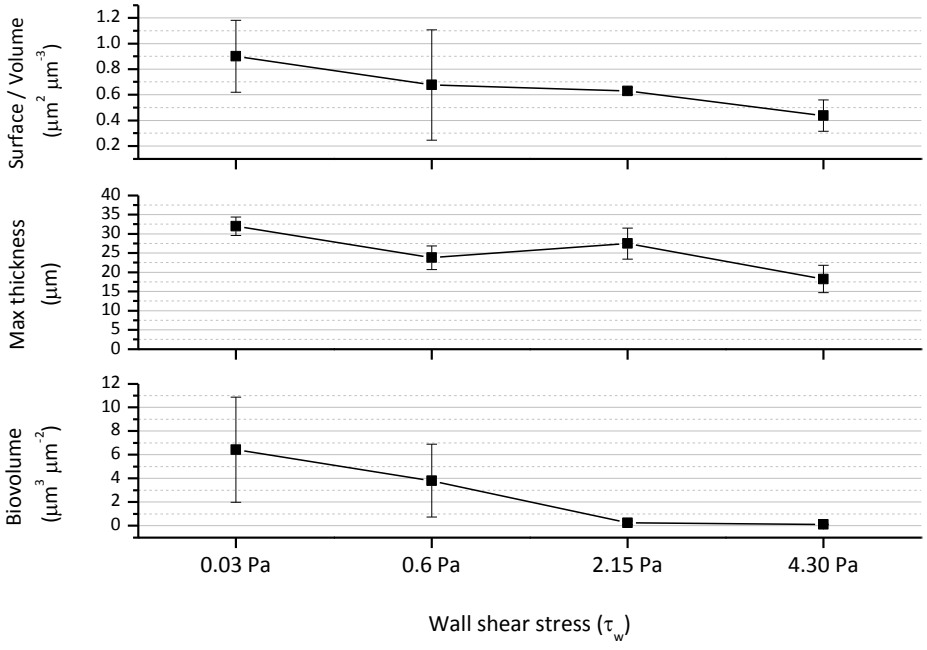

Figure 7.29. A graphical representation of the various parameters using COMSTAT analysis in Table 7.7.

The biofilm/bacterial vertical distribution from the glass surface to the fluid phase under the different shear stresses was determined from the 3D CLSM imaging data sets (Jeon et al. 2009), **Figure 7.30**. Interestingly, for the biofilms exposed at the lower shear stresses (0.03 and 0.6 Pa), the bulk of the biofilm biomass appear to be distributed at around 10 μm from the surface, displaying a distinctive architecture/morphology characterised by mushroom like structures (*e.g.* Hall -Stoodley et al. 2004), see **Figure 7.30a**. Conversely, biofilms grown under the higher shear stresses (2.15 and 4.30 Pa) display a very different morphology with bacterial biomass being distributed in a more compact way, with a more homogeneous dispersion throughout the cluster, especially for the highest shear stress grown biofilms (**Figure 7.30b**). In good agreement with the current work, van Loosdrecht (1995, 1997) demonstrated that at higher shear forces biofilm morphology was characterised by compact structures with less growth occurring in the outer filamentous biofilm and more in the base of the biofilm. It was suggested that at high shear stresses, the filamentous structures and protrusions are detached before they proliferate out.

Computational simulations have also shown that under low shear stresses (and subsequently low media/nutrient transport rates), porous and/or even filamentous biofilms can be formed (van Loosdrecht et al. 2002). In terms of biofilm porosity and nutrient (or any substrate) transport it was found that only at high flow rates, convection (as opposed to diffusion) will dominate media transport, while biofilm will adapt by becoming less porous and smoother, in a way that mass transfer is buffered (van Loosdrecht et al. 2002). Studies on biofilm mechanical properties have established a link between hydrodynamics, biofilm structure and strength (*e.g.* Stoodley et al. 2001, Dunsmore et al. 2002). In general, the higher the flow velocities the greater the nutrient flux towards the biofilm due to a diminished external resistance to the boundary layer (Picioreanu et al. 2001). Computational simulations revealed that at *Re* = 13.3, the biofilms remained thin suggesting that the higher the Re the stronger the forces that the biofilm must resist, while lower *Re* = 6.7, produced bulkier colonies/biofilms (Picioreanu et al. 2001).

Increasingly, several studies report differences in biofilm structure under hydrodynamic conditions. Rieu et al. (2008) investigated the biofilm structure of *Listeria monocytogenes* under flowing conditions, and they found that following initial adhesion as single cells, the developed biofilm consisted of dense, ball-shaped microcolonies separated by poorly colonized zones (16 h exposure). The cell morphology of *L. monocytogenes* was also affected

by the growth conditions, *i.e.* under static conditions bacteria were characterised by short rods while under dynamic conditions, long cells created a network of knitted chains (Rieu et al. 2008). They also showed that flow conditions (dynamic and static), besides biofilm structure of *L. monocytogenes*, deeply influenced the spatiotemporal patterns of gene expression.

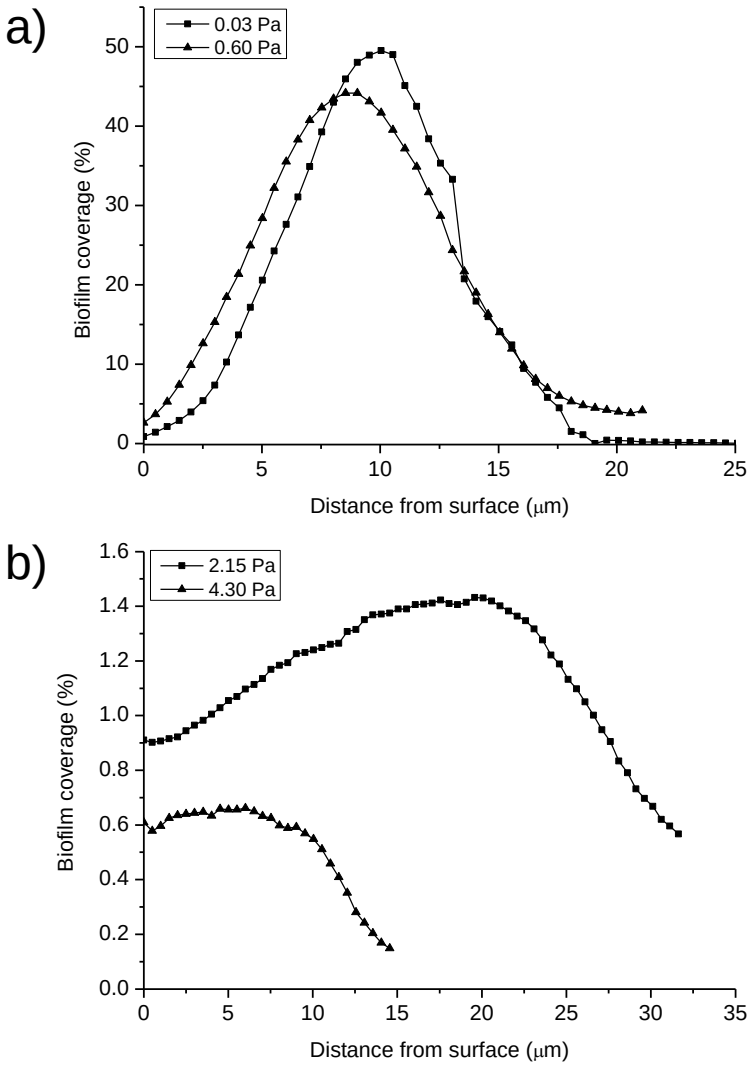

Figure 7.30. Representative profile of biofilm distribution following hydrodynamic exposure under a) 0.3 and 1.5 Pa and b) 2.4 and 4.5 Pa.

It would be very interesting to assess the biofilm's mechanical properties (using techniques such as cantilever-based indentation and "conventional" indentation) at the end-point to test whether bacterial clusters formed under higher shear stresses would result in stiffer structures.

7.4.4 Summary

In the current section, a novel microfluidic device (SoC) that allows parallel observations of bacterial attachment and biofilm formation under four shear stresses was assessed. Overall, it was found that the two lower shear stresses resulted in biofilms with distinctive morphologies characterised by mushroom-like structures, interstitial channels (similar to river banks) and internal voids. While for the two higher shear stresses compact clusters with large interspaces between them were formed. Both the device and the observations constitute novelties, *i.e.* the combination of parallel experiments under four different shear stresses along with the application of nucleic acid staining to reconstruct a biofilm's three-dimensional structures. Since the hydrodynamic environment/parameter is can influence biofilms, such a microfluidic device has a wide range of potential applications from the marine and the medical field (*e.g.* biofilms present in catheters, on teeth, etc.). The SoC device has the capability to provide a greater understanding of the processes occurring during biofilm formation providing good controllability, replication and relevance to realistic hydrodynamic conditions.

7.5 General summary and comparisons between the three flow cell systems

In the current work, three flow-cell systems were used in order to assess the initial biofilm formation in the presence/absence of inhibitors. Biofilm initial attachment and formation should be viewed as a dynamic process strongly influenced by the surrounding environmental parameters, *i.e.* physico-chemical affected. In the case of marine biofilms, the effect of flow plays a key role in the initial attachment/development and establishment of marine species since the marine environment has a wide range of hydrodynamic conditions. Additionally, under the scope of the current project where the aim was to assess anti-biofilm strategies for ship hulls, the investigation of biofilm responses under hydrodynamic conditions was found to be crucial.

Laboratory-based experiments that include hydrodynamic testing are by no means an easy task and several conditions/requirements must be met in order to obtain meaningful information/data such as, *i*) ease of use, *ii*) replication and reproducibility, *iii*) experimental versatility and, *iv*) cost. For this reason, the three flow cell systems tested in the current work are compared (see **Figure 7.31** for the main parameters compared in the current section).

***i*) Ease of use**

Although commercially available and frequently used in the literature, the **FC81** did not provide good controllability of the flow since the presence of bubbles within the chamber would influence the attaching/detaching behaviour of the cells. Also, leaks were frequently observed and constant care was necessary to eliminate this. The latter would additionally affect the local shear stresses within the chamber. Sterilisation of the **FC81** was conducted by means of autoclave and rinsing with EtOH which is time consuming and care must be taken in order to ensure complete removal of the solvent (EtOH) prior to the experiments.

The **BioFlux** was found to be considerably more user friendly, although in order to mount the pump controller on the modified 48-well plate the uncontrolled force often applied by the user during the mounting procedure may result in damaging the expensive well plate. In terms of sterilisation, the **BioFlux** system was found to fulfil the best procedural setting since

the modified 48-well plates were pre-sterilised by the manufacturer, avoiding this way, the time consuming sterilisation process found for FC81. However, the draw-back of the modified pre-sterilised 48-well plates is the fact that they can only be used once leading to higher costs (each plate costs > £150-170).

The prototype **SoC** was also found to be user friendly and although minor leaks did occur during pilot runs (data not shown), these were easily resolved. Assembling the **SoC** device was not problematic, although during the pilot runs the glass cover slip did break at the edges (due to increased force applied by the user), however, this was overcome by practising. The sterilisation procedure and the associated disadvantages were similar to those found for the **FC81** system.

***ii*) Replication and reproducibility**

In terms of replication, the **FC81** is comprised of a single chamber, therefore no replication is achievable. The possibility to run several **FC81** flow cells at the same time may be considered, however problems identified in (*i*) would make this task too problematic with the additional challenges of manoeuvring the connected flow cells to allow *in situ* microscopic observations (only single **FC81** fits under the microscope). Running a flow cell the size of **FC81** requires a large volume of media, especially when using a closed-loop set-up (as done here) is not an option, therefore running a number of **FC81** flow cells (at least three flow cells to obtain statistically relevant data) simultaneously would be laborious and expensive.

The **BioFlux** employs microfluidic technology through flow-cell microfabrication of up to 12 channels in one 48-well plate. This is an obvious advantage as the simultaneous observation of up to 12 biofilms is possible. The microfluidic nature/approach of BioFlux facilitates parallel channel observations under the microscope, especially when an automated stage is available. In the current work a number of experiments were conducted using the BioFlux and the experimental reproducibility was found to be very satisfactory, considering the admitted difficult/laborious nature of flow cell work throughout the literature.

The **SoC** system also employs the microfluidic technological advances that allow the overall miniaturisation of several flow cells in one device. The stepped **SoC** is comprised of a total of 24 micro-chambers that allow parallel observations of biofilm processes. In terms of replication, the **SoC** differs from the BioFlux by means of the number of shear stresses applied simultaneously, which is explained in the following paragraph. Experimental reproducibility

was found to be satisfactory, although further repeats are necessary to fully evaluate this aspect of the **SoC**.

***iii*) Experimental conditions/versatility: shear stresses, time scales and substrate addition**

Overall, the shear stresses applied within the three flow cell systems is largely dependent on the associated equipment such as the flow rate ranges achievable by standard laboratory peristaltic pumps that may restrict the desirable shear forces. However, discussing the technical restrictions on the development of relevant shear stresses in a flow cell is beyond the scope of this Section.

A test that aims to assess the effect of hydrodynamics on biofilm processes should include a range of shear stresses since in reality dynamic conditions are complex (*i.e.* more than one flow rates/shear stresses/speeds). For this reason, the **FC81** was found to be limited in providing this kind of experimental flexibility since it is comprised of a single channel, especially when the aim of the study is to assess the impact of more-than-one shear stress on biofilms, simultaneously. The **BioFlux** can achieve the parallel application of maximum two shear stresses in the same experiment, and is therefore more versatile. Being even more resourceful, the **SoC** system can achieve 4 shear stresses simultaneously which makes it ideal for highly dynamic experimental set-ups.

The experimental time is a crucial part of every assay and therefore the choice of flow cell system would largely depend on how well this parameter is addressed. Both the **FC81** and **SoC** systems were able to accommodate long experimental time scales (hours to days –though the latter was not attempted) since a closed-loop set-up is achievable. However, due to the size differences between the two systems, it is imperative to note that the same shear stress would require different medium volumes (as explained previously), especially on a non-recycling system, therefore the experimental time would be limited for the **FC81**. On the contrary, the microfluidic approach employed for the SoC flow cell system can support long experimental time scales, as smaller volumes are required, making this system ideal. As for the **BioFlux** system, the experimental time scale achievable was found to be an important limitation, since the maximum medium volume is 1 mL which restricts the application of a high shear stress over long periods of time (example: highest shear stress achievable with BioFlux is 20 Pa, experiment can last up to few minutes).

The main limitation of a microfluidic approach for the assessment of biofilm processes is the risk of chamber clogging due to excessive biofilm growth and the overall changes in local pressure differences created within the chambers. Indeed, this was observed in the current work for BioFlux during biofilm growth experiments (14 h). As described in the materials and methods of **Section 7.3**, the chamber height is 70 μm which is considerably restricting, especially for bacterial species that are known to form thick biofilms within short time scales. For the **SoC** system, clogging is not expected since the largest chamber is 1 mm high, nevertheless, this cannot be fully addressed in the current discussion as biofilm growth was not assessed and whether the last chamber (110 μm high) would get clogged, remains to be answered. It should be noted though, that in the current work, assessing initial attachment was the main focus and since there was no such phenomenon observed during the 4 h, the **SoC** was concluded to be appropriate for this application.

Since biofilm formation is a surface-dependent phenomenon, a variety of substrates are often assessed, especially for the marine environment (and the EDA project) which necessitates the testing of coated surfaces. For this reason, it is imperative for a flow system to accommodate this requirement which was not met by the BioFlux system, as the modified 48-well plate could not be disassembled. On the contrary, both the FC81 and SoC systems were designed to facilitate the addition of modified surfaces.

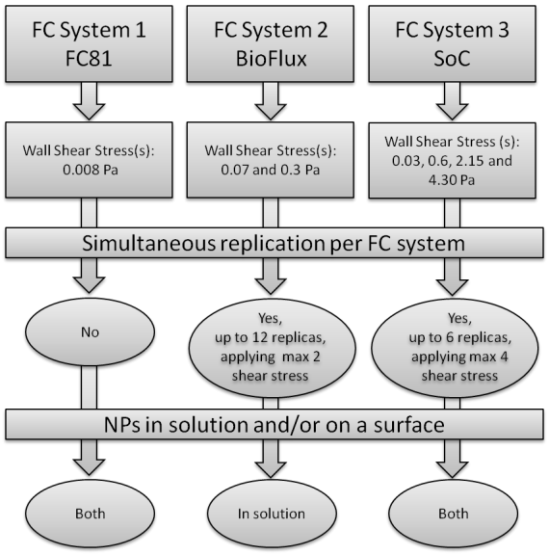

Figure 7.31. Schematic illustrating differences between the three flow cell systems tested in the current Chapter.

Chapter 8

8. General conclusions

Although a set of comprehensive summaries have been provided at the end of each Chapter, this Section intends to draw together the key findings in order to establish a general overview of the experimental discussion and outline future directions.

Novel bioassays were developed that allowed a rapid *in situ* assessment of newly attached bacteria using microtiter plates combined with nucleic acid staining and plate reader technology (**Chapters 4 & 5**). These bioassays were then used for the evaluation and/or screening of two terrestrial NPs (juglone and usnic acid) as environmental friendly compounds and one crude extract from a marine source (the red seaweed *Chondrus crispus*) that could potentially be used as natural anti-biofilm agents. The results showed that although all NPs demonstrate some degree of anti-biofilm effect, this was found to be species specific. However, juglone was selected as the final choice of NP for further investigation as this compound illustrated the best anti-biofilm performance (at concentrations of 5 – 20 ppm) against both of the bacterial species tested here (*C. marina* and *M. hydrocarbonoclasticus*). Importantly, when compared to data available in the literature, juglone demonstrated better activity against marine bacteria than commercially available booster biocides.

The development of a novel bioassay that assessed NP-containing coatings against marine biofilms was achieved (**Chapter 6**). Although this bioassay illustrated promising reproducibility and greater relevance for AF technologies (than the conventional toxicity bioassays), the lack of information on NP release rates was found to be a limiting factor. Specifically, marine NP-coatings (formulation 1) containing *C. crispus* and *B. bifurcata* illustrated very good AF activity against *Pseudoalteromonas* sp., while terrestrial NP-coatings (formulation 2) containing usnic acid and juglone did not show AF activity against *Pseudoalteromonas* sp. Differences between the two formulations may have been due to *i*) the choice of binder, *i.e.* the inert PMMA (formulation 1) *vs*. the erodible Metamare B175™ and/or *ii*) selective activity of marine products against *Pseudoalteromonas* sp. over the

terrestrial NPs. Since the main limitation of this protocol was concluded to be the lack of knowledge on NP's leaching rates, a set of experiments were specifically designed to address this issue.

Specifically, the NP with the best anti-biofilm efficacy (juglone) was mixed with 2 different binders and the compound's release was characterised over the experimental period, i.e. 48 h prior to bioassays. Overall, the protocol was optimised in terms of *i*) experimental binder, *ii*) establishing juglone leaching from the coating, *iii*) *in situ* biofilm quantification directly on the coated surfaces using two different techniques, *i.e.* the commercial and high-throughput plate reader and the highly sensitive CLSM, both gave consistent results. Juglone exhibited good AF efficacy, significantly inhibiting biofilm formation when incorporated into a coating giving comparable results with the commercially available booster biocide Cu_2O. No apparent decrease in planktonic growth between the experimental (juglone containing coatings) and the controls ((-)ve controls: just the binder, biocidal: binder + Cu_2O) indicates that only biofilm formation was inhibited, however, more physiological studies are necessary to conclude on the compounds' effect on the cell's biology.

In **Chapter 7**, the effect of hydrodynamics on bacterial attachment and initial biofilm formation in the presence and/or absence of NPs in solution, as well as part of a coating, were investigated. For the latter, usnic acid was incorporated into a simple coating formulation and tested for attachment inhibition under hydrodynamic conditions. This NP was chosen as it had shown a relatively satisfactory AF performance in field trials (data not shown). Although previous static bioassays did not reveal significant anti-biofilm effect for this NP (**Chapter 5**) against *C. marina*, when incorporated into the coating and subjected to flow conditions, marked differences in biofilm morphology were revealed in comparison to a control coating. However, the hydrodynamic conditions applied here, were very low due to experimental limitations regarding the flow cell used (see **Section 7.5.2**).

A more controlled hydrodynamic environment was achieved with the use of a commercially available microfluidic system (BioFlux) where the NP with the best anti-biofilm performance (juglone) was tested under flow conditions. Novel protocols were developed for monitoring NP compounds under distinct shear stresses and although, both factors were simultaneously tested (*i.e.* shear stress and juglone treatment), comparisons with controls illustrated that juglone was the main component affecting biofilm initial formation, as opposed to shear stress. Importantly, the use of this system allowed for a deeper understanding of biofilm formation under flow conditions since *in situ* high resolution sampling was possible and

the application of two shear stresses on the control biofilms illustrated significant differences on biofilm growth rates. Data obtained from this technique were directly comparable with static bioassays, supporting in this way the anti-biofilm efficacy of juglone. Interestingly, hydrodynamic growth assays illustrated that bacterial attachment was impaired when treated with juglone, and as a response, phenotypic changes were evident with elongated cell chains and reduced biofilm density.

The exploration (pros and cons) of the two previous experimental techniques (above) lead to the design and fabrication of a novel microfluidic flow cell (**SoC**) that exploits the advantages of a *lab-on-a-chip* approach, *i.e.* by incorporating a wide range of well-defined shear stresses (CFD simulations) and replication (6 replicas) in a single device. Initial results illustrated significant differences in biofilm architecture with increasing shear stresses, *i.e.* under low shear stresses biofilm morphologies were characterised by mushroom-like structures, with interstitial channels (similar to river banks) and internal voids, while at high shear stresses compact clusters with large interspaces between them were formed. Although not attempted in the current work, the SoC is designed in such a way that the addition of different substrates is possible, which makes the device highly versatile and appropriate for a wide spectrum of applications and settings.

Chapter 9

9. Future Directions

9.1 Natural Products (NPs)

As already discussed in **Section 3**, surface textures and microtopographic modifications appear to be a promising AF approach. Common model systems studied and used in surface texture biomimetics, closely simulate surfaces of marine origin, such as shark and whale skin as well as mussel and bivalve shells, *etc*. The micro-textured surfaces however, have yet to establish a long term AF activity in the marine environment. It is often believe that the surface texturing alone might not be sufficient to prevent biofouling, as surface organic materials/compounds, such as proteins appear to additionally enhance the overall AF performance observed by marine organisms, therefore a combinatorial approach should be investigated.

In the current project, hatched egg cases of an elasmobranch species, *Scyliorhinus canicula* (**Fig. 9.1**), were obtained (October 2010 from the Isle of Wight marine centre) to assess potential AF activity. Initial thoughts on the investigation of elasmobranch egg cases derived from *in situ* observations of un-fouled specimens found hatched on the UK south coast. Incubation time for elasmobranch egg cases can reach up to 2 years in some species, during which the egg needs to be fouling-free since its semi-permeable case allows for oxygen supply to the embryo. The long incubation time translates to long activity against biofouling which makes this product an ideal candidate. Additionally, egg cases are generally characterised by a hydrodynamic shape which, once attached on a substrate, may be facilitated by the surrounding flow conditions (*e.g.* waves, tidal currents) to remain fouled-free.

Figure 9.1. Egg case of the elasmobranch *Scyliorhinus canicula* in hydrated state (for scale the Petri dish has a diameter 90 mm).

The first step was to characterise surface topography of the egg case using the Alicona - 3D optical metrology. Preliminary imaging results are presented in **Figure 9.2** for 2D and **Figure 9.3** for 3D reconstructions. The surface texture of an elasmobranch egg case was characterised using the Alicona 3D surface profiler for the first time and has not previously been reported in the published literature. Clearly defined complex vertical and perpendicular ripple-like patterns were observed, illustrating an interesting finding in a microtopography context. With the exception of only a few diatom cells, the egg case was found to be remarkably foul-free, both macro and micro (see Fig 9.2b). Thus, this suggests that elasmobranch egg cases are worthy of further investigation to establish their AF performance, in terms of NPs and surface texturing.

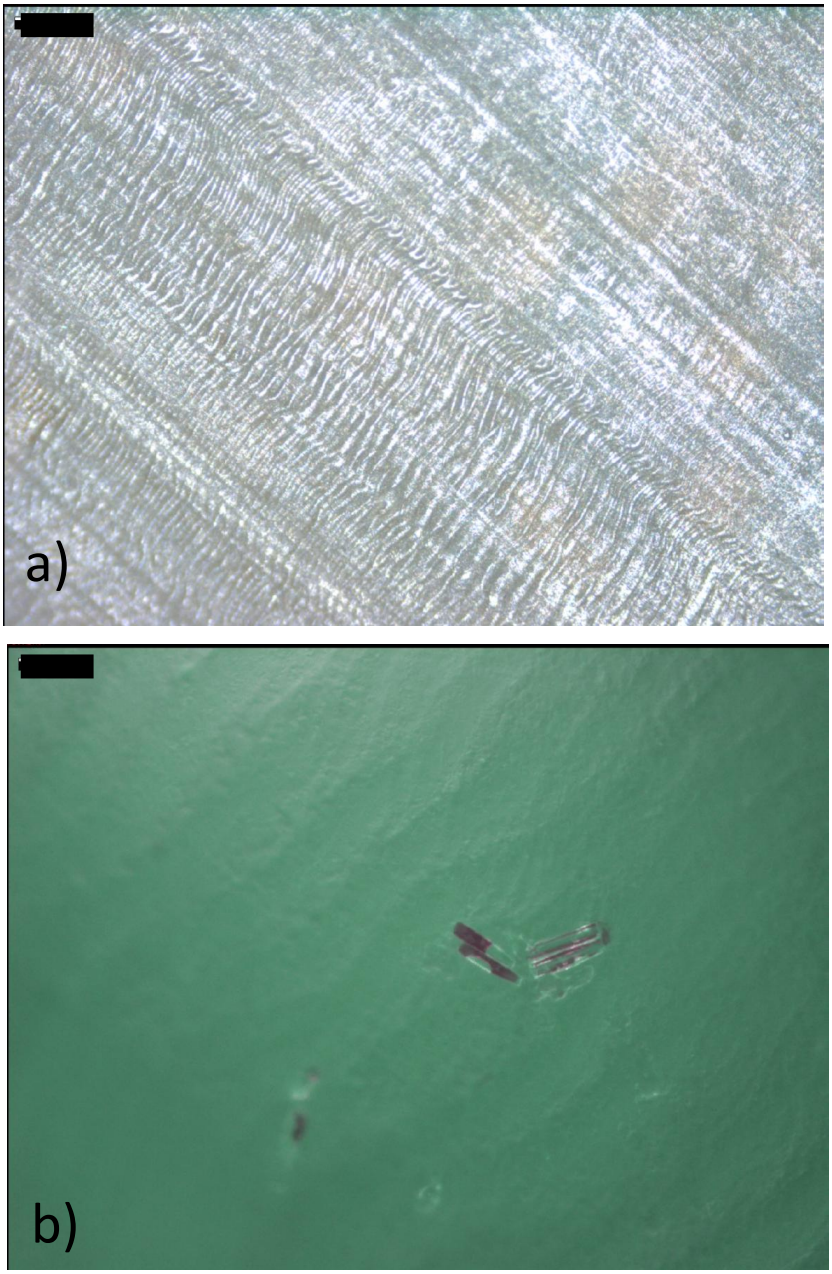

Figure 9.2. Alicona images of: a) the *Scyliorhinus canicula* egg case surface texture (scale bar = 20 µm) and b) a polarised and higher magnification image showing an isolated cluster of diatom cells (scale bar = 200 µm)

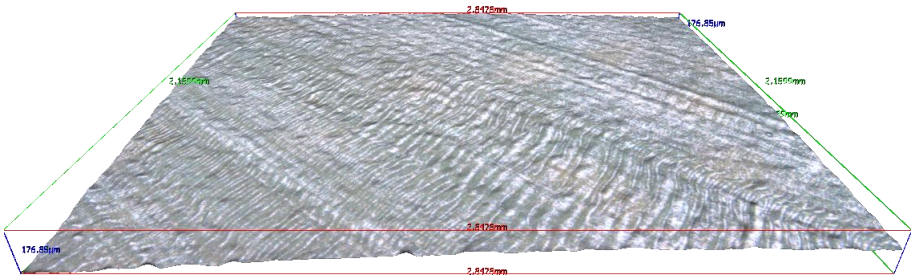

Figure 9.3. Alicona 3D projection of the *Scyliorhinus canicula* egg case surface texture (length: 2.1 mm, width 2.8 mm, height 0.176 mm).

9.2 Mechanical properties of single bacterial cells and biofilm

Single cells

The current study identified the importance in understanding adhesion and attachment mechanisms/strategies of both single bacterial cells and also the biofilm matrix. For this reason, future studies will include experimental work on the adhesion strength/attachment strength of single cells on a NP-containing surface using AFM. A preliminary test has already been undertaken to assess the experimental practicalities / methodology and to explore the initial single cell separation, visualisation and overall protocol development. Overnight culture of *C. marina* was inoculated on a mica surface and left to attach for 20 minutes. Following washing steps with ASW, the sample was imaged by means of AC mode (Amplitude Channel, dynamic mode) AFM (Asylum Research – MFP 3D) in air, see **Figure 9.4.**

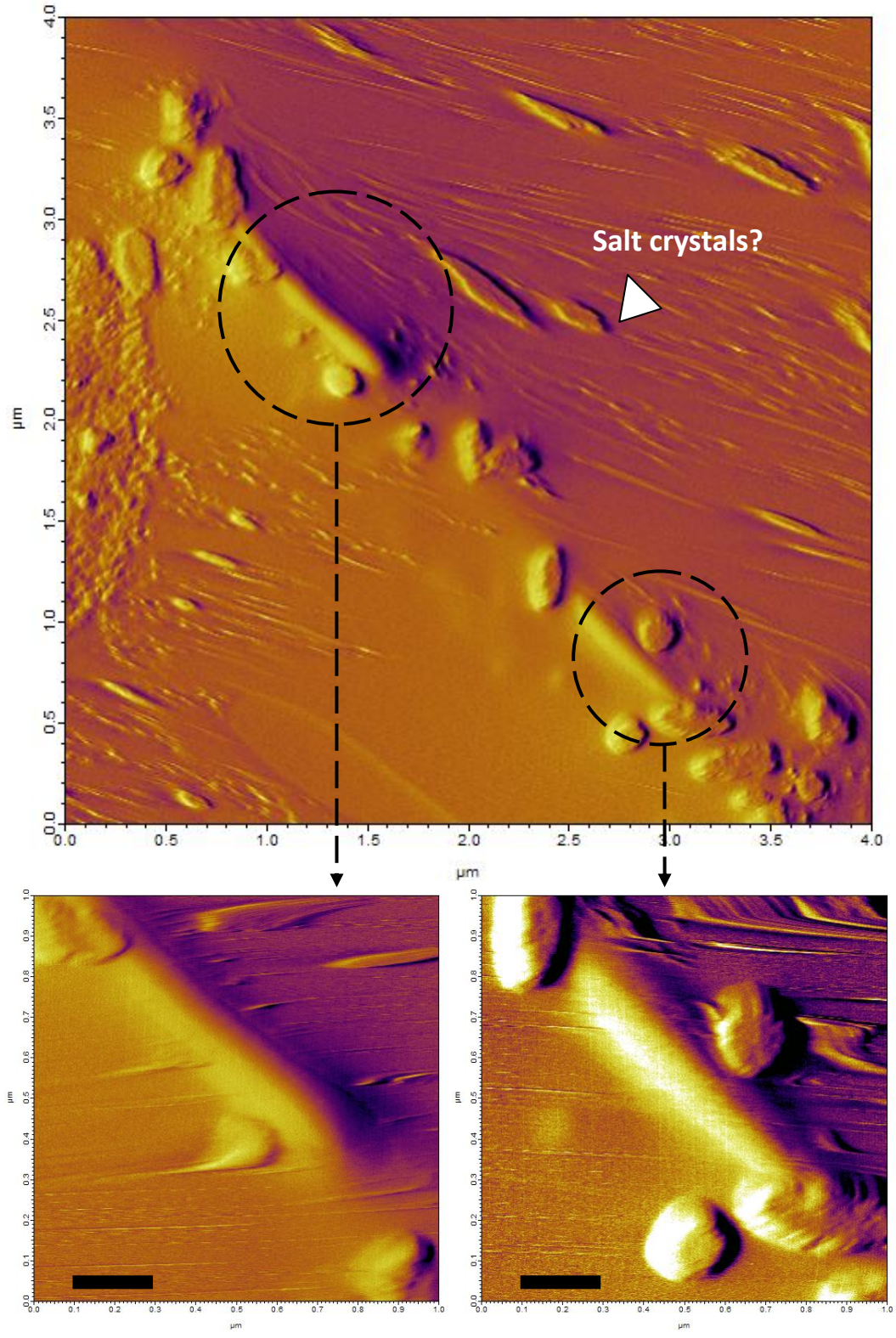

Figure 9.4. AFM images (amplitude channel) of *C. marina* on mica. Dashed circles indicate individual bacteria which are shown at greater magnification below (Scale bars = 0.2 µm).

Bulk biofilm

Marine biofilm attachment strength on a surface is a parameter that has not been fully characterised in the published research literature. The current work aims to characterise adhesion strength of the bulk biofilm on different surfaces including NP-coated, FRC-coated and compare them against controls control surface. This will be achieved by using available equipment within the SES Tissue Laboratory, *i.e.* the BOSE Electro-Force which allows several mechanical testing modalities including uniaxial tension and compression. Protocol establishment is currently under development, however initial pilot experiments have been conducted to validate the ability of the equipment to measure biofilm attachment strength. Protocol challenges include: *i)* successful attachment and growth of the biofilm between two parallel surfaces and *ii)* the definition of the appropriate parameters for the mechanical testing/measurements.

Promisingly a bacterial biofilm was successfully grown between the two surfaces (polystyrene plates) within 4 hours, resulting in a well attached biofilm. The attachment strength was evaluated through a series of "pull off" experiments using a custom designed configuration/set-up for the Electro-Force machine. In brief, the two surfaces were glued onto removable mounting disks of the Electro-Force, and were uniaxially stretched by keeping the strain rate (500 µm s^{-1}) constant (**Fig. 9.5**). Stress – Strain curves were produced by dividing the force values (N) (Force – Displacement curves) by the measured biofilm area.

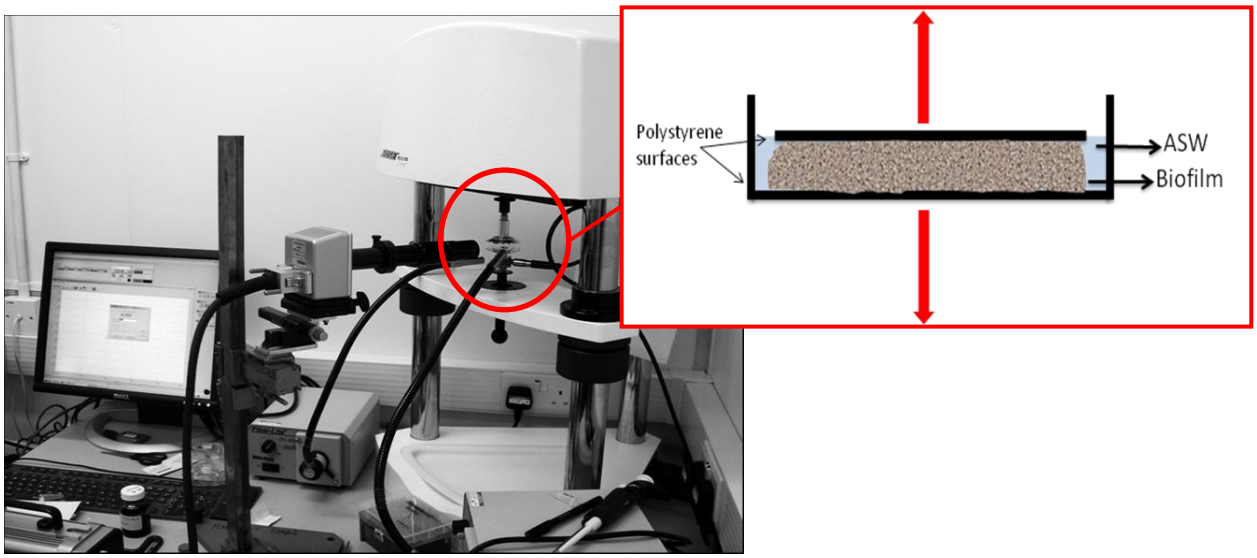

Figure 9.5. BOSE electro-force lay-out. Schematic diagram on the "pull off" set-up with red arrows indicating the force direction.

Preliminary results are shown in **Figure 9.6**. Those results indicate that a biofilm's attachment strength was able to be measured by this new approach. Most importantly, the contribution of capillary forces – *plate-liquid* (*ASW*)*-plates interface* – was ~ 5 times smaller than the measured signal. Furthermore, a linear region is also evident on biofilm sample, indicating the loading of a stiffer phase/material in comparison with the ASW controls.

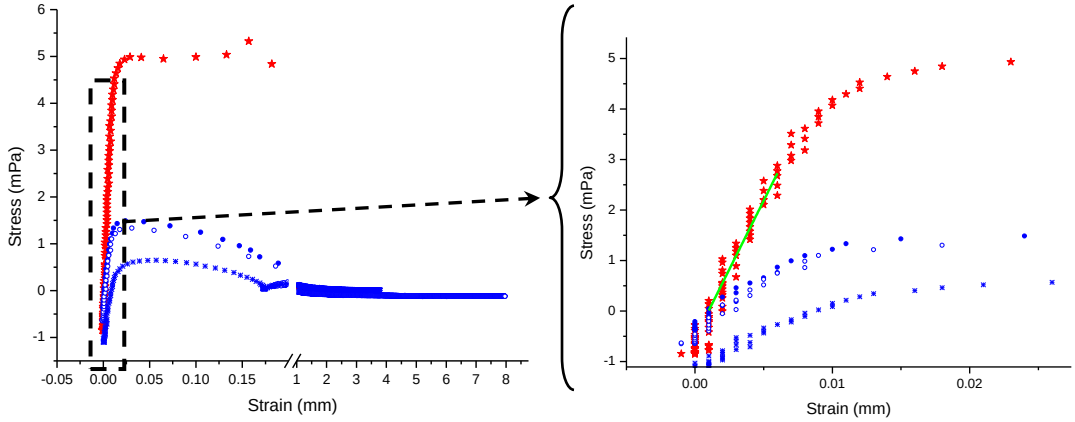

Figure 9.6. Stress *vs*. strain curves of a *C. marina* bacterial biofilm (Red line) and ASW controls (Blue lines). Biofilm maximum load = 4.95 mPa; Biofilm slope = 543.6 mPa mm^{-1}; ASW mean maximum load = 1.10 mPa.

References

Abarzua S, Jakubowski S (1995) Biotechnological investigation for the prevention of biofouling. 1. Biological and biochemical principles for the prevention of biofouling. Marine Ecology Progress Series 123: 301-312

Akesso L, Pettitt M, Callow J, Callow M, Stallard J, Teer D, Liu C, Wang S, Zhao Q, Willemsen P (2009) The potential of nano-structured silicon oxide type coatings deposited by PACVD for control of aquatic biofouling. Biofouling 25: 55-67

Anderson CD, Atlar M, Callow M, Candries M, Milne A, Townsin RL (2003) The development of foul-release coatings for seagoing vessels. Journal of Marine Design and Operations B4: 11-23

Andrews JM (2001) Determination of minimum inhibitory concentrations. Journal of Antimicrobial Chemotherapy 48: 5

Asbeck WK, Loo MV (1949) Critical Pigment Volume Relationships. Industrial & Engineering Chemistry 41: 1470-1475

Atta AM, El-Saeed SM, Farag RK (2006) New vinyl ester resins based on rosin for coating applications. Reactive and Functional Polymers 66: 1596-1608

Bacabac R, Smit T, Cowin S, Van Loon J, Nieuwstadt F, Heethaar R, Klein-Nulend J (2005) Dynamic shear stress in parallel-plate flow chambers. Journal of biomechanics 38: 159-167

Baier R (1980) Substrate influences on adhesion of microorganisms and their resultant new surface properties. In: (ed) Bitton G, Marchall KC (eds) *In* Adsorption of microorganisms to surfaces. John Wiley & Sons, Inc, New York

Bakker D, Klijnstra J, Busscher H, van der Mei H (2003) The effect of dissolved organic carbon on bacterial adhesion to conditioning films adsorbed on glass from natural seawater collected during different seasons. Biofouling 19: 391-397

Bao W, Satuito C, Yang J, Kitamura H (2007) Larval settlement and metamorphosis of the mussel Mytilus galloprovincialis in response to biofilms. Marine Biology 150: 565-574

Baty A, Frølund B, Geesey G, Langille S, Quintero E, Suci P, Weiner R (1996) Adhesion of biofilms to inert surfaces: a molecular level approach directed at the marine environment. Biofouling 10: 111-121

Baum C, Meyer W, Stelzer R, Fleischer L-G, Siebers D (2002) Average nanorough skin surface of the pilot whale (*Globicephala melas*, Delphinidae): considerations on the self-cleaning abilities based on nanoroughness. Marine Biology 140: 653-657

Baumann L, Baumann P, Mandel M, Allen R (1972) Taxonomy of aerobic marine eubacteria. Journal of Bacteriology 110: 402-429

Baumann L, Bowditch R, Baumann P (1983) Description of Deleya gen. nov. created to accommodate the marine species *Alcaligenes aestus*, *A. pacificus*, *A. cupidus, A. venustus*, and *Pseudomonas marina*. International Journal of Systematic Microbiology 33: 793-802

Benoit MR, Conant CG, Ionescu-Zanetti C, Schwartz M, Matin A 2010 New device for high-throughput viability screening of flow biofilms. Applied and Environmental Microbiology 76: 4136-4142

Berg H, Brown D (1972) Chemotaxis in Escherichia coli analysed by three-dimensional tracking. Nature 239: 500-504

Berney M, Hammes F, Bosshard F, Weilenmann H, Egli T (2007a) Assessment and interpretation of bacterial viability by using the LIVE/DEAD BacLight kit in combination with flow cytometry. Applied and Environmental Microbiology 73: 3283-3290

Berney M, Hammes F, Bosshard F, Weilenmann HU, Egli T (2007b) Assessment and interpretation of bacterial viability by using the LIVE/DEAD BacLight kit in combination with flow cytometry. Applied and Environmental Microbiology 73: 3283-3290

Bers A, Wahl M (2004) The influence of natural surface microtopographies on fouling. Bioufouling 20: 43-51

Bertin C, Yang X, Weston LA (2003) The role of root exudates and allelochemicals in the rhizosphere. Plant and Soil 256: 67-83

Beyenal H, Lewandowski Z (2002) Internal and external mass transfer in biofilms grown at various flow velocities. Biotechnology progress 18: 55-61

Bhaskar P, Bhosle N (2006) Bacterial extracellular polymeric substance (EPS): A carrier of heavy metals in the marine food-chain. Environment international 32: 191-198

Biggerstaff J, Le Puil M, Weidow B, Prater J, Glass K, Radosevich M, White D (2006) New methodology for viability testing in environmental samples. Molecular and Cellular Probes 20: 141-146

Bohlander G (1991) Biofilm effects on drag: measurements on ships. Polymers in a Marine Environment 16: 1-4

Brading MG, Jass J, Lappin-Scott HM (1995) Dynamics of bacterial biofilm formation. In: Lappin-Scott H,

Costerton, J.W. (ed) Microbial biofilms. Cambridge University Press, pp 46-63

Briand JF (2009) Marine antifouling laboratory bioassays: an overview of their diversity. Biofouling 25: 297-311

Bryan PJ, Rittschof D, McClintock JB (1996) Bioactivity of echinoderm ethanolic body-wall extracts: an assessment of marine bacterial attachment and macroinvertebrate larval settlement. Journal of Experimental Marine Biology and Ecology 196: 79-96

Burkholder J, Wetzel R, Klomparens K (1990) Direct comparison of phosphate uptake by adnate and loosely attached microalgae within an intact biofilm matrix. Applied and Environmental Microbiology 56: 2882-2890

Burns E, Ifrach I, Carmeli S, Pawlik JR, Ilan M (2003) Comparison of anti-predatory defenses of Red Sea and Caribbean sponges. I. Chemical defense. Marine Ecology Progress Series 252: 105-114

Burns E, Ilan M (2003) Comparison of anti-predatory defenses of Red Sea and Caribbean sponges. II. Physical defense. Marine Ecology Progress Series 252: 115-123

Calabrese EJ (2001) Nitric oxide: biphasic dose responses. CRC Critical Reviews in Toxicology 31: 489-501

Caldwell D, Korber D, Lawrence J (1992) Confocal laser microscopy and digital image analysis in microbial ecology. Advances in microbial ecology 12: 1-67

Callow J, Callow M (2009) Advanced nanostructured surfaces for the control of Biofouling: The AMBIO project. In: Hellio C, Yebra D (eds) Advances in marine antifouling coatings and technologies. Woodhead, Cambridge, UK

Callow M, Jennings A, Brennan A, Seegert C, Gibson A, Wilson L, Feinberg A, Baney R, Callow J (2002) Microtopographic cues for settlement of zoospores of the green fouling alga Enteromorpha. Biofouling 18: 237-245

Callow ME (1986) Fouling Algae from 'In-service' Ships. Botanica Marina XXXIX: 351-357

Campanella L, Delfini M, Ercole P, Iacoangeli A, Risuleo G (2002) Molecular characterization and action of usnic acid: a drug that inhibits proliferation of mouse polyomavirus in vitro and whose main target is RNA transcription. Biochimie 84: 329-334

Campbell AH, Meritt DW, Franklin RB, Boone EL, Nicely CT, Brown BL (2011) Effects of age and composition of field-produced biofilms on oyster larval setting. Biofouling: The Journal of Bioadhesion and Biofilm Research 27: 255 - 265

Camps M, Briand J-Fo, Guentas-Dombrowsky L, Culioli Gr, Bazire A, Blache Y (2011) Antifouling activity of commercial biocides vs. natural and natural-derived products assessed by marine bacteria adhesion bioassay. Marine Pollution Bulletin 62: 1032-1040

Carman M, Estes T, Feinberg A, Schumacher J, Wilkerson W, Wilson L, Callow M, Callow J, Brennan A (2006) Engineered antifouling microtopographies–correlating wettability with cell attachment. Biofouling 22: 11-21

Casse F, Swain GW (2006) The development of microfouling on four commercial antifouling coatings under static and dynamic immersion. International Biodeterioration & Biodegradation: 179-185

Chambers L (2009) The development of a marine antifouling system using environmentally acceptable and naturally occuring products. FACULTY OF ENGINEERING, SCIENCE & MATHEMATICS, SCHOOL OF ENGINEERING SCIENCES, nCATS, Ph.D. Thesis, Engineering Sciences

Chambers LD, Hellio C, Stokes K, Dennington S, Goodes L, Wood R, Walsh F (2011) Investigation of *Chondrus crispus* as a potential source of new antifouling agents. International Biodeterioration & Biodegradation 65: 939-946

Chiu J, Zhang R, Wang H, Thiyagarajan V, Qian P (2008) Nutrient effects on intertidal community: from bacteria to invertebrates. Mar Ecol Prog Ser 358: 41-50

Chobot V, Hadacek F (2009) Milieu-dependent pro-and antioxidant activity of juglone may explain linear and nonlinear effects on seedling development. Journal of Chemical Ecology 35: 383-390

Christensen GD, Simpson W, Younger J, Baddour L, Barrett F, Melton D, Beachey E (1985) Adherence of coagulase-negative staphylococci to plastic tissue culture plates: a quantitative model for the adherence of staphylococci to medical devices. Journal of Clinical Microbiology 22: 996-1006

Chung H, Lee O, Huang Y, Mok S, Kolter R, Qian P (2010) Bacterial community succession and chemical profiles of subtidal biofilms in relation to larval settlement of the polychaete *Hydroides elegans*. The ISME Journal 4: 817-828

Clare AS (1996) Marine natural product antifoulants: status and potential. Biofouling 9: 211-229

Colvin KM, Gordon VD, Murakami K, Borlee BR, Wozniak DJ, Wong GCL, Parsek MR The Pel Polysaccharide Can Serve a Structural and Protective Role in the Biofilm Matrix of Pseudomonas aeruginosa. PLoS pathogens 7

Combaut G, Piovetti L (1983) A Novel acyclic aiterpene from the brown alga *Bifurcaria bifurcata*. Phytochemistry 22: 1787-1789

Comber S, Franklin G, Gardner M, Watts C, Boxall A, Howcroft J (2002) Partitioning of marine antifoulants in the marine environment. The Science of the Total Environment 286: 61-71

Costerton J, Stewart P, Greenberg E (1999) Bacterial biofilms: a common cause of persistent infections. Science 284: 1318

Cox S, Abu-Ghannam N, Gupta S (2010) An assessment of the antioxidant and antimicrobial activity of six species of edible Irish Seaweeds. International Food Research Journal 17: 205–220

Culioli G, Daoudi M, Mesguiche V, Valls R, Piovetti L (1999b) Geranylgeraniol-derived diterpenoids from the brown alga *Bifurcaria bifurcata*. Phytochemistry 52: 1447-1454

Culioli G, Di Guardia S, Valls R, Piovetti L (2000) Geranylgeraniol-derived diterpenes from the brown alga Bifurcaria bifurcata: comparison with two other Cystoseiraceae species. Biochemical systematics and ecology 28: 185-187

Culioli G, Mesguiche V, Piovetti L, Valls R (1999) Geranylgeraniol and geranylgeraniol-derived diterpenes from the brown alga *Bifurcaria bifurcata* (Cystoseiraceae). Biochemical systematics and ecology 27: 665-668

Culioli G, Ortalo-Magne A, Richou M, Valls R, Piovetti L (2002) Seasonal variations in the chemical composition of *Bifurcaria bifurcata* (Cystoseiraceae). Biochemical systematics and ecology 30: 61-64

D'Souza F, Bruin A, Biersteker R, Donnelly G, Klijnstra J, Rentrop C, Willemsen P (2010) Bacterial assay for the rapid assessment of antifouling and fouling release properties of coatings and materials. Journal of Industrial Microbiology and Biotechnology 37: 363-370

Dahms H, Jin T, Qian P (2004) Adrenoreceptor Compounds Prevent the Settlement of Marine Invertebrate Larvae: Balanus amphitrite (Cirripedia), Bugula neritina (Bryozoa) and Hydroides elegans (Polychaeta). Biofouling 20: 313-321

Dang H, Lovell C (2000) Bacterial primary colonization and early succession on surfaces in marine waters as determined by amplified rRNA gene restriction analysis and sequence analysis of 16S rRNA genes. Applied and Environmental Microbiology 66: 467

Dang H, Lovell CR (2002) Numerical dominance and phylotype diversity of marine Rhodobacter species during early colonization of submerged surfaces in coastal marine waters as determined by 16S ribosomal DNA sequence analysis and fluorescence in situ hybridization. Applied and Environmental Microbiology 68: 496-504

Davey M, O'toole G (2000) Microbial biofilms: from ecology to molecular genetics. Microbiology and molecular biology reviews 64: 847

Davis AR, Targett, N.M., McConnell, O.J. & Young, C.M. (1989) Epibiosis of marine algal and benthic invertebrates: natural products chemistry and other mechanisms inhibiting settlement and overgrowth. Bioorganic Marine Chemistry 3: 85-114

de Beer D, Stoodley P (1995) Relation between the structure of an aerobic biofilm and transport phenomena. Water Science and Technology 32: 11-18

De Beer D, Stoodley P, Lewandowski Z (1996) Liquid flow and mass transport in heterogeneous biofilms. Water Research 30: 2761-2765

de Beer D, Stoodley P, Lewandowski Z (1997) Measurement of local diffusion coefficients in biofilms by microinjection and confocal microscopy. Biotechnology and bioengineering 53: 151-158

de Beer D, Stoodley P, Roe F, Lewandowski Z (1994) Effects of biofilm structures on oxygen distribution and mass transport. Biotechnol Bioeng 43: 1131-1138

De Haan EJ, Charles R (1969) The mechanism of uncoupling of oxidative phosphorylation by 2-methyl-1,4-naphthoquinone. Biochimica et Biophysica Acta (BBA) - Bioenergetics 180: 417-419

de Nys R, Dworjanyn SA, Steinberg PD (1998) A new method for determining surface concentrations of marine natural products on seaweeds. Marine Ecology Progress Series 162: 79-87

de Nys R, Steinberg PD, Willemsen P, Dworjanyn SA, Gabelish CL, King RJ (1995) Broad spectrum effects of secondary metabolites from the red alga delisea pulchra in antifouling assays. Biofouling 8: 259-271

De Voe I, Oginsky E (1969) Antagonistic effect of monovalent cations in maintenance of cellular integrity of a marine bacterium. Journal of Bacteriology 98: 1355-1367

Dempsey M (1981) Marine bacterial fouling: a scanning electron microscope study. Marine Biology 61: 305-315

Derjaguin BV (1992) Selected works of B.V. Derjaguin. Vol. 1. Surface forces in thin films and disperse systems. In: Davison SG, Liu WK (eds) *In* Progress in Surface Science. Pergamon Press, New York

Dobretsov S, Xiong HR, Xu Y, Levin LA, Qian PY (2007) Novel antifoulants: Inhibition of larval attachment by proteases. Marine Biotechnology 9: 388-397

Donlan R (2002) Biofilms: microbial life on surfaces. Emerging Infectious Diseases 8: 881

Dunsmore B, Jacobsen A, Hall-Stoodley L, Bass C, Lappin-Scott H, Stoodley P (2002) The influence of fluid shear on the structure and material properties of sulphate-reducing bacterial biofilms. Journal of Industrial Microbiology & Biotechnology 29: 347-353

Dusenbery D (2009) Living at micro scale. Harvard University Press, Cambridge, MA

Dworjanyn SA (2001) Chemically mediated antifouling and the cost of producing secondary metabolites in a marine alga., Sidney

Dworjanyn SA, De Nys R, Steinberg PD (1999) Localisation and surface quantification of secondary metabolites in the red alga Delisea pulchra. Marine Biology 133: 727-736

Dworjanyn SA, de Nys R, Steinberg PD (2006) Chemically mediated antifouling in the red alga Delisea pulchra. Marine Ecology-Progress Series 318: 153-163

Efimenko K, Finlay J, Callow M, Callow J, Genzer J (2009) Development and testing of hierarchically wrinkled coatings for marine antifouling. Applied Materials & Interfaces 1: 1031-1040

Ekblad T, Bergstrom G, Ederth T, Conlan S, Mutton R, Clare A, Wang S, Liu Y, Zhao Q, D'Souza F, Donnelly G, Willemsen P, Pettitt M, Callow M, Callow J, Liedberg B (2008) Poly (ethylene glycol)-containing hydrogel surfaces for antifouling applications in marine and freshwater environments. Biomacromolecules 9: 2775-2783

Faimali M, Garaventa F, Terlizzi A, Chiantore M, Cattaneo-Vietti R (2004) The interplay of substrate nature and biofilm formation in regulating Balanus amphitrite Darwin, 1854 larval settlement. Journal of Experimental Marine Biology and Ecology 306: 37-50

Fay F, Linossier I, Carteau D, Dheilly A, Silkina A, Vallee-Rehel K (2010) Booster biocides and microfouling. Biofouling 26: 787-798

Fitt WK, Coon SL, Walch M, Weiner RM, Colwell RR, Bonar DB (1990) Settlement behavior and metamorphosis of oyster larvae (*Crassostrea gigas*) in response to bacterial supernatants. Marine Biology 106: 389-394

Fletcher M, Floodgate G (1973) An electron-microscopic demonstration of an acidic polysaccharide involved in the adhesion of a marine bacterium to solid surfaces. Journal of General Microbiology 74: 325

Fletcher M, Loeb G (1979) Influence of substratum characteristics on the attachment of a marine pseudomonad to solid surfaces. Applied and Environmental Microbiology 37: 67-72

Ford T, Maki J, Mitchell R (1987) The role of metal-binding bacterial exopolymers in corrosion processes. Corrosion 87/380, Paper no. 380, NACE Publications, California

Francolini I, Norris P, Piozzi A, Donelli G, Stoodley P (2004) Usnic acid, a natural antimicrobial agent able to inhibit bacterial biofilm formation on polymer surfaces. Antimicrobial Agents and Chemotherapy 48: 4360-4365

Fusetani N (2004) Biofouling and antifouling. Natural Product Report 21: 94-104

Gauthier M, Lafay B, Christen R, Fernandez L, Acquaviva M, Bonin P, Bertrand J (1992) *Marinobacter hydrocarbonoclasticus* gen. nov., sp. nov., a new, extremely halotolerant, hydrocarbon-degrading marine bacterium. International Journal of Systematic and Evolutionary Microbiology 42: 568-576

Green-Rhino-Energy (2012) Tidal Streem Energy, http://www.greenrhinoenergy.com/renewable/marine/tidal_stream.php

H-U. D, Hellio C (2009) Laboratory bioassays for screening marine antifouling compounds. In: Hellio C, Yebra D (eds) Advances in marine antifouling coatings and technologies. Woodhead, Cambridge, UK

Haack T, McFeters G (1982) Nutritional relationships among microorganisms in an epilithic biofilm community. Microbial Ecology 8: 115-126

Hall-Stoodley L, Costerton J, Stoodley P (2004) Bacterial biofilms: from the natural environment to infectious diseases. Nature Reviews Microbiology 2: 95-108

Hamer JP, Walker G, Latchford JW (2001) Settlement of *Pomatoceros lamarkii* (Serpulidae) larvae on biofilmed surfaces and the effect of aerial drying. Journal of Experimental Marine Biology and Ecology 260: 113-131

Hannig C, Follo M, Hellwig E, Al-Ahmad A Visualization of adherent micro-organisms using different techniques. Journal of Medical Microbiology 59: 1-7

Hansen O, Stougaard P (1997) Hexose oxidase from the red alga *Chondrus crispus*. Journal of Biological Chemistry 272: 11581

Hanssen A, Spangehl M (2004) Practical applications of antibiotic-loaded bone cement for treatment of infected joint replacements. Clinical Orthopaedics and Related Research 427: 79-85

Harder T, Lau S, Dahms H, Qian P (2002) Isolation of bacterial metabolites as natural inducers for larval settlement in the marine polychaete *Hydroides elegans* (Haswell). Journal of Chemical Ecology 28: 2029-2043

Harder T, Yee L (2009) Bacterial adhesion and marine fouling. In: Hellio C, Yebra D (eds) Advances in marine antifouling coatings and technologies. Woodhead, Cambridge, UK

Hellio C, Berge J, Beaupoil C, Le Gal Y, Bourgougnon N (2002) Screening of marine algal extracts for anti-settlement activities against microalgae and macroalgae. Biofouling 18: 205-215

Hellio C, Bremer G, Pons A, Le Gal Y, Bourgougnon N (2000) Inhibition of the development of microorganisms (bacteria and fungi) by extracts of marine algae from Brittany, France. Applied microbiology and biotechnology 54: 543-549

Hellio C, De La Broise D, Dufossé L, LeGal Y, Bourgougnon N (2001) Inhibition of marine bacteria by extracts of macroalgae: potential use for environmentally friendly antifouling paints. Marine Environmental Research 52: 231-247

Hellio C, Marechal J-P, Véron B, Bremer G, Clare A, Le Gal Y (2004) Seasonal variation of antifouling activities of marine algae from the Brittany coast (France). Marine Biotechnology 6: 67-82

Hellio C, Thomas-Guyon H., Culioli, G., Poivetti, L., & Bourgougnon (2001) Marine antifoulants from Bifurcaria bifurcata (Phaeophyceae, Cystoseiracea) and other brown macroalgae. Biofouling 17: 189-201

Heydorn A, Nielsen AT, Hentzer M, Sternberg C, Givskov M, Ersboll BK, Molin S (2000) Quantification of biofilm structures by the novel computer program COMSTAT. Microbiology-Uk 146: 2395-2407

Hoffman LR, D'Argenio DA, MacCoss MJ, Zhang Z, Jones RA, Miller SI (2005) Aminoglycoside antibiotics induce bacterial biofilm formation. Nature 436: 1171-1175

Holland R, Dugdale T, Wetherbee R, Brennan A, Finlay J, Callow J, Callow M (2004) Adhesion and motility of fouling diatoms on a silicone elastomer. Biofouling 20: 323-329

Holm E, Schultz M, Haslbeck E, Talbott W, Field A (2004) Evaluation of hydrodynamic drag on experimental fouling-release surfaces, using rotating disks. Biofouling 20: 219-226

Horn H, Reiff H, Morgenroth E (2003) Simulation of growth and detachment in biofilm systems under defined hydrodynamic conditions. Biotechnology and bioengineering 81: 607-617

Hougaard L, Anthoni U, Christophersen C, Nielsen P (1991b) Two new diterpenoid dihydroxy- -butyrolactones from *Bifurcaria difurcata* (Cystoseiraceae). Tetrahedron letters 32: 3577-3578

Hougaard L, Anthoni U, Christophersen C, Nielsen PH (1991a) Eleganolone Derived Diterpenes from *Bifurcaria bifurcata*. Phytochemistry 30: 3049-3051

Howell D (2009) Testing the impact of biofilms on the performance of marine antifouling coatings. In: Hellio C, Yebra D (eds) Advances in marine antifouling coatings and technologies Woodhead, Cambridge, UK

Huang S, Hadfield M (2003) Composition and density of bacterial biofilms determine larval settlement of the polychaete *Hydroides elegans*. Marine Ecology Progress Series 260: 161-172

Huang Y-L, Li M, Yu Z, Qian P-Y (2011) Correlation between pigmentation and larval settlement deterrence by Pseudoalteromonas sp. sf57. Biofouling: The Journal of Bioadhesion and Biofilm Research 27: 287-293

Huang YL, Dobretsov S, Ki JS, Yang LH, Qian PY (2007) Presence of acyl-homoserine lactone in subtidal biofilm and the implication in larval behavioral response in the polychaete *Hydroides elegans*. Microbial Ecology 54: 384-392

Huggett M, Nedved B, Hadfield M (2009) Effects of initial surface wettability on biofilm formation and subsequent settlement of *Hydroides elegans*. Biofouling 25: 387-399

Hung O, Thiyagarajan V, Qian P (2008) Preferential attachment of barnacle larvae to natural multi-species biofilms: Does surface wettability matter? Journal of Experimental Marine Biology and Ecology 361: 36-41

Hung O, Thiyagarajan V, Wu R, Qian P (2005) Effect of ultraviolet radiation on biofilms and subsequent larval settlement of Hydroides elegans. Marine Ecology Progress Series 304: 155-166

Hung OS, Lee OO, Thiyagarajan V, He HP, Xu Y, Chung HC, Qiu JW, Qian PY (2009) Characterization of cues from natural multi-species biofilms that induce larval attachment of the polychaete *Hydroides elegans*. Aquatic Biology 4: 253-262

Inbakandan D, Sriyutha Murthy P, Venkatesan R, Ajmal Khan S (2010) 16S rDNA sequence analysis of culturable marine biofilm forming bacteria from a ship's hull. Biofouling 26: 893-899

Inbaraj J, Chignell C (2004) Cytotoxic action of juglone and plumbagin: a mechanistic study using HaCaT keratinocytes. Chem. Res. Toxicol 17: 55-62

Ingolfsdottir K (2002) Usnic acid. Phytochemistry 61: 729-736

Jackson S (1991) Microalgae: their status as fouling organisms. Oebalia 17: 295-303

Jacob SW, Bischel M, Herschler RJ (1964) Dimethyl Sulfoxide (DMSO): A new concept in pharmacotherapy. Current therapeutic research, clinical and experimental 6: 134

Jeon JH, Lee CH, Kim MK, Lee HS (2009) Antibacterial effects of juglone and its derivatives against oral pathogens. Journal of the Korean Society for Applied Biological Chemistry 52: 720-725

Joint I, Callow ME, Callow JA, Clarke KR (2000) The attachment of Enteromorpha zoospores to a bacterial biofilm assemblage. Biofouling 16: 151-158

Jones P, Cottrell M, Kirchman D, Dexter S (2007) Bacterial community structure of biofilms on artificial surfaces in an estuary. Microbial Ecology 53: 153-162

Kazy SK, Sar P, Singh SP, Sen AK, D'Souza SF (2002) Extracellular polysaccharides of a copper-sensitive and a copper-resistant <i>Pseudomonas aeruginosa</i> strain: synthesis, chemical nature and copper binding. World Journal of Microbiology and Biotechnology 18: 583-588

Kerr A, Cowling M (2003) The effects of surface topography on the accumulation of biofouling. Philosophical Magazine 83: 2779-2795

Khatoon H, Yusoff F, Banerjee S, Shariff M, Bujang JS (2007) Formation of periphyton biofilm and subsequent biofouling on different substrates in nutrient enriched brackishwater shrimp ponds. Aquaculture 273: 470-477

Kirchman D, Mazzella L, Alberte R, Mitchell R (1984) Epiphytic bacterial production on *Zostera marina*. Marine ecology progress series. Oldendorf 15: 117-123

Kristensen JB, Meyer RL, Laursen BS, Shipovskov S, Besenbacher F, Poulsen CH (2008) Antifouling enzymes and the biochemistry of marine settlement. Biotechnology Advances 26: 471-481

Kristensen JB, Olsen SM, Laursen BS, Kragh KM, Poulsen CH, Besenbacher F, Meyer RL (2010) Enzymatic generation of hydrogen peroxide shows promising antifouling effect. Biofouling 26: 141-153

Kristmundsdottir T, Jonsdottir E, Ogmundsdottir HM, Ingolfsdottir K (2005) Solubilization of poorly soluble lichen metabolites for biological testing on cell lines. European Journal of Pharmaceutical Sciences 24: 539-543

Kuechle D, Landon G, Musher D, Noble P (1991) Elution of vancomycin, daptomycin, and amikacin from acrylic bone cement. Clinical Orthopaedics and Related Research 264: 302-308

Kugel A, Stafslien S, Chisholm BJ (2011) Antimicrobial coatings produced by â€œtetheringâ€ biocides to the coating matrix: A comprehensive review. Progress in Organic Coatings 72: 222-252

Kwok W, Picioreanu C, Ong S, Van Loosdrecht M, Ng W, Heijnen J (1998) Influence of biomass production and detachment forces on biofilm structures in a biofilm airlift suspension reactor. Biotechnology and bioengineering 58: 400-407

Lakowicz J (2006) Principles of Fluorescence Spectroscopy. Springer, New York

Lam C, Harder T, Qian P (2003) Induction of larval settlement in the polychaete *Hydroides elegans* by surface-associated settlement cues of marine benthic diatoms. Marine Ecology Progress Series 263: 83-92

Lau S, Qian P (2001) Larval settlement in the serpulid polychaete *Hydroides elegans* in response to bacterial films: an investigation of the nature of putative larval settlement cue. Marine Biology 138: 321-328

Lau S, Thiyagarajan V, Cheung S, Qian P (2005) Roles of bacterial community composition in biofilms as a mediator for larval settlement of three marine invertebrates. Aquatic Microbial Ecology 38: 41-51

Lau S, Thiyagarajan V, Qian P (2003) The bioactivity of bacterial isolates in Hong Kong waters for the inhibition of barnacle (*Balanus amphitrite* Darwin) settlement. Journal of Experimental Marine Biology and Ecology 282: 43-60

Lauga E, Powers T (2009) The hydrodynamics of swimming microorganisms. Reports on Progress in Physics 72: 096601

Lauterwein M, Oethinger M, Belsner K, Peters T, Marre R (1995) In vitro activities of the lichen secondary metabolites vulpinic acid,(+)-usnic acid, and (-)-usnic acid against aerobic and anaerobic microorganisms. Antimicrobial Agents and Chemotherapy 39: 2541-2543

Lawrence J, Korber D, Hoyle B, Costerton J, Caldwell D (1991) Optical sectioning of microbial biofilms. Journal of Bacteriology 173: 6558-6567

Lee H, Dellatore SM, Miller WM, Messersmith PB (2007) Mussel-inspired surface chemistry for multifunctional coatings. Science 318: 426-430

Leroy C, Delbarre Ladrat C, Ghillebaert F, Rochet M, Compere C, Combes D (2007) A marine bacterial adhesion microplate test using the DAPI fluorescent dye: a new method to screen antifouling agents. Letters in Applied Microbiology 44: 372-378

Lewandowski Z, Stoodley P (1995) Flow induced vibrations, drag force, and pressure drop in conduits covered with biofilm. Water Science and Technology 32: 19-26

Lewis G (2009) Properties of antibiotic loaded acrylic bone cements for use in cemented arthroplasties: A state of the art review. Journal of Biomedical Materials Research Part B: Applied Biomaterials 89: 558-574

Lewis J (2002) Hull Fouling as a Vector for the Translocation of Marine Organisms: Report 1 - Hull Fouling Research. In: Department of Agriculture F, and Forestry (ed). Commonwealth of Australia, pp 129

Lewthwaite J, Molland A, Thomas K (1985) An investigation into the variation of ship skin frictional resistance with fouling. Transactions of the Royal Institution of Naval Architects 126: 269-284

Li X, Yan Z, Xu J (2003) Quantitative variation of biofilms among strains in natural populations of *Candida albicans*. Microbiology 149: 353-362

Liermann L, Barnes A, Kalinowski B, Zhou X, Brantley S (2000) Microenvironments of pH in biofilms grown on dissolving silicate surfaces. Chemical Geology 171: 1-16

Lim M, Jeon J, Jeong E, Lee C, Lee H (2007) Antimicrobial activity of 5-hydroxy-1, 4-naphthoquinone isolated from *Caesalpinia sappan* toward intestinal bacteria. Food Chemistry 100: 1254-1258

Linares JF, Gustafsson I, Baquero F, Martinez JL (2006) Antibiotics as intermicrobial signaling agents instead of weapons. Proceedings of the National Academy of Sciences 103: 19484-19489

Lincoln SF, Richens DT, Sykes AG, Editors-in-Chief:Â Â JAM, Meyer TJ (2003) 1.25 - Metal Aqua Ions Comprehensive Coordination Chemistry II. Pergamon, Oxford, pp 515-555

Magin C, Long C, Cooper S, Ista L, López G, Brennan A (2010) Engineered antifouling microtopographies: the role of Reynolds number in a model that predicts attachment of zoospores of *Ulva* and cells of *Cobetia marina*. Biofouling 26: 719-727

Maki J, Mitchell R (1985) Involvement of lectins in the settlement and metamorphosis of marine invertebrate larvae. Bulletin of Marine Science 37: 675-683

Maki J, Rittschof D, Mitchell R (1992) Inhibition of larval barnacle attachment to bacterial films: an investigation of physical properties. Microbial Ecology 23: 97-106

Maréchal J-P, Culioli G, Hellio C, Thomas-Guyon H, Callow ME, Clare AS, Ortalo-Magné A (2004) Seasonal variation in antifouling activity of crude extracts of the brown alga *Bifurcaria bifurcata* (Cystoseiraceae) against cyprids of *Balanus amphitrite* and the marine bacteria *Cobetia marina* and *Pseudoalteromonas haloplanktis*. Journal of Experimental Marine Biology and Ecology 313: 47-62

Marshall K, Joint I, Callow M, Callow J (2006) Effect of marine bacterial isolates on the growth and morphology of axenic plantlets of the green alga *Ulva linza*. Microbial Ecology 52: 302-310

Marshall KC (1985) Mechanisms of bacterial adhesion at solid-water interfaces. In: Savage DL, Fletcher MF (eds) *In* Bacterial Adhesion. Plenum Press, New York

Massol-Deya AA, Whallon J, Hickey RF, Tiedje JM (1995) Channel structures in aerobic biofilms of fixed-film reactors treating contaminated groundwater. Applied and Environmental Microbiology 61: 769-777

Maximilien R, de Nys R, Holmstrom C, Gram L, Givskov M, Crass K, Kjelleberg S, Steinberg PD (1998a) Chemical mediation of bacterial surface colonisation by secondary metabolites from the red alga Delisea pulchra. Aquatic Microbial Ecology 15: 233-246

Maximilien R, De Nys R, Holmstrom C, Gram L, Kjelleberg S, Steinberg P (1998b) Bacterial fouling is regulated by secondary metabolites from the red alga Delisea pulchra. Aquat. Microbial. Ecol 15: 233-246

McNamara CJ, Bearce Lee K, Russell MA, Murphy LE, Mitchell R (2009) Analysis of bacterial community composition in concretions formed on the USS Arizona, Pearl Harbor, HI. Journal of Cultural Heritage 10: 232-236

Méndez J, Abraham G, Fernández M, Vázquez B, Román J (2002) Self curing acrylic formulations containing PMMA/PCL composites: Properties and antibiotic release behavior. Journal of Biomedical Materials Research 61: 66-74

Meyer MT, Roy V, Bentley WE, Ghodssi R (2011) Development and validation of a microfluidic reactor for biofilm monitoring via optical methods. Journal of Micromechanics and Microengineering 21

Mihm JW, Leob GI (1988) The effects of microbial biofilms on organotin release rate by an antifouling paint. Biodeterioration 7: 309-314

Molino PJ, Campbell E, Wetherbee R (2009*b*) Development of the initial diatom microfouling layer on antifouling and fouling-release surfaces in temperate and tropical Australia. Biofouling 25: 685-694

Molino PJ, Childs S, Hubbard MR, Carey JM, Burgman MA, Wetherbee R (2009*a*) Development of the primary bacterial microfouling layer on antifouling and fouling release coatings in temperate and tropical environments in Eastern Australia. Biofouling 25: 149-162

Molino PJ, Wetherbee R (2008) The biology of biofouling diatoms and their role in the development of microbial slimes. Biofouling 24: 365-379

Moller S, Sternberg C, Andersen JB, Christensen BB, Ramos JL, Givskov M, Molin S (1998) In situ gene expression in mixed-culture biofilms: evidence of metabolic interactions between community members. Applied and Environmental Microbiology 64: 721-732

Mori R, Nakai T, Enomoto K, Uchio Y, Yoshino K (2010) Increased Antibiotic Release from a Bone Cement Containing Bacterial Cellulose. Clinical Orthopaedics and Related Research 469: 600-606

Murthy PS, Venugopalan VP, Nair KVK, Subramoniam T (2009) Larval settlement and surfaces: implications in development of antifouling strategies. In: Flemming HC, Murthy PS, Venkatesan R, Cooksey KE (eds) Marine and Industrial Biofouling. Springer Verlag, Berlin, pp 233-264

Nagayama K, Iwamura Y, Shibata T, Hirayama I, Nakamura T (2002) Bactericidal activity of phlorotannins from the brown alga *Ecklonia kurome*. Journal of Antimicrobial Chemotherapy 50: 889-893

National-Physical-Laboratory (2012) Prysical properties of sea water, http://www.kayelaby.npl.co.uk/general_physics/2_7/2_7_9.html

Nayar S, Goh BPL, Chou LM (2005) Settlement of marine periphytic algae in a tropical estuary. Estuarine Coastal and Shelf Science 64: 241-248

Neely R, Wetzel R (1995) Simultaneous use of 14C and 3H to determine autotrophic production and bacterial protein production in periphyton. Microbial Ecology 30: 227-237

Nylund G, Gribben P, De Nys R, Steinberg P, Pavia H (2007) Surface chemistry versus whole-cell extracts: antifouling tests with seaweed metabolites. Marine Ecology Progress Series 329: 73-84

Nylund GM, Pavia H (2003) Inhibitory effects of red algal extracts on larval settlement of the barnacle *Balanus improvisus*. Marine Biology 143: 875-882

O'Brien P (1991) Molecular mechanisms of quinone cytotoxicity. Chemico-biological interactions 80: 1-41

O'Connor N, Richardson D (1996) Effects of bacterial films on attachment of barnacle (*Balanus improvisus* Darwin) larvae: laboratory and field studies. Journal of Experimental Marine Biology and Ecology 206: 69-81

Ogden MI, Beer PD (2006) Water & O-Donor Ligands Encyclopedia of Inorganic Chemistry. John Wiley & Sons, Ltd

Olivier F, Tremblay R, Bourget E, Rittschof D (2000) Barnacle settlement: field experiments on the influence of larval supply, tidal level, biofilm quality and age on *Balanus amphitrite* cyprids. Marine ecology. Progress series 199: 185-204

Olsen SM, Kristensen JB, Laursen BS, Pedersen LT, Dam-Johansen K, Kiil S (2010) Antifouling effect of hydrogen peroxide release from enzymatic marine coatings: Exposure testing under equatorial and Mediterranean conditions. Progress in Organic Coatings 68: 248-257

Omae I (2003) General aspects of tin-Free antifouling paints. Chemical Review 103: 3431-3448

Park TH, Shuler ML (2003) Integration of Cell Culture and Microfabrication Technology. Biotechnology progress 19: 243-253

Patel P, Callow ME, Joint I, Callow JA (2003) Specificity in the settlement–modifying response of bacterial biofilms towards zoospores of the marine alga *Enteromorpha*. Environmental Microbiology 5: 338-349

Patil JS, Anil AC (2005) Biofilm diatom community structure: Influence of temporal and substratum variability. Biofouling 21: 189-206

Picioreanu C, van Loosdrecht MCM, Heijnen JJ (2000) Modelling and predicting biofilm structure. Society of General Microbiology Symposium 59. Cambridge; Cambridge University Press, pp 129-166

Picioreanu C, van Loosdrecht MCM, Heijnen JJ (2001) Two-dimensional model of biofilm detachment caused by internal stress from liquid flow. Biotechnology & Bioengineering 72: 205-218

Pitts B, Hamilton M, Zelver N, Stewart P (2003) A microtiter-plate screening method for biofilm disinfection and removal. Journal of Microbiological Methods 54: 269-276

Price R, Patchan M, Clare A, Rittschof D, Bonaventura J (1992) Performance enhancement of natural antifouling compounds and their analogs through microencapsulation and controlled release. Biofouling 6: 207-216

Qian PY, Thiyagarajan V, Lau SCK, Cheung SCK (2003) Relationship between bacterial community profile in biofilm and attachment of the acorn barnacle *Balanus amphitrite*. Aquatic Microbial Ecology 33: 225-237

Ragan M (1976) Physodes and the phenolic compounds of brown algae. Composition and significance of physodes in vivo. Bot. mar 19: 145-154

Railkin AI (2004) Marine biofouling: colonization processes and defenses. CRC Press

Rasmussen K, Ostgaard K (2003) Adhesion of the marine bacterium Pseudomonas sp. NCIMB 2021 to different hydrogel surfaces. Water Research 37: 519-524

Reading NC, Sperandio V (2005) Quorum sensing: the many languages of bacteria. Fems Microbiology Letters 254: 1-11

Riber H, Wetzel R (1987) Boundary-layer and internal diffusion effects on phosphorus fluxes in lake periphyton. Limnology and Oceanography 32: 1181-1194

Richter L, Stepper C, Mak A, Reinthaler A, Heer R, Kast M, Bruckl H, Ertl P (2007) Development of a microfluidic biochip for online monitoring of fungal biofilm dynamics. Lab on a Chip 7: 1723-1731

Riedl J, Altenburger R (2007) Physicochemical substance properties as indicators for unreliable exposure in microplate-based bioassays. Chemosphere 67: 2210-2220

Rieu A, Briandet R, Habimana O, Garmyn D, Guzzo J, Piveteau P (2008) *Listeria monocytogenes* EGD-e biofilms: no mushrooms but a network of knitted chains. Applied and Environmental Microbiology 74: 4491-4497

Riffel A, Medina L, Stefani V, Santos R, Bizani D, Brandelli A (2002) In vitro antimicrobial activity of a new series of 1, 4-naphthoquinones. Brazilian Journal of Medical and Biological Research 35: 811-818

Rochex A, Godon J, Bernet N, Escudié R (2008) Role of shear stress on composition, diversity and dynamics of biofilm bacterial communities. Water Research 42: 4915-4922

Salerno M, Logan B, Velegol D (2004) Importance of molecular details in predicting bacterial adhesion to hydrophobic surfaces. Langmuir 20: 10625-10629

Salta M, Wharton J, Stoodley P, Dennington S, Goodes L, Werwinski S, Mart U, Wood R, Stokes K (2010) Designing biomimetic antifouling surfaces. Philosophical Transactions of the Royal Society A: Mathematical, Physical and Engineering Sciences 368: 4729-4754

Satheesh S, Wesley S (2010) Influence of substratum colour on the recruitment of macrofouling communities. Journal of the Marine Biological Association of the UK 90: 941-946

Savary BJ, Hicks KB, O'Connor JV (2001) Hexose oxidase from *Chondrus crispus*: improved purification using perfusion chromatography. Enzyme and Microbial Technology 29: 42-51

Scardino A, Guenther J, De Nys R (2008) Attachment point theory revisited: the fouling response to a microtextured matrix. Biofouling 24: 45-53

Scardino A, Hudleston D, Peng Z, Paul N, De Nys R (2009*a*) Biomimetic characterisation of key surface parameters for the development of fouling resistant materials. Biofouling 25: 83-93

Scardino A, Zhang H, Cookson D, Lamb R, Nys R (2009*b*) The role of nano-roughness in antifouling. Biofouling 25: 757-767

Scardino AJ, de Nys R (2004) Fouling deterrence on the bivalve shell *Mytilus galloprovincialis*: a physical phenomenon? Biofouling 20: 249-257

Scardino AJ, de Nys R (2011) Mini review: Biomimetic models and bioinspired surfaces for fouling control. Biofouling 27: 73-86

Schneider R (1997) Bacterial adhesion to solid substrata coated with conditioning films derived from chemical fractions of natural waters. Journal of Adhesion Science and Technology 11: 979-994

Schreiber R, Altenburger R, Paschke A, Kuster E (2008) How to deal with lipophilic and volatile organic substances in microtiter plate assays. Environmental Toxicology and Chemistry 27: 1676-1682

Schultz M (2007) Effects of coating roughness and biofouling on ship resistance and powering. Biofouling 23: 331-341

Schultz M, Swain G (1999) The effect of biofilms on turbulent boundary layers. Journal of Fluids Engineering 121: 44

Schultz M, Swain G (2000) The Influence of Biofilms on Skin Friction Drag. Biofouling 15: 129-139

Schultz MP, Bendick JA, Holm ER, Hertel WM (2011) Economic impact of biofouling on a naval surface ship. Biofouling 27: 87-98

Schumacher JF, Aldred N, Callow ME, Finlay JA, Callow JA, Clare AS, Brennan AB (2007) Species-specific engineered antifouling topographies: correlations between the settlement of algal zoospores and barnacle cyprids. Biofouling 23: 307-317

Schwartz T, Hoffmann S, Obst U (2003) Formation of natural biofilms during chlorine dioxide and uv disinfection in a public drinking water distribution system. Journal of applied microbiology 95: 591-601

Semmak L, Zerzouf A, Valls R, Banaigs B, Jeanty G, Francisco C (1988) Acyclic diterpenes from *Bifurcaria bifurcata*. Phytochemistry 27: 2347-2349

Shi L (2000) Development and application of a three-dimensional water quality model in a partially-mixed estuary, Southampton Water, UK. School of Ocean and Earth Science, Southampton

Shikuma NJ, Hadfield MG (2006) Temporal variation of an initial marine biofilm community and its effects on larval settlement and metamorphosis of the tubeworm *Hydroides elegans*. Biofilms 2: 231-238

Silence S, Scott J, Stankus J, Moerner W, Moylan C, Bjorklund G, Twieg R (1995) Photorefractive polymers based on dual-function dopants. The Journal of Physical Chemistry 99: 4096-4105

Soderquist CJ (1973) Juglone and allelopathy. Journal of Chemical Education 50: 782

Stafslien S, Bahr J, Feser J, Weisz J, Chisholm B, Ready T, Boudjouk P (2006) Combinatorial materials research applied to the development of new surface coatings I: a multiwell plate screening method for the high-throughput assessment of bacterial biofilm retention on surfaces. J. Comb. Chem 8: 156-162

Stafslien S, Daniels J, Chisholm B, Christianson D (2007a) Combinatorial materials research applied to the development of new surface coatings III. Utilisation of a high-throughput multiwell plate screening method to rapidly assess bacterial biofilm retention on antifouling surfaces. Biofouling 23: 37-44

Stafslien S, Daniels J, Mayo B, Christianson D, Chisholm B, Ekin A, Webster D, Swain G (2007b) Combinatorial materials research applied to the development of new surface coatings IV. A high-throughput bacterial biofilm retention and retraction assay for screening fouling-release performance of coatings. Biofouling 23: 45-54

Stafslien SJ, Bahr JA, Daniels JW, Wal LV, Nevins J, Smith J, Schiele K, Chisholm B (2007c) Combinatorial materials research applied to the development of new surface coatings VI: An automated spinning water jet apparatus for the high-throughput characterization of fouling-release marine coatings. Review of Scientific Instruments 78: 072204-072204-072206

Steinberg P, De Nys R (2002) Chemical mediation of colonization of seaweed surfaces. Journal of Phycology 38: 621-629

Steinberg PD, de Nys R, Kjelleberg S (2002) Chemical Cues for Surface Colonization. Journal of Chemical Ecology 28: 1935-1951

Stewart P, Franklin M (2008) Physiological heterogeneity in biofilms. Nature Reviews Microbiology 6: 199-210

Stewart PS (2003) Diffusion in biofilms. Journal of Bacteriology 185: 1485-1491

Stocks S (2004) Mechanism and use of the commercially available viability stain, BacLight. Cytometry Part A 61: 189-195

Stoodley P, Cargo R, Rupp C, Wilson S, Klapper I (2002) Biofilm material properties as related to shear-induced deformation and detachment phenomena. Journal of Industrial Microbiology and Biotechnology 29: 361-367

Stoodley P, deBeer D, Lewandowski Z (1994) Liquid flow in biofilm systems. Applied and Environmental Microbiology 60: 2711

Stoodley P, Lewandowski Z, Boyle J, Lappin-Scott H (1998) Oscillation characteristics of biofilm streamers in turbulent flowing water as related to drag and pressure drop. Biotechnology and bioengineering 57: 536-544

Stoodley P, Lewandowski Z, Boyle J, Lappin-Scott H (1999) Structural deformation of bacterial biofilms caused by short-term fluctuations in fluid shear: an in situ investigation of biofilm rheology. Biotechnology and bioengineering 65: 83-92

Stoodley P, Warwood B (2003) Use of flow cells and Annular Reactors to study biofilms. In: Lens O, O'Flaherty V, Moran A, Stoodley P, Mahony T (eds) Biofilms in Industry,

Medicine and Environmental Biotechnology - Characteristics, analysis and control. IWA Publishing, London, pp 197-213

Stoodley P, Wilson S, Hall-Stoodley L, Boyle JD, Lappin-Scott HM, Costerton J (2001) Growth and detachment of cell clusters from mature mixed-species biofilms. Applied and Environmental Microbiology 67: 5608-5613

Stupak ME, García MT, Perez MC (2003) Non-toxic alternative compounds for marine antifouling paints. International Biodeterioration & Biodegradation 52: 49-52

Sudatti D, Rodrigues S, Coutinho R, da Gama B, Salgado L, Amado Filho G, Pereira R (2008) Transport and defensive role of elatol at the surface of the red seaweed *Laurencia obtusa* (Ceramiales, Rhodophyta). Journal of Phycology 44: 548-591

Sullivan J, JD, Ikawa M (1973) Purification and characterization of hexose oxidase from the red alga *Chondrus crispus*. Biochimica et Biophysica Acta (BBA)-Enzymology 309: 11-22

Taherzadeh D, Picioreanu C, Küttler U, Simone A, Wall W, Horn H (2009) Computational study of the drag and oscillatory movement of biofilm streamers in fast flows. Biotechnology and bioengineering 105: 600-610

Teitzel GM, Parsek MR (2003) Heavy metal resistance of biofilm and planktonic *Pseudomonas aeruginosa*. Applied and Environmental Microbiology 69: 2313-2320

Thiyagarajan V, Lau SCK, Cheung SCK, Qian PY (2006) Cypris habitat selection facilitated by microbial films influences the vertical distribution of subtidal barnacle Balanus trigonus. Microbial Ecology 51: 431-440

Thomas K, Brooks S (2009) The environmental fate and effects of antifouling paint biocides. Biofouling 26: 73-88

Thomas KV, Fileman, T.W., Readman, J.W. & Waldock, M.J. (2001) Antifouling Paint Booster Biocides in the UK Coastal Environment and Potential Risks of Biological Effects. Marine Pollution Bulletin 42: 677-688

Thompson R, Norton T, Hawkins S (1998) The influence of epilithic microbial films on the settlement of *Semibalanus balanoides* cyprids – a comparison between laboratory and field experiments. Hydrobiologia 375-376: 203-216

Townsin R, Anderson C (2009) Fouling control coatings using low surface energy, foul release technology. In: Hellio C, Yebra D (eds) Advances in marine antifouling coatings and technologies. Woodhead, Cambridge, UK

Tran T, Saheba E, Arcerio A, Chavez V, Li Q, Martinez L, Primm T (2004) Quinones as antimycobacterial agents. Bioorganic & medicinal chemistry 12: 4809-4813

Tsai Y (2005) Impact of flow velocity on the dynamic behaviour of biofilm bacteria. Biofouling 21: 267-277

Unabia CRC, Hadfield MG (1999) Role of bacteria in larval settlement and metamorphosis of the polychaete *Hydroides elegans*. Marine Biology 133: 55-64

Valls R, Banaigs B, Francisco C, Codomier L, Cave A (1986) An acyclic diterpene from the brown alga *Bifurcaria bifurcata*. Phytochemistry 25: 751-752

Valls R, Banaigs B, Piovetti L, Archavlis A, Artaud J (1993a) Linear Diterpene with Antimitotic Activity from the Brown Alga *Bifurcaria bifurcata*. Phytochemistry 34: 1585-1588

Valls R, Banaigs B, Piovetti L, Zerzouf A (1993b) Geographical Variations in the Diterpene Composition of *Bifurcaria bifurcata* on the Atlantic Coasts of Morocco. Annales De L Institut Oceanographique 69: 215-223

Valls R, Piovetti L, Banaigs B, Archavlis A, Pellegrini M (1995) (S)-13-Hydroxygeranylgeraniol-Derived Furanoditerpenes from *Bifurcaria bifurcata*. Phytochemistry 39: 145-149

van Loosdrecht M, Lyklema J, Norde W, Zehnder A (1989) Bacterial adhesion: a physicochemical approach. Microbial Ecology 17: 1-15

van Loosdrecht M, Lyklema J, Norde W, Zehnder A (1990) Influence of interfaces on microbial activity. Microbiological Reviews 54: 75

van Loosdrecht MCM, Heijnen JJ, Eberl H, Kreft J, Picioreanu C (2002) Mathematical modelling of biofilm structures. Antonie Van Leeuwenhoek International Journal of General and Molecular Microbiology 81: 245-256

Virto M, Frutos P, Torrado S, Frutos G (2003) Gentamicin release from modified acrylic bone cements with lactose and hydroxypropylmethylcellulose. Biomaterials 24: 79-87

Ward JB, Berkeley RCW (1980) The microbial cell surface adhesion. In: Berkeley RCW, Lynch MJ, Melling J, Rutter PR, Vincent B (eds) *In* Microbial adhesion to surfaces. Ellis Horwood, Chichester

Waters CM, Bassler BL (2005) Quorum sensing: Cell-to-cell communication in bacteria. Annual Review of Cell and Developmental Biology 21: 319-346

Webster NS, Battershill CN, Negri AP (2006) Recruitment of Antarctic marine eukaryotes onto artificial surfaces. Polar Biology 30: 1-10

Webster NS, Negri AP (2006) Site-specific variation in Antarctic marine biofilms established on artificial surfaces. Environmental Microbiology 8: 1177-1190

Webster NS, Smith LD, Heyward AJ, Watts JEM, Webb RI, Blackall LL, Negri AP (2004) Metamorphosis of a Scleractinian Coral in Response to Microbial Biofilms. Appl. Environ. Microbiol. 70: 1213-1221

Weinell C, Olsen K, Christoffersen M, Kiil S (2003) Experimental study of drag resistance using a laboratory scale rotary set-up. Biofouling 19: 45-51

Wetzel R (1993) Microcommunities and microgradients: linking nutrient regeneration, microbial mutualism, and high sustained aquatic primary production. Aquatic Ecology 27: 3-9

Wieczorek S, Clare A, Todd C (1995) Inhibitory and facilitatory effects of microbial films on settlement of *Balanus amphitrite amphitrite* larvae. Marine ecology progress series 119: 221-228

Wieczorek SK, Todd CD (1998) Inhibition and facilitation of bryozoan and ascidian settlement by natural multi-species biofilms: effects of film age and the roles of active and passive larval attachment. Marine Biology 128: 463-473

Wikstrom SA, Pavia H (2004) Chemical settlement inhibition versus post-settlement mortality as an explanation for differential fouling of two congeneric seaweeds. Oecologia 138: 223-230

Wood DC, Wood J (1975) Pharmacologic and biochemical considerations of dimethyl sulfoxide. Annals of the New York Academy of Sciences 243: 7-19

Wright D, Dawson R, Cutler S, Cutler H, Orano-Dawson C, Graneli E (2007) Naphthoquinones as broad spectrum biocides for treatment of ship's ballast water: Toxicity to phytoplankton and bacteria. Water Research 41: 1294-1302

Yoon MY, Lee KM, Park Y, Yoon SS (2011) Contribution of cell elongation to the biofilm formation of *Pseudomonas aeruginosa* during anaerobic respiration. PloS one 6: e16105

Young D, Howard B, Fenical W (1980) Subcellular localization of brominated secondary metabolites in the red alga Laurencia snyderae. Journal of Phycology 16

Zalavras C, Patzakis M, Holtom P (2004) Local antibiotic therapy in the treatment of open fractures and osteomyelitis. Clinical Orthopaedics and Related Research 427: 86-93

Zardus J, Nedved B, Huang Y, Tran C, Hadfield M (2008) Microbial biofilms facilitate adhesion in biofouling invertebrates. The Biological Bulletin 214: 91-98

List of publications

Conferences

Salta M., Capretto, L., Carugo, D., Wharton JA., Stoodley P., Dennington S., Stokes KR. (2012) A novel microfluidic approach for the assessment of antifouling technologies, 16th International Conference for Marine Corrosion and Fouling, Seattle, USA (Oral)

Salta M., Dennington S, Capretto, Wharton JA., Stokes KR. (2012) *In situ* assessment of biofilm growth and structure on natural product-containing antifouling coatings, 16th International Conference for Marine Corrosion and Fouling, Seattle, USA (Poster)

Salta M., Capretto, L., Carugo, D., Wharton JA., Dennington S., Stokes KR. Assessment of marine biofilm attachment and growth for antifouling surfaces under static and controlled hydrodynamic conditions, MRS Spring meeting 2011, KK Microbial Life on Surfaces – Biofilm-Material Interactions, San Francisco, USA (Oral)

Salta M., Wharton JA., Stoodley P., Wood RJ., Dennington S., Stokes KR. (2010) Bacteria and diatom bioassay screening for antifouling performance of natural products, Challenger 2010, Southampton, UK (Poster)

Salta M., Wharton JA., Stoodley P., Wood RJ., Dennington S., Stokes KR. (2010) Bioinspired antifouling using natural products against marine biofilms. Biofilms 4, Winchester, UK (Poster)

Salta M., Wharton JA., Stoodley P., Dennington S., Iglesias-Rodriquez D., Stokes KR. , Wood RJK. (2010), Bioassay screening and imaging for antifouling performance of novel natural products, 15th International Conference for Marine Corrosion and Fouling, New Castle, UK (Oral)

Salta M., Hellio C., Wharton JA., Wood RJ., Stokes KR, (2009) Natural products as marine antifoulants: the importance of biofilms, ASM Conferences: Biofilms 09, Cancun, Mexico (Poster)

Salta M., Chambers L., Wharton JA., Wood RJ, Briand JF., Blache Y., Stokes KR., (2009), Marine fouling organisms and their use in antifouling bioassays, EUROCORR 09, Nice, France (Oral)

Publications

Salta M., Wharton JA., Stoodley P., Dennington SP., Goodes L., Werwinski S., Mart U., Wood RJK., Stokes KR., (2010), Designing Biomimetic Antifouling Surfaces, Phil. Trans. R. Soc. A, 368, 4729-4753

Salta M., Chambers L., Wharton JA., Wood RJ, Briand JF., Blache Y., Stokes KR., (2009), Marine fouling organisms and their use in antifouling bioassays, EUROCORR 09 Proceedings, Nice, France.

Salta M., (2009), Natural Products as Marine Antifoulants: observing biofouling activity in Drake Passage. *In*:Hamersley DRC & McDonagh EL (eds) Cruise Report No 39, RRS James Cook Cruise JC031, 03 Feb-03 Mar 2009. Hydrographic sections of the Drake Passage. Southampton, UK, National Oceanography Centre Southampton, 170pp.

Salta M., Wharton., JA, Briand, JF. (2012) Marine biofilms on man-made surfaces: structure and dynamics, Environmental Microbiology, (submitted)

Salta M., Wharton, JA., Dennington, S., Stoodley P., Stokes KR., (2012) Antifouling performance against marine bacterial attachment for 3 natural products: *Chondrus crispus* crude extract, usnic acids and juglone. Marine Pollution Bulletin, (submitted)

Publication Strategy

Salta M., Wharton, JA., Dennington, S., Stokes KR., Novel method for the i*n situ* assessment of biofilm growth and structure on antifouling coatings, (in preparation for Biofouling)

Salta M., Wharton, JA. Effect of juglone on bacterial attachment under controlled hydrodynamic conditions (in preparation for Biofouling)

Salta M., Tsaloglou, MN., Wharton JA., Iglesias-Rodriquez D., Wood RJ., Dennington S., Stokes KR., Natural Products as Marine Antifoulants: comparing biofilm diversity through *in-situ* experiments in Drake Passage (in preparation for Microbial Ecology)

Salta M., Capretto, L., Carugo, D., Wharton JA., Stokes KR., A novel microfluidic approach for the assessment of antifouling technologies: *Ship-on-a-Chip* (in preparation for Lab-on-a-Chip)

Salta M., Katsamenis, O. Wharton JA., Dennington S., Stokes KR., Characterisation of the mechanical properties and adhesion strength of marine biofilm forming bacteria for antifouling coatings (in preparation)

APPENDIX A7.1 SoC OPTIMISATION, DESIGN AND FABRICATION

A7.1.2 Computational Fluid Dynamic simulations

The fluid flow field within the microfluidic device was numerically simulated with a three-dimensional model using ANSYS Fluent 12.1.4 (ANSYS Inc., Canonsburg, PA, USA). Computational fluid dynamics simulations based on the finite volume method (FVM) were performed on a geometry applying 1,200,000 cubic hexahedra (3D) mesh elements. The flow field within the device was modelled using single phase three-dimensional continuity and full Navier-Stokes equations for incompressible fluid flow. The governing conservation equations of mass and momentum are given respectively by the following expressions:

$$\nabla \cdot (\rho \vec{v}) = 0 \tag{A7.1}$$

$$\rho\left(\frac{\partial \vec{v}}{\partial t} + \vec{v} \cdot \nabla \vec{v}\right) = -\nabla p + \mu \nabla^2 \vec{v} + \rho \vec{g} \tag{A7.2}$$

where v is the fluid velocity, ρ is the density, μ is the dynamic viscosity, p is the pressure. The parameters: ρ and μ of 1024.75 kg·m^{-3} and 1.08×10^{-3} Pa·s, respectively, were set for seawater at temperature of 20 °C (National Physical Laboratory, 2012). The velocity at the flow inlet boundary was assumed to have uniform profile, while a constant pressure (101,325 Pa) was imposed at the outlet boundary. Finally, no-slip conditions were applied at the solid walls of the modelled device.

The governing equations and their boundary conditions were solved iteratively until solution convergence was reached. Note that under-relaxation technique was adopted to avoid divergence during the iterative solution procedure. Moreover, during the meshing step, care was taken in order to have a large number of elements in the grid, and to have edges parallel to flow direction.

A7.1.2 Design optimisation

The microfluidic device design, in terms of chamber depth was performed by adopting a computational-based optimization approach (**Figure A7.1**) in which the microchannel architecture was iteratively refined in order to obtain the desired shear stress values on the substrate surface. A range of hydrodynamic shear stress values with relevance in marine antifouling coating applications was determined from ASTM standards (ASTM D3949, 2007). Shear stress values correspond to those that can occur on a ship hull, either during the tidal phase (*i.e*. vessel in the dock) or during vessel motion, leading to this biomimetic inspired design for the SoC microfluidic device. In particular, typical values in the range 1-15 knots were considered in the device design step, and the corresponding shear stress values generated on a ship surface are reported in **Table A7.1** (as from ASTM standard determinations).

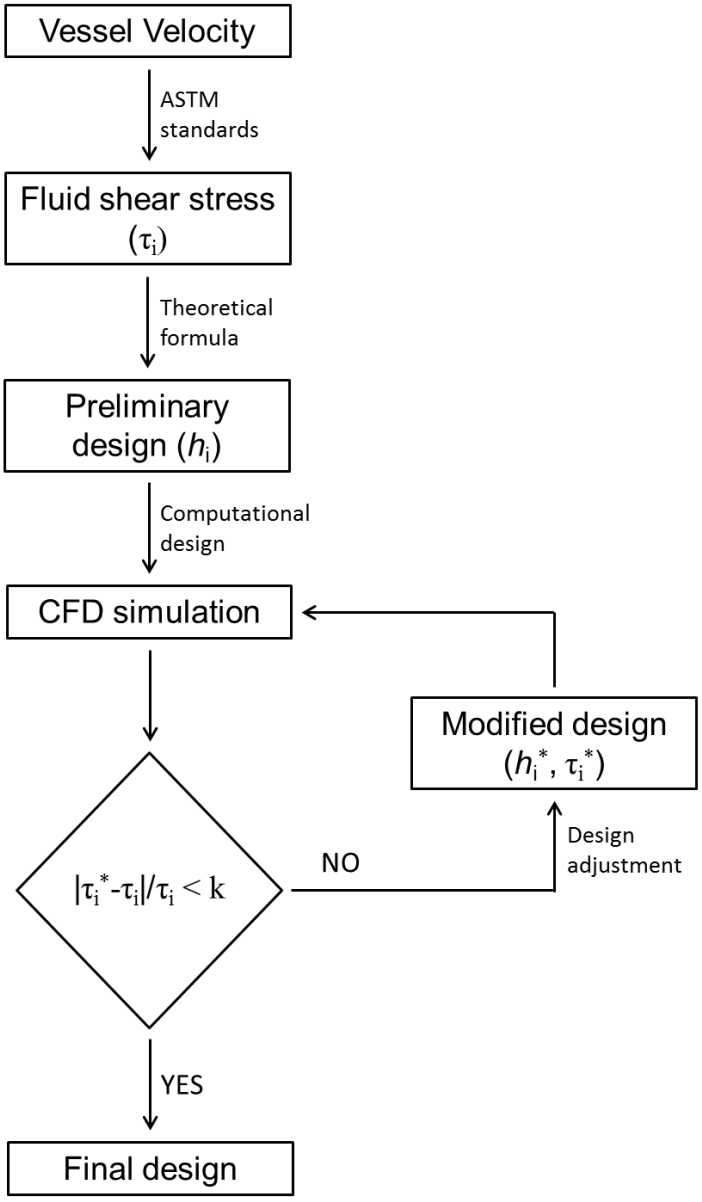

Figure A7.1. Schematic of the procedure of SoC device design and optimization.

Table A7.1. Fluid velocities (in knots) and corresponding fluid shear stress values (in Pa), as determined from ASTM (ASTM D3949, 2007) international standards.

τ_1 (Pa)	τ_2 (Pa)	τ_3 (Pa)	τ_4 (Pa)
0.5	10.3	36.8	77.5
v_1 (knots)	v_2 (knots)	v_3 (knots)	v_4 (knots)
1	5	10	15

Following the selection of the desired shear stress values to be generated within the device, a preliminary design of the flow cell was performed. Specifically, the designed is characterised by stair-like geometry that create four chambers with different heights, as shown in **Figure A7.2**. The stair-like geometry of the channel was proposed to obtain four different regions with homogeneous wall-shear stress regions within each chamber, maintaining a constant flow rate. During the optimisation step, the well-known theoretical equation for the fluid shear stress field within a squared cross-section channel was employed (Equation A7.3) to determine the optimal chamber depth (**Figure A7.2**).

Figure A7.2. Stair-like geometry of the channel illustrating the four micro-chamber heights.

Notably, the width of the chamber represents a compromise between a large enough area of study and the requirement of keeping the total flow rate (with a tube of 3.1 mm ID) and the back pressure (be up to 2 bars) in a range easily achievable with standard laboratory peristaltic pumps. In this respect, channel width (w) was kept constant and equal to 1 mm, while the local channel height (h_i) was determined from Equation A7.3 for rectangular chambers (Bacabac *et al.* 2005), as a function of the local shear stress (τ_i) and the volume flow rate at the device inlet (Q_{in}):

$$h_i = \sqrt{\frac{6 \cdot \mu \cdot Q_{in}}{\tau_i \cdot w}} \qquad \text{with } i = 0, 1, 2, 3 \qquad \text{(A7.3)}$$

Q_{in} was set equal to 8.5 mL min^{-1}, which fell within the range of volume flow rates provided by the peristaltic pump used for standard experimental procedures.

Due to fabrication restrictions associated with the micro-milling technique employed here, chamber height was adjusted with respect to the theoretical value. The effect of this modified height (h_i*) on the flow field characteristics (*i.e.* modified fluid shear stress, τ_i*) was

evaluated numerically by implementing a computational fluid dynamic (CFD) model. The h_i* values were subsequently refined in order to obtain satisfactorily agreement between numerical shear stress values and ASTM standards. This was achieved upon satisfaction of the following condition:

$$\frac{\left|\tau_i^* - \tau_i\right|}{\tau_i} < k = 0.05 \qquad \text{(A7.4)}$$

Equation A7.4 was verified for i = 0, 1, 2 and 3; with a maximum percent difference between τ_i* and τ_i of 4 % within the chamber. The final chamber height and corresponding shear stress values on the substrate surface of the device (as determined from numerical simulations) are reported in **Table A7.2**.

Table A7.2. Final microfluidic device design. Numerical fluid shear stress values (in Pa) are reported together with the corresponding microchannel height (in mm).

τ_1 (Pa)	τ_2 (Pa)	τ_3 (Pa)	τ_4 (Pa)
0.52	10.01	37.2	75.04
h_1 (mm)	h_2 (mm)	h_3 (mm)	h_4 (mm)
2.00	0.32	0.16	0.11

A7.1.3 CFD analysis

As obtained from the iterative process for the optimization of the depths, the chambers were selected to be 2.00, 0.32, 0.16 and 0.11 mm high and 1.00 mm wide. Following the dimension optimisation a series of simulations were run controlling the inlet flow rate from 0.5 mL min^{-1} to 15 mL min^{-1} (which represent values attainable within the peristaltic pump range). The values of the shear stresses obtained for each single chamber at different flow rates were interpolated to create the calibration **Table A7.3**. The lowest total flow rate point (*i.e*. 0.5 mL min^{-1}) was used to allow direct comparisons with the Bioflux study/experiments (**Section 4.3**).

Table A7.3. Computed shear stresses for the SoC over a wide range of flow rates

Flow rate (mL min^{-1})	τ_1 (Pa)	τ_2 (Pa)	τ_3 (Pa)	τ_4 (Pa)
0.5	0.02684505	0.5967	2.14501	4.31249
1	0.0518	1.2279	4.3101	8.6293
1.5	0.08155	1.8048	6.44925	12.9422
2	0.1113	2.3817	8.5884	17.2551
2.5	0.14105	2.9586	10.72755	21.568
3	0.1708	3.5355	12.8667	25.8809
3.5	0.20055	4.1124	15.00585	30.1938
4	0.2303	4.6893	17.145	34.5067
4.5	0.26005	5.2662	19.28415	38.8196
5	0.2898	5.8431	21.4233	43.1325
5.5	0.31955	6.42	23.56245	47.4454
6	0.335	7.15	25.78	51.77
6.5	0.37905	7.5738	27.84075	56.0712
7	0.4088	8.1507	29.9799	60.3841
7.5	0.43855	8.7276	32.11905	64.697
8	0.4683	9.3045	34.2582	69.0099
8.5	0.52	10.01	37.2	75.04
9	0.5278	10.4583	38.5365	77.6357
9.5	0.55755	11.0352	40.67565	81.9486
10	0.5873	11.6121	42.8148	86.2615
10.5	0.61705	12.189	44.95395	90.5744
11	0.6468	12.7659	47.0931	94.8873
11.5	0.67655	13.3428	49.23225	99.2002
12	0.7063	13.9197	51.3714	103.5131
12.5	0.73605	14.4966	53.51055	107.826
13	0.7658	15.0735	55.6497	112.1389
13.5	0.79555	15.6504	57.78885	116.4518
14	0.8253	16.2273	59.928	120.7647
14.5	0.85505	16.8042	62.06715	125.0776
15	0.8848	17.3811	64.2063	129.3905

Figure A7.3 shows the computed results of the shear stress values at flow rate of 0.5 mL min^{-1} in **Figure A7.3A** illustrates that four different regions with virtually homogeneous wall-shear stress can be created using the current geometry. These results are further demonstrated by the plot of the shear stress distribution along both the cross-section of the chamber (see **Figure A7.3B**) and the channel longitudinal direction (see **Figure A7.3C**). In

addition **Figure A7.3C** shows the stair-like increase of the shear stress along the channel as expected by the stair-like decrease in channel depth.

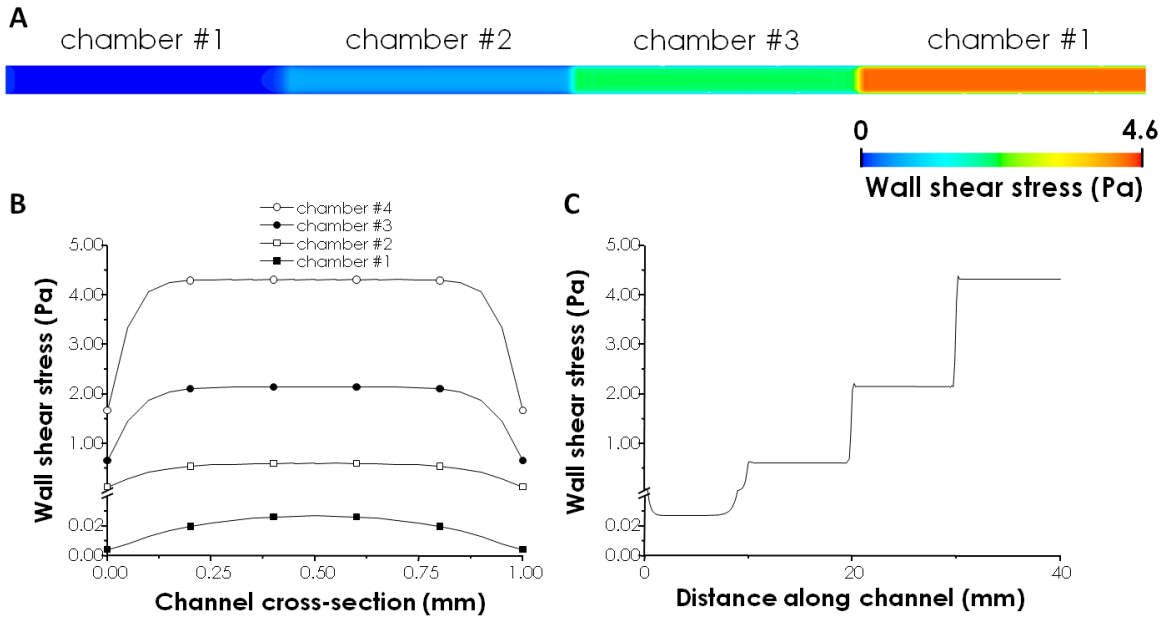

Figure A7.3. The flow field established in the channel with a constant flow rate of 0.5 mL min^{-1} at the inlet has been simulated using CFD package. (A) Colour map contour of the computed wall shear stress on the substrate surface where the biofilm attached. (B) Wall shear stress along the cross section as computed at the middle length of each chamber. (C) Wall shear stress at different positions along the channel, computed at half-width length of the channel showing the characteristic stair-like increase of the wall shear stress.

A7.1.4 SoC fabrication

The top plate was drawn in CAD software (AutoCAD, Autodesk, Inc.) and machined by micro milling on a PMMA (poly(methyl) methacrylate)) layer with a micro-mill (Datron CAT3D-M6, Datron Dynamic, Inc.). The surface roughness of the milled channel was reduced by means of treatment with chloroform vapour as previously reported (Ogilvie et al. 2010). Briefly, the face to be processed was cleaned with detergent then rinsed with DI water and ethanol and subsequently dried with air steam. The PMMA layer was placed on metal stand (6 mm in height) in a flat bottom crystallizing dish which was previously filled with chloroform in order to have the level of solvent 2-3 mm below the layer surface (*i.e.* face to be treated). A lid

was placed over the assembly to form a vapour exposure chamber. The surface was exposed for 6 min and subsequently left overnight in a water bath.

The gasket was fabricated casting a PDMS layer (polydimethylsiloxane) with a thickness of 0.11 mm. The top part of the template for the cast, which contains the reliefs to produce the through cut features of the gasket was fabricated on PMMA by micromilling and subsequently treated to reduce the surface roughness as previously reported (see previous paragraph). The bottom part of the template consisted of the substrate layer to be included in the final device. To produce the PDMS gasket, PDMS (Sylgard 184, Dow Corning) monomer and curing agent were mixed in a ratio of 10:1 by weight, degassed under reduced pressure, injected into the casting template and placed in the oven at 65 °C for 4 h.

I R G Ogilvie, V J Sieben, C F A Floquet, R Zmijan, M C Mowlem and H Morgan, 2010, Reduction of surface roughness for optical quality microfluidic devices in PMMA and COC20, *Journal of Micromechanics and Microengineering*, Volume 20, Issue 6, pp. 065016

APPENDIX A7.2 – TIME LAPSE IMAGING FOR 4 FLOW CELL CHAMBERS: C1, C2, C3 & C4

Flow cell C1, wall shear stress: 0.03 Pa

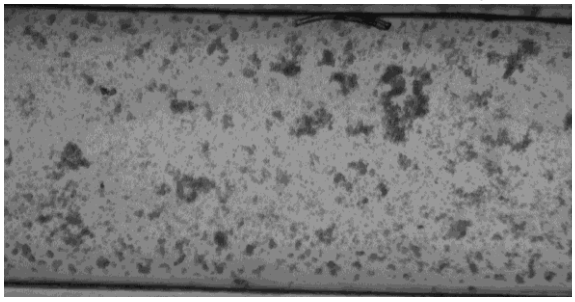

0.5 h

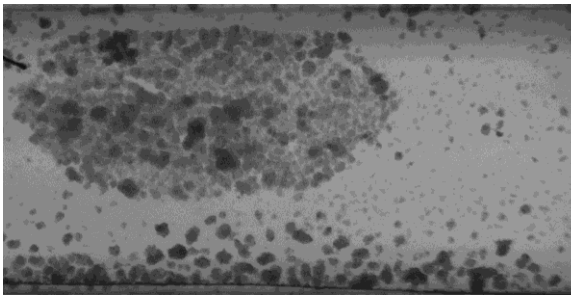

2.5 h

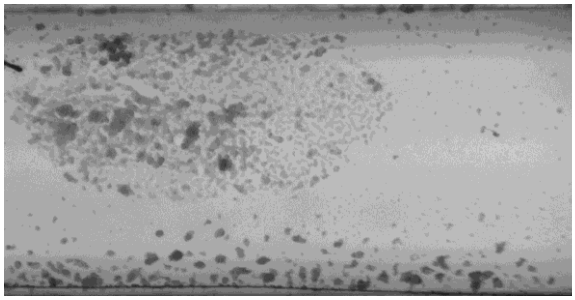

1 h

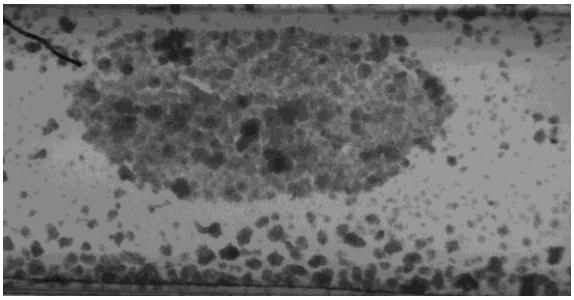

3 h

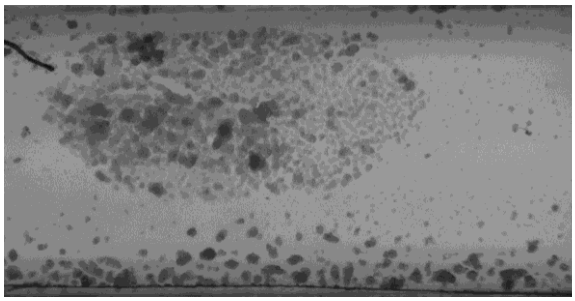

1.5 h

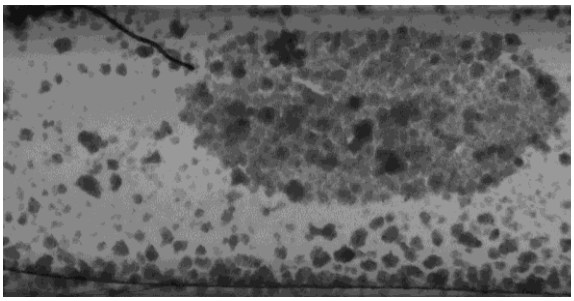

3.5 h

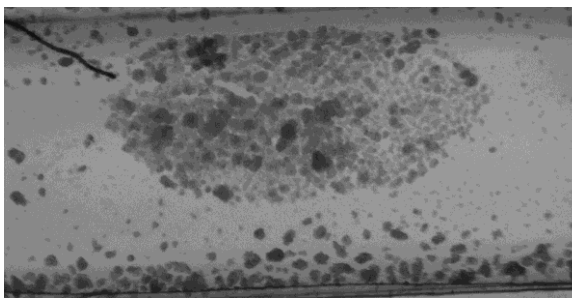

2 h

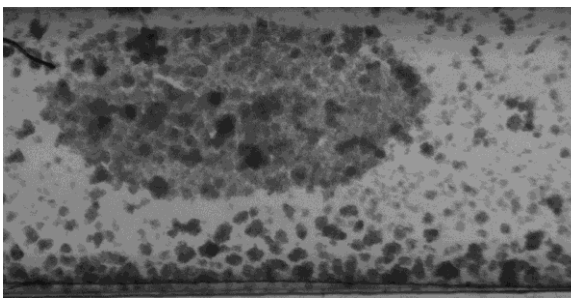

4 h

Flow cell C2, wall shear stress: 0.60 Pa

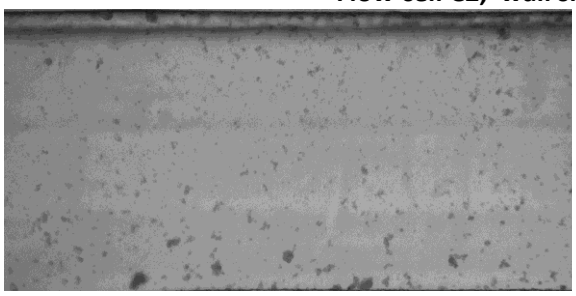

0.5 h

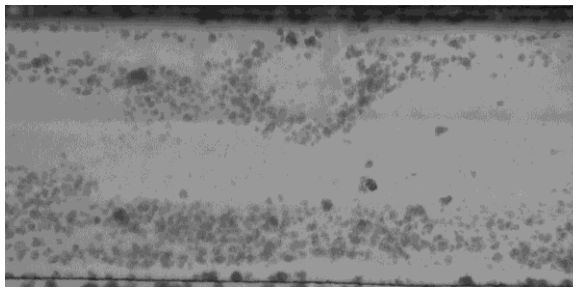

2.5 h

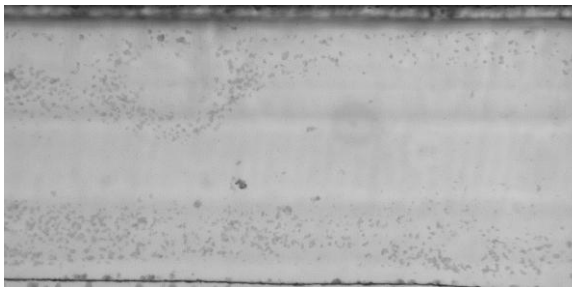

1 h

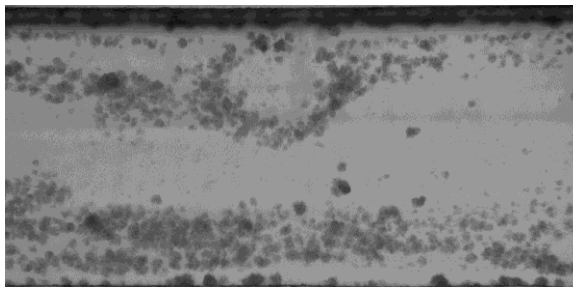

3 h

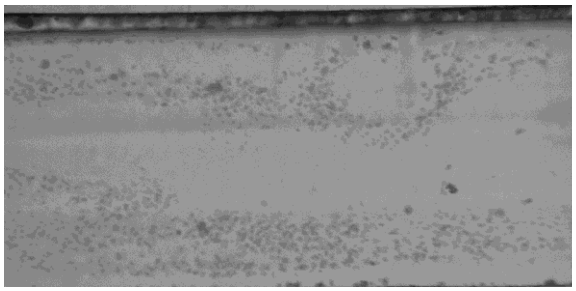

1.5 h

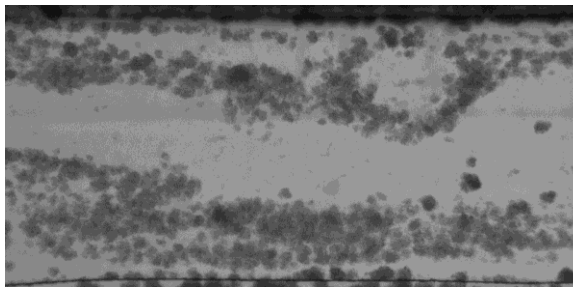

3.5 h

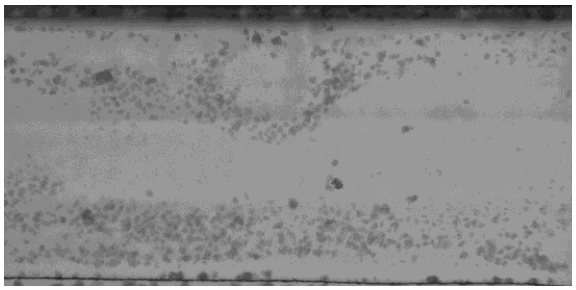

2 h

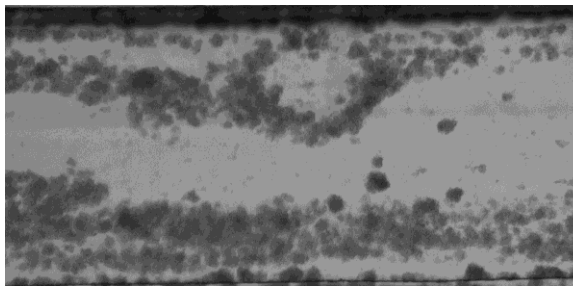

4 h

Flow cell C3, wall shear stress: 2.15 Pa

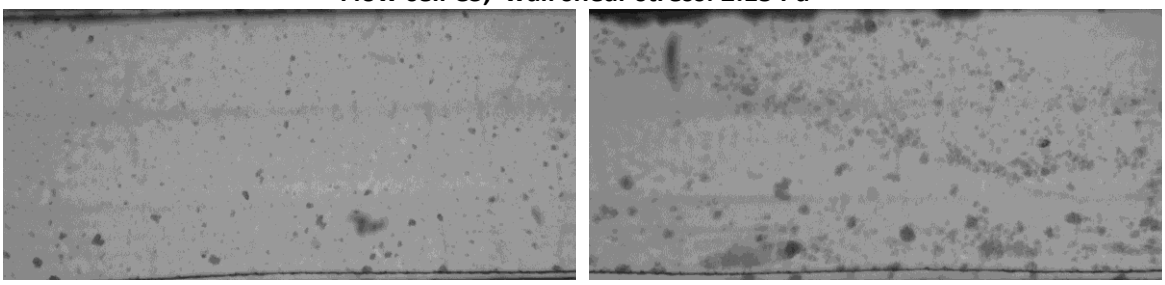

0.5 h

2.5 h

1 h

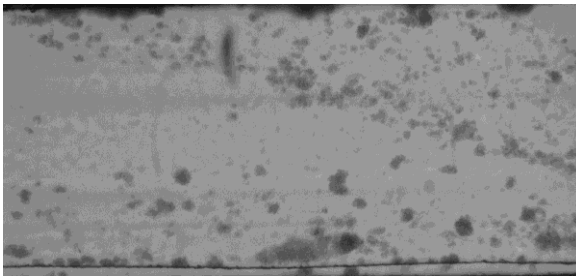

3 h

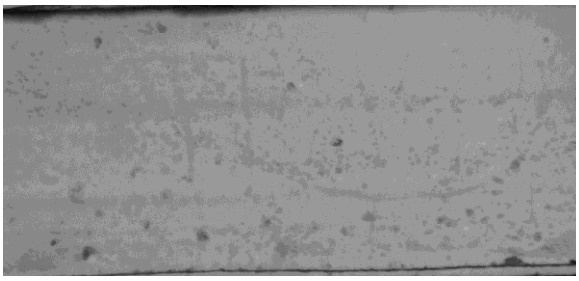

1.5 h

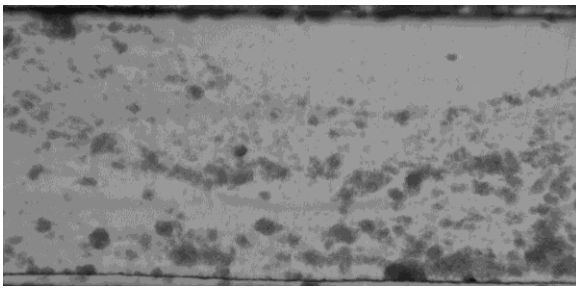

3.5 h

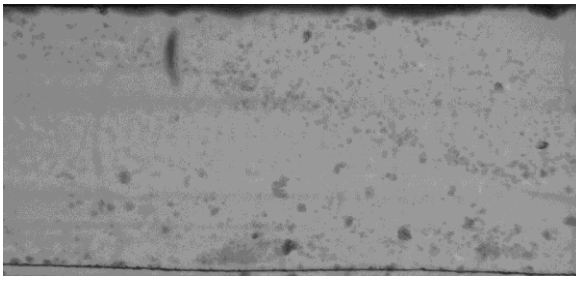

2 h

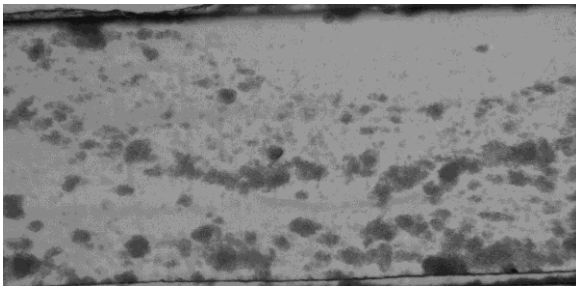

4 h

Flow cell C4, wall shear stress: 4.30 Pa

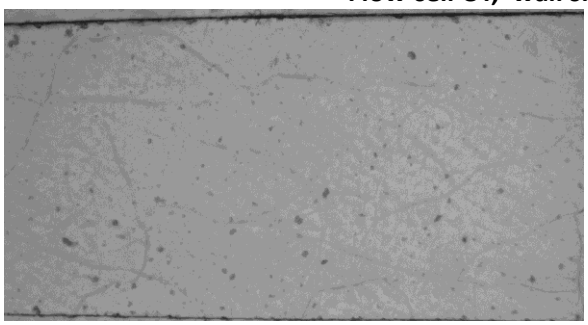

0.5 h

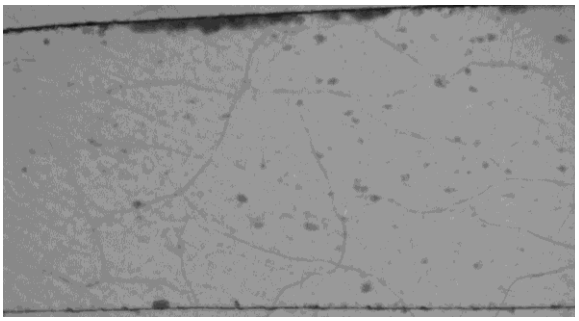

2.5 h

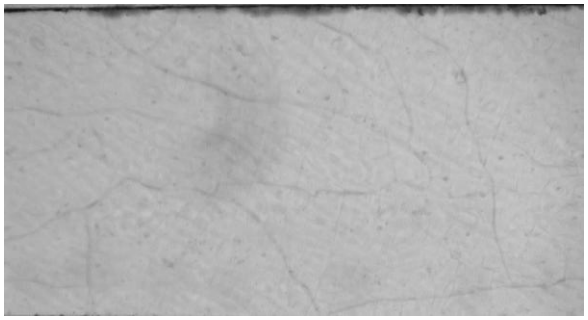

1 h

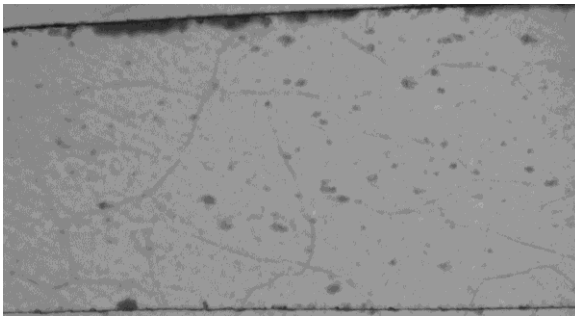

3 h

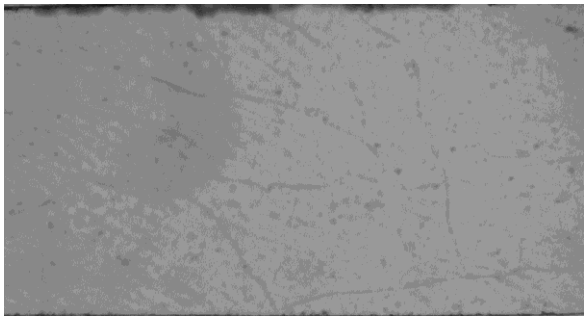

1.5 h

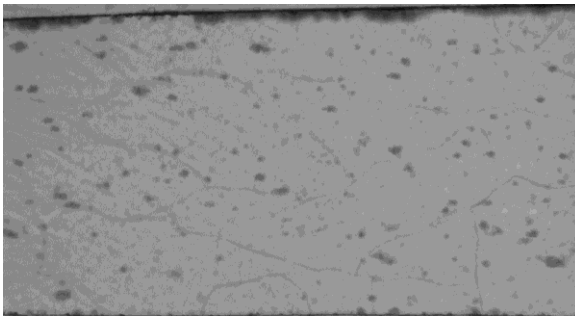

3.5 h

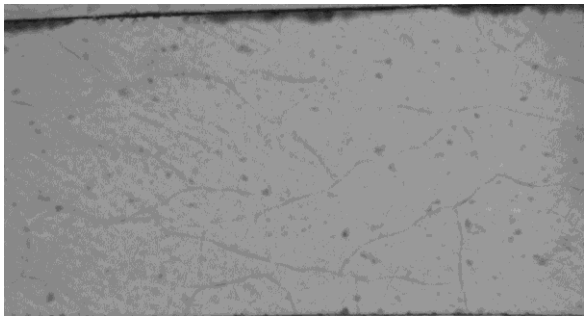

2 h

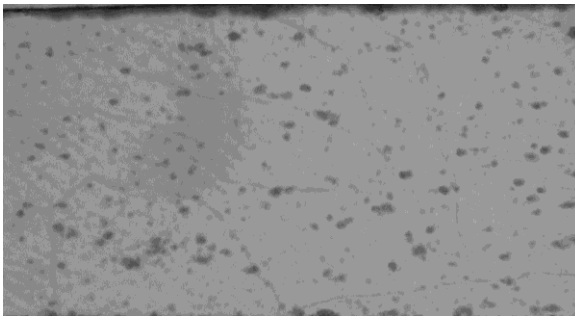

4 h